GLOBCER'24

Global Conference on Engineering Research

16-19 October 2024

4th GLOBAL CONFERENCE on ENGINEERING RESEARCH

Proceedings Book

ISBN: 978-625-94317-3-4

PROCEEDINGS BOOK

4th GLOBAL CONFERENCE on ENGINEERING RESEARCH

16-19 October 2024

4th GLOBAL CONFERENCE ON ENGINEERING RESEARCH (GLOBCER'24)

16-19 October 2024

ISBN: 978-625-94317-3-4

4th Global Conference on Engineering Research (GLOBCER'24)

16-19 October 2024

Organizination Board

Prof. Dr. Muhammet Nuri SEYMAN
Assist. Prof. Dr. Barış Gürcan HAKANOĞLU

Scientific Board

Prof. Dr. Ahmed Kadhim Hussein
Prof. Dr. Alexandre Jean Rene SERRES
Prof. Dr. Degan ZHANG
Prof. Dr. Feyzullah TEMURTAŞ
Prof. Dr. Goran Putnik
Prof. Dr. Hui CHEN
Prof. Dr. İbrahim DEVELİ
Prof. Dr. Jianjun WANG
Prof. Dr. Jue-Sam CHOU
Prof. Dr. Ke-Lin DU
Prof. Dr. Lianggui LIU
Prof. Dr. Mehmet TEKTAŞ
Prof. Dr. Miladin Stefanović
Prof. Dr. Mustafa GÜNAY
Prof. Dr. Necmi TAŞPINAR
Prof. Dr. Paweł LULA
Prof. Dr. Recep ÇALIN
Prof. Dr. Zitaun CAI
Prof. Dr. R. Gökhan TÜRECİ
Prof. Dr. Mahmut BÖYÜKATA
Prof. Dr. Gökçe NUR YILMAZ
Prof. Dr. Ziyodulla YUSUPOV
Prof. Dr. Halit ÖZTEKİN
Prof. Dr. Selim ÖNCÜ
Prof. Dr. Oğuz Akın DÜZGÜN
Prof. Dr. Ahmet AKKÖSE
Prof. Dr. Semet ÇELİK
Prof. Dr. Rıdvan KOÇYİĞİT
Assoc. Prof. Dr. Abdullah YEŞİL
Assoc. Prof. Dr. Bülent BÜYÜK
Assoc. Prof. Dr. Emre ÇELİK
Assoc. Prof. Dr. Fahmina TARANUM
Assoc. Prof. Dr. Filmor MURILLO
Assoc. Prof. Dr. H.Oktay ERKOL
Assoc. Prof. Dr. Héctor F. MIGALLON
Assoc. Prof. Dr. M. Hanefi CALP
Assoc. Prof. Dr. Muharrem PUL
Assoc. Prof. Dr. Neelamadhab PADHY
Assoc. Prof. Dr. Ning CAI
Assoc. Prof. Dr. Harun ÖZBAY
Assoc. Prof. Dr. Adem DALCALI
Assoc. Prof. Dr. İsmail KOÇAK
Assoc. Prof. Dr. Oye Nathaniel DAVID
Assoc. Prof. Dr. Hayri YAMAN
Assoc. Prof. Dr. Alican KARACA
Assoc. Prof. Dr. Sasmita MOHAPATRA
Assoc. Prof. Dr. Serhat DUMAN
Assoc. Prof. Dr. Onur ÜLKER

TABLE OF CONTENTS

Classification of Skin Cancer Lesions Using Machine Learning and Image Processing Methods 1

The Effect on Model Performance of Increasing the Batch Size during Training 14

Design and Optimization of Renewable Energy-Based Electric Vehicle Charging Stations: A Case Study in Yalova 21

Performance Investigation of Bridge Type Parallel-Resonance Fault Current Limiter in Power Distribution Systems 37

Sustainable Management of Water Resources: Strategies, Challenges, And Implementation Recommendations 46

Brain Tumor Detection and Classification from MRI Image 51

Breast Tumor Classification on Ultrasound Images Using Image Processing and Machine Learning Methods 64

Çok Kriterli Karar Verme Yöntemleri İle Tedarikçi Seçimi 77

Derin Öğrenme Yöntemleriyle Akarsu Debisi Tahmini 82

Self-Gravitational Solitary Potential In Degenerate Quantum Plasmas 96

Effects of Different Nitrogen Levels on Some Agronomical Characteristics of Echinacea Purpurea L. Moench 103

Effect Of Fumed Silica on Cutting Carrying Performance of Spud Type Drilling Muds 114

Kentsel Geri Dönüşüm Atık Yönetimi için Belirsiz Talepler Altında Araç Rotalama Problemine Yönelik Matematiksel ve Sezgisel Çözüm Yaklaşımları 120

A Hybrid DEA-AHP Approach for Assessing the Calorific Efficiency of Softwoods 133

Towards Intelligent Industry: Optimizing Processes through AI and Blockchain Integration 145

Yüksek Sıcaklık Faktörünün Karbon Lif Katkılı Çimentolu Harçların Mekanik Özellikleri Üzerine Etkisi 159

Bulut Servisi Sağlayıcı Seçiminde Çok Kriterli Karar Verme Yaklaşımları: AHS ve TOPSIS Uygulaması 171

Boşluklu Betonarme Kirişlerin Davranışı Üzerine Nümerik Bir Çalışma 181

Arbitrary Amplitude Solitary Potential in Ultra-Relativistic Degenerate Plasma 191

Modeling the light-dependent growth kinetics of the green microalga Chlorella zofingiensis 199

Eksantrik Mesnetli Basit Kirişlerin Serbest Titreşim Analizi 207

Machine Learning-Based IoT Device Classification through Network Traffic Feature Extraction 217

Establishment of Citrus suhuiensis Adventitious Root Culture 225

Preparation Of Ti_3SiC_2 Max Phase Via Sol-Gel Process.....226

Investigation of the Oxidation Behavior and Mechanical Properties of TiB_2-$MoSi_2$ Composites 227

Investigation Of the Densification, Mechanical Properties and Oxidation Behavior of CrB_2-SiC Composites.....228

Local well-posedness and blow-up solutions of a fourth-order pseudo-parabolic equation.....229

Evaluation of the Degree of Biological Decay of Wood Based on Climate Index Values in Türkiye 230

The Role of CuIr Alloys and Magnetic Damping in NiFe Thin Films.....231

Processing and Characterization of CoCrFeNiAlx (x=0.2 x=0.6 x=1 x=1.5 mol) High Entropy Alloy by Mechanical Alloying and Spark Plasma Sintering.....232

Influence of Halogen Heater and Fluidized Bed Drying on Color, Total Phenolic Content and Drying Kinetics of Green Pepper (Capsicum L.) 233

Tuz Hidrat Faz Değişim Malzemeleri ve Performanslarını İyileştirmek için Kullanılan Nanoparçacıklar.....234

Kısa Elyaf Takviyeli Kompozit Timoshenko Kirişlerinin Titreşiminde Dönel Yay Mesnetlerinin Etkisi.....236

Morphological Features in Radiological Images: Python-Based Image Processing Solutions.....238

Optimizing Load-Bearing Capacity of Sand: The Role of Stiffness Modulus Ratio 239

Analysis of Piled Concrete Foundation for an Offshore Structure 240

Classification of Skin Cancer Lesions Using Machine Learning and Image Processing Methods

Enis ÖZKAN[*,1], Kayra Berk CİHAN[1], Mahmut BÜYÜKBAŞ[1]

[*]enis.ozkan@agu.edu.tr, ORCID: 0009-0004-4605-5135
[1]*Department of Electrical & Electronics Engineering, School of Engineering, Abdullah Gül University, Kayseri, Turkey*

Abstract: Skin cancer is a critical health problem and early diagnosis is important for effective treatment. Correct differentiation of benign and malignant skin lesions is important for early diagnosis and appropriate treatment. The biopsy method, which is frequently used in diagnosis, gives almost 100% accurate results and this process takes about 10 minutes. With new techniques brought about by developments in image processing and machine learning skin cancer diagnosis is getting more accurate and effective. Some of the image processing techniques, such as segmentation and analysis, can be utilized in enhancing skin lesion images. Also, machine learning algorithms can be trained and can perform as well as biopsy in certain scenarios. In addition, machine learning algorithms can be trained and can perform as well as biopsy in certain scenarios. In this research, image processing and machine learning were used to classify skin lesions as benign and malignant, to improve the performance of the classification, and to accelerate and facilitate the diagnosis process of skin cancer. Benign and malignant test and train skin cancer dataset was obtained from Kaggle. In the studies conducted, it was seen that the highest accuracy rate achieved using machine learning algorithms was 0.791% in the study of Marques S et al.[7]. To achieve higher accuracy rate noise removal, segmentation and feature extraction in the samples were implemented with MATLAB, and feature selection and classification were implemented using Weka. 8 different classification methods and 6 different selection models were evaluated using cross-validation and a 79.27% accuracy rate (Classification via Regression and ReliefF) and 79.39% accuracy rate (Logistic Model Trees and ReliefF) were achieved. Each model was evaluated using standard measurements such as accuracy, precision, recall (sensitivity), confusion matrix. Although perfect accuracy is not achieved, a cost-effective and simplified solution is presented. By expanding the data set and improving the algorithms created, misdiagnoses can be prevented and diagnosis can be made more easily.

Keywords: *Skin Cancer, Machine Learning, Image Processing, Feature Extraction*

I. INTRODUCTION

Skin cancer is one of the biggest health problems worldwide. Despite this, in diagnosing skin cancer, visual examination of skin lesions still negatively affects the disease process in terms of the reliability of the diagnosis, and pathological tests negatively affect the disease process due to the length of the diagnosis period. The limitations of traditional methods used to distinguish different types of skin cancer have led to the need for a faster, cost-effective, and reliable diagnostic approach. In this research, we used image processing and artificial intelligence techniques to determine whether a skin lesion is benign or malignant. Using the data set obtained from Kaggle, we achieved the classification of malignant and benign lesions with noise removal, segmentation, feature extraction, feature selection and classification. With this method we developed, we offered a fast and cost-effective solution instead of

pathology that could take 7 days.

When compared to other studies using machine learning, we can conclude that the accuracy of the method we created is highest (Table I).

TABLE I
ACCURACY RESULTS IN DIFFERENT RESEARCH

Reference	Accuracy with ML
Marques S et al. [7]	0.791
Kanca et al. [3]	0.68
Proposed method	0.7939

ML: Machine Learning

II. METHODOLOGY

In the research, the "Skin Cancer: Malignant vs. Benign" [8] data set obtained from Kaggle was used. The data set contains two different folders, "benign" and "malignant", under two headings "train" and "test". The data consists of these two folders with each 1800 images.

The workflow for classification of skin cancer is shown in Figure 1. The workflow includes the steps of skin cancer image acquisition, pre-processing, segmentation, feature extraction, feature selection and evaluation, and classification as benign or malignant. This process was applied to achieve the highest accuracy percentage.

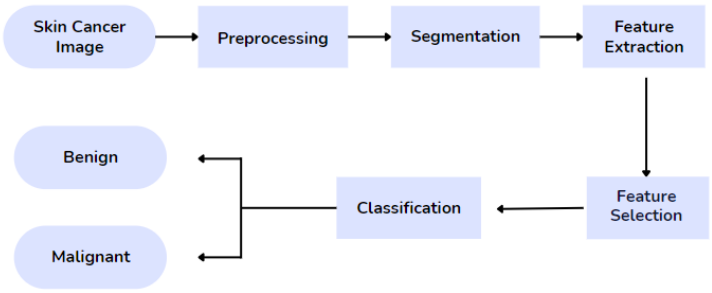

Fig. 1. Workflow for skin cancer classification

A. PRE-PROCESSING

The preprocessing part is the preparation phase for image processing and machine learning and is critical. This important step was taken to improve the data image quality and facilitate classification in the classification of skin cancer. This step was done with MATLAB. In the first step, the images were converted from RGB to grayscale. Converting to grayscale is an important and mandatory step for the subsequent application of the "Black Hat Filter". Black Hat Filter was used to highlight dark areas, that is, to highlight hairs, spots or structures of interest that would cover the lesions and prevent image processing. After using the filter, dark and light areas were separated by applying "Adaptive Thresholding". This process allowed clear separation of hairs, stains, or structures of interest. "Binary Mask" allowed the hairs to be isolated by showing the unwanted structures as white (1) and the background as black (0). Images with unwanted structures removed are shown in Figure 7.

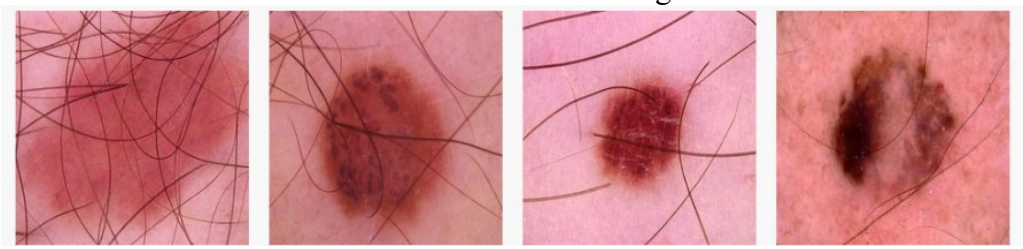

Fig. 2. The initial-colored image of skin cancer. [7]

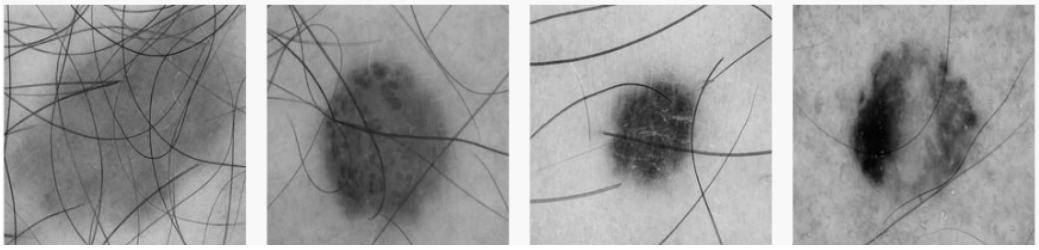

Fig. 3. Images converted to grayscale.

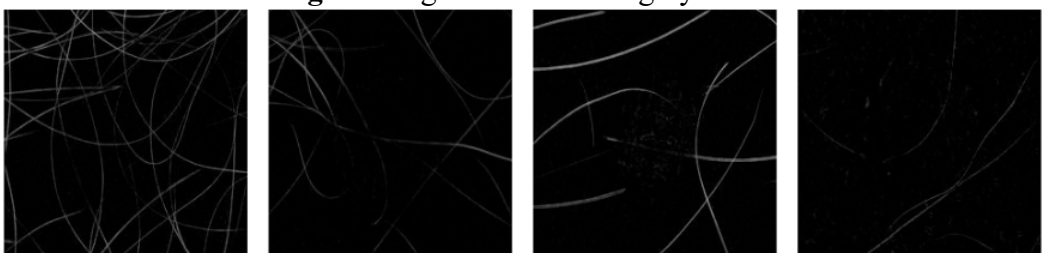

Fig. 4. Images with black hat filter applied.

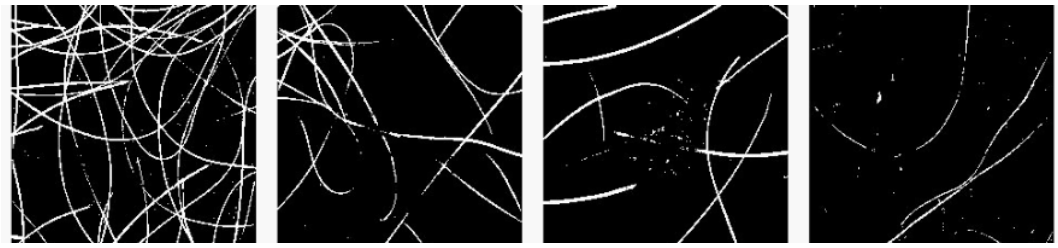

Fig. 5. Images with adaptive thresholding applied.

Fig. 6. Images with binary mask applied.

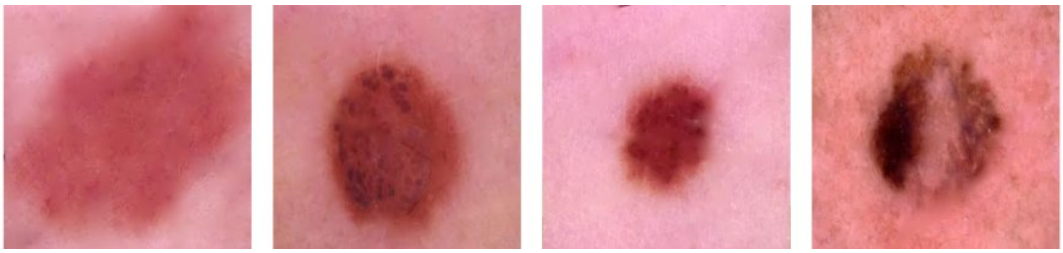

Fig. 7. Images that have been noise-removed through preprocessing.

B. SEGMENTATION

Segmentation is a technique in image processing that finds lesion boundaries in skin cancer images and separates and isolates them from the background.

This step was done with the MATLAB program. In the first step, lesions were selected and identified using Otsu's Thresholding Method in the images converted to grayscale. Then, Median Filter and Opening-Closing Operation were applied to reduce noise and achieve a cleaner image.

Pre-processing batch results were converted from RGB to grayscale. In the first step, Otsu's Thresholding Method was applied to these converted images. This method is done by

automatically binarizing the image using the optimal threshold value. Otsu's Thresholding Method for histogram analysis establishes the boundary that maximizes inter-class variance on an image's brightness histogram to separate black pixels from white ones according to their level of brightness.

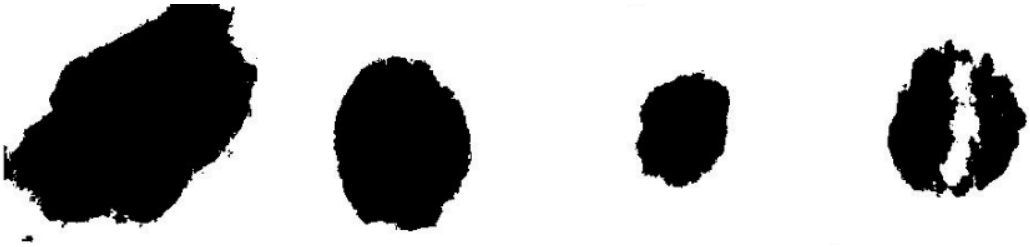

Fig. 8. Images applied Otsu's Thresholding Method.

An attempt was made to find the appropriate Median Size value for the filter by applying different values. The images show values of 15 Median Size (Figure 9), 9 Median Size (Figure 10), and 3 Median Size (Figure 11), respectively. Although more values were tried, these values were added to observe the difference. The most appropriate value was found to be 3 Median Size. Thanks to this value, noise is cleaned more clearly, while edge detection and accurate cropping of edges are more successful.

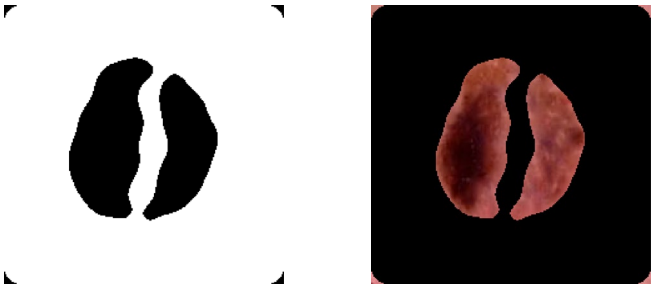

Fig. 9. Median filtered image with a neighborhood region of 15.

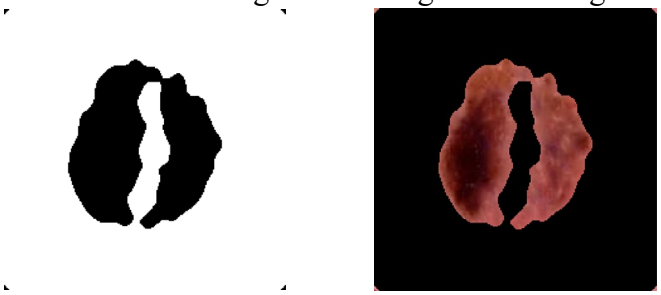

Fig. 10. Median filtered image with a neighborhood region of 9.

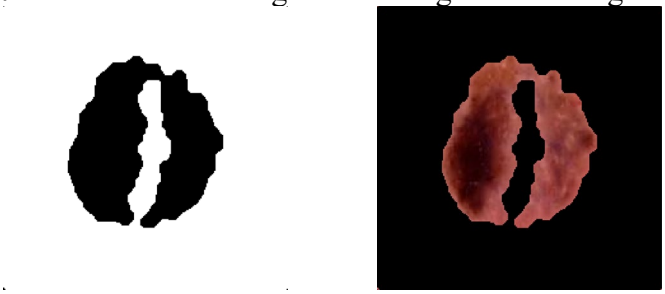

Fig. 11. Median filtered image with a neighborhood region of 3.

Opening and Closing Operations were used to make the filtered image cleaner and clearer. It is the process of identifying and deleting white pixels. Closing process is the step of filling the gaps created during the opening process. The configuration item size value for Opening-

Closing is selected as 5. Comparison of Median Filter result and Opening-Closing operation results are shown in Figure 12, respectively.

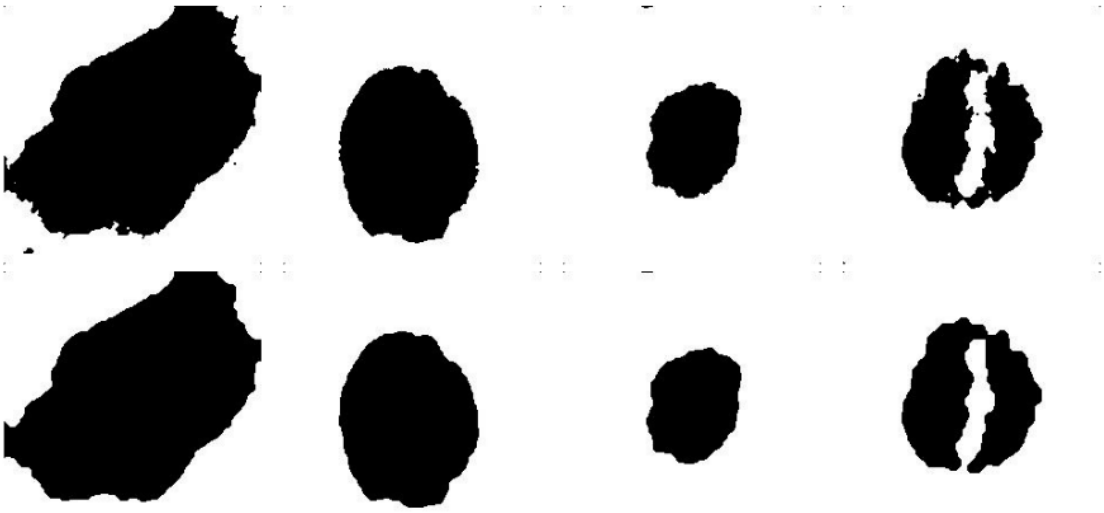

Fig. 12. Comparison of Median Filter and Opening-Closing operation results.

In the last step, the images were returned to their original color, and in the segmentation step, the images prepared before the feature extraction step became ready for use. Although The Chan-Vese algorithm was also tried in the segmentation step, the method was not used in this research because it gave lower accuracy.

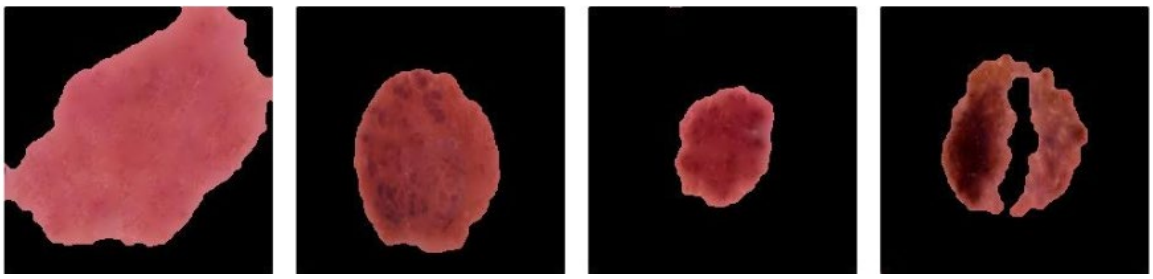

Fig. 13. Images results after segmentation.

C. FEATURE EXTRACTION

In the study, the feature extraction method is important in determining the lesion type. There are two classes: malignant and benign, and at this point, MATLAB was used in the feature extraction step. As a result of the literature study, forty-eight feature extraction techniques were used in the regions determined as a result of segmentation, taking into account texture, shape, intensity, statistical, volume and surface area.

GLCM, GLSZM, GLDM, and GLRLM are matrices and methods used in the study to extract different textural features in image processing and texture analysis. Each method is designed to capture a different texture feature.

- GLCM: The GLCM technique used to detect the texture of an image by calculating the amount of pixel combinations with a certain value in a particular direction [4].
- GLRLM: The technique known as GLRLM determines the length or number of consecutive pixels with the same gray level value [4].
- GLSZM: A technique called GLSZM measures pixels whose values fall into the same gray level [4].
- GLDM: The number of connected pixels inside the distance connected to a center pixel is measured using the GLDM method [4].

The obtained features were saved from MATLAB to the Excel file. These extracted features were used to obtain better results in skin cancer diagnosis.

TABLE II
FEATURES' VALUES

Features	Benign 1	Benign 2	Malignant 1	Malignant 2
Angular Second Moment	0,554064728	0,587693956	0,894203873	0,616432663
Area	18522	618,125	2413	229,75
Compactness	0,000678456	0,000847076	0,005207779	0,001243087
Contrast	780,5	780,5	780,5	780,5
Convexity	18522	14835	2413	10109
Correlation	5,750886767	4,879401748	6,912258778	6,639913338
Contrast (GLCM)	0,170163357	0,442825112	0,08504164	0,324391416
Correlation (GLCM)	0,935914444	0,956456238	0,939530936	0,918277248
Dissimilarity	0,695547726	0,630285074	0,134168802	0,5583720372
Dissimilarity(GLCM)	1561	1561	1561	1561
Eccentricity	0,890480963	0,496351092	0,818445369	0,459568842
Elongation	0,414801369	3,80586048	0,683981442	2,108175733
Energy	14698122	12034584	1999394	8623395
Energy (GLSZM)	1100198088	13112363448	2253394362	1572087682
Energy (GLDM)	1382503586	14666415312	2231219564	1538124200
Energy (GLCM)	1100198088	13112363448	2253394362	1572087682
Entropy (GLSZM)	0,942163169	0,997180399	0,942163169	0,982316608
Entropy (GLDM)	0,982316608	0,91299914	0,69621226	0,974489403
Entropy (GLCM)	-480492,8311	-488494,4506	-525899,9661	-496947,9784
Fractal Dimension	-6,024734285	-1,573256405	-4,869540836	-2,188663305
Ferets Diameter	230,6306174	9,235646075	73,76370436	7,786621547
Flatness	0,181683362	0,509652515	0,233301337	0,369870289
Gray Level Variance	0,02942702	0,093522993	0,03882701	0,03382701
Homogeneity	48336,96667	48136,99881	49530,15952	48069,33333
Homogeneity(GLCM)	0,967668295	0,963665095	0,991555083	0,962310485
Interquartile Range	0,31372549	0,623529412	0	0,015686275
Intensity Range	0,615686275	0,890196078	0,7522941176	0,666666667
Kurtosis	4,167487755	2,685599473	24,66059214	4,145764968
Long Run Low Gray Level Emphasis	0,000160154	4,00384E-05	0,000100096	0,000200192
Long Run High Gray Level Emphasis	0,014353637	0,012943283	0,00275903	0,01218055
Long Run High Gray Level Emphasis (GLRLM)	228186709,3	192975402,7	38874154,67	161514154,7
Mean	34,4918952	52,81151015	6,621797938	25,39720849
Mean Intensity	0,130226544	1,99875732	0,026650269	0,101457458
Minimum Intensity	0	0	0	0
Maximum Intensity	0,615676285	0,890196078	0,752941176	0,666666667
Maximum Probability	0,718429693	0,746296445	0,944847053	0,769058296
Perimeter	749,801	38,38204167	210,553	29,27004545
Roundness	1,7734709	2,61926772	2,25861389	2,709837193

Standard Deviation	54,26791328	83,75739637	30,04619567	50,4556835
Skewness	1,543997433	1,150603034	4,714228776	1,681684636
Surface Area	63564	53572	10419	45907
Sphericity	0,414801369	3,80586048	0,683981442	2,108185733
Short Run Low Gray Level Emphasis	0,912776909	0,921067868	0,983161692	0,926609092
Short Run High Gray Level Emphasis	0,099675689	0,090226618	0,01919843	0,83900545
Short Run High Gray Level Emphasis (GLRLM)	2,45228814	2,261581224	0,581294679	4,193590881
Solidity	0,916703786	0,956081747	0,928076923	0,945224398
Total Energy	2327,433126	6697,062822	732,5006536	2464,637693
Volume	63564	53572	10519	45907

The values obtained as a result of the features applied to the images are too wide apart for some features. This increases the margin of error in machine learning. To prevent this, the maximum and minimum values of the values for each feature were found and normalized between 0 and 1. When it was later tested with the selected classification methods, it was observed that the accuracy rate of the classification increased by approximately 3 percent. For this reason, normalized data was used throughout the study.

D. FEATURE SELECTION

Feature selection is utilized to increase model performance and generalization ability by identifying and selecting the most important and relevant features in the machine learning process. This is done through eliminating unnecessary or low-information feature extraction methods from the model. The aim here is to increase model performance, prevent overfitting, facilitate interpretability, and increase accuracy. Weka was used in the feature selection part.

Various feature selection algorithms have been used to select a subset of features for the purposes. Weka offers a wide range of classifiers and feature selectors that can be combined in various ways to automatically detect the relationship between extracted features and the target class (benign or malignant). The best configuration that maximized classification accuracy was found by experimenting with different combinations of classifiers and feature selection methods. According to the applied methods, 12 feature extraction methods that worked best for 6 different feature selection methods were selected. 8 different classification methods were applied for each dozen feature extraction methods. Selected feature selection methods are, Info Gain, Correlation, Gain Ratio, OneR, ReliefF, and Symmetrical Uncert. And the selected classification methods are, Bagging, J48, LMT, Random Forest, Iterative Classifier, Attribute Selected, Classification Via Regression, and Logistic.

E. VALIDATION

In each feature selection method, experiments were carried out by selecting the first 12 features listed according to the discrimination success percentage. Different models appear in the tables below. Calculations were made by selecting 10 folds using the Cross Validation technique.

RESULTS

1. Information Gain (Info Gain): Information gain measures the reduction in entropy resulting from the transformation of a data set. On the dependent variable, it is used to determine how much information is lost from independent variables.

TABLE III
RESULTS FOR INFO GAIN

Classifier	Accuracy	Precision	Recall
Bagging	0.7317	0.731	0.732
J48	0.6959	0.697	0.696
LMT	0.728	0.727	0.728
Random Forest	0.7274	0.727	0.727
Iterative Classifier	0.6922	0.694	0.692
Attribute Selected	0.6828	0.685	0.683
Classification Via Regression	0.7265	0.727	0.727
Logistic	0.7241	0.731	0.724

2. Correlation: Correlation measures the statistical relationship between two variables. It evaluates how successful a feature is related to the target variable in the context of feature selection. Pearson correlation coefficient is often used for this purpose.

TABLE IV
RESULTS FOR CORRELATION

Classifier	Accuracy	Precision	Recall
Bagging	0.7411	0.741	0.741
J48	0.7083	0.710	0.708
LMT	0.7432	0.745	0.743
Random Forest	0.7584	0.758	0.758
Iterative Classifier	0.6977	0.698	0.698
Attribute Selected	0.6877	0.693	0.688
Classification Via Regression	0.7432	0.745	0.743
Logistic	0.7271	0.733	0.727

3. Gain Ratio: It is a normalized version of Info Gain. Accounting for the natural knowledge of a feature results in adjustment that combats information gain towards those features that possess more levels.

TABLE V
RESULTS FOR GAIN RATIO

Classifier	Accuracy	Precision	Recall
Bagging	0.7614	0.762	0.761
J48	0.7426	0.746	0.743
LMT	0.7641	0.766	0.764
Random Forest	0.7675	0.768	0.768
Iterative Classifier	0.7474	0.751	0.747
Attribute Selected	0.7329	0.745	0.733
Classification Via Regression	0.7569	0.759	0.757
Logistic	0.7192	0.722	0.719

4. One Rule (OneR): This method creates a rule for each feature and selects the feature with the lowest error rate, which is rule-based method.

TABLE VI
RESULTS FOR ONE RULE

Classifier	Accuracy	Precision	Recall
Bagging	0.7402	0.740	0.740
J48	0.6995	0.700	0.700
LMT	0.7405	0.740	0.741
Random Forest	0.7423	0.742	0.742
Iterative Classifier	0.7089	0.709	0.709
Attribute Selected	0.6858	0.686	0.686
Classification Via Regression	0.7350	0.734	0.735
Logistic	0.7162	0.723	0.716

5. ReliefF: It is an iterative feature selection algorithm that evaluates the importance of attributes according to the extent to which they differentiate samples close to each other. It considers nearest neighbors that have the same class and those that have different classes.

TABLE VII
RESULTS FOR RELIEF

Classifier	Accuracy	Precision	Recall
Bagging	0.7781	0.778	0.778
J48	0.7643	0.764	0.762
LMT	0.7918	0.792	0.792
Random Forest	0.7881	0.788	0.788
Iterative Classifier	0.7635	0.763	0.764
Attribute Selected	0.7556	0.761	0.756
Classification Via Regression	0.7918	0.793	0.792
Logistic	0.7760	0.776	0.776

6. Symmetrical Uncert: It is a combination of Information Gain and Gain Rate. It is based on information theory. It is measuring the symmetric relationship between mutual knowledge and knowledge gain.

TABLE VIII
RESULTS FOR SYMMETRICAL UNCERT

Classifier	Accuracy	Precision	Recall
Bagging	0.7341	0.734	0.734
J48	0.7110	0.714	0.711
LMT	0.7274	0.727	0.727
Random Forest	0.7393	0.739	0.739
Iterative Classifier	0.6937	0.695	0.694
Attribute Selected	0.4946	0.694	0.695
Classification Via Regression	0.7220	0.721	0.722
Logistic	0.7165	0.723	0.717

Calculations were made by selecting 10 folds with different feature selection and classification techniques and cross validation techniques. To achieve higher accuracy, feature numbers were reduced by 2 and accuracy percentages were tabulated with the help of MATLAB.

The two most successful models in this research are ReliefF-LMT (Logistic Model Trees) and ReliefF-Classification Via Regression models. ReliefF-LMT achieved an accuracy rate of 79.39%, and ReliefF-Classification Via Regression achieved an accuracy rate of 79.27%.

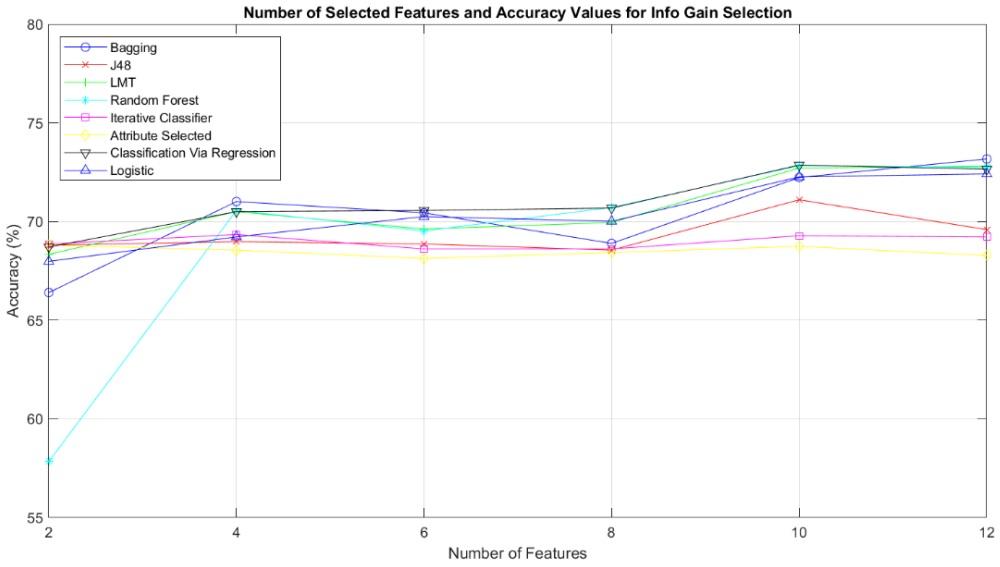

Fig. 14. Info Gain Selection Accuracies

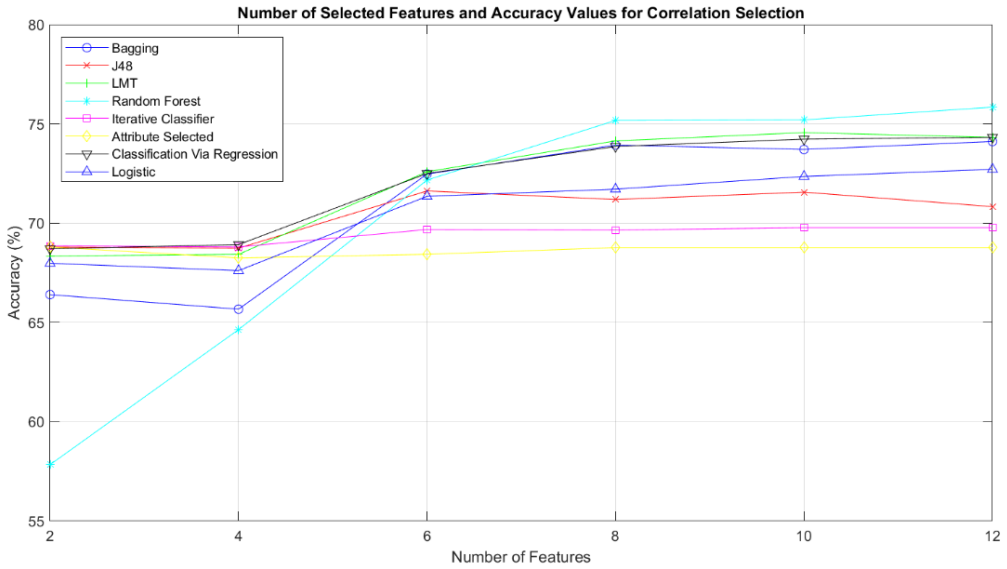

Fig. 15. Correlation Selection Accuracies

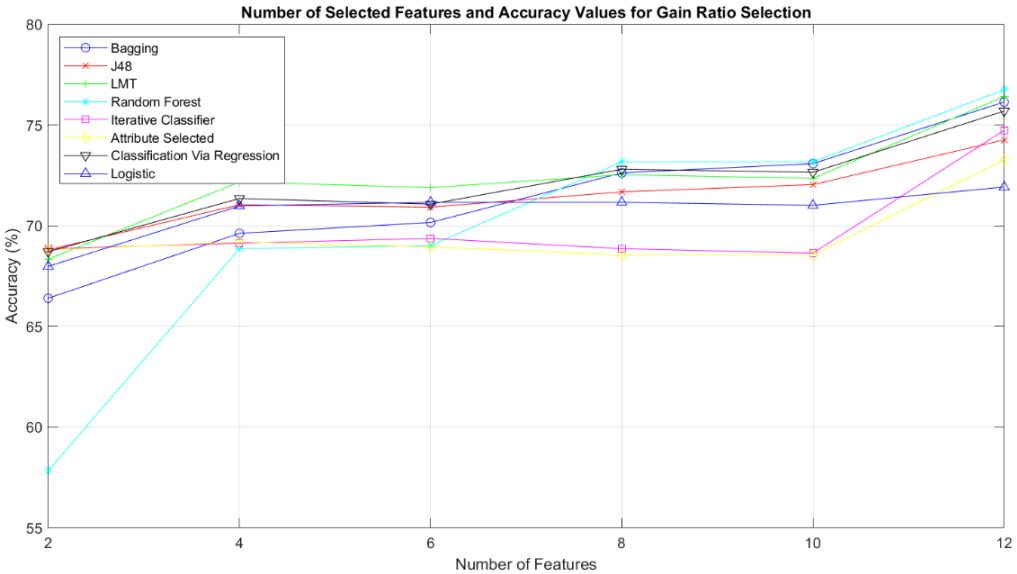

Fig. 16. Gain Ratio Selection Accuracies

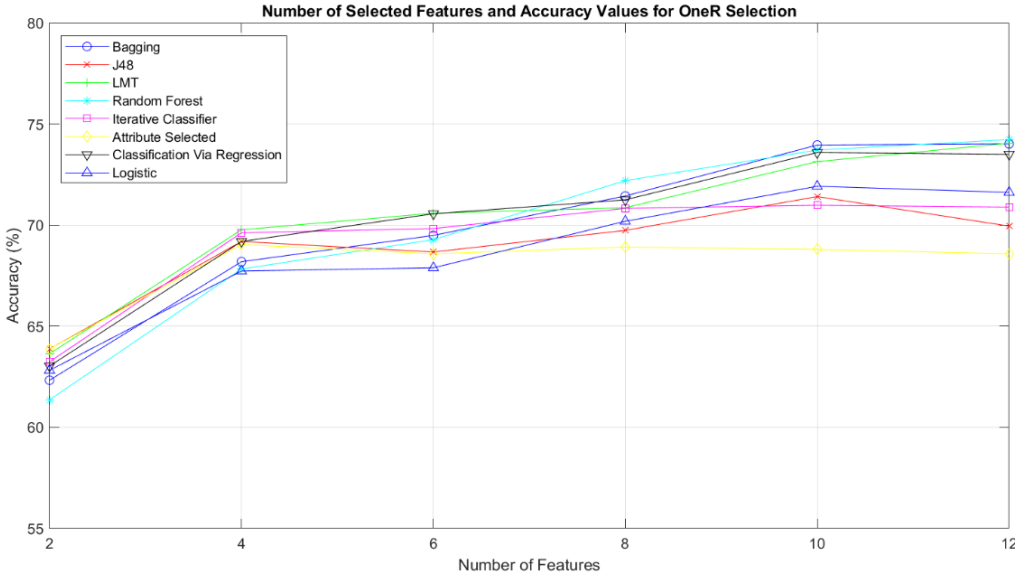

Fig. 17. OneR Selection Accuracies

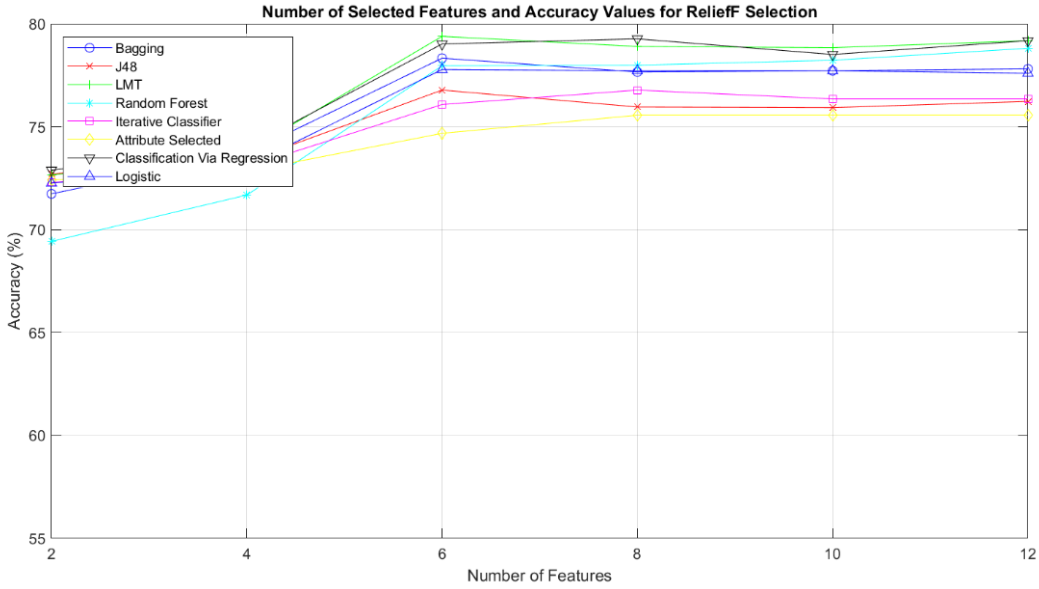

Fig. 18. ReliefF Selection Accuracies

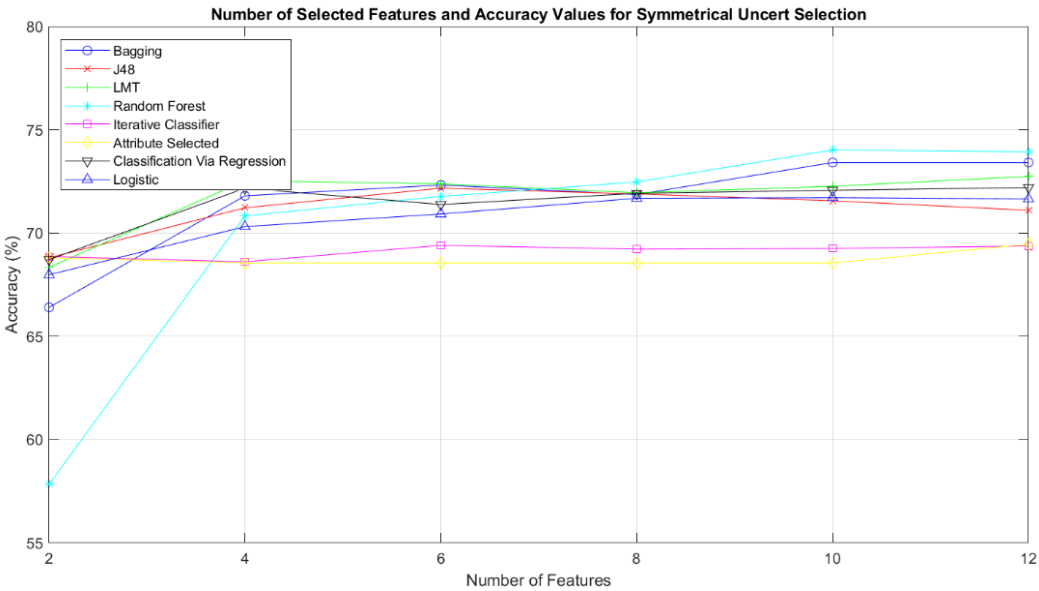

Fig. 19. Symmetrical Uncert Selection Accuracies

It has been observed that the accuracy rate also changes as the number of features changes. Mostly, the accuracy rate increases as the number of features increases, but this is not the case for every classification technique. A sudden increase in accuracy was seen when the feature number was increased to 4 and 6. In later increases, this sudden increase decreased and a low-slope increase was observed.

When the model put forward in this research is compared with existing machine learning models, it is seen that the research is successful. When the average accuracy, precision, and recall results of the created models were compared, we observed that the highest percentage for all criteria was in the ReliefF feature selection method.

TABLE IX
FEATURE SELECTION METHOD'S AVERAGE RESULTS

Feature Selecting Method	Accuracy	Precision	Recall
Info Gain	0.7136	0.7149	0.7136
Correlation	0.7258	0.7279	0.7258
Gain Ratio	0.7490	0.7524	0.7490
OneR	0 7210	0.7218	0.7211
ReliefF	0.7762	0.7769	0.7760
Symmetrical Uncert	0.6923	0.7184	0.7174

III. DISCUSSION AND CONCLUSION

Compared to other research results, the accuracy rate achieved result of the study is reasonable. Although it has lower accuracy compared to traditional methods, it is faster and more cost-effective. The accuracy rate obtained can be further increased with improved methods, and better results can be obtained with advanced image processing techniques. In addition, improving the data set is among the studies aimed at improving and increasing model performance. No matter how promising the study is, the risks of this method should be taken into consideration. It is necessary to be cautious against misdiagnosis of the disease and harm to the patient. Since at this point, results as accurate as pathology cannot be obtained, it may be possible to increase its reliability or combine it with this method in the future. Studies in the field of skin cancer diagnosis and classification are ongoing, and efforts are being made to make it accessible to healthcare personnel and presented to the user. These studies are important and critical for doctors, healthcare professionals and patients.

REFERENCES

[1] A. O. Salau and S. Jain "Feature Extraction: A Survey of the Types, Techniques, Applications", IEEE Xplore, March 2019.

[2] B. Arivuselvam , S. Tanisha , S. Shalini , and V.S. Subhalaksmi, "Skin Cancer Detection And Classification Using Svm Classifier", Turkish Journal of Computer and Mathematics Education, Vol.12 No.13 (2021), 1863-1871

[3] E. Kanca, S. Ayas, "Learning Hand-Crafted Features for K-NN based Skin Disease Classification" IEEE Xplore, Ankara, Turkey, 9–11 June 2022;pp. 1–4.

[4] F. Al-Areqi and M. Z. Konyar, "Effectiveness Evaluation of Different Feature Extraction Methods for Classification of Covid-19 from Computed Tomography Images: A High Accuracy Classification Study", ResearchGate, March 2022.

[5] G. Arora, A. Kumar Dubey, Z. A. Jaffery, and A. Rocha, "Bag of feature and support vector machine based early diagnosis of skin cancer", Neural Computing and Applications (2022), 34:8385–8392.

[6] G. Kumar and P. Kumar Bhatia, "A Detailed Review of Feature Extraction in Image Processing Systems", IEEE Xplore, April 2014, doi: 10.1109/ACCT.2014.74.

[7] J. S. Marques, C. Barata, and T. Mendonca, "On the Role of Texture and Color in the Classification of Dermoscopy Images", 34th Annual International Conference of the IEEE EMBS San Diego, California USA, 28 August-1 Sepetember 2012.

[8] Kaggle, "Skin Cancer: Malignant vs. Benign," Kaggle, [Online]. Available: https://www.kaggle.com/datasets/fanconic/skin-cancer-malignant-vs-benign/code?datasetId=174469&searchQuery=+Feature+Extraction

[9] R. Maurya, S. K. Singh, A. K. Maurya, and A. Kumar, "GLCM and Multi Class Support vector machine based automated skin cancer classification", IEEE Xplore, March 2014.

[10] S.A. Medjahed, "A Comparative Study of Feature Extraction Methods in Images Classification," in International Journal of Image, Graphics and Signal Processing, vol. 7, pp. 16-23, 2015.

The Effect on Model Performance of Increasing the Batch Size during Training

İsmail Akgül[*,1]

[*] iakgul@erzincan.edu.tr, ORCID: 0000-0003-2689-8675
[1] *Departmant of Computer Engineering, Faculty of Engineering and Architecture, Erzincan Binali Yıldırım University, Erzincan, Türkiye*

Abstract: Many hyperparameters are used for classification in convolutional neural networks (CNNs). Optimum tuning of hyperparameters plays an important role in the classification success of CNN. One of the important hyperparameters used in CNNs is batch size (BS). Changing the BS, just like changing other hyperparameters during training, is a research topic. However, changing the BS during training has been less investigated than other hyperparameters. In this study, the effect on the performance of CNNs of increasing the BS during training was examined. For this purpose, the test loss value was checked with early stopping during training, and BS was increased if the loss value increased by the determined number of steps. To examine the effect of increasing the BS, training was performed on the MNIST dataset using pre-trained MobileNet and MobileNetV2 models. The results showed that increasing the BS during training provided slightly higher accuracy and lower loss compared to using a constant BS.

Keywords: *Convolutional Neural Network, Early Stopping, Increasing Batch Size, Classification*

I. INTRODUCTION

Many hyperparameters are needed when training CNNs. One of these hyperparameters is BS. BS determines the number of simultaneously processed samples before updating the base model parameters during training [1,2]. BS, which is an important hyperparameter in training deep learning models [3], is widely used in neural network training [4]. BS is a hyperparameter defined as the number of images used to train a single forward and backward pass. For CNNs to perform more robust classification, BS, like many hyperparameters, must be tuned appropriately [5].

The BS value, one of the most effective hyperparameters when training a neural network, can lead to various training and testing successes [6]. However, the selection of appropriate BS is a fundamental problem faced by researchers [7]. It is still not completely clear how to tune hyperparameters such as learning rate and BS to achieve a more robust classification [8]. Additionally, theories that quantitatively explain how large or how small the BS should be are lacking [4]. Successful classification is affected by the interaction of learning rate and BS [9]. Considering the significant interaction between learning rates and BS, adaptive BS strategies are needed [10].

BS can only fit in the remaining memory after the model is loaded and depending on the data size. BS becomes smaller as model and data size increases [11]. The selection of BS often has a significant effect on training results. Choosing the BS too small may result in a long training time and choosing it too large may cause it to get closer to the local optimal value [12]. Although BS increases the resource requirement, it has a decisive effect on image recognition

accuracy in CNNs and many other networks.

There are some studies in the literature that examine the BS effect. Smith et al. (2017) found that the same learning curve would generally be obtained in the training and test datasets as a result of increasing the BS by 5 times at each step during training [13]. Kandel et al. (2020) carried out studies on the VGG16 model using different BSs without making any changes during training. They observed that using higher BS generally does not result in higher accuracy [5].

In the study by Radiuk (2017), the effect of BS on performance was examined on MNIST and CIFAR-10 datasets using various CNN architectures. It has been observed that a higher BS value increases the recognition accuracy [14]. Lin (2022) tried to find the most appropriate BS range by training some CNNs using Mnist, Fashion Mnist, and CIFAR-10 datasets. As a result of the study, it was concluded that the probability of training a CNN model is high when the BS is selected between 16 and 32 [6].

Gao et al. (2022) proposed an adaptive BS strategy to solve stochastic optimization problems. Instead of giving the mini-BS and the step-size values constant, they developed a two-scale adaptive (TSA) method that adaptively increases the BS when an appropriate error criterion is encountered. As a result of their classification experiments using MNIST and CIFAR-10 datasets, they showed that adaptive tuning of mini-BS is useful in practice [15]. Choudhury and Soni (2023) proposed an adaptive BS-based CNN-LSTM model from 128 to 1024 to recognize different human activities in an uncontrolled environment. They achieved good performance in their proposed model by using the human activity recognition (HAR) dataset they created [16].

In this study, the effect on model performance of increasing the BS during training in CNNs was examined. For this purpose, a series of experiments were carried out on the MNIST dataset using MobileNet and MobileNetV2 models. By comparing the BS results that were left constant throughout the model training with the BS results that were increased during training, the effect on the model performance of increasing the BS during training was examined.

II. MATERIALS AND METHODS

A. Dataset and Preprocessing

In this study, the Modified National Institute of Standards and Technology (MNIST) dataset was used to examine the effect on the model performance of increasing the BS during training. Each of the 70000 images in this dataset consisting of 10 classes is 28x28x1 in size [17]. To use it in this study, the image dimensions were resized to 32x32x3 pixels.

B. MobileNet and MobileNetV2 Models

MobileNets are based on a streamlined architecture that uses depth-wise separable convolutions to create lightweight deep neural networks that offer a wide range of applications such as object detection, fine-grain classification, face attributes, and large-scale geo-localization [18]. In this study, the effect on the performance of increasing the BS during training was examined using MobileNet and MobileNetV2 models.

C. Training Parameters and Metrics

In the experiments carried out on the MNIST dataset using MobileNet models, the Adamax optimization algorithm was used with default parameters. The loss function is implemented as Categorical Crossentropy and the classification activation function is implemented as Softmax. During the training, the minimum level of the test loss value was checked with the early stopping feature, with patience=2. Both the BS value was kept constant throughout the training at 32, 64, and 128, and the BS value was increased at these values during the training. To

determine the classification success of the models, accuracy and loss metrics were examined.

D. Increasing BS

The training was started with pre-trained weights of MobileNet and MobileNetV2 models. The training was carried out by updating the weights in all layers without partial layer freezing. The BS value was initially set to 32. During the training, if the test loss value, which was checked with the early stopping feature, did not decrease twice in a row, the BS value was increased to 64 and the training was continued. Likewise, the decrease in the test loss value was checked, and if the loss value did not decrease during 2 repetitions, the BS value was increased to 128 and the training was continued. After that, the training was terminated by looking at the test loss value in the same way. The training was completed by changing the BS value to 32, 64, and 128 during the training.

III. RESULT AND DISCUSSION

To examine the effect on model performance of increasing the BS during training, a series of experiments were conducted on the MNIST dataset using the MobileNet and MobileNetV2 models discussed in the study. Experiments were carried out by first keeping the BS values constant as 32, 64, and 128 throughout the training, and then increasing them during training. The experiments were repeated 3 times for each case, and the classification accuracy of the models on the MNIST test dataset is given in Table 1.

TABLE I
TEST SUCCESS ACCURACY

Model	Batch Size (BS)	Experiment 1 (%)	Experiment 2 (%)	Experiment 3 (%)	Average (%)
MobileNet	32	*99.23*	99.23	99.10	99.19
	64	*99.35*	99.29	99.14	99.26
	128	99.07	98.93	*99.15*	99.05
	Increasing BS	99.40	99.39	*99.49*	**99.43**
MobileNetV2	32	99.18	99.17	*99.28*	99.21
	64	*99.15*	99.08	99.13	99.12
	128	98.74	*98.77*	98.59	98.70
	Increasing BS	99.33	*99.37*	99.30	**99.33**

When the test success accuracies given in Table 1 are examined, it is seen that the highest success accuracy is achieved with increased BS in both MobileNet and MobileNetV2 models. In the MobileNet model, the average success rates were found to be 99.43% for increased BS, 99.26% for BS=64, 99.19% for BS=32, and 99.05% for BS=128, respectively, from largest to smallest. In the MobileNetV2 model, the increased BS=99.33%, BS(32)=99.21%, BS(64)=99.12% and BS(128)=98.70%. In both models, the increased BS provided a performance increase of only approximately 0.1%-0.2%.

According to the test success accuracies presented in Table 1, the best-performing experiments in the MobileNet model were Experiment 1 for BS(32) and BS(64), Experiment 3 for BS(128), and increasing BS. The model train-test accuracy graphs of these best-performing experiments in the MobileNet model are given in Fig. 1, and the train-test loss graphs are given in Fig. 2.

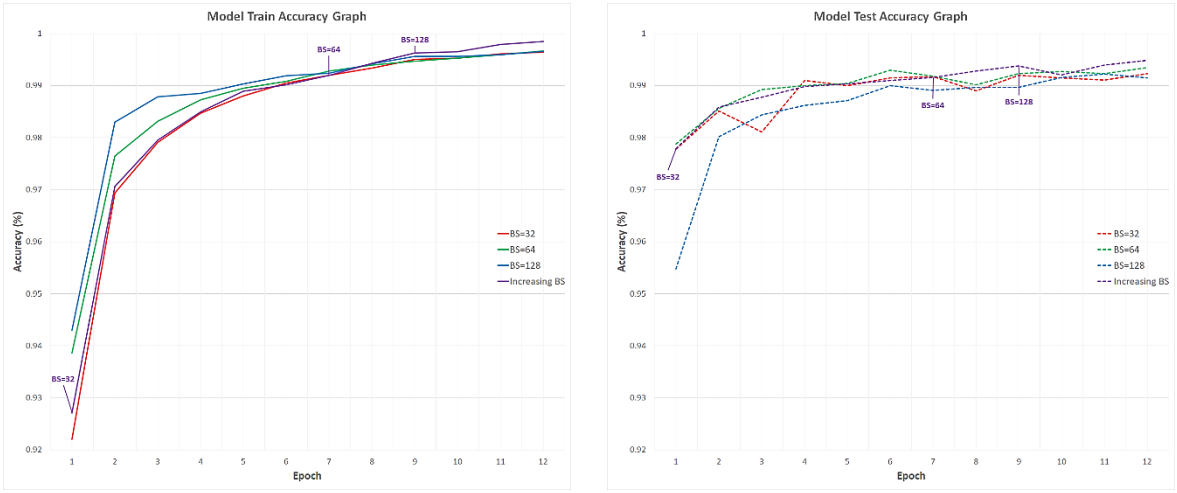

(a) Train set (b) Test set

Fig. 1. Train-test accuracy graphs of the MobileNet model (a) Train set, (b) Test set.

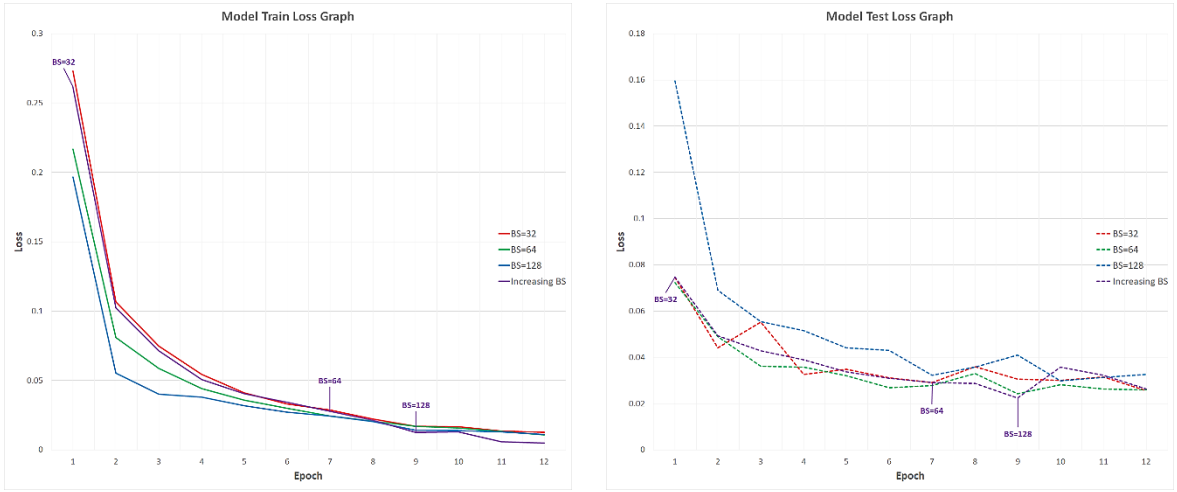

(a) Train set (b) Test set

Fig. 2. Train-test loss graphs of the MobileNet model (a) Train set, (b) Test set.

In Fig. 1 and Fig. 2, the training and test results of the 32, 64, and 128 BS values that were left constant throughout the training of the MobileNet model and the increasing BS value are seen together. As can be seen in the figure, training started with 32 BS in the increasing BS application. Since the test loss value increased twice in a row after the 7th epoch, the BS value was increased to 64 in this epoch and the training was continued from the 7th epoch. Again, after the 9th epoch, when the test loss value increased twice in a row, the BS value was set to 128 and the training was continued from the 9th epoch. As seen in Fig. 1 and Fig. 2, in the training carried out with the MobileNet model, it was determined that the application of increasing BS had a positive effect on the model performance, albeit slightly.

In addition, according to the test success accuracies presented in Table 1, the best-performing experiments in the MobileNetV2 model were Experiment 3 for BS(32), Experiment 1 for BS(64), Experiment 2 for BS(128), and increasing BS. The model train-test accuracy graphs of these best-performing experiments in the MobileNetV2 model are given in Fig. 3, and the train-test loss graphs are given in Fig. 4.

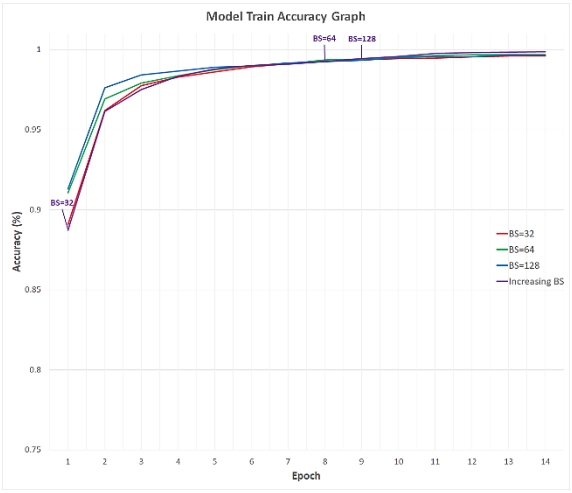

(a) Train set

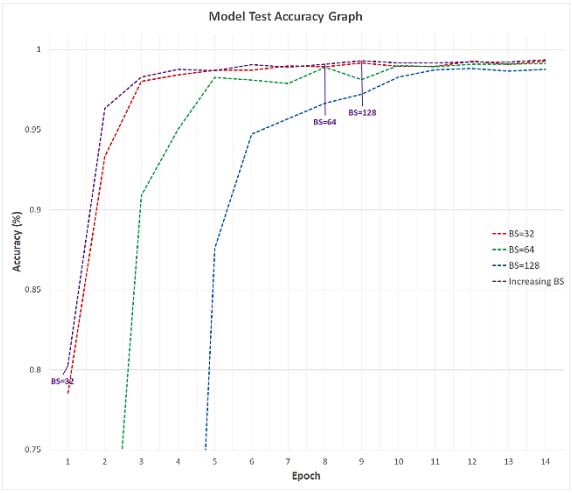

(b) Test set

Fig. 3. Train-test accuracy graphs of the MobileNetV2 model (a) Train set, (b) Test set.

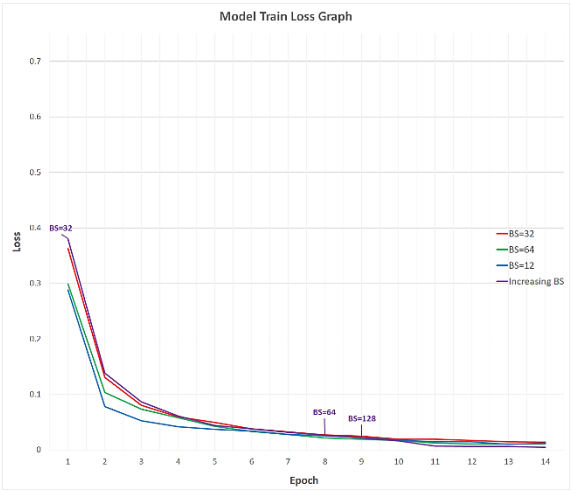

(a) Train set

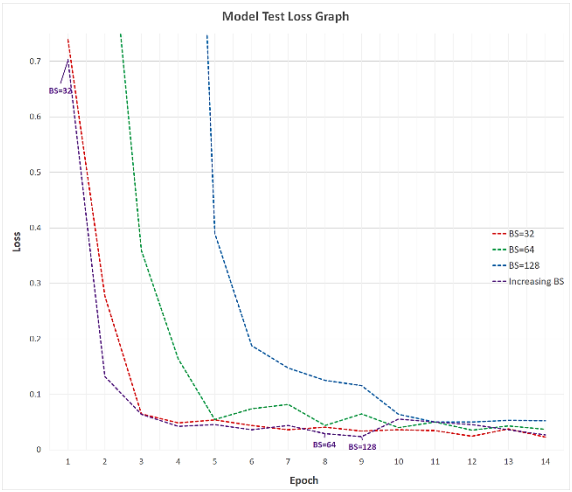

(b) Test set

Fig. 4. Train-test loss graphs of the MobileNetV2 model (a) Train set, (b) Test set.

In Fig. 3 and Fig. 4, the training and test results of the 32, 64, and 128 BS values that were left constant throughout the training of the MobileNetV2 model and the increasing BS value are seen together. As can be seen in the figure, training started with 32 BS in the increasing BS application. Since the test loss value increased twice in a row after the 8th epoch, the BS value was increased to 64 in this epoch, and after the 9th epoch, when the test loss value increased twice in a row, the BS value was increased to 128 and the training was continued. As seen in Fig. 3 and Fig. 4, in the training carried out with the MobileNetV2 model, it was determined that the application of increasing BS had a positive effect on the model performance, albeit slightly.

IV. CONCLUSION

In this study, training was carried out with the MNIST dataset using MobileNet and MobileNetV2 versions to examine the effect on model performance of increasing the BS during training. Training started with a BS value of 32, and the test loss value was checked during training, if this value increased twice in a row, the BS value was increased twice, first to 64 and then to 128. To compare the effect on the model performance of increasing the BS, training was also carried out with fixed 32, 64, and 128 BS values throughout the training.

As a result of a series of experiments, it was concluded that increasing the BS during training

performed slightly better than giving a constant BS value throughout the training. Since the models considered in the study showed a success of 99% (close to 100%) at BS values that were kept constant throughout the training, the performance increase obtained by increasing BS was approximately 0.1%-0.2%. Although this performance increase is very small, it is worth examining the effect of increasing BS in different datasets, different models, and different BS values in future studies.

ACKNOWLEDGMENT

This work was supported by Research Fund of the Erzincan Binali Yıldırım University. Project Number: FHD-2024-1007.

REFERENCES

[1] B. Panda, and P. Singh, "A deep convolutional-LSTM neural network for signal detection of downlink NOMA system," AEU-International Journal of Electronics and Communications, 170, 154797, 2023.

[2] R. Amamath, and V.V. Kumar, "Pruning Distorted Images in MNIST Handwritten Digits," arXiv preprint arXiv:2307.14343, 2023.

[3] C.I. Kerley, L.Y. Cai, Y. Tang, L.L. Beason-Held, S.M. Resnick, L.E. Cutting, and B.A. Landman, "Batch size go big or go home: counterintuitive improvement in medical autoencoders with smaller batch size," In Medical Imaging 2023: Image Processing, vol. 12464, pp. 106-115, SPIE, 2023.

[4] R. Marino, and F. Ricci-Tersenghi, "Phase transitions in the mini-batch size for sparse and dense neural networks," arXiv preprint arXiv:2305.06435, 2023.

[5] I. Kandel, and M. Castelli, "The effect of batch size on the generalizability of the convolutional neural networks on a histopathology dataset," ICT express, 6(4), 312-315, 2020.

[6] R. Lin, "Analysis on the selection of the appropriate batch size in CNN neural network," In 2022 International Conference on Machine Learning and Knowledge Engineering (MLKE), pp. 106-109, IEEE, 2022.

[7] B. Schmeiser, "Batch size effects in the analysis of simulation output," Operations Research, 30(3), 556-568, 1982.

[8] F. He, T. Liu, and D. Tao, "Control batch size and learning rate to generalize well: Theoretical and empirical evidence," Advances in neural information processing systems, 32, 2019.

[9] I.A. Usmani, M.T. Qadri, R. Zia, F.S. Alrayes, O. Saidani, and K. Dashtipour, "Interactive effect of learning rate and batch size to implement transfer learning for brain tumor classification," Electronics, 12(4), 964, 2023.

[10] T.T.K. Lau, H. Liu, and M. Kolar, "AdAdaGrad: Adaptive Batch Size Schemes for Adaptive Gradient Methods," arXiv preprint arXiv:2402.11215, 2024.

[11] X. Piao, D. Synn, J. Park, and J.K. Kim, "Enabling Large Batch Size Training for DNN Models Beyond the Memory Limit While Maintaining Performance," IEEE Access, 11, 102981-102990, 2023.

[12] H. Shao, E. Ma, M. Zhu, X. Deng, and S. Zhai, "MNIST Handwritten Digit Classification Based on Convolutional Neural Network with Hyperparameter Optimization," Intelligent Automation & Soft Computing, 36(3), 3595-3606, 2023.

[13] S.L. Smith, P.J. Kindermans, C. Ying, and Q.V. Le, "Don't decay the learning rate, increase the batch size," arXiv preprint arXiv:1711.00489, 2017.

[14] P.M. Radiuk, "Impact of training set batch size on the performance of convolutional neural networks for diverse datasets," Information Technology and Management Science, 20(1), 20-24, 2017.

[15] Z. Gao, A. Koppel, and A. Ribeiro, "Balancing rates and variance via adaptive batch-size for stochastic optimization problems," IEEE Transactions on Signal Processing, 70, 3693-3708, 2022.

[16] N.A. Choudhury, and B. Soni, "An adaptive batch size-based-CNN-LSTM framework for human activity recognition in uncontrolled environment," IEEE Transactions on Industrial Informatics, 19(10), 10379-10387, 2023.

[17] Y. LeCun, L. Bottou, Y. Bengio, and P. Haffner, "Gradient-based learning applied to document recognition," Proceedings of the IEEE, 86(11), 2278-2324, 1998.

[18] A.G. Howard, M. Zhu, B. Chen, D. Kalenichenko, W. Wang, T. Weyand, ... and H. Adam, "Mobilenets: Efficient convolutional neural networks for mobile vision applications," arXiv preprint arXiv:1704.04861, 2017.

Design and Optimization of Renewable Energy-Based Electric Vehicle Charging Stations: A Case Study in Yalova

Aykut Fatih Güven[*,1]

[*]afatih.guven@yalova.edu.tr, ORCID: 0000-0002-1071-9700
[1]*Department of Electrical and Electronics Engineering, Yalova University, Yalova, Turkey*

Abstract: Energy consumption in the transportation sector has become a significant issue involving the sustainable use of global energy resources. Environmental concerns related to fossil fuel consumption and the need for energy efficiency have made the transition from traditional internal combustion engine vehicles to electric vehicles (EVs) imperative. Along with the widespread adoption of EVs, improving charging infrastructure and supporting this infrastructure with environmentally friendly energy sources have become crucial.
In this study, a renewable energy-based charging station design and optimization for EVs at a shopping center in Yalova was conducted. Simulation models were created using HOMER Grid software, and four different scenarios with different components were developed. Among these scenarios, scenario 4 was chosen as the optimal solution in terms of energy efficiency and cost-effectiveness. In this scenario, the net present cost of the charging station was $1.18 million, with an initial cost of $1.05 million, and the renewable energy usage rate reached 97%. The results demonstrate that renewable energy-based charging stations offer significant environmental and economic benefits.

Keywords: *Renewable Energy, Electric Vehicle Charging Stations, Energy Optimization, HOMER Grid Simulation, Sustainable Transportation*

I. INTRODUCTION

Energy is a fundamental element of economic growth, sustainability, and social welfare in modern societies [1]. As global energy demand rapidly increases and fossil fuel resources become increasingly limited, energy management and efficient utilization have become more critical than ever [2]. Carbon emissions and climate change caused by fossil fuels have made the transition to renewable energy sources (RES) a global necessity [3]. In this context, the use of renewable energy sources and energy-efficient systems plays a crucial role in ensuring future energy security and promoting environmental sustainability.

The transportation sector is a major contributor to global energy consumption, and the environmental impacts of fossil fuel-powered vehicles pose significant challenges [4]. Electric vehicles (EVs) are emerging as an innovative solution that reduces the dependency on fossil fuels and offers significant opportunities to improve energy efficiency. Research shows that EVs have much higher energy-conversion efficiency than traditional internal combustion engine vehicles and significantly reduce carbon emissions. However, the widespread adoption of EVs also requires the development of charging infrastructure. The proliferation of fast-charging stations is crucial for providing reliable and user-friendly solutions for EV owners while promoting sustainable transportation [5].

Several studies in the literature have focused on developing charging infrastructure for EVs. Rigas et al. developed a charging station design using the EVLibSim library to simulate and

analyze various charging station scenarios, examining factors such as charging capacity, demand, and grid load [6]. Wang et al. proposed an off-grid solar- and hydrogen-based charging station that can provide electricity to electric and hydrogen vehicles. Their design included a water electrolyzer powered by solar systems to generate and store hydrogen with a backup diesel generator. The system's solar capacity was increased from 1612 to 1818 kW, while the diesel generator capacity was raised from 48 to 64 kW [7].

Bicer designed a charging station that utilizes H2 and NH3 fuel cells in combination with concentrated photovoltaics (CPV) and wind turbines, highlighting increased system efficiency, especially in space-constrained areas. The system employs two fuel cells for greater flexibility in electricity generation and storage, with the main energy contribution coming from the fuel cells, which account for about 80% of the system's output [8]. Çobanoğlu et al. analyzed the economic feasibility of grid-connected solar-assisted charging stations in İzmir by using MATLAB/Simulink to simulate various configurations. Their findings indicated that systems without battery storage could amortize their costs in five years, whereas those with battery storage contributed to grid stability by reducing load fluctuations [9]. Li et al. explored the optimization of EV charging infrastructure using renewable energy and battery storage systems by applying Monte Carlo simulations and multi-objective genetic algorithms to minimize total costs and carbon emissions [10].

In Morocco, Allouhi et al. applied HOMER Grid software to design an optimal hybrid renewable energy system (HRES) for supermarkets in three cities. The design integrated solar PVs, wind turbines, and battery storage to achieve a renewable energy fraction of 71.66% in Dakhla, resulting in a COE of $0.0841/kWh and annual operating costs of $0.124M [11]. Similarly, Chisale et al. examined the energy challenges in Malawi, where only 15% of the population had reliable access to electricity. They proposed a hybrid system that combined solar panels, biogas, wind, and battery storage to reduce school grid demand and electricity costs. The system achieved a cost of $0.095/kWh, lower than Malawi's average of $0.11/kWh, with biogas being primarily generated from human waste [12].

In the study by Güven, the integration of HRES into electric vehicle (EV) charging infrastructure is explored. Using solar panels, wind turbines, and battery storage, this research focuses on designing sustainable energy systems for university campuses and nearby electric vehicle stations. This study demonstrates that the system significantly reduces energy costs and carbon emissions while supporting EV charging. Simulations conducted with MATLAB 2022b indicated that the proposed system can meet both the university's energy demands and EV charging needs effectively [13]. Joseph et al. explored renewable energy storage systems in EV charging stations, focusing on the integration of solar panels. They designed a hybrid forward converter to improve the power transfer efficiency under fluctuating energy conditions, achieving a maximum overall efficiency of 95% [14]. Atawi et al. developed a photovoltaic-powered standalone charging station employing a closed-form design equation for the system components. The system was modeled in MATLAB/Simulink, and the experimental results showed that the system exhibits stable charging performance under various solar irradiance levels [15]. Kurtz et al. used HOMER to optimize hydrogen-powered microgrids for data centers and identified scenarios for integrating RESs to achieve carbon-free power solutions [16]. In Bangladesh, Karmaker et al. addressed the rapid rise in EV demand by proposing hybrid solar/biogas EV charging stations to reduce the load on the national grid, with an energy cost of $0.1302/kWh and a total net present cost (NPC) of $56,202 [17]. Singh et al. conducted a study in India using PVsyst software to design a solar-powered EV charging station. The system, equipped with 8.1 kWp of PV capacity and two days of battery autonomy, reduced CO2 emissions by 7,950 kg annually while achieving an optimal performance ratio [18]. Narasipuram et al. provided a comprehensive review of various EV charging station designs, categorizing stations by power levels and examining optimization algorithms for improved design efficiency [19]. Ebrahimi et al. used Monte Carlo methods and queueing theory to address uncertainties in renewable energy supply for EV charging stations, minimize total

costs, and improve grid performance [20]. Güven et al. extended the research into hybrid microgrid systems by optimizing EV charging infrastructure using RESs. Their work emphasized the potential of vehicle-to-grid (V2G) and grid-to-vehicle (G2V) models in reducing grid stress. Using a range of optimization algorithms, including the Coati Optimization Algorithm (COA) and Turbulent Flow of Water-based Optimization (TFWO), their simulations demonstrated a 69.87% reliance on renewable energy [21]. Güven et al. also investigated the use of HRES at Yalova University, finding that a system that utilizes 73% renewable energy could significantly reduce carbon emissions with a 5.7-year payback period [22]. In another study, Güven et al. analyzed the integration of RES into EV charging stations and evaluated seven different scenarios. Scenario 3, which combined photovoltaic systems, batteries, and biodiesel generators, was identified as the most efficient method, reducing CO2 emissions by 29.40% [23]. In addition, their research in Manisa showed that optimized EV charging stations had an annual energy generation capacity of 3,049,337 kWh and lower energy costs than fossil fuels [24]. These findings underscore the importance of renewable energy systems for environmental sustainability and cost-effectiveness.

In summary, these literature reviews highlight the significant potential of renewable energy-based EV charging infrastructure in reducing energy costs, improving energy efficiency, and promoting environmental sustainability.

This study focuses on the design and optimization of a renewable energy-based electric vehicle charging station for a shopping center in Yalova, and examines its cost-effectiveness and environmental sustainability. Shopping centers, due to their high visitor traffic flows, are strategic locations for charging stations, playing a key role in promoting sustainable transportation.

II. MATERIAL AND METHOD

A. Homer Grid Software

HOMER Grid is a software application used for designing and analyzing systems that generate electricity from RES. The proposed model shares the same mathematical foundation as HOMER Pro for calculating energy production but is specifically designed for grid-connected applications and can handle more complex tariff structures. This software is particularly useful for configuring EV charging stations and connecting them to HRES.

HOMER Grid offers users a comprehensive set of tools for analyzing energy demands and sources, balancing energy production and consumption, and optimizing the use of energy storage systems. This allows for the design of the most efficient system by considering multiple RESs (e.g., solar, wind) and energy storage options (e.g., batteries). Through advanced optimization algorithms, HOMER Grid enables users to model various energy scenarios and design systems that minimize costs while maximizing efficiency. It is especially useful for providing strategic decisions regarding the proper sizing and management of EV charging stations, ensuring that energy demands are met while reducing environmental impact.

B. System Design

The proposed renewable energy-based electric vehicle charging station was designed using HOMER Grid software. In this design process, four different scenarios were created using various system components. The schematic diagrams of these scenarios are presented in Figure 3. The main objective of the design was to create a system that operates at the lowest NPC and cost of energy (COE). As shown in Figure 1, the methodological framework comprises three main steps: initial assessment, design optimization, and results analysis.

In the initial stage, the available energy sources and meteorological data (such as solar radiation, wind speed, and ambient temperature) for the study area were thoroughly examined. This examination was conducted to understand the potential of energy sources and to accurately evaluate the system components. Using HOMER Grid, several scenarios were created to determine the optimal system design.

Finally, among the four scenarios, the most cost-effective and environmentally friendly system was selected and analyzed. Figure 2 schematizes the scenarios tested in the program. Based on the evaluation of these scenarios, the system that offered the best balance between cost and environmental sustainability was selected as the optimal solution.

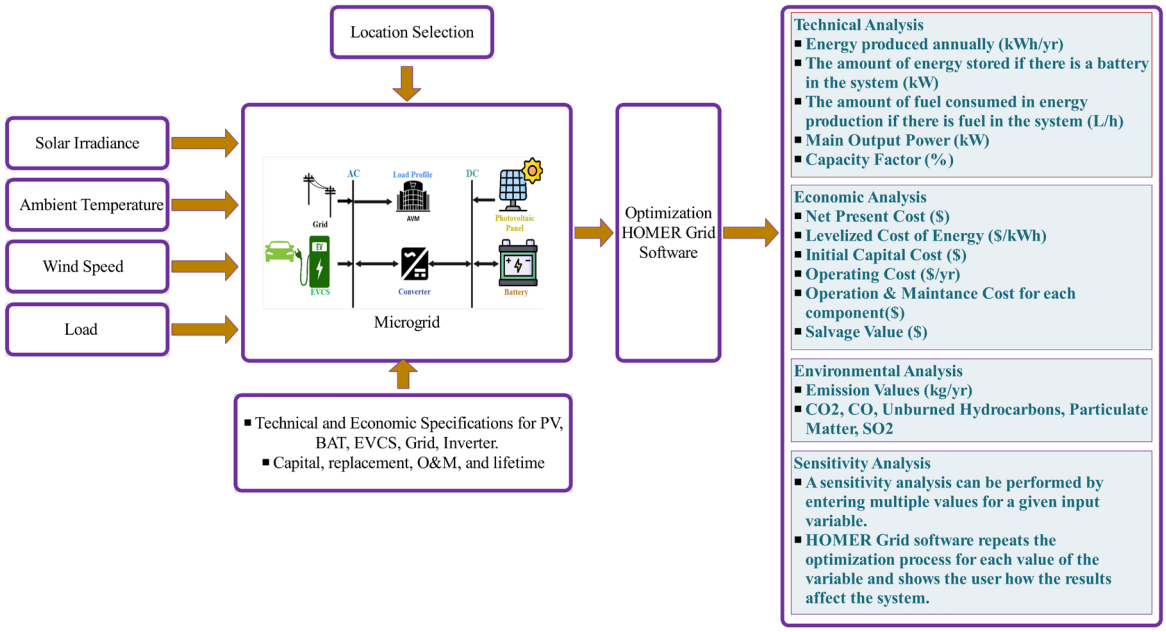

Fig. 1. Schematic representation of study techniques.

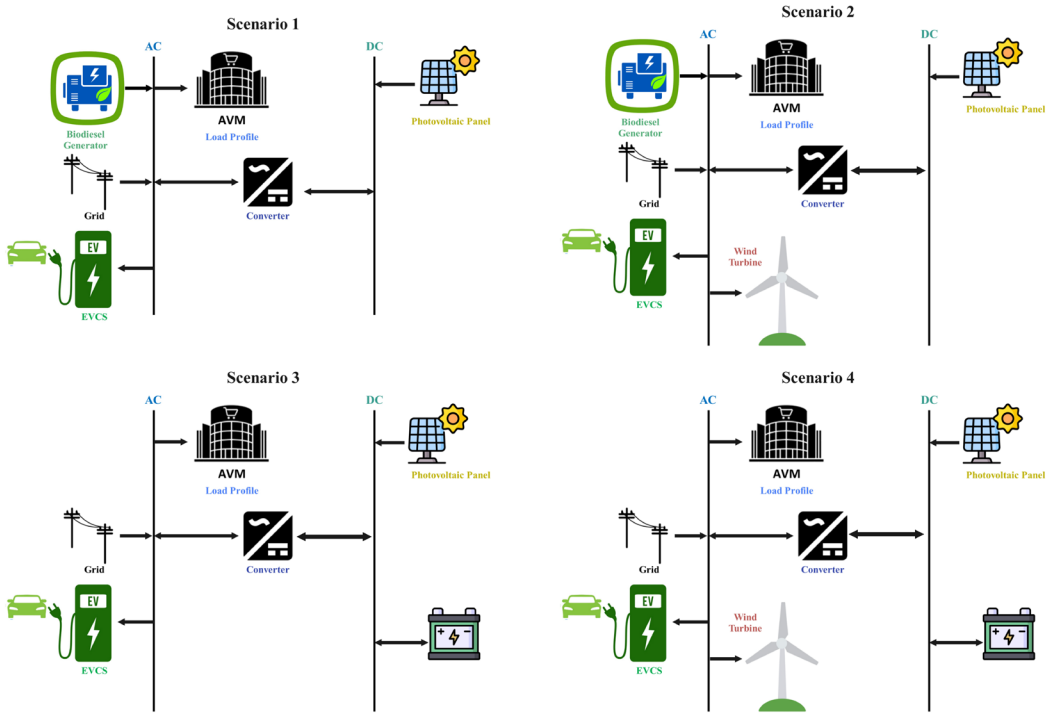

Fig. 2. Schematic diagrams of the four scenarios.

C. Location Selection

The study area is a shopping center located in the central district of Yalova. To meet the energy demand of the charging stations planned for shopping centers, a grid-connected hybrid energy system comprising RES was evaluated. Meteorological data used in this study were provided by the Turkish Meteorological Service. To create a detailed profile of the study area, annual wind speed, solar radiation, ambient temperature, and load data were collected.

Figure 3 presents the hourly solar radiation profile over the course of a year, while Figure 4 shows the monthly wind speed profiles at 10 m above ground level. Figure 5 illustrates the monthly ambient temperature profiles in the form of time series graphs. As shown in Figure 3, the solar energy potential of the study area is higher during summer than during winter. Wind turbines can serve as supplementary energy sources when solar energy is insufficient during the winter months, thus complementing solar power. These two energy sources are the most preferred in hybrid systems.

The annual, daily, and seasonal load demand profiles are also presented in Figure 6. The economic analysis, a nominal discount rate of 25% and an inflation rate of 20% were considered. The project lifespan of the HRES was set to 25 years [25].

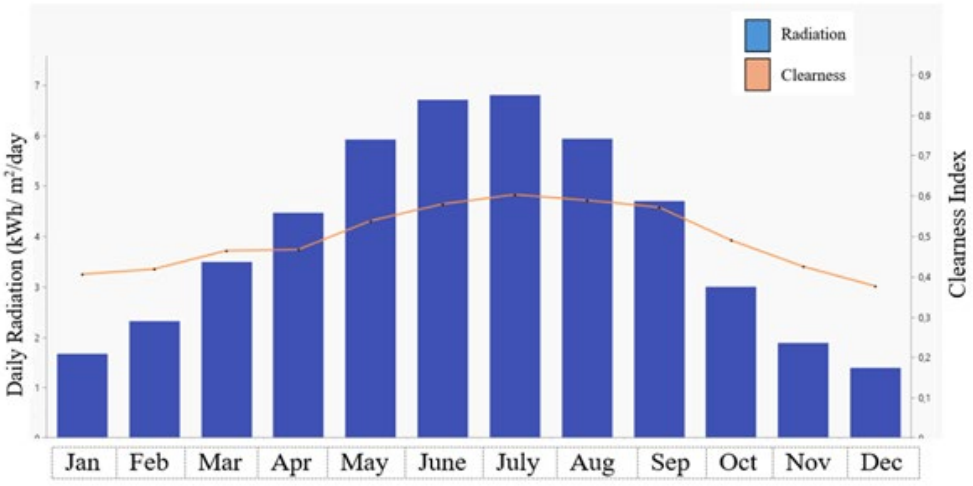

Fig. 3. The radiation profile of the study area.

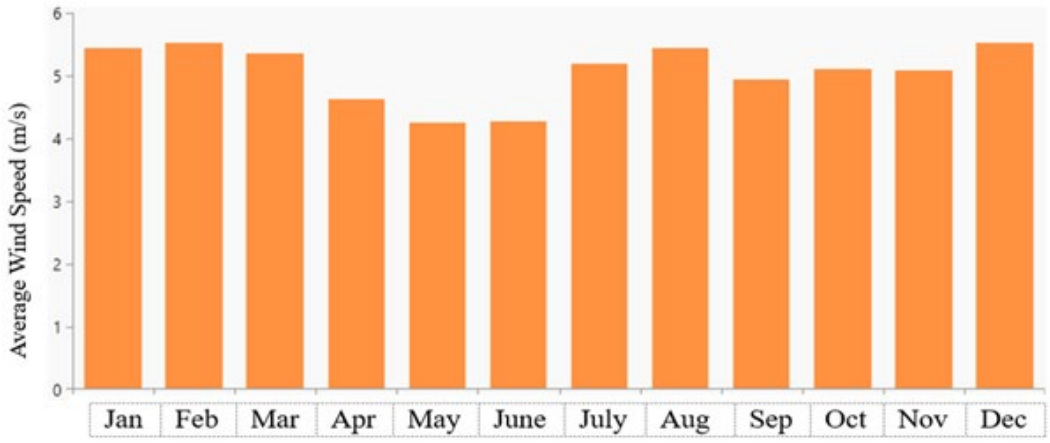

Fig. 4. Wind speed in the study area.

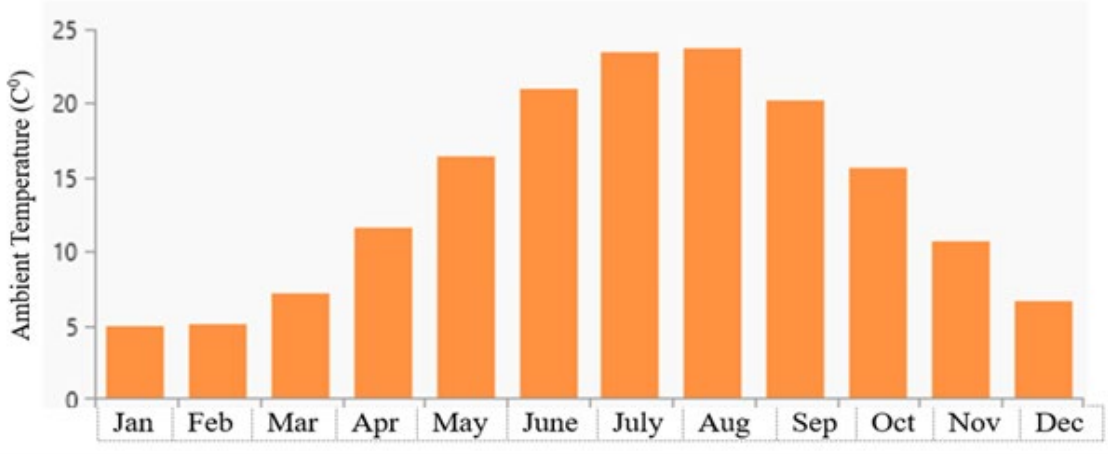

Fig. 5. Ambient temperature of the study area.

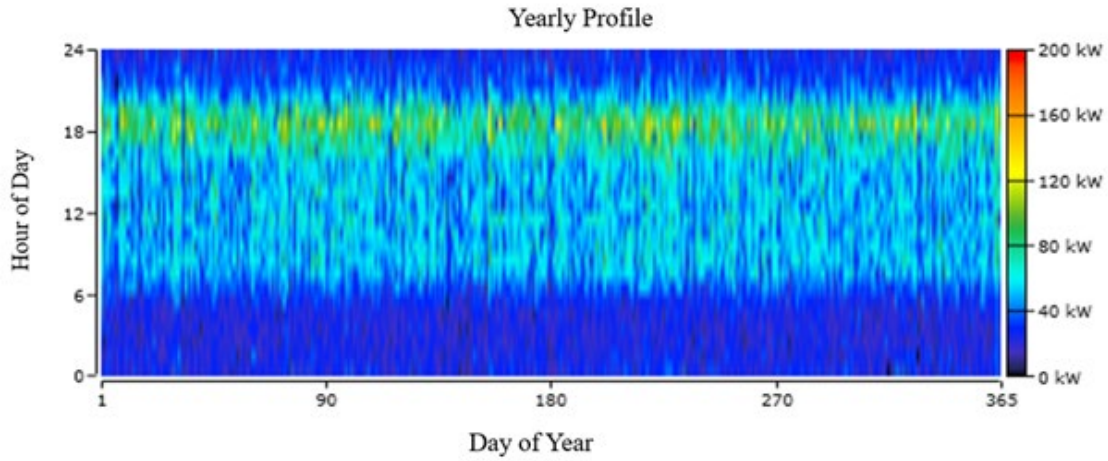

Fig. 6. Load profile of the study area

D. Grid

To supply power to electric vehicle charging stations, a connection to the grid is typically established. This step is essential for evaluating the economic costs associated with the system based on the proportion of renewable energy production and for analyzing the carbon emissions in each scenario. In all scenarios considered, a grid connection was used. The electricity cost varies depending on the time of day, with a rate of $0.40/kWh during the day (06:00-17:00), $0.35/kWh during peak hours (17:00-22:00), and $0.30/kWh during nighttime (22:00-06:00). Additionally, electricity sold back to the grid is priced at $0.15/kWh [26].

E. Solar Panels

Solar energy is one of the most important RES due to its inexhaustible nature. Given Turkey's high solar energy potential, solar power is considered one of the best renewable sources for hybrid energy systems. Solar radiation reaches its peak in March and April, and drops to its lowest in December and January. Solar panels convert the heat energy they collect from the sun into direct current (DC) electricity stored in batteries. The solar panel output power can be calculated using the following equation [27]:

$$P_{PVout} = Y_{PV} * f_{PV} * \frac{G_T}{G_{T,STC}} * \left[1 + \alpha_P * \left(T_c - T_{c,STC}\right)\right] \quad (1)$$

where P_{PVout} represents the output power of the solar panel in watts, Y_{PV} is the rated capacity

of the solar panel under standard test conditions, and f_{PV} is the derating factor of the panel. G_T is the solar radiation incident on the panel at any given time, while $G_{T,STC}$ is the radiation under standard test conditions. α_P is the temperature coefficient of power, T_c is the cell temperature, and $T_{c,STC}$ is the cell temperature under standard test conditions. The installation cost of a 1-kW solar panel is approximately $700, with the same amount for the replacement cost, and the annual maintenance cost is estimated to be $70. The expected lifespan of a solar panel is 25 years.

F. Wind Turbine

The wind turbine selected for this study was an XANT M21 with a nominal power of 100 kW. This model was chosen because it can be constructed using the essential engineering parts principle, thereby reducing manufacturing costs, and is portable. The wind turbine has a starting speed of 3 m/s, nominal speed of 11 m/s, and cut-off speed of 20 m/s. It was installed at a height of 31.8 m, and the rotor had a diameter of 21 m. The installation and replacement costs were $250,000 each, and the annual maintenance cost was $62.5. The expected lifespan of a wind turbine is 20 years [28].

HOMER analyzes wind turbine electricity generation on an hourly basis four steps. To estimate wind speed, the following power law equation was used:

$$U_{hub} = U_{anem} * \left(\frac{Z_{hub}}{Z_{anem}}\right)^{\propto} \tag{2}$$

HOMER adjusts the calculated power values to match real-life conditions by multiplying the calculated power values by the air density ratio. The air density was measured at standard temperature and pressure (1.225 kg/m³). The equation is as follows:

$$P_{WTG} = \left(\frac{\rho}{\rho_0}\right) * P_{WTG,STP} \tag{3}$$

where P_{WTG} is the power generated by the wind turbine, ρ is the air density at the site, ρ_0 is the air density under standard temperature and pressure (1.225 kg/m³), and $P_{WTG,STP}$ is the power generated by the wind turbine under standard test conditions.

G. Converter

The converter connects the DC and alternating current (AC) components of the system. It operates bidirectionally, depending on the energy flow, and ensures smooth energy conversion between DC and AC systems. The installation cost of the converter was approximately $400, with the same cost for replacement, and the annual maintenance cost was $50. The lifespan of the converter is estimated to be 15 years. The power output of the converter can be calculated using the following equation:

$$P_{inv} = \frac{PV_{ic}}{n_{inv} * N_{inv}} \tag{4}$$

where P_{inv} represents the output power of the converter, PV_{ic} is the installed capacity of the solar panels, n_{inv} is the efficiency of the inverter, and N_{inv} is the number of inverter units [29].

H. Battery

Batteries, which store electrical energy in chemical form, are crucial components of hybrid energy systems. They are used to store excess energy produced when generation exceeds consumption. The installation and replacement costs for a 1-kW battery are approximately

$550, and the annual maintenance cost is $55. The lifespan of the battery is expected to be 15 years. The state of charge (SOC) of the battery during charge and discharge modes can be calculated using the following equation [30]:

$$SOC\ (t) = (1 - Q) * SOC(t - 1) + \frac{P_{cd} * \Delta(t) e_{cd}}{E} \quad (5)$$

where Q represents the hourly discharge rate, P_{cd} is the charge and discharge power, e_{cd} is the charge and discharge efficiency, and E is the total energy stored in the battery.

İ. Electric Vehicle Charging Station

The charging station planned for the shopping center is designed to accommodate various EV types. The charging characteristics of the vehicles to be charged are presented in Table 1. Although the electric vehicle market is rapidly growing, there are still limited data on the actual operation of charging stations. Therefore, the system was modeled based on probable data regarding vehicle charging requirements and population estimates.

TABLE I
CHARGING CHARACTERISTICS OF THE VEHICLES

Vehicle type	Population	Maximum charging power per vehicle (kW)	Required charging energy per vehicle (kWh)
SUV EV	30	150	260
Small EV	70	50	260

The data used in this study assume a growing EV population, and the charging station design reflects a realistic mix of different vehicle types. As the global adoption of EVs continues to increase, the chosen vehicle population and charging characteristics parameters are in line with industry expectations for future EV charging demands.

III. RESULTS AND DISCUSSION

Using HOMER Grid software, four scenarios were generated to evaluate the economic and environmental performance of a renewable energy-based EV charging station. The results summarized in Table 2 show that Scenario 4 emerges as the optimal solution, exhibiting the lowest NPC of $1.18M and renewable energy fraction 97%. This high renewable fraction indicates that the majority of the station's energy is sourced from renewable resources, minimizing the dependency on fossil fuels and significantly reducing carbon emissions.

In comparison, Scenario 4 also achieves the lowest operating cost of $8,398 and an initial cost of $1.05M, making it the most financially sustainable option. While Scenario 2 records a slightly lower COE of $0.0554/kWh, its higher initial and operational expenses make it less favorable than Scenario 4. On the other hand, Scenario 1, with an NPC of $2.06 million and the lowest renewable fraction of 87.6%, ranks as the least efficient in terms of both cost and environmental sustainability.

Ultimately, Scenario 4 is the ideal implementation choice, offering an optimal balance between cost efficiency and environmental performance. The scalability and reliance on renewable energy make it a suitable model for future projects, especially in urban areas such as shopping centers. As the demand for electric vehicle charging infrastructure grows, Scenario 4 can be replicated or expanded to meet these needs while contributing to long-term environmental sustainability and financial savings.

TABLE II
COST OPTIMIZATION RESULTS.

	NPC($)	COE($)	OPERATING COST($)	INITIAL COST($)	RENEWABLE FRACTION (%)
Scenario1	2.06M	0.0818	60.339	1.14M	87.6
Scenario2	1.53M	0.0554	9.641	1.39M	93.3
Scenario3	1.47M	0.0653	15.970	1.22M	97.3
Scenario4	1.18M	0.0628	8.398	1.05M	97

The various scenarios for installing charging stations in shopping centers in Yalova are presented in Table 2. Among the systems created with different components, Scenario 4, which includes photovoltaic (PV) panels, wind turbines, batteries, and a converter, as shown in Figure 8, is the most suitable system in terms of NPC, initial cost, and renewable energy fraction.

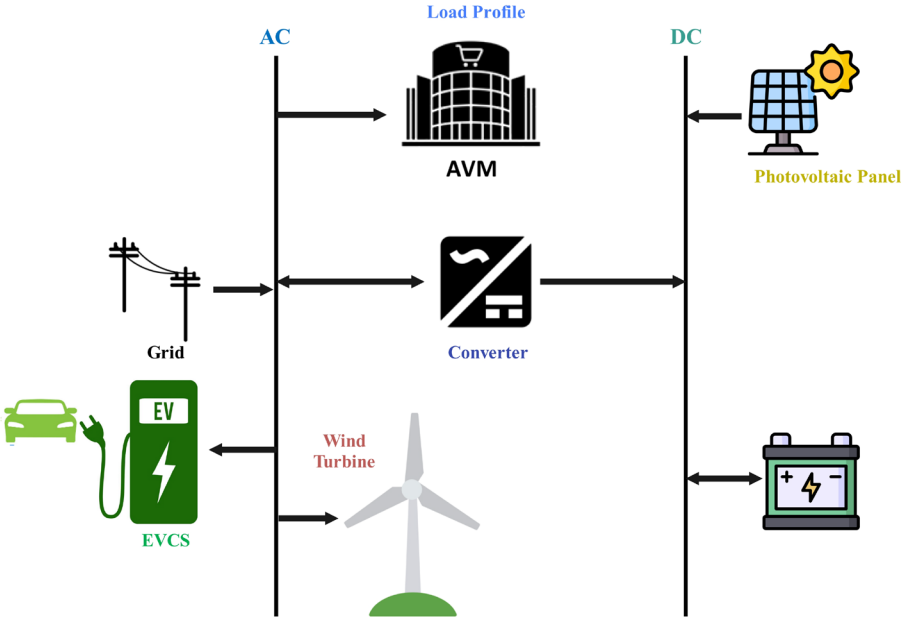

Fig. 7. Diagram of the selected system.

The monthly and annual performance of the optimized system is depicted in Figure 8, and the respective contributions of wind, grid, and solar panel electricity production are illustrated in Figure 9. The system consumes 1,424 kWh of energy per day, with a peak demand of 164 kW, and predominantly relies on RES for its electricity needs. As shown in the figures, combined electricity generation from solar panels and wind turbines exceeds the grid's contribution. Specifically, the system generates 1,062,698 kWh/year from PV panels and 244,794 kWh/year from wind turbines, covering 97.2% of the total energy demand.

In the proposed system, the nominal capacity of solar PVs is 795 kW, with an average daily output of 2,912 kWh/day. As shown in Figure 10, solar PV production occurs between 06:00 and 18:00. Figure 11 highlights the daily performance of wind turbines, which serve as complementary energy sources, particularly during periods when solar energy is insufficient.

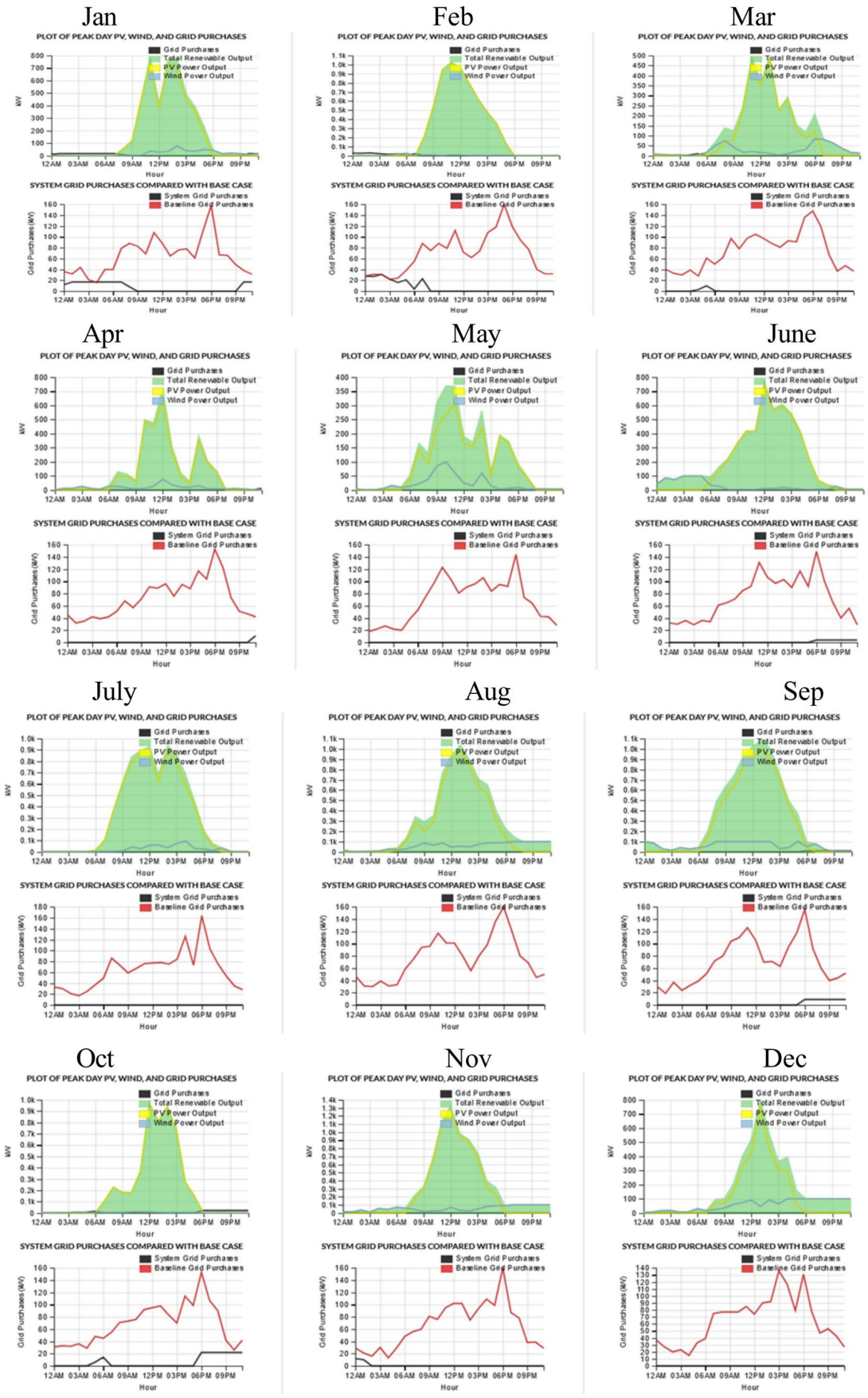

Fig. 8. Monthly load profile of electricity consumption.

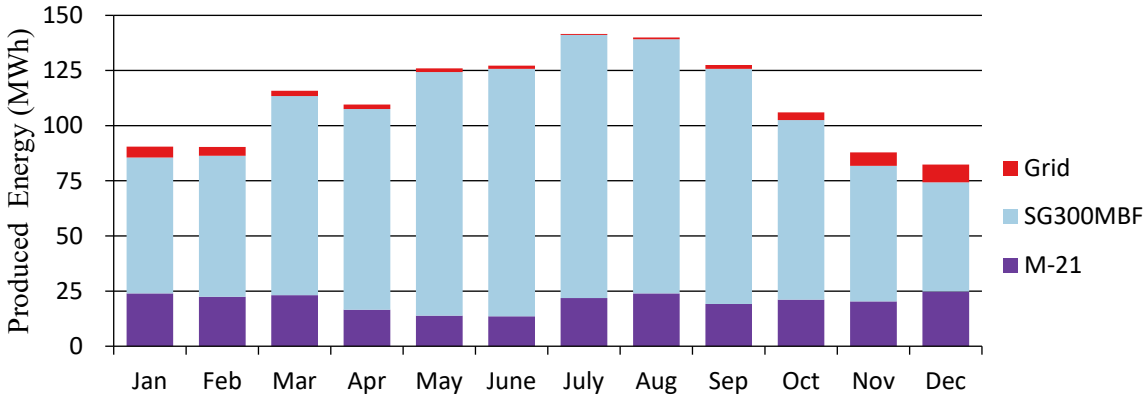

Fig. 9. Monthly electricity production of solar, wind and grid.

The monthly electricity production from solar panels (SG300MBF), wind turbines (M-21), and the grid for the system are shown in Figure 9. It can be observed that solar energy generation is the dominant source across all months, with peak production occurring during the summer months of June, July, and August. The wind energy production, shown in purple, remains relatively constant throughout the year, providing supplementary power. The grid represented by the red section contributes only a small portion of the total electricity, demonstrating the system's heavy reliance on renewable energy sources. This highlights the effectiveness of integrating solar and wind energy sources to meet energy demands while minimally relying on grid electricity.

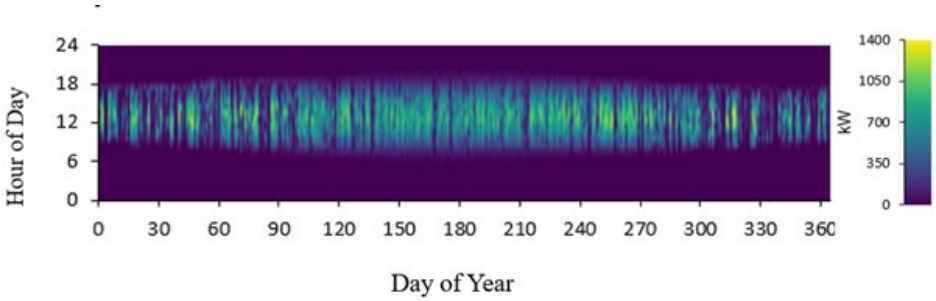

Fig. 10. Daily PV performance.

Figure 10 illustrates the daily performance of the solar PV system over the course of a year. The graph displays the solar output in kilowatts (kW) at various hours of the day across the 365 days of the year. The color gradient indicates the intensity of solar power generation, where darker areas represent low production and lighter shades indicate higher energy generation. As expected, the highest solar output occurs during the daytime, typically between 6:00 AM and 6:00 PM, with peak production around noon. Consistent horizontal energy production bands suggest reliable daily electricity generation throughout the year, with minor fluctuations due to seasonal changes and weather variations.

Figure 11 illustrates the daily performance of the wind turbine system over the course of a year. The graph shows the power output in kW at different hours of the day plotted against the 365 days of the year. The color scale indicates the intensity of wind power generation, with darker colors representing lower production levels and lighter colors indicating higher output. Unlike solar energy, wind energy production does not follow a fixed daily pattern because wind speeds fluctuate throughout the day and across different seasons. The graph shows that wind energy production is more sporadic, with noticeable variations occurring throughout both day and night. However, despite these fluctuations, wind power provides a consistent source of

energy throughout the year.

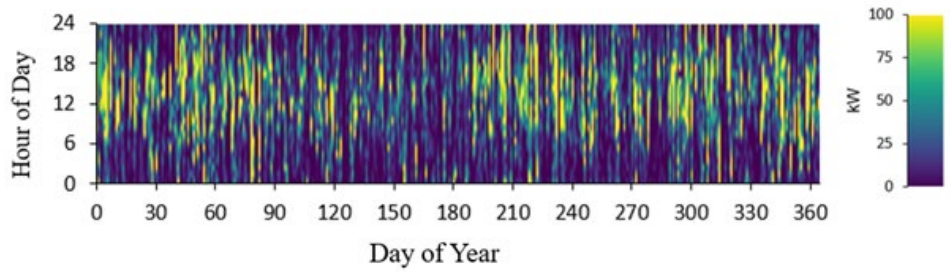

Fig. 11. Daily wind turbine performance.

The converter in the system has a capacity of 480 kW, with an average output power of 110 kW and a maximum output power of 480 kW. Based on the simulation results, the converter's capacity factor was found to be 22.9%, with a total annual operation time of 7,385 hours. Annually, the converter processes 17,311 kWh of energy, with an output of 16,446 kWh, resulting in an energy loss of 866 kWh. As shown in Figure 13, the converter's performance is closely linked to solar PV generation. The graphical representation shows that the converter's peak output generally aligns with the daily solar production hours, highlighting its reliance on solar energy for efficient operation.

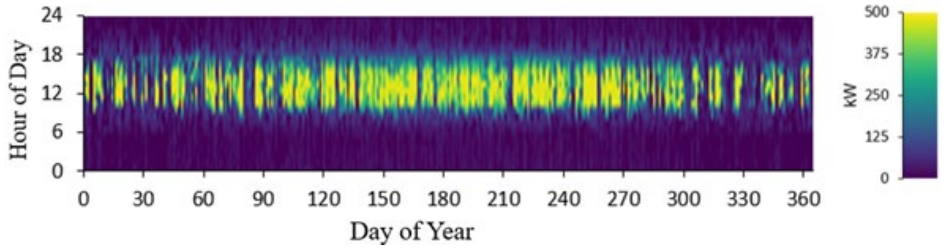

Fig. 12. Daily converter performance.

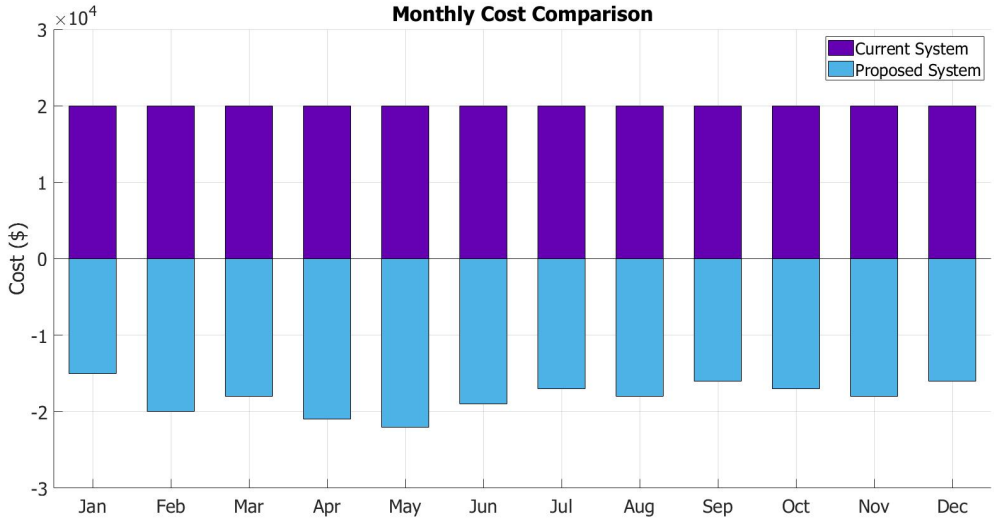

Fig. 13. Monthly cost comparison between the current and proposed systems.

The economic performance of the hybrid energy charging stations designed using RESs was evaluated through a techno-economic analysis. This analysis considered all costs incurred over the system's lifespan. To identify the most cost-effective system, the NPC was prioritized in HOMER Grid software, and the system with the lowest NPC was selected as optimal. Other

key parameters included the renewable fraction and the COE, which were also vital for determining the optimal system configuration. Figure 13 displays the monthly electricity bill savings of the proposed system compared to the existing one. As the chart indicates, the proposed system offers significant cost savings across all months, with the most notable reductions occurring during the spring and summer periods. This highlights the economic advantage of integrating renewable energy into the system.

As shown in Table 3, the proposed system resulted in an annual emission of 23,554 kg of carbon dioxide (CO_2), 102 kg of sulfur dioxide (SO_2), and 49.9 kg of nitrogen oxides (NO_x). Notably, the emissions of carbon monoxide (CO), unburned hydrocarbons, and particulate matter (PM) were zero, indicating a significant reduction in the harmful pollutants. This environmentally friendly system helps reduce atmospheric gas emissions, which can contribute to mitigating global warming and improving air quality.

TABLE III
EMISSION RESULTS

	Emission value (KG/YEAR)
Carbon Dioxide	23,554
Carbon Monoxide	0
Unburned Hydrocarbons	0
Particulate Matter	0
Sulfur Dioxide	102
Nitrogen Oxides	49.9

Reductions in emissions are especially important in the context of climate change mitigation, as lower CO_2 levels contribute to slowing down the greenhouse effect, while reduced NO_x and SO_2 levels minimize acid rain formation and respiratory health risks. Overall, the proposed renewable energy system offers both economic and environmental advantages by significantly cutting emissions.

IV. CONCLUSION

HRES have been proven to offer reliable and uninterrupted electricity despite the intermittent nature of RES. This study focused on the design of an EV charging station for a shopping center using RES, addressing both energy reliability and cost efficiency. The system's goal was to reduce energy costs while utilizing clean, sustainable energy sources. The study modeled four scenarios, each incorporating various combinations of RES, and evaluated their performance using HOMER Grid software.

Among the modeled scenarios, Scenario 4, which combines solar energy, wind energy, battery storage, and converters within a grid-connected hybrid energy system, emerged as the optimal solution. This scenario exhibited a NPC of $1.18 million, an initial cost of $1.05 million, and achieved a renewable fraction of 97%, making it the most cost-effective and environmentally friendly option compared to the other models.

The simulation results demonstrate that the proposed hybrid energy system can generate significantly more energy from renewable sources than from the grid. Specifically, the system is expected to deliver 97% of its energy from renewable sources, thus reducing reliance on fossil fuels and minimizing environmental impacts. The use of renewable energy not only decreases the carbon footprint of EV charging stations but also contributes to long-term energy security and cost savings.

1. **Key Findings and Recommendations:**
2. **Environmental Benefits**: The transition to renewable energy significantly reduces carbon emissions, as shown by the system's ability to cut annual CO_2 emissions by over 23,554 kg. This will support global efforts to combat climate change and promote sustainable development.
3. **Economic Efficiency**: Scenario 4, with its optimized combination of solar, wind, and battery storage, provides the lowest NPC and initial investment and demonstrates the financial viability of adopting HRES in EV charging infrastructure.
4. **Scalability and Adaptability**: The success of this model in a commercial shopping center setting indicates that similar systems can be scaled up and adapted for broader applications, such as industrial zones, residential complexes, or even entire city districts, where renewable energy can meet growing energy demands.
5. **Policy Implications**: Policymakers should consider incentivizing the integration of renewable energy systems into EV charging networks to significantly reduce dependency on non-renewable energy, lower energy costs, and contribute to national and international sustainability targets.
6. **Future Work and Recommendations:**

- **Technological Advancements**: Further research should focus on integrating emerging technologies, such as V2G solutions, which can enhance system flexibility and efficiency by allowing stored energy in EVs to be fed back into the grid.
- **Extended Sensitivity Analysis**: Conducting a more detailed sensitivity analysis under various weather and market scenarios can provide deeper insights into system resilience and financial outcomes.
- **Expansion to Other Locations**: Future studies should also explore the potential of hybrid renewable systems in regions with different climatic conditions and energy demands to assess the scalability and adaptability of the proposed solutions across diverse geographies.

This study demonstrates that HRES are not only feasible but also crucial in supporting the transition to cleaner energy, especially for EV charging infrastructure. Implementing such systems will significantly contribute to environmental sustainability, energy security, and economic benefits, aligning with global renewable energy and decarbonization goals.

REFERENCES

[1] A. Fatih Guven, A. Y. Abdelaziz, M. Mahmoud Samy, and S. Barakat, "Optimizing energy Dynamics: A comprehensive analysis of hybrid energy storage systems integrating battery banks and supercapacitors," *Energy Convers. Manag.*, vol. 312, no. May, p. 118560, 2024, doi: 10.1016/j.enconman.2024.118560.

[2] A. F. Güven and N. Yörükeren, "A comparative study on hybrid GA-PSO performance for stand-alone hybrid energy systems optimization," *Sigma J Eng Nat Sci.*, vol. 42, no. 5, pp. 1410–1438, 2024, doi: 10.14744/sigma.2024.00.

[3] A. F. Güven ve C. Hatipoğlu, "Şebekeden Bağımsız güneş/rüzgâr/biyogaz/yakıt hücresi/batarya tabanlı hibrit enerji sisteminin tekno-ekonomik analizi: Muğla zaferler köyü vaka çalışması", *EMO Bilimsel Dergi*, c. 12, sy. 1, ss. 53–65, 2022.

[4] A. F. Güven, "Bahçelievler Belediye Başkanlık Binasının Enerji İhtiyacının Güneş ve Rüzgar Sistemi ile Karşılanması, Optimizasyonu ve Maliyet Analizi," *Sinop Üniversitesi Fen Bilim. Derg.*, vol. 2, no. 1, pp. 24–36, 2017, [Online]. Available: http://dergipark.gov.tr/sinopfbd/issue/28364/255023.

[5] S. Barakat, A. I. Osman, E. Tag-Eldin, A. A. Telba, H. M. Abdel Mageed, and M. M. Samy, "Achieving green mobility: Multi-objective optimization for sustainable electric

vehicle charging," *Energy Strateg. Rev.*, vol. 53, no. August 2023, p. 101351, 2024, doi: 10.1016/j.esr.2024.101351.

[6] E. S. Rigas, S. Karapostolakis, N. Bassiliades, and S. D. Ramchurn, "EVLibSim: A tool for the simulation of electric vehicles' charging stations using the EVLib library," *Simul. Model. Pract. Theory*, vol. 87, no. June, pp. 99–119, 2018, doi: 10.1016/j.simpat.2018.06.007.

[7] Y. Wang, M. Kazemi, S. Nojavan, and K. Jermsittiparsert, "Robust design of off-grid solar-powered charging station for hydrogen and electric vehicles via robust optimization approach," *Int. J. Hydrogen Energy*, vol. 45, no. 38, pp. 18995–19006, 2020, doi: 10.1016/j.ijhydene.2020.05.098.

[8] Y. BİCER, "Thermodynamic Analysis of a Renewable Energy-Driven Electric Vehicle Charging Station with On-Site Electricity Generation from Hydrogen and Ammonia Fuel Cells," *Int. J. Automot. Sci. Technol.*, vol. 4, no. 4, pp. 223–233, 2020, doi: 10.30939/ijastech..754580.

[9] A. Çobanoğlu, G. Demirkıran, and M. Güneş, "İzmir İlinde Elektrikli Kara Araçları için Güneş Enerjisi Destekli Bir Şarj İstasyonun Tasarlanması," *Eur. J. Sci. Technol.*, no. 21, pp. 635–648, 2021, doi: 10.31590/ejosat.777874.

[10] T. Li *et al.*, "An optimal design and analysis of a hybrid power charging station for electric vehicles considering uncertainties," *Proc. IECON 2018 - 44th Annu. Conf. IEEE Ind. Electron. Soc.*, vol. 1, pp. 5147–5152, 2018, doi: 10.1109/IECON.2018.8592855.

[11] A. Allouhi and S. Rehman, "Grid-connected hybrid renewable energy systems for supermarkets with electric vehicle charging platforms: Optimization and sensitivity analyses," *Energy Reports*, vol. 9, pp. 3305–3318, 2023, doi: 10.1016/j.egyr.2023.02.005.

[12] S. W. Chisale, S. Eliya, and J. Taulo, "Optimization and design of hybrid power system using HOMER pro and integrated CRITIC-PROMETHEE II approaches," *Green Technol. Sustain.*, vol. 1, no. 1, p. 100005, 2023, doi: 10.1016/j.grets.2022.100005.

[13] F. I. Conference, T. Engineering, A. May, and E. S. Engineering, "Dandelion-Optimizer based power sharing in hybrid renewable energy system optimum sizing with EV : grid-connected , wind , solar , battery , electric vehicles," pp. 1–3, 2023.

[14] P. K. Joseph and E. Devaraj, "Design of hybrid forward boost converter for renewable energy powered electric vehicle charging applications," *IET Power Electron.*, vol. 12, no. 8, pp. 2015–2021, 2019, doi: 10.1049/iet-pel.2019.0151.

[15] I. E. Atawi, E. Hendawi, and S. A. Zaid, "Analysis and design of a standalone electric vehicle charging station supplied by photovoltaic energy," *Processes*, vol. 9, no. 7, 2021, doi: 10.3390/pr9071246.

[16] J. Kurtz, Z. Ma, G. Saur, J. A. Wrubel, R. Mount, and S. Hammond, "Analysis of hydrogen infrastructure for the feasibility, economics, and sustainability of a fuel cell powered data center," *Sustain. Energy Technol. Assessments*, vol. 58, no. July, p. 103357, 2023, doi: 10.1016/j.seta.2023.103357.

[17] A. K. Karmaker, M. R. Ahmed, M. A. Hossain, and M. M. Sikder, "Feasibility assessment & design of hybrid renewable energy based electric vehicle charging station in Bangladesh," *Sustain. Cities Soc.*, vol. 39, no. January, pp. 189–202, 2018, doi: 10.1016/j.scs.2018.02.035.

[18] A. Singh, S. S. Shaha, P. G. Nikhil, Y. R. Sekhar, S. Saboor, and A. Ghosh, "Design and analysis of a solar-powered electric vehicle charging station for Indian cities," *World Electr. Veh. J.*, vol. 12, no. 3, 2021, doi: 10.3390/wevj12030132.

[19] R. P. Narasipuram and S. Mopidevi, "A technological overview & design considerations for developing electric vehicle charging stations," *J. Energy Storage*, vol. 43, no. September, p. 103225, 2021, doi: 10.1016/j.est.2021.103225.

[20] J. Ebrahimi, M. Abedini, M. M. Rezaei, and M. Nasri, "Optimum design of a multi-form energy in the presence of electric vehicle charging station and renewable resources

considering uncertainty," *Sustain. Energy Grids Networks*, vol. 23, p. 100375, 2020, doi: 10.1016/j.segan.2020.100375.

[21] A. F. Güven, "Integrating electric vehicles into hybrid microgrids: A stochastic approach to future-ready renewable energy solutions and management," *Energy*, vol. 303, no. May, p. 131968, 2024, doi: 10.1016/j.energy.2024.131968.

[22] A. F. Güven, Ş. Türkmen, and F. Karayiğit, "Sustainable energy integration in microgrids and HOMER grid optimization: enhancing efficiency with electric vehicle Charging Solutions," no. August, 2024.

[23] A. F. Güven and E. Yücel, "Sustainable energy integration and optimization in microgrids: enhancing efficiency with electric vehicle charging solutions," *Electr. Eng.*, 2024, doi: 10.1007/s00202-024-02619-x.

[24] A. F. Güven, N. Yörükeren, and M. M. Samy, "Design optimization of a stand-alone green energy system of university campus based on Jaya-Harmony Search and Ant Colony Optimization algorithms approaches," *Energy*, vol. 253, 2022, doi: 10.1016/j.energy.2022.124089.

[25] A. F. Güven and E. Yücel, "Application of HOMER in assessing and controlling renewable energy-based hybrid EV charging stations across major Turkish cities," *Int. J. Energy Stud.*, vol. 8, no. 4, pp. 747–780, 2023, doi: 10.58559/ijes.1324236.

[26] A. F. Güven, N. Yörükeren, and O. Ö, "Mengi, Multi-objective optimization and sustainable design: a performance comparison of metaheuristic algorithms used for on-grid and off-grid hybrid energy systems, " *Neural Computing and Applications,* vol. 36, no. 13. 2024.

[27] A. F. Güven and O. Ö. Mengi, "Assessing metaheuristic algorithms in determining dimensions of hybrid energy systems for isolated rural environments: Exploring renewable energy systems with hydrogen storage features," *J. Clean. Prod.*, vol. 428, no. October, 2023, doi: 10.1016/j.jclepro.2023.139339.

[28] A. F. Güven and N. Yörükeren, "Bir hibrit enerji sisteminin parçacık sürüsü optimizasyon algoritması- genetik algoritma ve gri kurt optimizasyon algoritma tekniği ile enerji yönetimi ve optimizasyonu: Yalova Üniversitesi için bir vaka çalışması," *Karadeniz Fen Bilim. Derg.*, vol. 12, no. 2, pp. 853–879, 2022, doi: 10.31466/kfbd.1169643.

[29] A. F. Güven and E. Poyraz, "Feasibility study and techno-economic analysis of stand-alone hybrid energy system for Muğla province köyceğiz," *Karadeniz Fen Bilim. Derg.*, vol. 11, no. 1, pp. 70–85, 2021, doi: 10.31466/kfbd.880437.

[30] A. F. Guven, N. Yorukeren, E. Tag-Eldin, and M. M. Samy, "multi-objective optimization of an islanded green energy system utilizing sophisticated hybrid metaheuristic approach," *IEEE Access*, vol. 11, no. July, pp. 103044–103068, 2023, doi: 10.1109/ACCESS.2023.3296589.

Performance Investigation of Bridge Type Parallel-Resonance Fault Current Limiter in Power Distribution Systems

Evren ISEN[*,1]

[*]eisen@bandirma.edu.tr, ORCID: 0000-0002-3107-9255
[1]*Electrical Engineering, Bandirma Onyedi Eylul University, Bandirma, Turkey*

Abstract: In this study, the performance of a bridge type fault current limiter using parallel LC resonant circuit in a power distribution system is investigated. The system is simulated in Simulink/Matlab and its success in fault current limitation and common point voltage regulation is investigated. The effect of the resistor R_{SH} used in resonance suppression in the fault current limiter on the common point voltage is presented. The results obtained show that this limiter can successfully suppress the high current that occurs in the short circuit fault condition. Again, it is seen that the common coupling point voltage can be kept at the nominal level if the circuit elements are used at their appropriate values.

Keywords: *Fault current limiter, Parallel resonance, Resonance FCL*

I. INTRODUCTION

With increasing population and industrialization, there is an increase in energy consumption. The use of alternative energy sources has increased and integrated into the electrical energy system due to the decrease in fossil fuels used to meet the electrical energy demand and their negative environmental impacts. With the increase in energy use and the inclusion of different energy sources in the system, there is an increase in the possibility of short circuit failure. Therefore, the importance of fault current limiters is increasing.

Fault current limiters have been in the electrical energy system from past to present. In the literature, superconductor fault current limiter [1], solid-state fault current limiter [2], series resonance type fault current limiter [3], parallel resonance fault current limiter [4], hybrid fault current limiter [5], magnetic flux type fault current limiter [6] and bridge type fault current limiter [7] exist. The most important features expected from fault current limiters are that they do not show impedance during normal operation and do not cause losses, show high impedance in case of fault, react quickly to the fault, provide regulation at the common coupling point voltage, reduce the current value to a safe level, and ensure that the current recovers as soon as possible by disabling quickly at the end of the fault [8].

There are various studies in the literature on the bridge-type parallel resonant circuit examined in this study. In this study, a bridge type FCL is used to improve the performance of the low voltage continuous ride-through (LVRT) performance of wind turbine power plants in the event of failure, and active power output control is provided by creating a variable capacitor with the FCL [9]. In an operation using a thyristor bridge circuit, the inductance in the series resonant circuit on the line is short-circuited with the help of the bridge circuit in case of a fault. Thus, since the resonance is disabled, the impedance of the circuit increases and the fault current is reduced by the effect of capacitor impedance [10]. In one of the two different bridge circuits consisting of diodes, a high-temperature superconductor is used, while the other uses a power capacitor and a semiconductor switch in addition to the superconductor. Both structures were investigated in the system with wind turbine. It has been shown that the

capacitor circuit is much more effective than the other one [11]. In another study using a diode bridge, a switching element in the middle of the bridge and a small dc inductance used to slow down the switch current and a second inductance parallel to the switch are used. In the event of a fault, the switch is deactivated and the high value inductance is activated, showing high impedance and suppressing the fault current [12]. In addition to fault current suppression, a bifunctional FCL has been developed to correct grid voltage fluctuations. The FCL is able to successfully suppress fault current while smoothly switching between current suppression and voltage correction functions [13]. A new FCL that can be connected to DC and AC systems suitable for use in AC/DC microgrids has been developed and the successful performance of the current limiter in a laboratory environment is presented. In addition to current suppression, the developed FCL is also capable of controlling the energy flow from AC system to DC system [14]. The developed FCL, which provides reduced power loss and harmonic distortion in line current, has been tested in a simulation environment in a system with a wind turbine and 2 generators. The FCL circuit, which provides simple construction and control, is compared with classical diode bridge, series dynamic braking resistor and active diode bridge FCL types [15]. The developed interconnecting bridge type FCL circuit is connected in series to the feeders connected to the common coupling point. The connection of multiple FCLs to a single limiting resistor on the DC bus provides a significant cost reduction. As a result of the simulation studies, it was observed that the developed FCL achieved a cost-effective success [16]. In the parallel resonance based FCL system developed for use at high voltage, the rectifier bridge short circuits the parallel resonant circuit under normal operating conditions. The semi-controlled rectifier is disabled in the event of a fault, allowing the parallel resonant circuit to be connected to the line and show high impedance. High fault current is thus suppressed [17].

In this study, the performance of a bridge-type parallel resonant fault current limiter is investigated in the event of a short circuit in the electrical power grid. System simulation is done in Simulink environment. Phase-ground (*PG*), phase-phase (*PP*), phase-phase-ground (*PPG*), phase-phase-phase (*PPP*) and phase-phase-phase-ground (*PPPG*) faults are analyzed in the simulation study in three-phase network. In all fault conditions, the bridge-type parallel resonant fault current limiter is able to suppress the current.

In the content of the study, information about the working principle of the fault current limiter is given in section 2. In section 3 the simulation results are given and in the last section the results obtained are presented.

II. PRINCIPLES OF PARALEL RESONANCE FAULT CURRENT LIMITER

The FCL examined in the study is shown in Fig. 1. This FCL consists of two parts. The upper part has a parallel resonance section and the lower part has a bridge structure. During normal operation, the bridge part is activated while the parallel resonance part is activated in case of failure. The operating principles and circuit structures in the two operating states are given below.

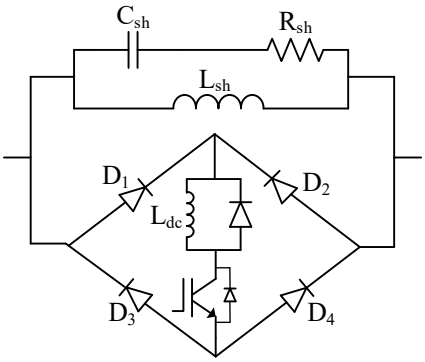

Fig. 1. Bridge type parallel resonance fault current limiter

A. Normal Operation

It is the operating state in which there is no fault in the system. In this case, since the system impedance should not be interfered with, the parallel resonant part at the top of the limiter should not be activated. Therefore, the path for the current to flow is provided by the bridge part. As seen in Fig. 2, the bridge diodes, DC inductance and semiconductor are in the circuit during normal operation. Depending on the AC current alternation, D_1 and D_4 diodes are conducting in positive alternation while D_2 and D_3 diodes are conducting in negative alternation. Since the AC main current flows through the diode bridge, the current through the semiconductor is DC. It is therefore possible to use a unidirectional semiconductor.

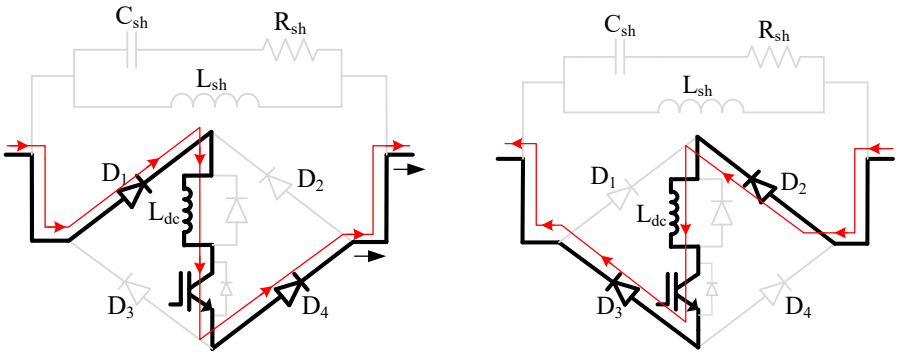

(a) Positive half-cycle **(b)** Negative half-cycle

Fig. 2. Normal operation

B. Fault Condition

This is when a short circuit fault occurs in the system. In this case, since the grid current starts to rise, the fault current limiter is activated to limit the current. When the fault condition is detected, the switching element in the bridge is opened. Thus, the current is diverted from the bridge circuit to the parallel resonant circuit as shown in Fig. 3. The parallel resonant circuit consisting of R-L-C elements shows high impedance and reduces the fault current.

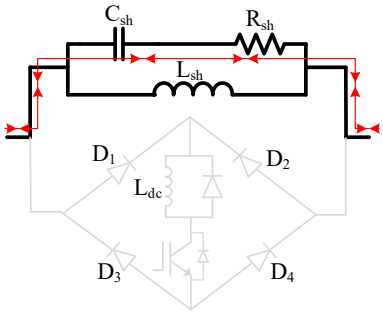

Fig. 3. Circuit operation in case of fault

III. SIMULATION STUDY

In order to analyze the performance of the bridge-type parallel resonant fault current limiter, the system is simulated in Simulink environment. Fig. 4 shows the Simulink circuit diagram of the system. The three-phase system consists of three-phase source, FCL, line impedance, fault point and load. Current level is used for fault detection in the system. If the absolute current reaches 500 A instantaneously, it is understood that a short circuit fault occurs in the system and a signal is sent to the FCL circuit in the relevant phase.

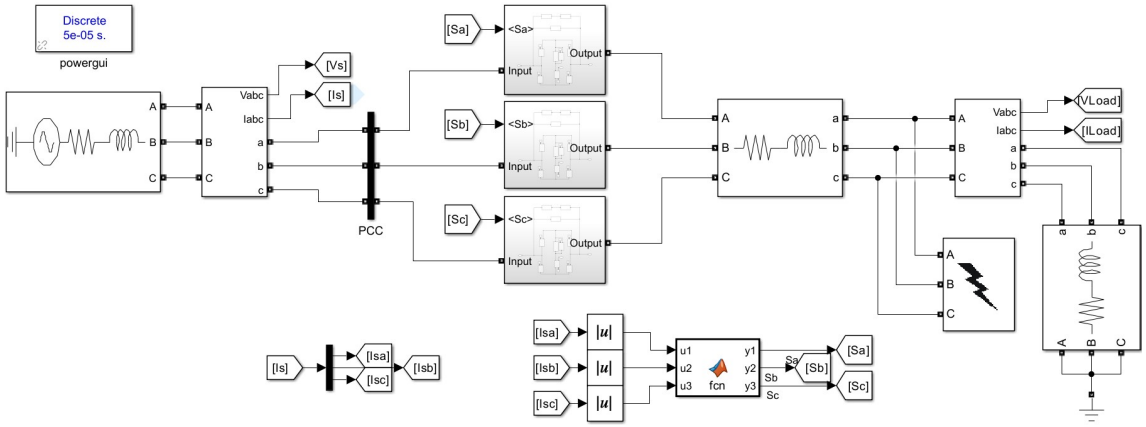

Fig. 4. Simulink circuit diagram of the system

Fig. 5 shows the Simulink circuit diagram of the FCL circuit used in the simulation. When fault current is detected in the system, the semiconductor switching element in the FCL circuit is opened and the high impedance in the relevant phase is activated to reduce the current. The parameters used in the circuit model created in the simulation of the system are given in TABLE I. The system to which FCL is applied has a frequency of 50 Hz and the values of L and C elements used in the FCL circuit are determined according to (1). In case of failure, oscillation occurs in the current with the activation of the parallel resonant circuit. R_{sh} resistor is used to suppress this oscillation.

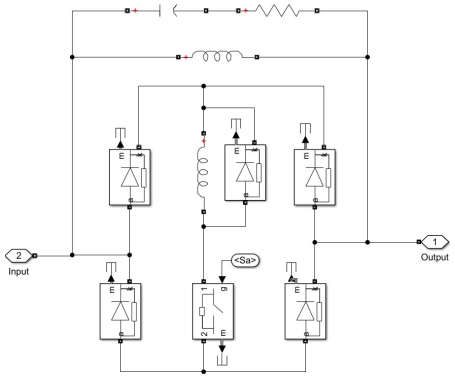

Fig. 5. FCL simulink circuit diagram

TABLE I
SYSTEM PARAMETERS

Sym	Quantity	Value
L_{dc}	dc side inductance	0.01 H
L_{sh}	resonance inductance	0.068 H
C_{sh}	resonance capacitor	150 µF
R_{sh}	resonance resistance	16 Ω
R_{load}	load resistance	15 Ω
L_{load}	load inductance	0.1 H
R_s	network resistance	1 Ω
L_s	network inductance	0.01 H
R_{line}	line resistance	2 Ω
L_{line}	line inductance	0.01 H
R_f	fault resistance	0.1 Ω

$$2\pi f = \frac{1}{\sqrt{LC}} \tag{1}$$

In order to determine the performance of the investigated FCL circuit, five different fault types are used. Fig. 6- Fig. 10 shows the grid currents during fault conditions. Fig. 6- Fig. 8 shows the currents in fault conditions occurring between phase and ground. When TABLE II, which shows the highest current value in the transient state at the time of failure, is examined, the maximum value of the current increases up to 599 A in the event of a fault (*PG*) between phase-A and ground. In case of a fault occurring between phase-A and phase-B and ground (*PPG*), it is 620 A. In the case of an inter-phase short circuit (*PP*) between phase-A and phase-B, the current is 736 A, while in the case of a short circuit between three phases (*PPP*), the current is 714 A. With the use of FCL, the current reduction rate in the current value is 78.57%, 77.83%, 77.83%, 77.83%, 68.89% and 74.47%, respectively, as shown in the table. In this case, the largest reduction is realized in the *PG* case. TABLE III shows the values and rates of change of the currents without FCL and with FCL at steady-state in case of fault. In case of *PP* fault, the current decreased from 2030 A to 373.1 A with the lowest rate of change of 91.62%. In other cases, the currents decreased from approximately 2330 A to 391 A, a change of 83.2%.

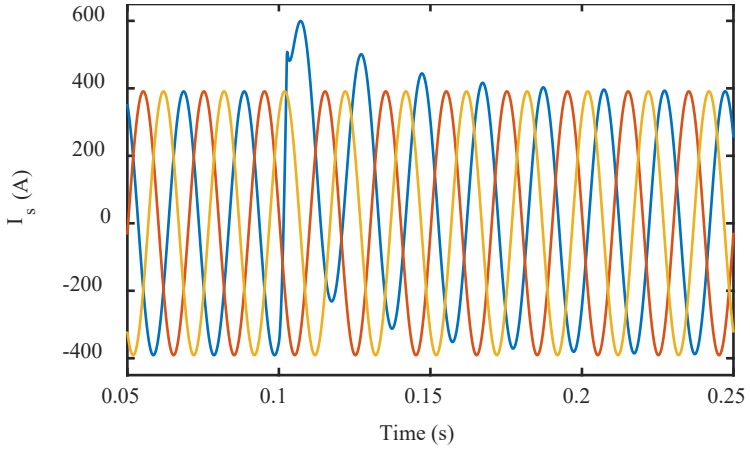

Fig. 6. Three-phase grid current variation in case of *PG* fault

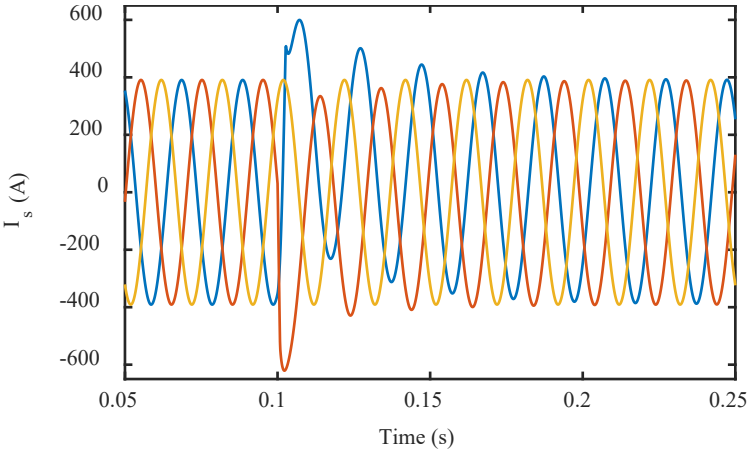

Fig. 7. Three-phase grid current variation in case of *PPG* fault

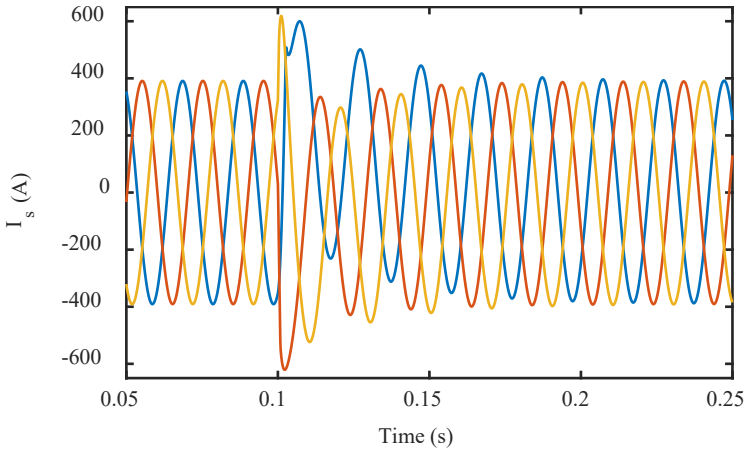

Fig. 8. Three-phase grid current variation in case of *PPPG* fault

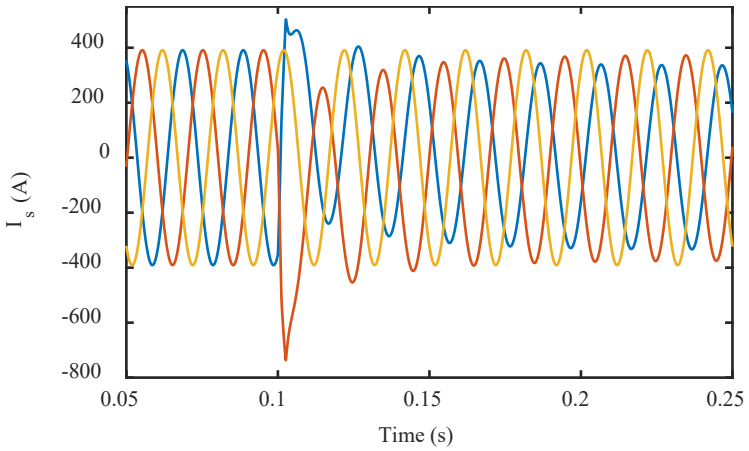

Fig. 9. Three-phase grid current variation in case of *PP* fault

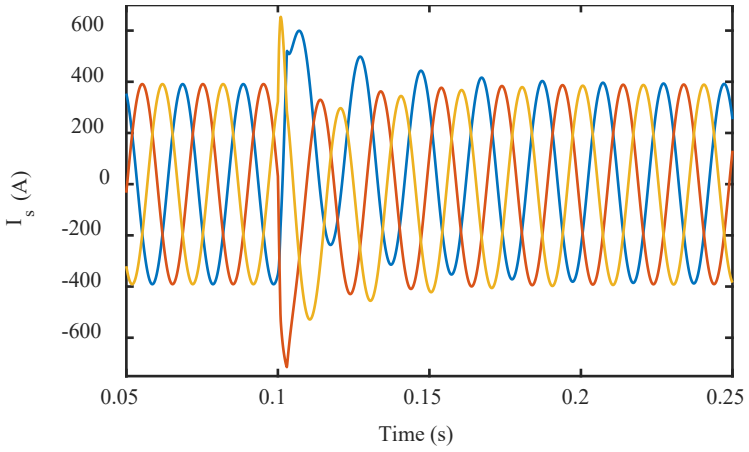

Fig. 10. Three-phase grid current variation in case of *PPP* fault

TABLE II
MAXIMUM CURRENT VALUES IN TRANSIENT

FAULT TYPE	CURRENT WITHOUT FCL	CURRENT WITH FCL	RATE OF CHANGE
PG	2,796 A	599.24 A	78.57%
PPG	2,800 A	620.78 A	77.83%
PPPG	2,800 A	620.90 A	77.83%
PP	2,368 A	736.66 A	68.89%
PPP	2,800 A	714.76 A	74.47%

TABLE III
MAXIMUM CURRENT VALUES IN STEADY-STATE

FAULT TYPE	CURRENT WITHOUT FCL	CURRENT WITH FCL	RATE OF CHANGE
PG	2,329 A	391 .4 A	83.19%
PPG	2,329 A	391.4 A	83.19%
PPPG	2, 330A	391.5 A	83.20%
PP	2,030 A	373.1 A	81.62%
PPP	2,330 A	391.1 A	83.21%

The R_{sh} resistor in the FCL resonance circuit is used to suppress the oscillation during resonance. Although the value of this resistance affects the damping amount, it also affects the PCC voltage value because it changes the current drawn from the grid at the time of the fault. TABLE IV shows the effective values of the PCC voltage depending on the R_{sh} resistance and the change rates compared to the nominal operation. If the resistance is 20 Ω, the PCC voltage at the fault moment and at the nominal operating moment remains constant. Fig. 11 shows the change in the rms value of the PPC voltage in case of *PPP* fault. Although the voltage value changes due to the oscillation at the time of the fault, the voltage value in steady state returns to its pre-fault value. Thus, other loads fed from the point of common are not affected by the situation. Therefore, when determining the value of this resistance, its effect on voltage as well as resonance damping should be taken into account.

TABLE IV
PCC VOLTAGE DUE TO FCL RESISTANCE

FCL RESISTOR (R_{SH})	PCC VOLTAGE (V_{PCC})	NOMINAL PCC VOLTAGE	RATE OF CHANGE
10	11.06192	10.64507	3.92%
13	10.91032	10.64507	2.49%
16	10.78277	10.64507	1.29%
20	10.64923	10.64507	0.04%
25	10.52971	10.64507	-1.08%
30	10.44743	10.64507	-1.86%

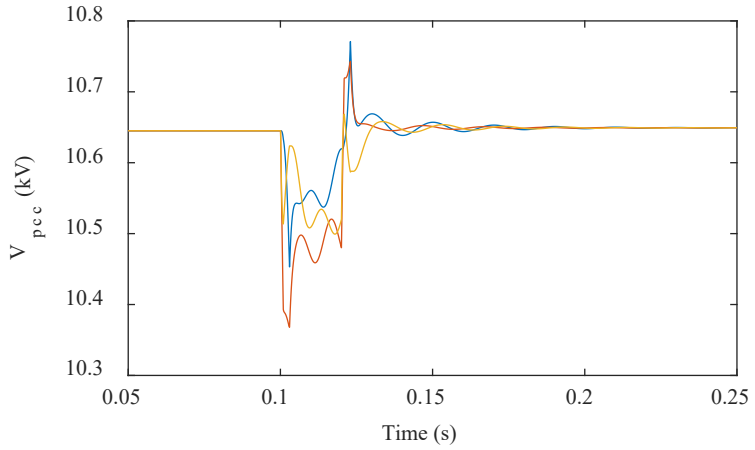

Fig. 11. PCC voltage for R_{sh}=20 Ω

IV. CONCLUSION

In this study, the performance of bridge type parallel resonance power electronics based FCL, which is one of the fault current limiters used to suppress the fault current in case of short circuit faults occurring in electrical networks, is examined in different short circuit situations. In the simulation study conducted in the Simulink, FCL performance is examined for phase-to-ground, two-phase-to-ground, three-phase-to-ground, phase-to-phase and three-phase short circuit faults. According to the results obtained, in the absence of FCL in these fault types, the highest temporary fault current was 2,800 A in *PPG*, *PPPG* and *PPP* fault cases, while the lowest fault current was 2,368 A in the *PP* fault case. In case of *PG* fault, the current reached 2,796 A. In case of using bridge type parallel resonance FCL examined in the study, a decrease of up to 78.57% is achieved in these fault current values. When the steady state values of the current are examined, the fault currents at 2,030 A and 2,330 A are reduced to 373.1 A and 391.4 A, and 81.62% and 83.2% change rates are obtained. In addition, the effect of the value of the damping resistor in the FCL circuit on the PCC voltage was examined, and it is seen that in this system, at a resistance value of 20 Ω, the value of the *PCC* voltage after the fault is the same as before the fault. Depending on the value of the resistance, there is an increase and decrease in voltage and this should be taken into account in the design. These results show that the bridge-type parallel resonant FCL circuit is an effective method against short circuit faults.

REFERENCES

[1] Q. Zhang, B. Xiang, L. Li, M. Yang, Z. Yuan, Z. Tang, Z. Liu, Y. Geng, and J. Wang "Current-Limiting Characteristics of a Variable Resistive Type SFCL With Different Branch Lengths," IEEE Transaction on Applied Superconductivity, vol. 34, no.8, Art no. 5601305.

[2] M. Gu, Z. Dongye, L. Qiu, and G. Li, "A Full-Bridge Self-Activated Solid State Fault Current Limiter," IEEE 6th International Electrical and Energy Conference (CIEEC), Hefei, China, 2023, pp. 2874-2877.

[3] O.H. Eyuboglu, B. Dindar, and O. Gul, "Series Resonance Type Fault Current Limiter for Fault Current Limitation and Voltage Sag Mitigation in Electrical Distribution Network," 2nd Global Power, Energy and Communication Conference (GPECOM), Izmir, Turkey, 2020, pp. 256-261.

[4] M. A. H. Sadi and M. H. Ali, "Lyapunov Function Controlled Parallel Resonance Fault Current Limiter for Transient Stability Enhancement of Power System," North American Power Symposium (NAPS), Fargo, ND, USA, 2018, pp. 1-6.

[5] A. T. Queiroz et al., "Development of a Hybrid Fault Current Limiter," in IEEE Transactions on Applied Superconductivity, vol. 34, no. 3, pp. 1-5, May 2024, Art no. 5601105.

[6] S. -C. Ko and S. -H. Lim, "Analysis on Magnetizing Characteristics Due to Peak Fault Current Limiting Operation of a Modified Flux-Lock-Type SFCL With Two Magnetic Paths," in IEEE Transactions on Applied Superconductivity, vol. 26, no. 4, pp. 1-5, June 2016, Art no. 5601605.

[7] M. Gu, Z. Dongye, L. Qiu and G. Li, "A Full-Bridge Self-Activated Solid State Fault Current Limiter," 2023 IEEE 6th International Electrical and Energy Conference (CIEEC), Hefei, China, 2023, pp. 2874-2877.

[8] S. Yadav, G.K. Choudhary and R.K. Mandal, "Review on Fault Current Limiters," International Journal of Engineering Research & Technology (IJERT), vol. 3, no. 4, pp. 1595-1603, April 2014.

[9] M. Ghorbani, M. Firouzi, B. Mozafari and F. Golshan, "Power flow management and LVRT enhancement by using multi-functional capacitive bridge-type fault current limiter in DFIG system," International Journal of Electrical Power & Energy Systems vol. 148, June 2023, Art no. 108810.

[10] H. Radmanesh and A. Heidary, "Bridge Type Series Resonance Transient Current Limiter for Medium-Voltage Smart Grids Application," 10th Smart Grid Conference (SGC), Kashan, Iran, 2020, pp. 01-05.

[11] J. Hasan, M. R. Islam, M. R. Islam, A. Z. Kouzani and M. A. Parvez Mahmud, "Implementation of Capacitive Bridge-Type Superconducting Fault Current Limiter to Improve the FRT Capability of DFIG Based Wind Generator," 2020 IEEE International Conference on Applied Superconductivity and Electromagnetic Devices (ASEMD), Tianjin, China, 2020, pp. 1-2.

[12] M. A. Islam, M. S. Alam, A. Rahman, M. A. Abido, F. S. AL-Ismail and M. F. Amink, "Modified bridge type fault current limiter based protective framework for Inverter Based Distributed Generation system," 2020 11th International Conference on Electrical and Computer Engineering (ICECE), Dhaka, Bangladesh, 2020, pp. 165-168.

[13] F. Jiang et al., "Design Consideration of a Dual-Functional Bridge-Type Fault Current Limiter," in IEEE Journal of Emerging and Selected Topics in Power Electronics, vol. 8, no. 4, pp. 3825-3834.

[14] M. Abdolkarimzadeh, M. Nazari-Heris, M. Abapour and M. Sabahi, "A Bridge-Type Fault Current Limiter for Energy Management of AC/DC Microgrids," in IEEE Transactions on Power Electronics, vol. 32, no. 12, pp. 9043-9050, Dec. 2017.

[15] D. Baimel et al., "New type of bridge fault current limiter with reduced power losses for transient stability improvement of DFIG wind farm," Electric Power System Research, vol. 197, August 2021, Art no. 107293.

[16] S.E. Naghibi, M. Mirzaie and T. Barforoshi, "Interline bridge-type fault current limiter: A novel approach for limiting fault current in distribution network," Electrical Energy Systems, vol. 30, no. 5, May 2020.

[17] H. Radmanesh and S.H. Fathi, "Parallel resonance type fault current limiting circuit breaker", High Voltage, vol. 5, no. 1, Feb 2020, pp. 76-82.

Sustainable Management of Water Resources: Strategies, Challenges and Implementation Recommendations

Özgül Çimen Mesutoğlu[*,1]

[*]: ozgulcimen@gmail.com, ORCID: 0000-0002-6704-8645
[1]: *Department of Environmental Engineering, Aksaray University, Aksaray, Türkiye*

Abstract: Water resources are facing a significant global crisis due to rapid population growth, industrialization, urbanization, and the pressures of climate change. The sustainable management of these resources is crucial to addressing this crisis and ensuring future water security. This study provides an in-depth analysis of the strategies proposed for the sustainable management of water resources, the challenges faced in this context, and the opportunities that can be leveraged to overcome these challenges. Integrated Water Resources Management (IWRM) and watershed management approaches are highlighted as critical tools for ensuring the equitable and balanced management of water resources. These approaches aim to safeguard both the quantity and quality of water while ensuring the sustainability of ecosystem services. Additionally, the integration of innovative technologies in water management, from advanced monitoring systems to the reuse of wastewater, offers a wide range of solutions that promote the efficient use of water. This study also examines the major challenges encountered in water management. Climate change has induced significant alterations in the water cycle, leading to issues such as droughts, floods, and severe degradation of water quality. In this context, the development and implementation of climate adaptation strategies are essential for the protection of water resources. Furthermore, enhancing institutional cooperation and public participation in water management is crucial for the effective implementation of policies. Finally, this study presents strategic recommendations based on successful case studies and key findings from the literature on sustainable water resource management. The protection, efficient use, and sustainable management of water resources are fundamental to securing a reliable water supply for future generations. In this regard, the development of new policies and strategies in water management is seen as a vital step towards resolving the water crisis.

Keywords: *Sustainable water management, IWRM, Innovative water technologies, Watershed management, Water security*

I. INTRODUCTION

Water resources are facing unprecedented pressures globally due to rapid population growth, urbanization, industrialization, and the intensifying effects of climate change. As the demand for water continues to rise, the availability and quality of freshwater are becoming increasingly uncertain, leading to significant challenges in water security. These challenges are compounded by the degradation of ecosystems, inefficient water use, and insufficient governance structures that fail to address the complexities of water management in a holistic manner [1-2].

In this context, the sustainable management of water resources has emerged as a critical priority for both policymakers and practitioners. Ensuring a balance between water use and ecosystem preservation, while meeting the needs of present and future generations, requires innovative strategies and collaborative efforts across sectors [3]. Integrated Water Resources

Management (IWRM) and watershed management approaches offer comprehensive frameworks for addressing these challenges, emphasizing equitable distribution, efficient use, and long-term sustainability [4].

This paper provides an in-depth analysis of sustainable water management strategies, the challenges posed by current environmental and socio-economic conditions, and the opportunities for leveraging new technologies and practices. Furthermore, it explores the role of institutional cooperation and public participation in enhancing water governance and policy implementation [5]. Through the review of successful case studies and literature, this study offers key recommendations for developing resilient water management policies that address both immediate needs and long-term sustainability goals.

II. GLOBAL WATER CRISES: CAUSES AND IMPLICATIONS

The global water crisis is driven by a combination of factors, including rapid population growth, urbanization, industrialization, and the increasing impacts of climate change. The world's population is expected to reach 9.7 billion by 2050, significantly increasing the demand for water in agriculture, industry, and domestic use [6]. Urbanization, particularly in developing countries, intensifies the pressure on local water supplies, as cities require vast amounts of water to sustain their populations. Additionally, industrial processes continue to consume and pollute significant water resources, exacerbating water shortages and quality degradation [7]. Climate change further complicates this scenario by altering precipitation patterns, reducing snowpack in critical regions, and intensifying the frequency and severity of droughts and floods. These changes not only disrupt water availability but also affect the quality of water resources, as increased flooding can lead to contamination of water supplies and damage to water infrastructure. The implications of this crisis are profound, affecting food security, economic development, and public health across the globe.

III. SUSTAINABLE WATER RESOURCE MANAGEMENT: THE ROLE OF INTEGRATED APPROACHES

Sustainable water resource management requires holistic and integrated approaches that consider the interconnectedness of water systems, ecosystems, and human activity. IWRM is one such approach that has gained significant traction in recent years. IWRM promotes the coordinated development and management of water, land, and related resources to maximize economic and social welfare without compromising the sustainability of vital ecosystems [8].

Watershed management, as a subset of IWRM, focuses on managing water resources within a defined watershed, ensuring that water use within the boundaries is sustainable and that ecosystems are preserved. This approach is particularly effective in regions facing water stress, as it helps allocate water equitably among various users while maintaining ecosystem services. Watershed management also encourages local stakeholders' involvement, ensuring that water management policies reflect the needs and priorities of the communities most affected by water scarcity [9].

IV. TECHNOLOGICAL INNOVATIONS IN WATER MANAGEMENT

One of the most promising aspects of modern water resource management is the application of advanced technologies to improve water efficiency, monitoring, and quality control. Emerging technologies, such as smart water meters, remote sensing, and real-time water quality monitoring systems, allow for more accurate data collection and decision-making in water management [10]. These tools help water managers optimize water distribution and usage, reducing waste and improving overall efficiency.

Additionally, the reuse of wastewater has become a critical component of sustainable water management. Wastewater treatment technologies allow for the recovery of clean water from

industrial, agricultural, and municipal waste streams, reducing the strain on freshwater sources. This circular approach to water uses not only extends the life cycle of water but also mitigates environmental impacts associated with wastewater discharge into natural water bodies.

V. CLIMATE CHANGE ADAPTATION IN WATER RESOURCE MANAGEMENT

Climate change is one of the greatest threats to water security, and adapting to its impacts is essential for ensuring sustainable water management. Climate adaptation strategies in water management focus on building resilience to changing precipitation patterns, reducing the risks of extreme weather events, and improving the flexibility of water supply systems [11]. For example, investments in water storage infrastructure, such as reservoirs and aquifers, can help mitigate the impacts of drought by providing reliable water supplies during dry periods.

Moreover, improving the efficiency of water use through the adoption of water-saving technologies and practices is critical in regions experiencing increasing water scarcity. Governments and water management institutions must prioritize the development of climate-resilient policies that account for future uncertainties, ensuring that water resources are managed in a way that anticipates and responds to the evolving challenges posed by climate change [12].

VI. INSTITUTIONAL COOPERATION AND PUBLIC PARTICIPATION IN WATER GOVERNANCE

Effective water management requires more than just technological solutions; it demands strong institutional cooperation and public participation. The fragmented nature of water governance, where different agencies and levels of government are responsible for various aspects of water management, often leads to inefficiencies and conflicts [13]. To address this, stronger coordination between institutions is essential to ensure that water policies are implemented effectively and equitably.

Public participation is another key element in achieving sustainable water management. Engaging local communities in decision-making processes fosters a sense of ownership and responsibility, leading to better compliance with water conservation measures. Public awareness campaigns and education programs also play a vital role in promoting water-saving behaviors and reducing water waste at the household and community levels [14].

VII. STRATEGIC POLICY RECOMMENDATIONS FOR SUSTAINABLE WATER MANAGEMENT

Based on successful case studies and the latest research, several strategic policy recommendations can be made to enhance the sustainable management of water resources. First, governments should prioritize the development of comprehensive water management policies that integrate environmental, social, and economic objectives [15]. These policies should focus on water conservation, improving infrastructure for water delivery, and protecting ecosystems that provide essential water services.

Second, investments in new water technologies should be promoted to improve water efficiency and management practices. This includes supporting research and development of innovations in water reuse, desalination, and advanced monitoring systems [3]. Finally, fostering institutional cooperation and ensuring that all stakeholders, including local communities, are involved in the water management process is crucial for the long-term sustainability of water resources [1].

VIII. CONCLUSION

The sustainable management of water resources is a pressing global challenge, driven by factors such as rapid population growth, industrialization, urbanization, and the increasingly severe impacts of climate change. This study has highlighted the importance of integrated

approaches, particularly IWRM and watershed management, as effective frameworks for addressing the complex demands on water resources. These approaches ensure not only the equitable distribution of water but also the preservation of critical ecosystem services, which are essential for long-term water security.

Technological innovations in water management, including advanced monitoring systems and wastewater reuse technologies, offer promising solutions for improving water efficiency and ensuring that limited freshwater resources are used sustainably. However, the challenges posed by climate change, such as more frequent droughts, floods, and water quality degradation, necessitate the adoption of climate adaptation strategies that enhance the resilience of water management systems.

Institutional cooperation and public participation are critical for the successful implementation of water management policies. Engaging communities and fostering collaboration among institutions ensure that policies are more effectively executed and that water resources are managed in a way that meets the needs of all stakeholders.

In conclusion, securing a reliable water supply for future generations requires the protection, efficient use, and sustainable management of water resources. This study emphasizes the need for comprehensive policy development, technological innovation, and stronger governance frameworks to address the ongoing water crisis. By adopting integrated strategies and fostering collaborative efforts, the path toward resolving the water crisis and ensuring water security for future generations becomes attainable.

REFERENCES

[1] P.H. Gleick, The World's Water Volume 8: The Biennial Report on Freshwater Resources, Island Press, 2018.

[2] United Nations, The United Nations World Water Development Report 2020: Water and Climate Change, Paris: UNESCO, 2020.

[3] C.J. Vörösmarty, P.B. McIntyre, M.O. Gessner, D. Dudgeon, A. Prusevich, P. Green, P.M. Davies, Global threats to human water security and river biodiversity. *Nature, 467*(7315), 555–561, 2010.

[4] Global Water Partnership, *Integrated Water Resources Management in Action*, Retrieved from https://www.gwp.org, 2017.

[5] C. Pahl-Wostl, P. Jeffrey, N. Isendahl, M. Brugnach, Maturing the New Water Management Paradigm: Progressing from Aspiration to Practice. *Water Resources Management, 25*(3), 837–856, 2010.

[6] A. Abou-Shady, M.S. Siddique, W. Yu, A Critical Review of Recent Progress in Global Water Reuse during 2019–2021 and Perspectives to Overcome Future Water Crisis. *Environments,* 10(9), 159, 2023.

[7] A. Saravanan, P. Senthil Kumar, S. Jeevanantham, S. Karishma, B. Tajsabreen, P.R. Yaashikaa, B. Reshma, Effective water/wastewater treatment methodologies for toxic pollutants removal: Processes and applications towards sustainable development, *Chemosphere*, 280, 130595, 2021.

[8] B.U. Ngene, C.O. Nwafor, G.O. Bamigboye, A.S. Ogbiye, J.O. Ogundare, V.E. Akpan, Assessment of water resources development and exploitation in Nigeria: A review of integrated water resources management approach, *Heliyon*, 7(1), e05955, 2021.

[9] G. Wang, S. Mang, H. Cai, S. Liu, Z. Zhang, L. Wang, J.L. Innes, Integrated watershed management: evolution, development and emerging trends. *Journal of Forestry Research,* 27, 967–994, 2016.

[10] J. Park, K.T. Kim, W.H. Lee, Recent Advances in Information and Communications Technology (ICT) and Sensor Technology for Monitoring Water Quality, *Water*, 12(2), 510, 2020.

[11] Y. Zhang, B.M. Ayyub, J.F. Fung, Z.M. Labe, Incorporating extreme event attribution into climate change adaptation for civil infrastructure: Methods, benefits, and research needs, *Resilient Cities and Structures*, 3(1), 103-113, 2024.

[12] S. Ahmad, H. Jia, A. Ashraf, D. Yin, Z. Chen, C. Xu, W. Chenyang, Q. Jia, Z. Xiaoyue, M. Israr, R. Ahmed, Water resources and their management in Pakistan: A critical analysis on challenges and implications, *Water-Energy Nexus*, 6, 137-150, 2023.

[13] M. Nouri, M. Homaee, L.S. Pereira, M. Bybordi, Water management dilemma in the agricultural sector of Iran: A review focusing on water governance, *Agricultural Water Management*, 288, 108480, 2023.

[14] J.M.A. Echeverría, Cross-country evidence for social dimensions of urban water consumption during droughts, *Journal of Cleaner Production*, 260, 120895, 2020.

[15] C. Seijger, P. Hellegers, How do societies reform their agricultural water management towards new priorities for water, agriculture, and the environment?, *Agricultural Water Management,* 277, 108104, 2023.

Brain Tumor Detection and Classification from MRI Images

Abdullah Burhan DOĞAN*[,1], Onur ERBAY[1], Enes DEVECİOĞLU[2], Mahmut BÜYÜKBAŞ[3]

[1:] abdullahburhan.dogan@agu.edu.tr, ORCID: 0009-0001-8693-5063
[1,2,3] *Department of Electrical & Electronics Engineering, School of Engineering, Abdullah Gül University, Kayseri, TÜRKİYE*

Abstract: Classification of brain tumors with good prediction accuracy is important for the treatment of patients. In this article, a comprehensive analysis is performed to determine whether the tumor is Glioma, Meningioma or Pituitary tumor type in brain MRI images. In the proposed project, tumor types will be analyzed by making necessary applications in terms of image processing and machine learning. Initially, pre-processing analysis is performed to improve the quality of MRI images and increase the accuracy of subsequent stages, and then the tumor parts of the images were segmented using the segmentations. After that, more than 100 Radiomic features of the images of the tumor area were extracted. Among these extracted features, 14 features were selected using the Correlation Attribute selection method, then these features were used to train the computer, and the images were classified using the Support Vector Machine (SVM) Algorithm. By optimizing this Support Vector Machine (SVM) Algorithm through the WEKA application, the accuracy rate was increased further. After classification, the results have shown that it can classify a total of 3064 MRI images into their own classes with approximately 93% accuracy.

Keywords: *Brain Tumor classification, feature extraction, feature selection, image segmentation*

I. INTRODUCTION

The brain is the most important human part in perceiving and reacting to external influences. It is the most important organ that controls a person's reactions and provides abilities such as thinking, feeling and remembering, that is, what makes a person human. Therefore, it is very important for people to have a healthy brain in order to sustain their lives. However, one of the biggest threats to the human brain is brain tumors. Brain tumors are caused by cancer cells. Brain tumor is a dangerous disease that reduces the efficiency of the human nervous system and causes abnormalities in the control of the immune system. There are generally two types of brain tumors: malignant and benign. While benign tumors are the type that do not harm them and can be treated with early diagnosis, malignant tumors are quite dangerous because they can spread to other cells and cause dangerous, irreversible damage to brain cells.

To be able to detect and analyze the tumors and their characteristics Magnetic Resonance Imaging (MRI) currently being used. It can sometimes be difficult to detect a brain tumor from images obtained using MRI technology due to various reasons such as the image being noisy. For this reason, in the proposed project, a system will be designed to assist doctors and radiologists by identifying tumor characteristics according to their presence using image processing and machine learning techniques. Thus, it is aimed to obtain a more accurate classification.

The chosen brain tumor dataset contains 3064 T1-weighted contrast-enhanced images from

233 patients with three kinds of brain tumors: meningioma (708 slices), glioma (1426 slices), and pituitary tumour (930 slices). The images were acquired at Nanfang Hospital, Guangzhou, China, and General Hospital, Tianjin Medical University, China, from 2005 to 2010 using spin-echo-weighted images with a 512 × 512 matrix. The pixel dimensions of the images are 0.49×0.49mm², the slice thickness is 6 mm, the slice gap is 1 mm and the Gd dose was 0.1 mmol/kg at a rate of 2 ml/s [2].

Hence, the fundamental motivation of this study is to detect and classify three different types of brain.

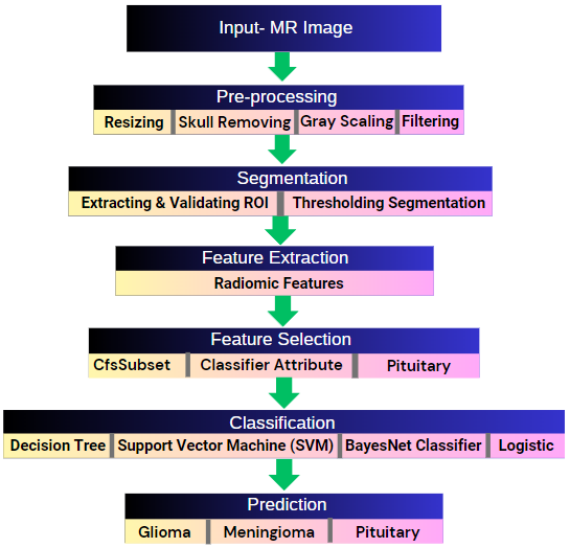

Fig. 1. *Block Diagram of the Proposed System*

II. LITERATURE REVIEW

The detection of brain tumor from MR images was searched by many researchers due to the significance of the problem. There is much research in the field of breast cancer diagnosis of ultrasonographic images. Magnetic Resonance Image (MRI) plays a significant role in diagnostic brain tumor imaging. The manual segmentation for cancer diagnosis of brain tumor and generation of MRI images in clinical routine is difficult and time-consuming [5]. For that reason, numerous works have been done on brain tumor classification in recent years. Yang et al. [3] proposed the CBIR (Content-Based Image Retrieval) method to evaluate a large image dataset. This method considers the tumor region as a query and tries to find a tumor that has the same pathological properties. The system used MID (Margin Information Descriptor) as the feature. It illustrates the image content by using the surrounding tissue of a tumor. Their proposed system was able to achieve a precision of 89.3%. But the distance metric determined by their methods is globally linear, and it disappoints to produce many local projections for separate regions. Furthermore, their system is developed using manual segmentation of the brain tumor. Furthermore, P. Gamage (2017) determined a brain tumor with the help of various image processing techniques. The objectives of medical image processing are to determine efficient and correct information about using images with minimum errors. MRI is used to get the images of cancerous tissue of the human body due to its better quality and high resolution as compared to some other imaging technologies. To take the image of a brain tumor by MRI image is difficult due to the complexity of the brain. MRI images are used for processing and to segment the brain tumor. Tumor can be segmented by using techniques of image segmentation. The process of determining brain tumor by using MRI images can be divided into four categories such as image classification, preprocessing, feature extraction and image segmentation [5]. Recent studies have highlighted the significance of deep feature extraction and classification in brain MR images. Machine learning algorithms have the advantage of directly learning representative features from images.

III. METHODOLOGY

For extracting the features from the images, a few important steps and processes need to be executed in rightly analyzing the machine learning project. Initially, the images are resized to achieve consistency in the size. Then, the images are converted to grayscale to facilitate the operations on the grayscale representation. Sharpening operations are applied to the images to enhance the overall sharpness and to emphasize the edge information. Median filtering technique also provides the controlled blur and reduces the noise. This method also preserves the parts of edges. Contrast-limited adaptive histogram equalization (CLAHE) is applied to enhance the contrast and highlight the differences between black and white regions. However, there exist possibilities that the processes will introduce the data loss and artifacts. To address this, the linked component technique is used to accurately remove the distractors and to detect the breast region. The Region of Interest (ROI) is extracted, and the masking operations are performed. The ROI-specific features are obtained after discarding the unnecessary parts of the picture. Gray Level Co-occurrence Matrix (GLCM), Gray Level Size Zone Matrix (GLSZM), Gray Level Run Length Matrix (GLRLM), shape-based features and first-order statistical features are some of the features that can be extracted using the radiomic packages. It must be noted that the feature selection is important as not all the characteristics extracted from the Radiomic matrices are relevant. The most relevant characteristics from the extracted set are selected using different techniques, such as feature selection algorithms. Finally, the investigation is carried out in the detailed modelling phase.

A. Pre-Processing

Preprocessing of images is crucial for subsequent tasks such as ROI extraction and feature extraction. By applying preprocessing steps, images become suitable for masking and ROI extraction. In the images of Glioma Pituitary and Meningioma tumors, which are 3 different tumor types in the data set, both the location of the tumors is different, and the MRI images are taken from different angles. This situation has increased the importance of the operations to be performed in pre-processing. To overcome these differences in the data set, the images were transferred to the MATLAB environment and the following methods were applied respectively. First, the images were converted to grayscale (Fig 2). Grayscale images occupy less space and make subsequent calculations simpler, reducing the processing time. Performing these operations does not affect the picture and the next steps because the picture is already gray. In addition, the images will already be binarized in the final stages of pre-processing. After this process, Skull Removing was applied to the images (Fig 3.a). The purpose of this process is to get rid of unnecessary areas in the image. In MRI images, pixels in the skull parts have high intensity values. Getting rid of these pixels also increases the efficiency in the segmentation section. After this step, the images were resized (Fig 3.b). The purpose of resizing is to facilitate future processes and increase processing speed by reducing the size of the image. Then, median filter was applied to the images. (Fig 4.a). The main reason for this is that the median filter filters out the noise in the image while preserving the details and edges in the image. This filter was chosen because tumors often have distinct edges. CLAHE (contrast limited adaptive histogram equalization) was used as the last step of pre-processing. (Fig 4.b). The reason for this is to make the details more visible by improving the contrast of the picture. At the same time, CLAHE divides the image into small blocks and applies histogram equalization separately, which gives homogeneity to the image. As a result of the difficulty in selecting some tumors in the data set, it was decided to use this method.

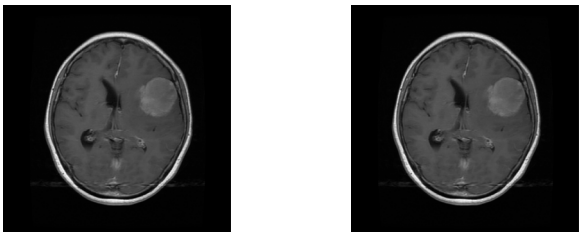

***Fig 2**, a. Original Dataset Image (left), b. Grayscale converted Image (right)*

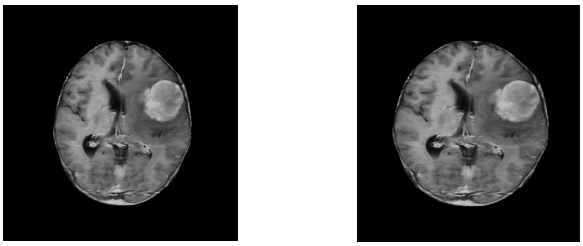

***Fig 3**, a. Skull Removed Image (left), b. Resizing Applied Image (right)*

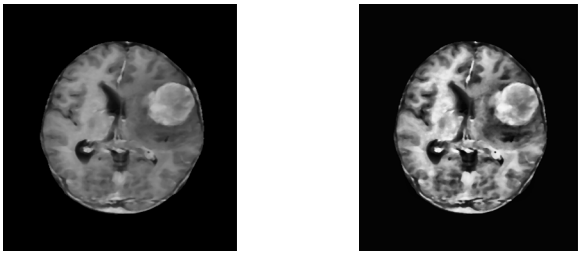

***Fig 4**, a. Median Filtered Image (left), b. CLAHE Applied Image (right)*

B. Extraction of ROI

In this study, thresholding segmentation was used to extract ROI to accurately segment three different brain tumors. Thresholding segmentation is a basic image processing technique that distinguishes objects in the image based on their intensity values. Since the pixel intensity values of the tumors in the images are generally high, above-average threshold values were determined and the tumor areas were extracted, and the surrounding brain tissue was isolated. This method enabled the identification and demarcation of tumors based on their unique density characteristics. The use of thresholding, accuracy and reliability of the segmentation process were ensured by comparing the mask images in the data set with our own segmented image (Fig 5). How the comparison is done; Mismatched pixel positions were determined by overlapping the two existing mask images (Fig 6). These non-matching pixels are marked in red. In addition, the percentage of matching parts was calculated, and a 98% match was observed.

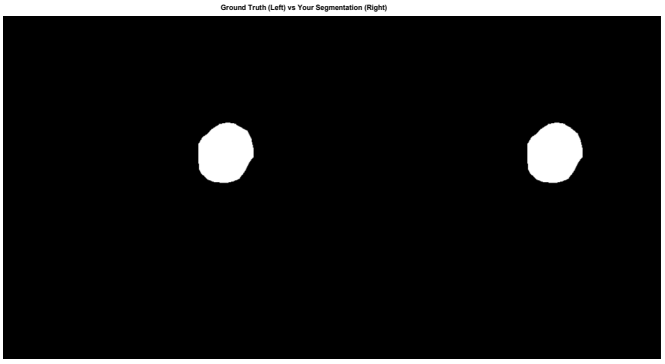

***Fig 5**, Data set mask (left), Result of Thresholding Segmentation (right)*

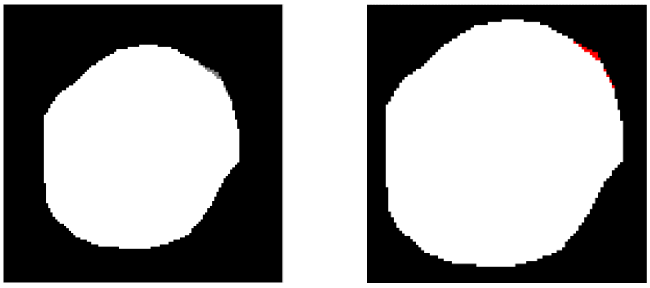

***Fig 6**, Overlayed and Zoomed Image (left), Unmatched pixels highlighted with red (right)*

C. Feature Extraction

Radiomic features are features that provide important quantitative information about disease diagnosis, prognosis and treatment processes with data obtained from medical images. In this project, the radiomic feature extraction method was applied as the feature extraction method. More than 100 features from 7 headings of Radiomic features were calculated using MATLAB with feature formulas and built-in functions, and an Excel file was printed. The names of these titles are: First Order Statistics, Shape-based (2D), Gray Leve Co-occurrence Matrix (GLCM), Gray Level Run Length Matrix (GLRLM), Gray Level Size Zone Matrix (GLSZM), Gray Level Dependence Matrix (GLDM). Small Area Low Gray Level Emphasis (SALGLE) [4].

First Order Statistics analyzes pixel intensities and distribution in images. These features are based on the histogram of each pixel value. Provides general information about textures in images. Median, variance, standard deviation, energy, and entropy can be given as examples of major first order features.

Shape-based (2D) features analyze the geometric and morphological features of the tumor region in the ROI in the images. Examples include Mesh Surface, Pixel Surface, Perimeter, Sphericity, Elongation, Major Axis Length.

Gray Level Co-occurrence Matrix (GLCM) analyzes the gray level relationships between pixels in an image with a given distance and direction. It is important in extracting textural features. Defines the characteristics of patterns and textures. Examples include Joint Average, Cluster Shade, Correlation, Difference Entropy. Gray Level Size Zone Matrix (GLSZM) analyzes the sizes of pixel regions that are at the same gray level in an image. It characterizes the textural structures and size distribution of homogeneous regions in images. Examples are Small Area Emphasis, Zone Variance, Zone Entropy, Small Area Low Gray Level Emphasis (SALGLE). Gray Level Run Length Matrix (GLRLM) focuses on the lengths of consecutive pixels at the same gray level. It is also used in the characterization of homogeneous regions and textural structures in the image. Examples include Short Run Emphasis, Long Run Emphasis, Run Length Non-Uniformity, Run Percentage. Gray Level Dependence Matrix (GLDM)

It measures the dependence between the gray level in a pixel and the gray level of neighboring pixels. It provides information about textural adherence and homogeneity from the picture. Small Dependence Emphasis, Large Dependence Emphasis, and Gray Level Non-Uniformity can be given as examples. Neighboring Gray Tone Difference Matrix (NGTDM) controls the gray tone differences of pixels in an image with neighboring pixels. These features determine textural patterns and local contrasts in the image. It calculates the gray tone differences between neighboring pixels and extracts statistical features. Examples include Busyness, Complexity, Strength, and Coarseness.

D. Feature Selection

The literature has a variety of feature selection methods, but not every one of them is appropriate for selection in terms of model accuracy and precision. The accuracy of these selection methods may vary from data set to data set, so the selection method that is most

suitable for the data set to be processed should be chosen. While feature selection was implemented through the Weka application, after research, it was decided that the CfsSubset, Classifier Attribute and Correlation Attribute selection methods were suitable for the selected data set.

Correlation Attribute selection method is directly measuring the first-order relationship to the class. Helps eliminate unnecessary features by identifying highly correlated features and finally reduces the complexity of the model and increases performance of the model. The working principle of the Correlation Feature selection method is that it first calculates the correlation of each feature with the class, then selects the features with high correlation and finally deletes unnecessary features as expressed in figure 7.

***Fig.** 7. Feature Selection Visualization*

After all these processes, 14 features were selected among more than 100 extracted features. Below, the extracted features used for the proposed project [4].

1. Large Area Low Gray Level Emphasis (LALGLE)
2. Long Run Low Gray Level Emphasis (LRLGLE)
3. Energy
4. Complexity
5. Low Gray Level Zone Emphasis (LGLZE)
6. Autocorrelation
7. Low Gray Level Run Emphasis (LGLRE)
8. Small Dependence Emphasis (SDE)
9. Low Gray Level Emphasis (LGLE)
10. Contrast
11. Cluster Shade
12. Mean
13. Total Energy
14. 90th percentile

E. Classification

In machine learning, classification is a form of supervised learning where an algorithm is trained on data with labels for each input. During the training phase, the classifier understands how the features, extracted from the MRI images, are related to the labels. After the training the classifier, it can predict the label of new, unseen MRI images based on their features. This prediction process assists in automating and enhancing the precision of diagnoses. Evaluating and comparing performance of classifier can be done by using a variety of classifiers, such as decision tree, support vector machine or neural network. It is critical to choose the classifier with the highest performance metrics includes accuracy, precision, recall and F1 score. Thus, the system can guarantee a strong and reliable model which improves the diagnostic process and possibly results in better patient outcomes.

In the proposed system, classification is a crucial step to automatically classify MRI images into specific categories which are glioma, meningioma, and pituitary tumor types. In this work, python was mostly utilized for the classification step. In addition, WEKA was used to compare

the results obtained from python and to be sure about the results. After selecting the features from WEKA by using correlation attribute function, different classifiers were implemented in python to classify three tumor types based on the selected features. The implemented classifiers are Logistic Regression classifier, Support Vector Machine (SVM), Decision Tree, K-Nearest – Neighbours (K-NN) and Bayesian Network. The main purpose of using different types of classification algorithms is to observe their performance and select the classifier with the best performance because the performance of these algorithms can vary from dataset to dataset. It is essential to describe the classifiers briefly to give basic ideas.

Decision tree is an algorithm for supervised machine learning that constructs tree-like models. It categorizes information into more and more specific groups: from "tree trunk," to "branches," to "leaves." It utilizes the if-then principle from math to generate sub-groups that fit within larger categories and enables accurate, organic classification [1].

The k-Nearest Neighbors (k-NN) algorithm is a technique in pattern recognition that saves and understands training data by assessing their relationships to other data points in an n-dimensional space. K-NN seeks to identify the k most similar data points in upcoming, unfamiliar data. In text analysis, k-NN assigns a specific word or phrase to a specific category by determining its closest neighbor, with the value of k determined by a majority vote of neighboring words. If k equals 1, it will be categorized into the class closest to 1 [1].

Support Vector Machines (SVM) are strong and efficient machine learning algorithms that convert your data into a linear decision space. The algorithm finds the best hyperplane in the linear decision space to divide your training data into various categories like meningioma or glioma. SVM excels at distinguishing things that are closely related. For example, all the instances within one category could be alike, whereas some instances in another category could be quite dissimilar. This makes it perfect for classification tasks that are easily separable with a linear boundary, which is not applicable to all classification tasks [1]

Logistic regression is essentially an expanded version of linear regression that permits the handling of classes. This is done by categorizing forecasts into a specific group using a certain probability limit. It is used for binary classification where sigmoid function is used, that takes input as independent variables and produces a probability value between 0 and 1. For that reason, logistic regression is not an appropriate classifier for this system [1].

Naive Bayes classifiers are a type of linear classifiers that assume a feature's value is unrelated to the value of any other feature. This implies that Bayes' theorem can be used to determine the likelihood of a specific label based on our data by examining each feature separately, without taking into account potential interactions between features. Naive Bayes classifiers are commonly utilized in text categorization due to the straightforward nature of calculating probabilities based on frequencies, and text usually contains a high volume of features (such as individual word tokens). They are also commonly used in identifying spam, as they can handle the complexity of email data without causing overfitting [1].

These classifiers were applied one by one on selected features in python. After application, these classifiers were again optimized in python. The reason for the optimization is to clearly see the classifier that gives the highest performance. For example, before optimization the decision tree may give a higher accuracy rate, whereas after optimization the highest performing classifier may be SVM. The performance evaluation includes accuracy, recall, precision and F1 score. Before providing the classifier results, it is beneficial to get an idea about these metrices. [1]

Accuracy evaluates the accuracy of the model by calculating the percentage of accurate predictions made throughout the dataset. It is determined by dividing the total of true positives (TP) and true negatives (TN) by the overall sample size.

$$Acc = \frac{TP+TN}{TP+TN+FP+FN} \quad (1)$$

Precision evaluates the ratio of accurate positive predictions to all positive predictions generated by the model. It is determined by dividing TP by the sum of TP and false positives (FP).

$$Precision = \frac{TP}{TP+FP} \tag{2}$$

Recall, also known as sensitivity, calculates the ratio of correct positive predictions out of all positive instances. The calculation is based on TP divided by the sum of TP and false negatives (FN).

$$Recall = \frac{TP}{TP+FN} \tag{3}$$

The F1 Score is a measurement that weighs both precision and recall equally. It is determined by taking the harmonic mean of precision and recall. The F1 Score is beneficial when aiming for a combination of high precision and high recall, as it punishes very low values of both aspects.

$$F1\ Score = 2 \times \frac{Precision \times Recall}{Precision+Recall} \tag{4}$$

In addition, training sets and test sets distributed with different percentages were used to obtain better performance metrics. In the results obtained, it was seen that the percentage split with 33% test set gave better performance, and the classification and optimization processes were applied according to this distribution.

F. Validation

In machine learning, merely training the model on the data is not enough to ensure accurate results on real-world data. It is essential to verify that the model has correctly grasped the patterns from the data and is not overfitting with excessive noise. The cross-validation technique is utilized in order to accomplish this in this study. K-fold cross validation and leave-one-out (LOOCV) were utilized and compared with each other to test the model and prevent overfitting. For the K-fold cross validation, different number of folds were tried to observe the effect of the number of folds on the performance of the classifier.

K-fold cross validation is a method utilized in machine learning for assessing how well a model performs on data it has not been trained on. This process includes separating the data into different sections or subsets, selecting one of these sections as a validation set, and training the model on the rest of the sections. This procedure is carried out several times, with a new fold being used as the validation set each time. Ultimately, the outcomes from every validation stage are combined to create a stronger evaluation of the model's performance. For example, number of folds (K) is chosen 10 for the figure 5.1. Thus, the dataset divided into 10 subsets, 10 iterations has been created and, in each iteration, there are 9 training set folds one 1 test fold as visualized in Figure 5.1. Each subset has the chance of becoming test fold for K-fold cross validation.

Fig.8. *Visualization of 10-fold Cross Validation*

For LOOCV cross validation method, it is performed training on the whole dataset but leaves only one data-point of the available dataset and then iterates for each data-point. In LOOCV, the model is trained on n-1 samples and tested on the one omitted sample, repeating this process for each data point in the dataset. It has some advantages as well as disadvantages also. An advantage of using this method is that we make use of all data points and hence it is low bias. The major drawback of this method is that it leads to higher variation in the testing model as it is testing against one data point. If the data point is an outlier it can lead to higher variation. Another drawback is it takes a lot of execution time as it iterates over 'the number of data points' times. It can be expressed that LOOCV is the extreme version of K-fold cross validation [6].

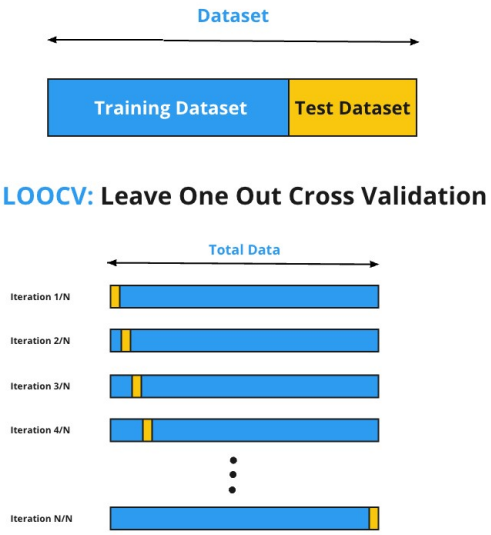

Fig.9. *Visualization of LOOCV*

IV. RESULTS

As a result, the images were processed as explained in the methodology. Before the feature extraction, pre-processing as resizing, grayscale conversion, skull removing, median filtering, and contrast limited adaptive histogram equalization (CLAHE) were successfully implemented on most of the images. Thanks to the pre-processing in MATLAB, the masks of the images were generated, and ROIs were extracted by using thresholding segmentation. However, there are visual problems on some of the images especially meningioma and pituitary tumor types, such that the masking could not detect the tumor region properly, and those images are not proper for further process which is ROI. During the pre-processing and extraction of ROI, the reason for getting along with MATLAB and not Python is that in the image processing side is having more experiences in MATLAB.

In the feature extraction part, radiomic features were extracted by using MATLAB-based feature extraction. There are more than 100 radiomic features extracted from ROI of the MR images via MATLAB. Among these features, the most outstanding features for classification were selected in WEKA by using correlation attribute. After the feature selection, classification step was implemented in python for five different classifiers to compare their performances. To choose the most appropriate one among selection methods, each of them was applied to the extracted features separately and Accuracy values were obtained as seen in table 1. Based on these accuracy values, the Correlation Attribute selection method was chosen.

Also, the performance of the classifiers was observed before the optimization and after the optimization. The results given are obtained from 33% test set and 66% training set percentage split.

As can be seen in table 2, decision tree has the best performance with the accuracy rate of 0.8711. In this case, it can be chosen as model classifier for further processing. However, it is crucial to optimize the whole classifier before choosing one of them.

Classifiers	Selection Method	Precision	Recall	F- Measure	Accuracy
J48 (Decision Tree)	CfsSubset	0.866	0.866	0.866	0.848
SMO (Support Vector Machine)		0.876	0.874	0.875	0.874
BayesNet		0.822	0.825	0.823	0.826
Logistic		0.898	0.898	0.895	0.896
J48 (Decision Tree)	Classifier Attribute	0.867	0.867	0.867	0.848
SMO (Support Vector Machine)		0.873	0.872	0.872	0.872
BayesNet		0.824	0.827	0.825	0.828
Logistic		0.899	0.899	0.899	0.896
J48 (Decision Tree)	Correlation Attribute	0.91	0.91	0.91	0.9097
SMO (Support Vector Machine)		0.902	0.902	0.902	0.9027
BayesNet		0.847	0.850	0.846	0.85101
Logistic		0.905	0.905	0.905	0.9078

Table 1. *Selection Techniques Comparison Table*

RESULTS / METHODS	Accuracy	Precision	Recall	F1 Score
Logistic Regression	0.464	0.154	0.333	0.211
Support Vector Machine	0.768	0.522	0.666	0.574
Decision Tree	0.8711	0.836	0.837	0.836
K Neighbors Classifier	0.836	0.796	0.784	0.785
BayesNet	0.784	0.736	0.6996	0.6698

Table 2*. Performance metrices before the optimization*

RESULTS / METHODS	Accuracy	Precision	Recall	F1 Score
Logistic Regression	0.915	0.895	0.893	0.893
Support Vector Machine	0.931	0.912	0.915	0.913
Decision Tree	0.889	0.859	0.862	0.860
K Neighbors Classifier	0.908	0.885	0.882	0.883
BayesNet	0.870	0.840	0.840	0.840

Table 3. *Performance metrices after the optimization*

After the optimization in python, the best performance metrices belongs to the Support Vector Machine with the accuracy rate of 0.931 as demonstrated in table 3. From this result, it should be noted the importance of classifier optimization. Moreover, the process implemented in python was done by using WEKA as well. It also concluded that the best classifier for this model was SVM. As a result, SVM was chosen as classifier of the proposed model with the accuracy of 0.931.

As mentioned before, cross validation must be implemented to prevent the model from overfitting because training the model on the data is not enough to ensure accurate results on real-world data. For this purpose, K-fold cross validation with different number of folds was applied in python

Cross Validation / Methods	CV Accuracy (10-fold)	CV Accuracy (25-fold)	CV Accuracy (50-fold)	CV Accuracy (75-fold)	CV Accuracy (100-fold)
Logistic Regression	0.9013	0.902	0.9042	0.938	0.9028
Support Vector Machine	0.914	0.913	0.914	0.916	0.915
Decision Tree	0.889	0.891	0.893	0.893	0.897
K Neighbors Classifier	0.899	0.896	0.900	0.899	0.900
BayesNet	0.776	0.783	0.783	0.784	0.785

***Table 4**. K-fold cross validation results*

It is concluded that the SVM classifier is the most appropriate algorithm for the model. It has the best accuracy rate for 75-fold. The validation result shows that SVM algorithm classifies the tumor types without overfitting.

Accuracy Table	Cross Validation Type	
Classifiers	K-fold Cross Validation	Leave-one-out Cross Validation
Logistic	0.901	0.904
Decision Tree	0.889	0.907
SVM	0.914	0.919
K- Nearest	0.889	0.907
BayesNet	0.776	0.78

***Table 5**. Comparison of K-fold cross validation and LOOCV*

The main purpose of implementation of LOOCV is to observe the difference between K-fold cross validation and leave -one -out cross validation. The observation is just a small increase in the LOOCV for the SVM. Also, LOOCV results verify that the SVM model is operating without significant overfitting and with a good performance.

For the percentage split, it was mentioned 33/66 percentage split was utilized for all processes it gives better performance metrices. The result in accuracy for 33/66 percentage was 0.931 and the result in accuracy for 20/80 percentage split was 0.91.

In addition, the ROC curve was plotted using python to show that SVM is a better algorithm for this model. It is good to have AUC ratio near to 1 because it illustrates the better detection of the tumor with high true positive rate figure 6. SVM has the highest AUC value with 0.91.

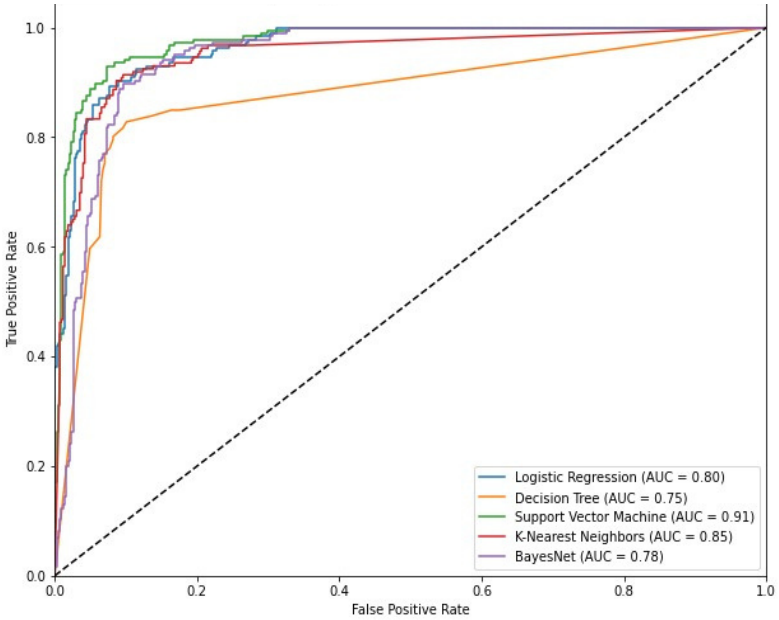

Fig 10. *ROC curve for classifiers*

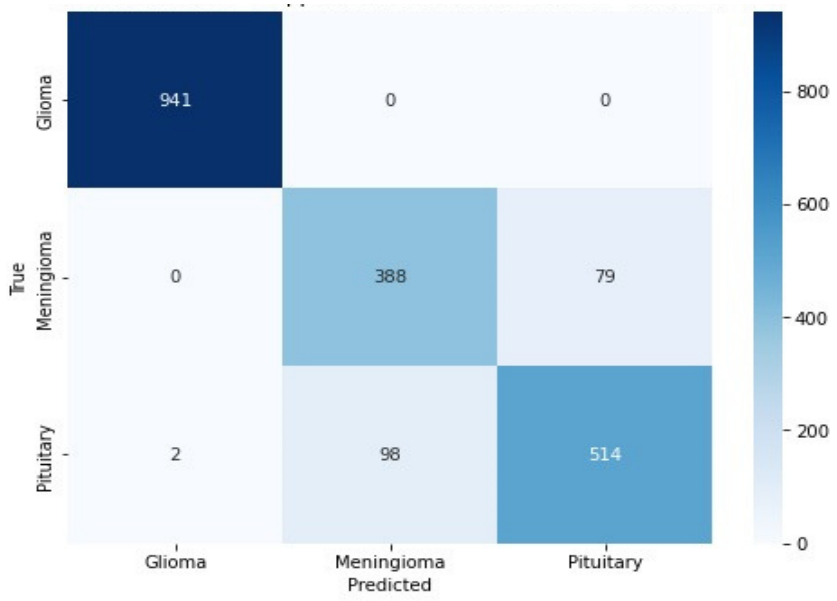

Fig 11. *Finalized confusion matrix of the system*

V. CONCLUSION

This research introduced an uncomplicated approach for categorizing tumor types from brain MR images. The method outlined in this study is useful for pinpointing tumor areas in MR images during digital processes. The approach included pre-processing the MR images to extract the ROI and get the image ready for masking. The region of interest was extracted by using the masks that were created in MATLAB. After extracting ROI, feature extraction involves taking out important characteristics from areas of interest following ROI. The features that were extracted were moved to the Weka software environment where additional tasks such as selecting features and categorizing them were carried out. After that, python was used for classification and validation tasks. The K-fold cross validation and leave one out cross validation (LOOCV) was employed as a model evaluation technique to mimic how the model will perform on new data samples. The outcomes of the evaluation show that the SVM algorithm is the most precise in terms of classification results for Correlation Attribute Selection. The study showed that the proposed method effectively identifies the tumor type, which is crucial for early detection. This research enhances tumor classification accuracy,

aiding in the creation of advanced diagnostic tools for brain tumor detection, resulting in better patient outcomes.

REFERENCES

[1] Abro, A. A., Khan, A. A., Talpur, M. S. H., Kayijuka, I., & Yaşar, E. (2021). Machine learning classifiers: a brief primer. University of Sindh Journal of Information and Communication Technology, 5(2), 63-68.

[2] Cheng, Jun (2017). brain tumor dataset. figshare. Dataset. https://doi.org/10.6084/m9.figshare.1512427.v5

[3] Das, S., Aranya, O. R. R., & Labiba, N. N. (2019, May). Brain tumor classification using convolutional neural network. In *2019 1st international conference on advances in science, engineering and robotics technology (ICASERT)* (pp. 1-5). IEEE. https://ieeexplore.ieee.org/stamp/stamp.jsp?tp=&arnumber=8934603

[4] Radiomic Features. Radiomic Features - pyradiomics v3.1.0rc2.post5+g6a761c4 documentation. (n.d.). https://pyradiomics.readthedocs.io/en/latest/features.html

[5] Varuna Shree, N., & Kumar, T. N. R. (2018). Identification and classification of brain tumor MRI images with feature extraction using DWT and probabilistic neural network. *Brain informatics*, *5*(1), 23-30. https://link.springer.com/article/10.1007/s40708-017-0075-5

[6] Wong, T. T. (2015). Performance evaluation of classification algorithms by k-fold and leave-one-out cross validation. *Pattern recognition*, *48*(9), 2839-2846.

Breast Tumor Classification on Ultrasound Images Using Image Processing and Machine Learning Methods

Yusuf SÜR*,1, Ahmet Serdar TUTAR[2], Serhat MIZRAK[3], Mahmut BÜYÜKBAŞ[4]

*yusuf.sur@agu.edu.tr, ORCID: 0009-0005-3315-2523
[1,2,3,4] *Department of Electrical & Electronics Engineering, School of Engineering, Abdullah Gül University, Kayseri, Turkey*

Abstract: Breast cancer is a dangerous type of cancer that is particularly common in women and can have fatal consequences. Early diagnosis plays a critical role as the risk of death increases considerably if it progresses. Ultrasound imaging is used in the detection phase. The purpose of using this type of imaging is that it gives better outputs according to the density of the breast tissue and can better select cancerous lesions. Detecting breast cancer in the early stages with ultrasound reduces the risk of death and allows for healthier conditions. In the project, tumor classification was tried to be completed by using a dataset containing a total of 789 images with online ready to use ultrasound breast outputs. The project basically aims to make breast images more easily processable, region segmentation, feature extraction from the segmented region and then tumor classification according to the extracted features. In this context, many features were extracted, especially radiomic features. In addition to machine learning, ResNet and Fully Connected Feedforward Neural Network deep learning algorithms were used to further improve the quality of the effect. The correlation-based feature selection approach used for classification then confirmed that radiomic features can produce even more accurate and effective results than other features extracted for ultrasound images. In the light of the results obtained, the highest accuracy rate with machine learning methods was 98.307% using the Random Forest method, while the Fully Connected Feed Forward Neural Network method, which deals with complex structures in deep learning, concluded the project with an accuracy rate of 97.967%.

Keywords: *Breast Tumor, Ultrasound Imaging, Early Diagnosis, Radiomic Features, Classification*

I. INTRODUCTION

In the last years of today's world, mankind is in a very serious battle with cancer. Cancer has become a serious event with a high probability of death. Breast cancer is one of the most dangerous of these. This type, which especially affects women, poses very serious problems. Among the main causes of this abnormal growth are unhealthy lifestyle, genetic favorability and environmental factors. Most cancer-based female deaths occur in patients with breast cancer. However, in case of early diagnosis, the risk of death is significantly reduced. For this reason, early diagnosis is especially vital in this type compared to other types. The growth of the detected cancerous tissues is prevented by various therapeutic methods and the quality of life is improved by increasing the chance of survival of the patients.

Breast cancer can be examined and investigated in many ways. The most used method is ultrasound imaging. Behind its widespread use, it also contains various problems. The measurements obtained can vary greatly depending on the patient's anatomy, the equipment used and the experience of the experts. Due to these variations, the algorithms developed can make it difficult to detect very sharp tumors on data sets obtained from people with different

anatomies. The quality of the elements in the dataset to be processed should be improved first and learning models with low margin of error and high generalization rate on different anatomical structures should be used. Another point to note is that tumor structures appearing on ultrasound images differ quite independently from each other. An illustrative example is that benign and malignant tumors have similar textural and dimensional characteristics. Likewise, there are tumors among benign types that appear benign but are malignant. The most important techniques to eliminate this problem are developing models using deep learning and neural networks.

In the light of these situations, the publicly available breast cancer dataset will be analyzed, and appropriate development and algorithms will be developed to address the above problems as a starting point. The basic principle is to develop a modeling that works in all disease versions and produces high results.

The main goal of the project is to help the experts working in this field as much as possible in early diagnosis and correct treatment stages in the light of algorithms that will accurately classify breast cancer as benign, malignant or non-cancerous based on ultrasound images. The developed models will be able to overcome the changes in US images and work with high accuracy in general patient variances and will speed up the process in clinical processing. As a result of this plot, the early diagnosis stage of individuals with breast cancer will be realized in the healthiest way and the quality of life will be improved.

II. MATERIALS AND METHODS

In this section, the operations performed on the dataset will be discussed in detail and explained section by section. The sections will be examined under headings such as pre-processing, segmentation, feature extraction, feature selection and classification. Residual Neural Network (ResNet) and Fully Connected Feedforward Neural Networks (FCFNN) sections will be focused on in depth.

2.1 DATASET

The data used in this study was obtained from the open-source Dataset of Breast Ultrasound Images with the link address https://doi.org/10.1016/j.dib.2019.104863 by Al-Dhabyani et al. (2020) was obtained as a result of their studies. There are a total of 780 breast ultrasound images in this dataset. The patients are between the ages of 25 and 75. There are 487 benign, 210 malignant and 133 normal images in the data set [1].

2.2 LITERATURE REVIEW

As we found in literature, university groups and researchers have various approaches to enhance the accuracy of cancer detection, especially for breast cancer. Researchers are providing approaches to the problem by proposing various way to extract the features and different neural network models to achieve the best accuracy. A specific area of research is comparing accuracy rates across different datasets, which helps identify the most effective methods for breast cancer diagnosis. Raino et al. [2] conducted a study focused on this aspect, examining the precision and reliability of various datasets to better understand which ones offer the best results. Our dataset is renamed as BC US in article and performance table, which corresponds to Breast Cancer Ultrasound, and researchers claims that maximum accuracy is 77.5% percent for the CNN models that used this dataset.

For instance, Zhuang et al. [3] developed an automated system for classifying benign and malignant breast tumors, achieving a precision rate of 92.86% with a comprehensive experimental process. Similarly, Eroglu et al. [4] combined features extracted from three different convolutional neural networks (CNN) in a hybrid structure to identify the optimal features for distinguishing benign, malignant, and normal breast tumors. The support vector

machine (SVM) classifier demonstrated the highest accuracy, reaching a remarkable rate of 95.6%. These studies underscore the significant progress in using machine learning to improve breast cancer diagnosis through ultrasound imaging.

The Ultrasound Breast Cancer dataset has been the focus of numerous research articles. Tagnamas et al. [5] applied a convolutional neural network (CNN) architecture to this dataset and achieved an accuracy of 94.02%. Wang et al. [6] introduced a unique multiple-feature extraction network called MF-Net, with accuracy ranging from 84.29% to 97.32%, depending on the methods used for benchmarking. These differences in accuracy rates show how various methods can affect results. This emphasizes the need to try different approaches to achieve the best ways and accuracy to detect breast cancer.

2.3 PRE-PROCESSING

The dataset of ultrasound images contains images of very different structures. Some images are in perfect condition, while others are very difficult to analyze without processing. Therefore, it is necessary to pre-process all the images to cover all of them and bring them to the most reasonable level of analysis. In this way, all the images will be brought to their best condition, artifact-like noise and distortions will be removed, and tumor regions will be made the most prominent. The most important purpose of preprocessing is tumor differentiation, which, as mentioned before, varies according to anatomy. When the dataset is carefully examined, there are noisy and distorted structures in some images that are not tumors but behave like tumors. To develop good machine learning, such problems should be overcome, and the best forms of the images should be processed. The biggest advantage of preprocessing is to accurately extract the region of interest in the segmentation part. Preprocessed images will be quite ready for ROI. As mentioned before, some of the images have tumor-like regions intertwined, while some images even have abdominal cavity detail. Even the abdominal cavity has the shape of a tumor in these images, but logically it is not a tumor. With Preprocess, such problems will be avoided, and more accurate results will be obtained.

In the first stage of the preprocess, the images were resized. Since each image contains data from different age groups, the image sizes vary. To avoid any problems in the later stages of the algorithm, all images were resized. As a result of the first stage, a dataset consisting of US images with the same dimensions was created. Immediately after resizing, grey scale operation was performed in MATLAB environment in order to use image processing tools more easily. All images taken to the workspace were converted to gray level. The gray level images were made available for thresholding and binarization operations.

After gray level conversion, filters were applied to remove small noise and artifacts in the images. In the previous stage of noise removal, a Gaussian filter was applied to remove blurs and to break the artifact effect for further filters. Immediately after the Gaussian filter, the median filter was applied. With the median filter, images were obtained that were free of noise and artifacts. These filters were applied sequentially, one after the other, rather than separately, to further enhance the effect. As a result of the median filter, some parts of the tumor regions were observed to become blurred and diffuse due to the removal of ultrasound artifacts. For these reasons, the median output images were immediately subjected to sharpening.

Sharpening was intended to make the filtered images sharper. The pictures that were cleaned of noise during the filtering phase were made even sharper and easier to recognize even by eye. That's the whole point of sharpening. It helps to make sharp transitions and curvilinear structures even more pronounced and improves processing performance. When the sharpened images were analyzed, morphological operations were applied for region extraction, which will be used even more effectively in the next steps. First, erosion was applied to enlarge the sharpened regions and then opening was applied to make the image

quality ready for segmentation.

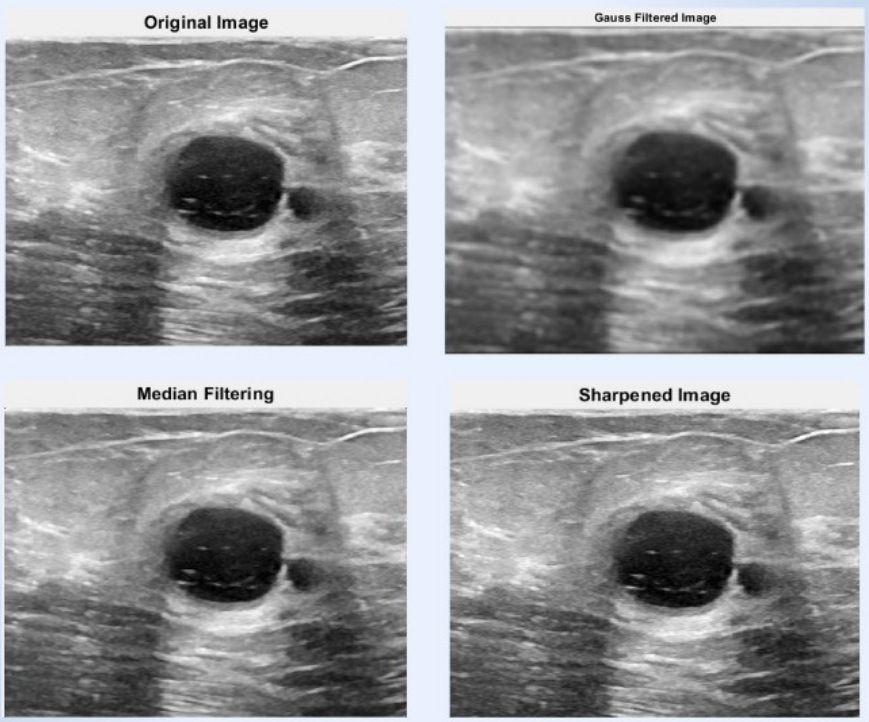

Figure 2.1. *Filtering Outputs*

2.4. SEGMENTATION

It is aimed to segment the images that are brought to the best form to be processed as a result of preprocessing. Segmentation is the process of identifying the tumor regions on the original image. Segmentation was achieved by applying multiple sub-stages one after the other [7]. The preprocessed images were first subjected to thresholding. Thresholding is a process that distributes according to the pixel values in the image and determines a threshold value and emphasizes the pixel values above it and reduces the dominance of the pixel values below it. This is the main purpose of the thresholding process. As mentioned before, some ultrasound images have distortion due to too much anatomical structure. These distorted regions will first be tried to be separated from their roughness as much as possible with the thresholding method. Another purpose of thresholding is to break the dominance of structures in the images that are not tumors but behave like tumors [8]. For example, in images where the abdominal cavity is included, the dominance of these cavity structures should be eliminated.

Thresholding has been used specifically for this purpose. It is well known that benign and malignant tumor structures cluster in a circular or rounded shape in certain regions. The pixel density of this clustering is quite high, but structures such as the abdominal and thoracic cavity are less dark and scattered in US images. Thresholding makes the densest clusters more prominent and reduces the effect of the remaining clusters that may cause misclassification [8]. Immediately after the thresholding process was completed, the complement, i.e. the inverse, of all the images was taken. This makes it easier to compare with the original masks in the dataset by whitening the tumor regions and blackening the remaining regions. In this way, it is possible to determine whether the correct region has been detected before proceeding to further steps.

After thresholding and complementing, Extraction of connected components was applied. Extraction of connected components image processing technique is an important method also used for feature extraction. It deals with the selection of the objects with the largest

relationship with each other. With the thresholding process, tumor regions were made more prominent. Extraction of connected components will ensure that these regions are extracted correctly. Before this, a few preliminary morphological operations have to be performed as in the preprocess [9]. In the complemented thresholded image, there are inevitably some spots and unwanted regions. Likewise, some parts of the tumor regions are broken and distorted. The best way to eliminate these problems is to use morphological operations. The unwanted small point structures located outside the tumor regions are first reduced and destroyed by the erosion process. Then, the structural defects in the tumor regions were solved with the dilation method and the tumor regions were made in the best harmony with each other.

The code logic tries to detect the largest and most interconnected region of the tumor or non-tumor image given as input, which is round or round-like. In this sequence of events, the tumor region is subtracted from the original image [7]. The images that were optimized as a result of morphological operations were linked to the Extraction of connected components event. In this command, cc2bw, available under the image processing toolbox of MATLAB version 2024, on further optimization, provides line-connected component extraction such that the best result can be obtained. The code logic tries to detect the largest and most interconnected region of the tumor or non-tumor image given as input, which is round or round-like. In this sequence of events, the tumor region is subtracted from the original image.

Comparing the ROI found by image processing algorithms and the ready-made mask data in the dataset itself, the results show a high degree of similarity [9]. As an example, a benign tumor was analyzed. A benign tumor is a benign tumor whose distribution is not random but evenly distributed compared to malignant tumors. This is the type where the cc2bw connected components decomposition is the best. Considering the ready-made mask and the output of the algorithm, the results are almost identical, and we conclude that the algorithm works correctly.

The last step is to overlay the ROI obtained by image processing techniques on the original image. For this case, the ROI extracted image is multiplied with the original image. As a result of the multiplication process, tumor regions are marked on the original images for both malignant and benign tumor images. The images leave only the marked tumor region in its original state, while the remaining parts are completely black.

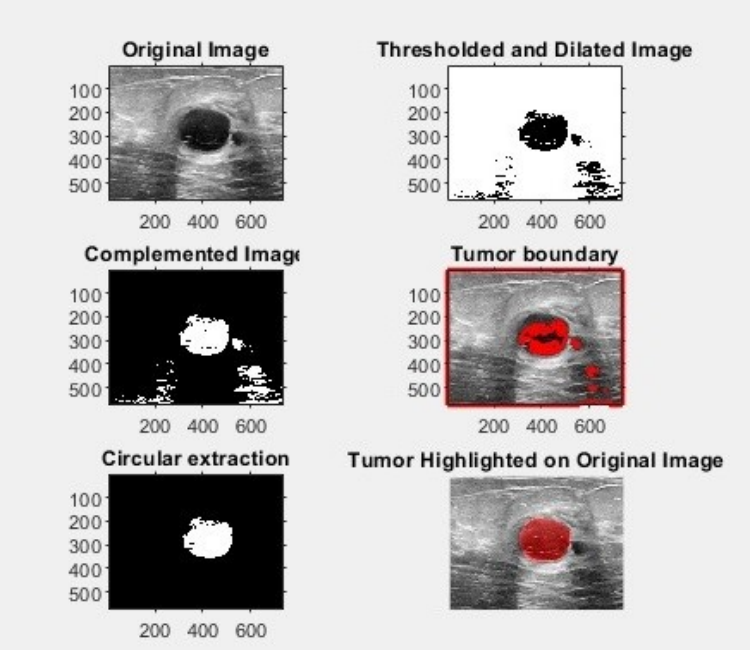

***Figure 2.2**. Image processing outputs*

2.5. FEATURE EXTRACTION

In recent years, the diagnosis of disease and the design of the necessary treatment plan has focused significantly on medical imaging. The most widely used method is ultrasound imaging. In order to extract the necessary features from the acquired images, objective analysis methods with high reproducibility and independence from human observation are tried to be obtained. The best way to accomplish this is feature extraction. Feature extraction is a measure of extracting distinctive segments of data from images in the most meaningful way [10]. The main goal is to arrive at small data sets that can make the images more navigable and the classification more useful and effective in the diagnostic phase. All discriminative factors such as patterns, textures, etc. are taken as input for further analysis methods. These features, which play a key role in important stages such as classification and segmentation, contain statistical, textural or subjective advance level information.

Ultrasound images are by their very nature the most difficult group of images to process and classify. The most difficult requirement is the sharp extraction of the right features. Therefore, radiomic features are most commonly extracted on the basis of accurate results. Radiomic features extract quantitative features from the data for classification characterization [11]. They are especially important in cancer status as they carry information about tumor distribution homogeneity, heterogeneity and microenvironment. The extraction of radiomic features ensures homogeneity by eliminating the different effects of the patient's anatomy. It represents the heterogeneity of the tissue and structure of the tumor mass, thus ensuring accurate diagnosis [12].

In the present study, radiomic feature extraction was considered for ultrasound breast images for the reasons described. Different methods and analysis techniques have been used for feature extraction. First order statistical features are one of them. It was used to analyze the intensity distribution and central tendencies of the image pixels, yielding a total of 19 features such as median mean deviation. Subsequently, the variable distribution of tumor intensity and distribution in the region allows the tumor type to be determined.

Afterwards, 2D and 3D features that are directly related to the shape and morphology of the ROI are extracted. The 3D features include 16 different features such as compactness, how much the shape resembles a sphere, volume, dimensions, etc., which contain information about the cancer type and make it easier to analyze the rate of spread. Likewise, in 2D features, 10 simple features such as cross-sectional area, radius and perimeter length were extracted.

The last feature extraction technique aims to extract texture features based on the direct structure of the tumor. The gray level co-probability matrix (GLCM) interprets the probabilistic relationship of two-pixel intensities. It contains a total of 24 features such as contrast, energy, and correlation, which provide data about the textural distribution. For example, the contrast value being higher than normal directly indicates the density of the tumor, while homogeneity, another criterion, examines the regular distribution.

The gray level run length matrix (GLRLM) considers the consecutive pixel lengths and frequency at the same gray level. Shape directionality and coarse structures therefore become more meaningful units. If the length is short, the malignant type is represented in the heterogeneous tissue distribution, if the length is long, the benign type is represented. In this way, 16 independent features were extracted based on such criteria.

The gray level size region matrix (GLSZM) provided 16 features that deal with the probabilistic size and dimensionality of homogeneously distributed regions. It analyzes how the regions vary in various gray level scales. Due to their nature, ultrasound images can be found in different shades of black, white and gray tones. For example, the presence of a large homogeneous region represents a denser tumor, while small regions represent a disseminated malignant tumor.

In the neighboring gray tone difference matrix (NGTDM) event, the tone difference is measured. The tone differences are found, and the difference order is extracted. Tumors with a complex and heterogeneous distribution show high tonal differences, while homogeneously distributed tumors show lower tonal differences. This is a feature that has the potential to be of great importance in distinguishing the type of cancer most clearly.

The gray level dependence matrix (GLDM) contains 14 features that analyze the statistical behavior of the intensity information and reveal its dependency. The dependency between pixels is revealed statistically. High dependency indicates homogeneous distribution, i.e. benign, while low level dependency represents heterogeneity, i.e. malignant.

As a result, the removal of radiomic features in ultrasound images allows for a more objective and highly processable analysis of the images. Disease types and the best treatment methods to be applied are diagnosed and detected at the earliest stages and patient health is protected [11]. In ultrasound outputs, where even specialist doctors can sometimes be in limbo and make wrong decisions, the best results are revealed by extracting such features and the aim is to classify the type of cancer, if any, and to apply the procedures to be applied accordingly without wasting time.

2.6. FEATURE SELECTION

Feature selection is one of the most important steps in machine learning to improve the performance of model evaluation and to interpret the results in a better quality [19]. Throughout the process, the features that will be most useful in classification should be selected and continued with these features. Otherwise, the model will be overwhelmed with unnecessary and repetitive features and produce disproportionate and illogical results. In addition, it reduces computational speed and cost in tumor detection in ultrasound imaging. Fast and accurate results are obtained by selecting the best data that gives the most accurate results.

In this project, a correlation-based approach was preferred in order to select the features correctly. The algorithm will check the connections between the features one by one and will not consider highly correlated features with the same information [12]. In MATLAB, this event corrcoef is used to examine the strength and direction information of the linear relationship between any two features. If the predetermined correlation coefficient of 0.95 between the pairs is above the threshold value, only one of these features is considered. This is a step taken to avoid repetition and to keep the model simple. It is important for machine learning interpretability to continue with only one of the pairs that are judged to have the same results.

The best 9 features with the highest correlation is selected at this stage. These can be considered as the most representative and meaningful structures of the model. These are Main Axis Length, Secondary Axis Length, Elongation, Volume Density, Area Density, Maximum Diameter, Area Density Convex Shell, Volume Density Convex Shell and Integrated Density. When processing in MATLAB, the correlation coefficients of the features are calculated with features array and those greater than 0.95 are selected. Therefore, sharp accuracy in determining the cancer type is established. Hence, model efficiency is increased overall, and reliable reproducible results are obtained independent of anatomical differences.

The feature selection process allows for increased model accuracy by removing redundant and repetitive data, and faster results at computational speed as less data is required [6]. Accordingly, the best and most information-rich features help to identify the cancer type. Subsequently, model accuracy and security are improved. Since the correlation method is the most efficient method, its importance is once again demonstrated.

2.7. CLASSIFICATION

Machine learning is an artificial intelligence discipline that involves computers learning

through experiences without the need for coding and using what they learn to facilitate complex tasks and make predictions on these tasks. There are different algorithms and applications developed for use in this field. In this study, Residual Neural Network, Fully Connected Feedforward Neural Networks, Support Vector Machine, Decision Tree and Random Forest methods will be explained.

2.7.1. RESIDUAL NEURAL NETWORK

In order to make the detection and early detection phase of breast cancer even easier to analyze, the use of a Residual Neural Network (ResNet) was applied in this phase of the study and satisfactory results were obtained.

The ResNet method is basically a structure developed to overcome the problem often referred to as gradient fading, which is used in deep learning [13]. Crossing the connections between the learning layers allows the operation of more complex networks. The ResNet algorithm tends to increase the learning capacity of the model by passing the data to be analyzed through the layers it determines within itself and then collecting the layer outputs obtained with the data entered into the structure [14]. Models with increased capacity can easily relate to deeper networks [15].

In this study, the ResNet algorithm was used to better define and analyze the models. The study produced results with a high accuracy rate that can be considered excellent in normal type, malignant type and benign type cases [14]. If the benign type is analyzed, a high accuracy value of 0.9705 was encountered as shown. For the malignant type, the accuracy value was 0.9666 and since there would be no distinction and difference in the normal part, a result of 1 was obtained. Considering the overall performance evaluation, the study was completed with a very satisfactory and high result of 98.76%.

When the confusion matrix is examined, the performance characteristics of the model in different types are shown. While 66 correct detections were found for the benign type, 2 were separated as false. The same analysis was done for the malignant type, but this time 29 correct discriminations were made with no incorrect ones. The same was done for normal with 20 correct cases. When it comes to the interpretation of the confusion matrix, it is observed that the model works with 100% accuracy for the normal and malignant type and with a high accuracy for the benign type due to reasons thought to be caused by the dataset.

The results show that using ResNet, breast cancer typing can be completed with a very high rate and clean results can be obtained. With an accuracy of 98.76%, the usability of the model is confirmed, and it is concluded that with the use of dataset, the model will play a critical role in typing and early detection.

2.7.2. FULLY CONNECTED FEEDFORWARD NEURAL NETWORKS

A fully connected feedforward neural network is a feedforward neural network with many layers of fully connected neurons. These types of networks are well suited and very well known for classification purposes in that sense. They learn deep structure in patterns, they can make accurate predictions. Fully connected layers in FCFNNs result in a multitude of architectures such that a neuron gets input from every neuron in the preceding layer to produce some output. This architecture is flexible in the sense that after learning the arbitrary function mapping between inputs and outputs, it can pass forward its activation generation to the next hidden layer. FCFNN operates in two main phases. They are feedforward and backpropagation phase. In the feedforward phase, input data is fed to the network and pushed through the network for each layer. In each hidden layer, it interprets the weighted sum of inputs by a nonlinear activation function to add nonlinearity to the model [16]. There are some differences between FCFNN and CNN. Although CNNs are created for exploiting the spatial hierarchies of feature in images, FCFNNs are best for the sequential datasets and other data in which the input-output relation is more complicated [17]. There are several

advantages of FCFNN over traditional CNN. Because of this, for example, they can process data where the relationships between the input and output are complex, and they are therefore more appropriate for tasks like breast cancer classification [18]. Additionally, since FCFNNs are computationally simpler than CNNs, they tend to be more computationally efficient in case of a large dataset [19].

The results of FCFNN in breast cancer classification is evaluated using some metrics. These include accuracy, precision, F-measure and confusion matrix. In our architecture, 98.8701% accuracy was achieved because of classification using FCFNN. Additionally, the complexity matrix shows the correct and incorrect classifications of the network.

2.7.3. SUPPORT VECTOR MACHINE

Support vector machines are also an effective method for solving classification and regression problems. This method, which is widely used, is preferred due to its fast estimation, low memory usage and accuracy rates [20].

The support vector machine will be actively used to classify the data in this study. SVM is an algorithm that tries to find the vector that will allow the most accurate classification of data points. Regardless of the capacity of the data set to decompose linearly creates the plane that will best separate and maximize the distance between the class planes [21]. Thanks to this decision limit, the data is tried to be classified in the most accurate way.

SVM first tries to find the hyperplane that is used to divide data into two classes in a multidimensional space. When finding this plane, the farthest distance between classes must be taken. When determining the distance, the data points closest to the hyperplane are called support vectors. Support vectors, which have a significant effect on the generalization capacity of the model, contribute to the determination of decision limits [22]. Even in cases where data is often not separated linearly in general, SVM ensures that data can be separated correctly thanks to vector planes.

With the SVM, our model achieved an impressive accuracy rate of 97.5169%, demonstrating its capability in effectively distinguishing between different types of breast tumors in ultrasound images.

Table 2.1. SVM Performance Table

Class	TP Rate	Precision	Recall	F-Measure	ROC Area
Benign	0,991	0,960	0,991	0,975	0,975
Malignant	0,914	0,980	0,914	0,946	0,969
Normal	1,000	1,000	1,000	1,000	1,000
Weighted	0,975	0,975	0.917	0,975	0,981

2.7.4. DECISION TREE

Another algorithm used in machine learning is the decision tree. It is widely used in classification problems. Visualizing it in the form of leaves and branches contributes to making the classification results more understandable. Low memory usage, pruning application, controls against overlearning, and fast classification of data in complex sets are among the reasons why it is preferred [23].

The decision tree creates nodes based on the selected features [24]. Of these nodes, the starting point is called the root node point, and the classification starts from there. Decision rules are applied at the nodes and branching points of the data. The endpoints of the decision tree are known as leaf nodes, and each leaf node gives rise to a class name in classification applications. The formation of branches or nodes is formed by criteria such as dataset and

information gain. Optimizing these criteria not only prevents over-learning, but also allows for a more accurate classification.

With the Decision Tree algorithm, our model achieved an impressive accuracy rate of 97.8555%, highlighting its effectiveness in accurately classifying various types of breast tumors in ultrasound images.

Table 2.2 Decision Tree Performance Table

Class	TP Rate	Precision	Recall	F-Measure	ROC Area
Benign	0,979	0,977	0,979	0,978	0,983
Malignant	0,979	0,962	0,952	0,957	0,979
Normal	1,000	0,996	1,000	0,998	0,999
Weighted	0,975	0,978	0,979	0,979	0,986

2.7.5. RANDOM FOREST

Random forest is one of the classification algorithms used in machine learning. Obtaining high-accuracy results and controlling overfitting is achieved by using at least two or more decision trees together [25]. However, the fact that it has a complex structure is one of its negative features in terms of cost and memory usage.

In the random forest method, data are randomly sampled, and different decision trees are created according to this distribution. The results of the values predicted by each decision tree are generated and voting is done on the predicted results and the result is generated by selecting the value with the most votes. Overfitting is prevented because the division points of the trees are randomly selected, and the results are located on these divisions. In addition, random sampling of data allows classification to be resilient to noise and missing data.

With the Random Forest algorithm, our model achieved an outstanding accuracy rate of 98.4199%, emphasizing its performance in classifying different types of breast tumors in ultrasound images.

Table 2.3 Random Forest Performance Table

Class	TP Rate	Precision	Recall	F-Measure	ROC Area
Benign	0.986	0.982	0.986	0.984	0.997
Malignant	0.962	0.971	0.962	0.967	0,995
Normal	1.000	1.000	1.000	1,000	1.000
Weighted	0.984	0.984	0.984	0.984	0.997

2.8. VALIDATION

Validation is one of the stages required to evaluate the performance of the model obtained in the machine learning process. The model is separated without connection, and performance values are obtained by performing train and test operations of the model through this separation. By randomly separating the model, it is learned how the model will perform on previously unknown sets [26]. Overfitting and underfitting situations are checked. There are methods such as hold-out, k-fold cross validation, stratified k-fold cross validation. Thanks to the Weka application, the number of folds required for validation was changed and validation was applied.

While validation, the data set is divided into training and test. Based on the 10-fold cross validation application made in the Weka, the process begins with the random separation of the set into 10 parts. Of these 10 parts, 9 parts are selected for train 1 part test Then this

process is repeated for k values and the results obtained are averaged. In this way, healthier and more reliable results can be obtained. The results are presented to the user such as accuracy, precision, recall and the success of the application is evaluated by the user.

The cross-validation application checks the overfitting status, examines the effects of the models on yet unknown sets, these features are one of the reasons why cross-validation is generally chosen in applications [27]. However, the disadvantages are that it requires high computational power and time and creates a complex structure. In addition, dividing the data set into appropriate values affects performance criteria.

Table 2.4 Cross Validation Table

Class	5 Fold Accuracy	10 Fold Accuracy	13 Fold Accuracy	16 Fold Accuracy
SVM	97.7427 %	97.5169 %	97.1783 %	97.6298 %
Decision Tree	97.8555 %	97.8555 %	98.0813 %	97.5169 %
Random Forest	98.4199 %	98.4199 %	98.307 %	98.4199 %
FCFNN	98.195%	98.415%	97.967%	98.076%
ResNet	98.220%	97.127%	97.089%	98.575%

Table 2.5 Overall Performance Table

Class	Accuracy	Precision	F-Measure
SVM	97.5169 %	0,975	0,975
Decision Tree	97.8555 %	0,978	0,979
Random Forest	98.307 %	0,984	0,984
FCFNN	98.8701 %	0.9858	0,9886
ResNet	98.76 %	0.9901	0,9838

III. CONCLUSION

This project has successfully created a detailed framework for classifying breast tumors using ultrasound images, focusing on radiomic feature extraction and leveraging sophisticated machine learning and deep learning algorithms. By employing meticulous pre-processing techniques to improve image quality and remove artifacts, we achieved accurate region segmentation, which served as a strong basis for precise feature extraction. Using a correlation-based feature selection method, we ensured that only the most pertinent features were included, enhancing both the efficiency and accuracy of our classification models.

The use of Residual Neural Networks (ResNet) and Fully Connected Feedforward Neural Networks demonstrated the power of deep learning in managing complex patterns and boosting classification accuracy. ResNet achieved an impressive overall accuracy of 98.76%, effectively distinguishing between benign, malignant, and non-cancerous cases. Similarly, the Fully Connected Feedforward Neural Network performed remarkably well, with an accuracy of 98.8701%.

Among the machine learning methods we used, the Random Forest algorithm proved to be the most effective, achieving the highest accuracy rate of 98.307%. This highlights the value of ensemble learning techniques in improving predictive performance. Additionally, Support Vector Machine and Decision Tree algorithms played significant roles in our comprehensive evaluation of various classification methods, each offering unique benefits in terms of speed, memory usage, and interpretability.

The validation process, cross-validation in MATLAB and Weka, confirmed the reliability and generalizability of our models. Interestingly, we observed minimal variation in performance metrics during cross-validation. We attribute this consistency to the large dataset size, which reduces fluctuations and ensures stable results across different validation folds. This crucial step ensured that our algorithms could perform effectively on unseen data, reducing the risks of overfitting and underfitting. The validation results demonstrated that our models maintained high accuracy and performance across various datasets.

In conclusion, integrating advanced pre-processing techniques, precise feature extraction, and advanced classification algorithms has led to a powerful tool for the early detection and accurate classification of breast tumors using ultrasound images. Our findings highlight the essential role of machine learning and deep learning in medical imaging, paving the way for future research and clinical applications. By enabling earlier and more accurate diagnoses, our models have the potential to significantly improve patient outcomes and enhance the effectiveness of breast cancer treatment. The success of this project underscores the importance of continuous innovation and the application of advanced computational techniques in the battle against breast cancer, ultimately aiming to improve patient's quality of life through timely and accurate medical interventions.

REFERENCES

[1] Al-Dhabyani, Walid, Mohammed Gomaa, Hussien Khaled, and Aly Fahmy. "Dataset of Breast Ultrasound Images." Data in Brief 28 (February 2020): 104863. https://doi.org/10.1016/j.dib.2019.104863.

[2] Rainio, O., Klén, R. Comparison of simple augmentation transformations for a convolutional neural network classifying medical images. *SIViP* 18, 3353–3360 (2024)

[3] Z. Zhuang, W. Ding, S. Zhuang, A.N. Joseph Raj, J. Wang, W. Zhou, C. Wei, Tumor classification in automated breast ultrasound (ABUS) based on a modified extracting feature network, Comput. Med. Imaging Graph. 90 (2021),

[4] Y. Eroglu, ˇ M. Yildirim, A. Çinar, Convolutional neural networks based classification of breast ultrasonography images by hybrid method with respect to benign, malignant, and normal using mRMR, Comput. Biol. Med. 133 (2021),

[5] Tagnamas, J., Ramadan, H., Yahyaouy, A. et al. Multi-task approach based on combined CNN-transformer for efficient segmentation and classification of breast tumors in ultrasound images. Vis. Comput. Ind. Biomed. Art 7, 2 (2024).

[6] Wang, J., Liu, G., Liu, D., & Chang, B. (2024). MF-Net: Multiple-feature extraction network for breast lesion segmentation in ultrasound images. Expert Systems with Applications, 249, 123798.

[7] Cervantes, J., Garcia-Lamont, F., Rodríguez-Mazahua, L., & Lopez, A. (2020). A comprehensive survey on support vector machine classification: Applications, challenges and trends. Neurocomputing, 408, 189-215.

[8] Khan, M. M., Islam, S., Sarkar, S., Ayaz, F. I., Kabir, M. M., Tazin, T., Albraikan, A. A., & Almalki, F. A. (2022). Machine learning based comparative analysis for breast cancer prediction. Journal of Healthcare Engineering, 2022, 1–15. https://doi.org/10.1155/2022/4365855

[9] Chen, C. W., Luo, J., & Parker, K. J. (1998). Image segmentation via adaptive K-mean clustering and knowledge-based morphological operations with biomedical applications. IEEE transactions on image processing, 7(12), 1673-1683.

[10] Scapicchio, C. et al., "A deep look into radiomics", La radiologia medica, 126(10):1296–1311, (2021).

[11] Liu, K., Kang, G., Zhang, N., & Hou, B. (2018). Breast cancer classification based on Fully-Connected Layer First Convolutional neural Networks.

https://www.semanticscholar.org/paper/Breast-Cancer-Classification-Based-on-Layer-First-Liu-Kang/2cd9dcc0fffaee438a7495778f9f4cea99d3095b

[12] Michael, E., Ma, H., Li, H., & Qi, S. (2022). An optimized framework for breast cancer classification using machine learning. BioMed Research International, 2022, 1–18. https://doi.org/10.1155/2022/8482022

[13] Gold, C., & Sollich, P. (2003). Model selection for support vector machine classification. Neurocomputing, 55(1-2), 221-249.

[14] Zhang, Y., Liu, Y. L., Nie, K., Zhou, J., Chen, Z., Chen, J. H., and Su, M. Y., "Deep Learning- based Automatic Diagnosis of Breast Cancer on MRI Using Mask R-CNN for Detection Followed by ResNet50 for Classification", Academic Radiology, (2023).

[15] Michalak, K., & Kwaśnicka, H. (2006). Correlation-based feature selection strategy in classification problems. International Journal of Applied Mathematics and Computer Science, 16(4), 503-511.

[16] Mayerhoefer, M.E. et al., "Introduction to radiomics", Journal of Nuclear Medicine, 61(4):488–495, (2020).

[17] Al-Haija, Q. A., & Adebanjo, A. (2020, September). Breast cancer diagnosis in histopathological images using ResNet-50 convolutional neural network. In 2020 IEEE International IOT, Electronics and Mechatronics Conference (IEMTRONICS) (pp. 1-7). IEEE. []

[18] Kohler, R. (1981). A segmentation system based on thresholding. Computer Graphics and Image Processing, 15(4), 319-338.

[19] Motlagh, M. H., Jannesari, M., Aboulkheyr, H., Khosravi, P., Elemento, O., Totonchi, M., & Hajirasouliha, I. (2018). Breast cancer histopathological image classification: A deep learning approach. BioRxiv, 242818.

[20] Aslam, M. A., Aslam, N., & Cui, D. (2020). Breast Cancer Classification using Deep Convolutional Neural Network. Journal of Physics. Conference Series, 1584(1), 012005. https://doi.org/10.1088/1742-6596/1584/1/012005

[21] Dai, B., Chen, R. C., Zhu, S. Z., & Zhang, W. W. (2018, December). Using random forest algorithm for breast cancer diagnosis. In 2018 International Symposium on Computer, Consumer and Control (IS3C) (pp. 449-452). IEEE.

[22] Pavlidis, P., Wapinski, I., & Noble, W. S. (2004). Support vector machine classification on the web. Bioinformatics, 20(4), 586-587.

[23] Sathiyanarayanan, P., Pavithra, S., Saranya, M. S., & Makeswari, M. (2019, March). Identification of breast cancer using the decision tree algorithm. In 2019 IEEE International conference on system, computation, automation and networking (ICSCAN) (pp. 1-6). IEEE.

[24] Venkatesan, E. V., & Velmurugan, T. (2015). Performance analysis of decision tree algorithms for breast cancer classification. Indian Journal of Science and Technology.

[25] Chudasama, D., Patel, T., Joshi, S., & Prajapati, G. I. (2015). Image segmentation using morphological operations. International Journal of Computer Applications, 117(18).

[26] Ahuja, A., Al-Zogbi, L., & Krieger, A. (2021). Application of noise-reduction techniques to machine learning algorithms for breast cancer tumor identification. Computers in Biology and Medicine, 135, 104576.

[27] Hall, M. A., "Correlation-based Feature Selection for Machine Learning", Department of Computer Scienc, (1999).

Çok Kriterli Karar Verme Yöntemleri ile Tedarikçi Seçimi

Supplier Selection with Multi Criteria Decision Making Methods

Miraçnur DOĞAN [*,1], Serkan KAYA [1]

[*] miracnurdogan@harran.edu.tr, ORCID: 0009-0007-3530-8645
[1] *Endüstri Mühendisliği Bölümü, Harran Üniversitesi, Şanlıurfa, Türkiye*

Özet: Firmaların sürdürülebilirliklerini korumaları ve rekabet avantajı elde etmeleri açısından tedarikçi seçimi önemli bir konu olmaktadır. Tedarikçi seçiminde karar vermeden önce tedarikçi seçim kriterlerinin ve alternatif tedarikçilerin seçiminde ve sıralamasında kullanılacak çok kriterli karar verme yöntemi önem arz etmektedir. Çok kriterli karar verme teknikleri, birçok kritere ve alternatife sahip organizasyonlara çözüm üreten yöntemlerdir. Çok kriterli karar verme problemlerinin çözümünde farklı yöntemler kullanılmaktadır ve bu yöntemler karar vericilere karar verme süreçlerinde önemli avantajlar sağlamaktadır. Bu çalışmanın amacı bir tekstil firmasının tedarikçi seçiminde etkili olacak olan kriterleri ve kriterlerin sahip oldukları önem ağırlıklarını belirlemek ve bu kriterler baz alınarak en uygun alternatifi seçmektir. Çalışmada kullanılmak üzere yedi adet kriter literatür ve alanında uzman kişilerden yararlanılarak belirlenmiştir. Problemin çözümü için MEREC ve CODAS teknikleri birleştirilerek hibrid bir yöntem geliştirilmiştir. Tedarikçi seçiminde belirlenen kriterlerin ağırlığını belirlemek amacıyla MEREC yöntemi kullanılmıştır. MEREC yöntemi, verilerin bağımsız ve objektif biçimde toplanmasına olanak tanımakla birlikte bireysel önyargıların en aza indirilmesine katkıda bulunduğu için tercih edilmiştir. MEREC yöntemi sonuçlarına göre en önemli kriter sektör deneyimi olurken en düşük önem seviyesine sahip kriter ürün fiyatı kriteri olmuştur. MEREC yöntemiyle hesaplanan kriter ağırlıkları göz önünde bulundurularak tedarikçi seçim ve sıralanmasında en güncel yöntemlerden olan CODAS yöntemi kullanılmıştır. CODAS yöntemi birbirleriyle çatışan kriterleri dengelemeye ve en iyi alternatif seçmeye olanak tanımaktadır. Dolayısıyla hem pozitif hem de negatif taraflar daha eşit bir şekilde göz önünde bulundurulabilir. CODAS yöntemi sonuçlarına göre A3 en uygun alternatif seçilirken bir sonraki en uygun alternatif tedarikçi ise A1 seçeneği olmaktadır. CODAS ve MEREC yöntemlerinin bütünleşik olarak kullanılması, karar vericilere karar verme süreçlerinde yardımcı olduğu görülmektedir. Elde edilen sonuçlar firmanın tedarikçi seçim probleminin en iyi şekilde çözüldüğünü göstermiştir.

Anahtar kelimeler: *Çok Kriterli Karar Verme, Tedarikçi Seçimi, MEREC, CODAS.*

Abstract: Supplier selection is an important issue for companies to maintain their sustainability and gain competitive advantage. Before deciding on supplier selection, the multi criteria decision making method to be used in the selection and ranking of supplier selection criteria and alternative suppliers is important. Multi criteria decision making techniques are methods that produce solutions to organizations with many criteria and alternatives. Different methods are used in solving multi criteria decision making problems and these methods provide significant advantages to decision makers in decision making processes. The aim of this study is to determine the criteria that will be effective in the supplier selection of a textile company and the importance weights of the criteria and to select the most appropriate alternative based on these criteria. Seven criteria were determined to be used in the study by using literature and experts in the field. A hybrid method was developed by combining MEREC and CODAS

techniques to solve the problem. MEREC method was used to determine the weight of the determined criteria in supplier selection. MEREC method was preferred because it allows data to be collected independently and objectively and contributes to the minimization of individual biases. According to the MEREC method results, the most important criterion was industry experience, while the criterion with the lowest level of importance was the product price criterion. Considering the criterion weights calculated with the MEREC method, the CODAS method, one of the most up-to-date methods, was used in supplier selection and ranking. The CODAS method allows balancing conflicting criteria and selecting the best alternative. Therefore, both positive and negative sides can be considered more equally. According to the CODAS method results, A3 is selected as the most suitable alternative, while the next most suitable alternative supplier is the A1 option. It is seen that the integrated use of CODAS and MEREC methods helps decision makers in their decision making processes. The results obtained showed that the company's supplier selection problem was solved in the best way.

Keywords: *Multi Criteria Decision Making, Supplier Selection, MEREC, CODAS.*

I. GİRİŞ

Tedarikçi seçimi, işletme için gerekli hammadde, mamul veya yarı mamul, hangi tedarikçiden temin edilmesini sağlayan bir karar verme sürecinden oluşmaktadır. Tedarikçi seçim sürecinde maliyetlerin azaltılması, müşteri hacminin artırılması ve rekabet avantajının sağlanması amaçlanmaktadır [1]. Son zamanlarda, tedarikçi firma seçiminde birçok kriterin farklı olduğu ve bu kriterlerin firmalarına göre değişkenlik gösterdiği, karar verme sürecinin karmaşık ve zor hale geldiği görülmektedir. Bu nedenle, tedarikçi seçimi genellikle çok kriterli karar verme (ÇKKV) sorunu olarak değerlendirilmektedir.

ÇKKV yöntemleri birden fazla kritere ve alternatife sahip işletmelere çözüm sunan yöntemlerdir [2]. ÇKKV problemlerinin çözümünde çeşitli yöntemler kullanılmaktadır. Alternatif kaynakların değerlendirilmesi ve uygun tedarikçinin belirlenebilmesinde bu yöntemlerin kullanılması, işletmedeki kaynakların daha etkin şekilde dağıtılmasını sağlamaktadır. Aynı zamanda, yöneticilerin karar alma süreçlerini hızlandırarak daha doğru karar vermelerine yardımcı olur [3]. Bu yöntemlerden AHP, TOPSIS, SWARA, MOORA en çok tercih edilen yöntemlerdir [4].

ÇKKV modelleri, karar vericilere etkin stratejiler ve metotlar sunarak onların karar alma sürecini destekler [5]. Referans [6] 7 kritere göre 7 adet alternatif arasından en uygun tedarikçi seçimini yapmak için TOPSIS yöntemini kullanmışlardır. Referans [7], çalışmalarında SWARA ve WASPAS yöntemlerini kullanarak tedarikçi seçim problemini ele almışlardır. Kriter ağırlıklarını tespit etmek amacıyla SWARA, bu ağırlıklara dayalı olarak alternatifler arasında seçim yapmak için WASPAS yöntemlerine başvurmuşlardır. Böylece bütünleşmiş bir karar verme süreci geliştirerek tedarikçi seçimine yönelik bir çözüm sunmuşlardır. Referans [8]'de Rize'deki bir konfeksiyon işletmesinin tercihli seçim problemini incelemişlerdir. Kriter ağırlıklarını belirlemek için MACBETH, tedarikçilerin sıralanması için MACBETH ve TOPSIS yöntemlerini kullanmışlardır. Referans [9], firmalar için kritik öneme sahip tedarikçi seçim problemini incelemiştir. Bu bağlamda, genel bir analiz yaparak en çok tercih edilen ÇKKV yöntemlerini araştırmıştır.

II. MATERYAL VE YÖNTEMLER

MEREC Yöntemi

MEREC yöntemi, 2021 yılında Keshavarz-Ghorabaee tarafından objektif kriteri ağırlıklandırma yöntemi olarak literatüre kazandırılmıştır. MEREC yöntemi kriterlerin alternatifler üzerindeki genel etkisini belirlemek için kriter ağırlıklarını kullanılır. Ayrıca alternatiflerin hem genel hem de spesifik performanslarını kullanmak amacıyla logaritmik bir fonksiyon kullanır. Yöntemde alternatiflerin performansında daha büyük bir etkiye sahip olan

kriter ağırlıklarına daha yüksek ağırlık vermektedir. Yöntemin ilk adımında karar matrisi oluşturulur ve bu matris fayda ve maliyet kriterleri baz alınarak normalize edilir. Sonraki adımda kriterlerin genel performans değerleri hesaplanır. Devamında her bir kriter kaldırılarak alternatiflerin performansları (mutlak sapma değerleri) hesaplanır ve bu işlem adımından sonra mutlak sapmaların toplamı hesaplanır. Son adımda ise nihai kriter ağırlıkları hesaplanır [10].

CODAS Yöntemi

CODAS (Kombine Mesafeye Dayalı Değerlendirme) yöntemi Keshavarz-Ghorabaee ve ark. (2017) tarafından alternatiflerin seçiminde ve sıralanmasında kullanılmak üzere literatüre kazandırılmış bir ÇKKV yöntemidir. Yöntemin diğer ÇKKV yöntemlerinden farkı ise alternatiflerin negatif ideal çözümü olan uzaklıklarını dikkate alarak Öklid ve Taksicab uzaklıklarını kullanmalarıdır. Bu yaklaşımla, alternatiflerin çözümünde daha sağlam ve duyarlı sonuçlar elde edilmektedir. Çalışmada problemin çözümü için Excel programı tercih edilmiştir. Tüm ÇKKV yöntemlerinde olduğu gibi öncelikle karar matrisi oluşturulur ve bu matris normalize edilir. Ardından ağırlıklı normalize karar matrisi oluşturulur, negatif ideal çözüm bulunur, Öklid ve Taksicab uzaklıkları hesaplanır, karar verici tarafından 0,01 ile 0,05 aralığındaki bir eşik değeri (τ) (genellikle bu değer 0,05 olarak alınmaktadır) belirlenir ve gerçekleşen matrisi oluşur, son olarak değerlendirme puanları hesaplanır ve en yüksek değerlendirme puanına sahip alternatif seçilir [11].

III. UYGULAMA

MEREC Yöntemi ile Kriter Ağırlıklarının Belirlenmesi:

Literatür çalışmaları sonucunda ve alanında uzman çalışanların değerlendirmeleri sonucunda 7 adet alternatif tedarikçi ve bu alternatif tedarikçilerin değerlendirilebilmesi amacıyla 7 adet kriter belirlenmiştir. Bunlar ürün kalitesi, üretim kapasitesi, ürünün fiyatı, tedarik süresi, tedarikçinin işletmeye uzaklığı, ürün paketleme yeteneği ve sektör deneyimidir. Ürün kalitesi tedarikçi işletmenin ürünün beklenen seviyede olmasını ifade etmektedir. MEREC yönteminin tüm işlem adımları gerçekleştirildikten sonra Tablo 1'de verilen kriter ağırlıkları elde edilmiştir.

TABLO I. KRİTER AĞIRLIKLARI

Ürün Kalitesi	Tedarikçinin Üretim Kapasitesi	Ürün Fiyatı	Tedarik Süresi	Tedarikçinin İşletmeye Olan Uzaklığı	Ürün Paketleme Yeteneği	Sektör Deneyimi
0,0843	0,0938	0,0556	0,1156	0,1979	0,1676	0,2853

Tablo 1'de görüldüğü üzere en yüksek önem ağırlığına sahip kriter sektör deneyimi olurken en düşük önem ağırlığına sahip kriter ürün fiyatı olmuştur. Tedarikçinin işletmeye olan uzaklığı kriteri ise 0.1979 değeri ile en yüksek önem ağırlığına sahip ikinci kriter olmaktadır. MEREC yöntemi ile elde edilen kriter önem ağırlıkları CODAS yönteminde alternatiflerin sıralanmasında kullanılmıştır.

CODAS Yöntemi Kullanarak Elde Edilen Sonuçlar:

MEREC yöntemi ile elde edilen kriter ağırlıkları baz alınarak ve CODAS yönteminin tüm işlem adımları gerçekleştirilerek Tablo 2'de verilen göreceli değerlendirme matrisi yani tedarikçi sıralamaları elde edilmiştir. Tablo 2'de yer alan değerlendirmeye göre, A3 alternatifi

1,02982 puanla en yüksek değerlendirme puanına sahip olup, sıralamada birinci sırayı almıştır. Bu sonuç, değerlendirme kriterlerine göre A3 alternatifinin diğer seçeneklerden daha üstün olduğunu göstermektedir.

Tablo II. GÖRELİ DEĞERLENDİRME MATRİSİ VE SIRALAMALAR

	A1	A2	A3	A4	A5	A6	A7	Hİ	Sıralama
A1	0	0,03941	-0,0878	0,02532	0,01801	0,05557	0,06135	0,11184	**2**
A2	-0,0371	0	-0,1144	-0,0128	-0,0204	0,01591	0,02063	-0,1482	**5**
A3	0,12952	0,17952	0	0,15923	0,15592	0,19828	0,20735	1,02982	**1**
A4	-0,0255	0,01283	-0,109	0	-0,0074	0,02961	0,03484	-0,0647	**4**
A5	-0,018	0,02007	-0,0974	0,00743	0	0,03569	0,0409	-0,0114	**3**
A6	-0,0528	-0,0159	-0,1274	-0,0279	-0,0366	0	0,00435	-0,2563	**6**
A7	-0,0557	-0,0199	-0,1271	-0,0313	-0,0401	-0,0044	0	-0,2785	**7**

IV. SONUÇ

Çalışmada, bir tekstil firması için yedi alternatif tedarikçi, yedi adet kriter (ürün kalitesi, tedarikçinin üretim kapasitesi, ürün fiyatı, tedarik süresi, tedarikçinin işletmeye olan uzaklığı, ürün paketleme yeteneği, sektör deneyimi) kullanılarak en uygun alternatif tedarikçinin seçimi yapılmıştır. Çalışmada kullanılan kriterler literatür çalışmaları sonucunda ve alanında uzman çalışanların değerlendirmeleri sonucunda seçilmiştir.

Çalışmanın uygulama kısmında, MEREC ve CODAS yöntemleri hibrit bir şekilde kullanılmıştır. Yöntemlerin hibrit olarak kullanılması karar verme sürecinde kriterlerin ve alternatif tedarikçilerin detaylı bir şekilde incelenmesine olanak tanımıştır.

Kriterlerin önem ağırlıklarının saptanmasında objektif bir yöntem olan MEREC yöntemi kullanılmıştır. MEREC yönteminin sonuçlarına göre en önemli kriter belirlenmiştir. Yöntemin sonuçlarına göre, en yüksek önem ağırlığına sahip kriter sektör deneyimi olurken en düşük önem ağırlığına sahip kriter ürün fiyatı olmuştur. Kriter ağırlıkları belirlendikten sonra en uygun tedarikçinin belirlenebilmesi için CODAS yöntemi kullanılmıştır. CODAS yöntemi sonuçlarına göre en uygun tedarikçi A3 tedarikçi olmaktadır.

Literatürde MEREC yöntemi ile ilgili çalışma sayısı oldukça az sayıda olduğundan bu çalışmanın literatüre önemli bir katkı sağlayacağı düşünülmektedir. Aynı zamanda MEREC yöntemi, subjektif değerlendirmeye ihtiyaç duymadan kullanılabilen bir yapıya sahiptir. Bu nedenle, kriter ağırlıklarının belirlenmesi süreçlerinde rahatlıkla kullanılabilir bir yöntem olarak kabul edilmektedir. Gelecekte, MEREC ve CODAS yöntemlerinin farklı alanlarda bir arada kullanılmasına ilişkin daha fazla çalışmaya yer verilmesi mümkündür. Tedarikçi seçim sürecinde, farklı yöntemlerin CODAS yöntemiyle birlikte kullanılmasıyla elde edilen sonuçlar, karşılaştırmalı bir şekilde değerlendirilebilir.

KAYNAKLAR

[1] Christopher M (2011) Logistics & Supply Chain Management (Pearson Education Limited, Essex).

[2] Bülbül, S. E., & Köse, A. (2016). Türk sigorta sektörünün PROMETHEE yöntemi ile finansal performans analizi. Marmara Üniversitesi İktisadi ve İdari Bilimler Dergisi, 38(1), 187-210.

[3] Yüksel, F.Ş., Kalan, O., Işık, M., 2022. Havaalanlarında Dijital Dönüşüm Risklerinin Değerlendirilmesi. Çukurova Üniversitesi Mühendislik Fakültesi Dergisi, 37(3),781-792.

[4] Zeydan, M., Çolpan, C., Çobanoğlu, C., 2011. A Combined Methodology for Supplier Selection and Performance Evaluation. Expert Systems with Applications, 38(3), 2741-2751.

[5] Şengül, Ü., Eren, M., Shiraz, S. E., Gezder, V., & Şengül, A. B. (2015). Fuzzy TOPSIS method for ranking renewable energy supply systems in Turkey. Renewable energy, 75, 617-625.

[6] Gündüz, H., Güler, M.E., 2015. Termal Turizm İşletmelerinde Çok Ölçütlü Karar Verme Teknikleri Kullanılarak Uygun Tedarikçinin Seçilmesi. Dokuz Eylül Üniversitesi İktisadi ve İdari Bilimler Fakültesi Dergisi, 30(1), 203-222.

[7] Adalı, EA ve Tuş, A. (2017). Bir Tedarikçi Seçim Problemi İçin Swara ve Waspas Yöntemlerine Dayanan Karar Verme Yaklaşımı. International Review of Economics and Management, 5(4), 56-77.

[8] Cevizci, D. K., & Kayacan, O. (2019). Konfeksiyon İşletmelerinde En Uygun Fason Seçimi Problemine MACBETH ve TOPSIS Yöntemlerinin Uygulanması. Dokuz Eylül Üniversitesi Mühendislik Fakültesi Fen ve Mühendislik Dergisi, 21(62), 331-344.

[9] Pınar, A. (2020). Tedarikçi seçiminde kullanılan çok kriterli karar verme metotları. Journal of Turkish Operations Management, 4(2), 449-478.

[10] Keshavarz-Ghorabaee, M. (2021). Assessment of distribution center locations using a multi-expert subjective–objective decision-making approach. *Scientific Reports*, *11*(1), 19461.

[11] Keshavarz-Ghorabaee, M., Amiri, M., Zavadskas, E. K., Hooshmand, R. ve Antuchevičienė, J. (2017). Fuzzy Extension of the CODAS Method for Multi-Criteria Market Segment Evaluation. Journal of Business Economics and Management. 18(1). 1-19.

Derin Öğrenme Yöntemleriyle Akarsu Debisi Tahmini

Stream Discharge Prediction with Deep Learning Methods

Mustafa Erden[1], Mehmet Seren Korkmaz[1], Ertuğrul Sunan[*, 2]

[*]ertugrul.sunan@samsun.edu.tr, ORCID: 0000-0003-1646-1752
[1]*Meteoroloji Mühendisliği Bölümü, Samsun Üniversitesi, Samsun, Türkiye*
[2]*Uçak Bakım ve Onarım Bölümü, Samsun Üniversitesi, Samsun, Türkiye*

Özet: Nüfus artışı ve iklim değişikliğinin etkilerinin artmasıyla birlikte tatlı su kaynaklarının izlenmesi giderek daha önemli hale gelmiştir. Bu kaynakların etkin bir şekilde yönetilmesi, içme suyu temini, tarım ve enerji üretimi için kritik bir rol oynamaktadır. Hidrolojik çalışmalar, akarsu havzalarının su potansiyelinin belirlenmesine odaklanır ve doğru debi tahmini su kaynaklarının yönetimi için önemlidir. Bu, gelecekte yaşanabilecek olası kuraklıklar ve taşkınlar gibi ekstrem olayların öngörülmesine olanak sağlar. Bu çalışmada, Samsun ilindeki Terme Çayı'nın günlük debi tahmini için [$Q_1(t)$], akarsu gözlem istasyonundan bir önceki güne ait debi değeri [$Q_1(t-1)$], menbasındaki akarsu gözlem istasyonunda önceki güne ait gözlenen debi değeri [$Q_2(t-1)$] ve havzada bir önceki güne ait gözlenen yağış değeri verileri [$P(t-1)$] kullanılarak, derin öğrenme yöntemleri olan Tekrarlayan Sinir Ağları (RNN), Uzun Kısa Süreli Bellek (LSTM) ve Uyarlamalı Ağ Tabanlı Bulanık Çıkarım Sistemi (ANFIS) yaklaşımlarının performansları sınanmıştır. Her bir modeli değerlendirmek için RMSE, R^2, NSE ve KGE performans metrikleri kullanılmıştır.
RNN modeli düşük ve orta debi değerlerinde başarılı tahminler yaparken, yüksek debi değerlerinde tahmin hatalarının arttığı görülmüştür. LSTM modeli ise RNN'e göre daha iyi bir performans sergilemiş, ancak yüksek debi değerlerinde benzer sapmalar görülmüştür. En iyi performansı gösteren ANFIS modeli ise düşük, orta ve yüksek debi değerlerinde tutarlı ve doğru tahminler yapmıştır. Korelasyon analizi, önceki dönem debi değerlerinin mevcut dönem debi değerlerini önemli ölçüde etkilediğini ortaya koymuştur. Ayrıca, Uzaktan Algılama tabanlı yağış veri setlerinin derin öğrenme yöntemlerinde kullanılabileceği tespit edilmiştir. Çalışmada, ANFIS modelinin Terme Çayı'ndaki debi tahminlerinde en iyi performansı gösteren model olduğu ve su kaynakları yönetimi için değerli bir araç olduğu sonucuna varılmıştır. Gelecek araştırmalar, daha kapsamlı veri setlerinin uyumunu ve hibrit modellerin geliştirilmesini dikkate almalıdır.

Anahtar Kelimeler: *Derin öğrenme, Debi, RNN, LSTM, ANFIS.*

Abstract: As the impacts of population growth and climate change intensify, monitoring freshwater resources has become increasingly important. Effective management of these resources is critical for ensuring drinking water supply, agriculture, and energy production. Hydrological studies focus on determining the water potential of river basins, and accurate discharge estimation is essential for water resources management. This enables the prediction of potential future extreme events such as droughts and floods. In this study, the performance of deep learning methods such as Recurrent Neural Networks (RNN), Long Short-Term Memory (LSTM), and Adaptive Network-Based Fuzzy Inference System (ANFIS) is evaluated for daily discharge prediction [$Q_1(t)$] of the Terme Stream in Samsun, using the previous day's discharge value [$Q_1(t-1)$] from the stream gage, the observed discharge value from the upstream observation gage on the previous day [$Q_2(t-1)$], and the observed total

rainfall in the basin from the previous day [P(t-1)]. RMSE, R^2, NSE, and KGE performance metrics are used to evaluate each model.
While the RNN model made successful predictions for low and medium discharge values, prediction errors increased for high discharge values. The LSTM model exhibited a better performance compared to RNN, but similar deviations were observed for high discharge values. The ANFIS model, which demonstrated the best performance, made consistent and accurate predictions for low, medium, and high discharge values. Correlation analysis revealed that previous period discharge values significantly affect current period discharge values. Additionally, it was determined that remote sensing-based rainfall datasets can be integrated into deep learning methods. The study concludes that the ANFIS model is the most effective model for discharge prediction in the Terme Stream and is a valuable tool for water resources management. Future research should consider the adaptation of more comprehensive datasets and the development of hybrid models.

Keywords: *Deep learning, Discharge, RNN, LSTM, ANFIS.*

I. GİRİŞ

Nüfus artışı ve iklim değişikliğiyle tatlı su kaynaklarının izlenmesi ve yönetimi kritik hale gelmiştir. Hidrolojik çalışmalar, akarsu havzalarının su potansiyelini belirlemek için debi ölçümüne büyük önem verir. Akarsuların debisi, yer altı sularının yeryüzüne çıkması ve yağış miktarı ile kar erimelerinin etkisiyle oluşur; ayrıca havzadaki meteorolojik ve hidrolojik olayların bir sonucu olarak değişir [4]. Debi tahmini, su kaynaklarının yönetilmesi için önemlidir ve gelecekte yaşanabilecek olası kuraklıklar ve taşkınlar gibi ekstrem olayların öngörülmesine olanak sağlar.

Yağış ve akım arasındaki ilişkinin regresyon tipi yaklaşımlar kullanılarak modellenmesi ve bu modeller aracılığıyla yağış olaylarının bir fonksiyonu olarak debi tahmini yapılmasına yönelik girişimler uzun bir geçmişe sahiptir [7]. Akarsu debi tahmininde geleneksel yöntemler, karmaşık modeller ve uzun süreli veri analizi gerektirir, ancak yağıştan akışa dönüşümdeki dinamikleri tam olarak yansıtamayabilir. Derin öğrenme yöntemleri ise büyük veri setlerinden anlamlı desenler çıkarabilme yetenekleriyle bu alanda güçlü bir alternatif sunar. Yapılan çalışmalarda, debi tahminleri için derin öğrenme yaklaşımının, temel modellere göre sürekli olarak daha iyi performans gösterdiği bildirilmiştir [3][19].

Anusree & Varghese, Karuvannur Nehir Havzası'nda ANFIS modelinin, ANN ve MNLR modellerine göre daha doğru tahminler sağladığını belirlemiştir [1]. Asaad, Konya'daki Meram Çayı'nın akım verilerini tahmin etmek için LSTM modelinin MLP ve ANFIS modellerine göre daha yüksek doğruluk sağladığını göstermiştir [2]. Cigizoglu, ANN'nin nehir akım tahmini için geleneksel modellere kıyasla daha yüksek doğruluk sağladığını ortaya koymuştur [9]. Gemici ve ark., Kızılırmak Nehri'nin yan kollarında ANFIS modelinin diğer yapay zeka yöntemlerine göre en yüksek performansı gösterdiğini belirtmiştir [13]. Girma & Berhanu, uydu tabanlı yağış verilerinin yer ölçüm istasyonlarının yetersiz olduğu bölgelerde hidrolojik modellemelerde önemli bir veri kaynağı olduğunu vurgulamıştır [14]. Kişi, Kuzey Platte Nehri'nde günlük akım tahminlerinde farklı ANN algoritmalarını karşılaştırmış ve ANN'lerin hidrolojik zaman serilerinde kısa dönemli tahminler yapmada etkili olduğunu göstermiştir [18]. Lohani ve ark., Sutlej Nehri'nde ANFIS modelinin, AR ve ANN modellerine göre daha doğru tahminler sunduğunu göstermiştir [21]. Rivera ve ark., CHIRPS veri setinin mevsimsel ve yıllık yağış değişimlerini doğru bir şekilde yeniden ürettiğini, ancak yerel verilerle kalibre edilmesi gerektiğini vurgulamıştır [22]. Sahoo ve ark., LSTM-RNN modelinin düşük akış tahminlerinde RNN ve naïve yöntemlere göre daha iyi performans sağladığını ortaya koymuştur [23]. Sulugodu & Deka, CHIRPS uydu yağış verilerinin akım tahminlerinde kullanılabilirliğini ve çeşitli hesaplama yöntemlerinin performansını değerlendirmiştir [25].

A. Çalışma Alanı

Terme Çayı, Türkiye'nin Karadeniz Bölgesi'nde, Samsun'un Terme ilçesinde bulunan ve kar suları ile yağmur sularıyla beslenen, mevsimsel olarak değişen debiye sahip önemli bir akarsudur. Terme Çayı havzası (Şekil 1), 420 km² yağış alanını kapsar, Salıpazarı ilçesindeki üç akarsu kolunun birleşmesiyle oluşur ve Karadeniz'e dökülür.

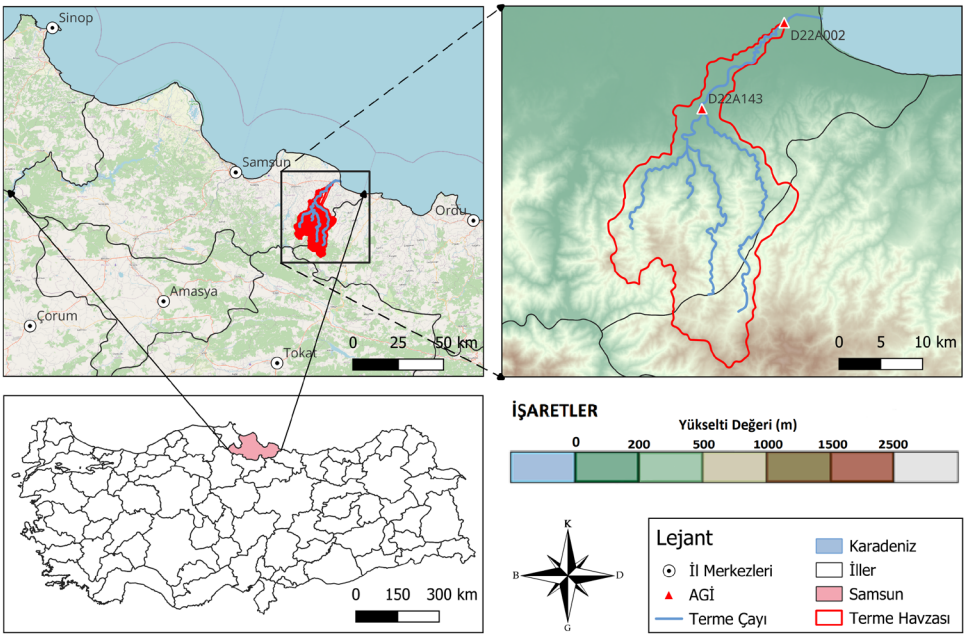

Şekil 1. Çalışma alanı ve AGİ'lerin konumlarını gösteren lokasyon haritası.

B. Veri

Çalışma alanı içerisinde Devlet Su İşleri (DSİ) tarafından işletilen TERME ve ŞEYHLİ adlı akım gözlem istasyonlarından (AGİ) elde edilen 01.10.2019 – 30.09.2022 tarihleri arasındaki günlük ortalama debi (m^3/s) verileri kullanılmıştır (Şekil 2). 01.10.2019 – 31.01.2022 tarihleri arası eğitim veri setini oluştururken, 01.02.2022 – 30.09.2022 tarihleri arası test veri setini oluşturmaktadır. Tablo 1'de çalışmada kullanılan AGİ'lere ait bilgiler verilmiştir.

TABLO 1
Çalışmada kullanılan akım gözlem istasyon bilgileri.

İstasyon No	İstasyon Adı	Enlem	Boylam
D22A002	TERME	41°12'33"K	36°58'22"D
D22A143	ŞEYHLİ	41°07'13"K	36°51'00"D

Veri setinde, veri bulunmayan günlerin doldurulması için bir önceki günün ve bir sonraki günün ortalaması kullanılmıştır. Modellerin ekstrem değerlerden dolayı olumsuz etkilenmemesi için veri seti minimum 0 m^3/s ile maksimum 200 m^3/s debi değerleri arasında olacak şekilde filtrelenmiştir.

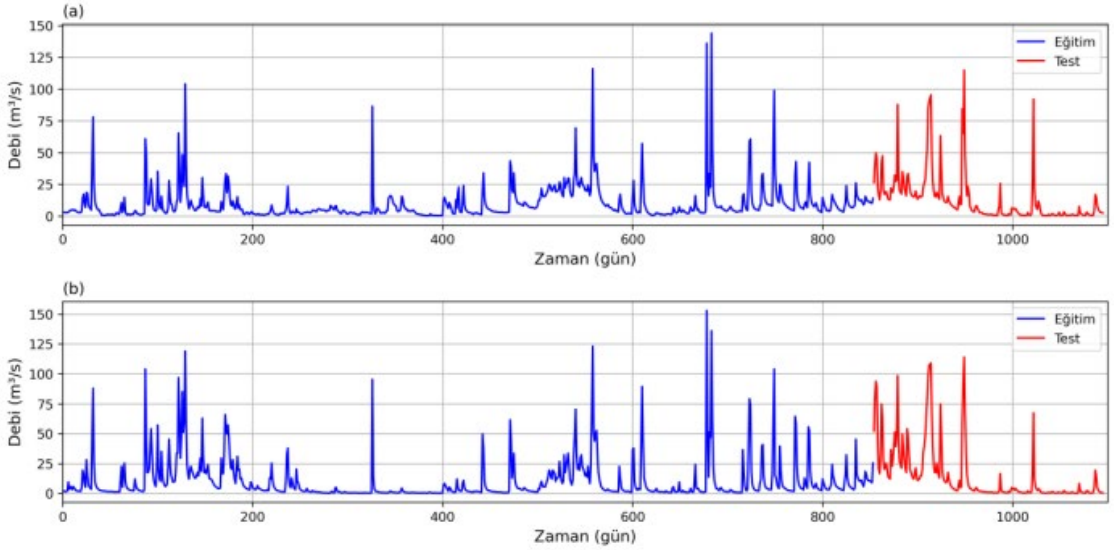

Şekil 2. (a) D22A002 numaralı istasyona ve (b) D22A143 numaralı istasyona ait debi verilerinin zaman içerisindeki değişimi. Veri setinin eğitim için kullanılan kısmı mavi, test için kullanılan kısmı ise kırmızı renkle gösterilmiştir.

Bu çalışmada kullanılan günlük toplam yağış verileri (Şekil 3), Google Earth Engine Code Editor arayüzünde JavaScript betiği (Şekil 4) ile UCSB – CHG/CHIRPS/DAILY veri setinden alınmıştır. CHIRPS veri seti, uydu gözlemleri ve yer istasyonu verilerinin yenilikçi bir karışım prosedürü ile birleştirilmesiyle elde edilir. CHIRPS, hem yüksek çözünürlüklü (0.05°) hem de uzun dönemli (1981 – günümüz) bir iklimsel veri setidir ve uydu tabanlı soğuk bulut süresi (CCD) gözlemlerine dayalı olarak geliştirilen akıllı interpolasyon teknikleriyle oluşturulmuştur [12].

CHIRPS, yerel ölçümlerin yetersiz olduğu bölgelerde hidrolojik modellemeler için değerli bir kaynak olabilir [14]. CHIRPS verileri bazen tahminlerde sapma gösterse de, yer ölçümlerinin yetersiz olduğu bölgelerde değerli bir alternatif olarak görülmektedir [10]. Çalışmalarda, hidrolojik modellerde kullanılabilecek yeterliliğe sahip olduğu belirtilsede [25], mümkün olduğunca yerel yağış ölçüm verileri ile kalibre edilmesi önerilmektedir [22] fakat bu çalışmada ham veri seti kullanılmıştır.

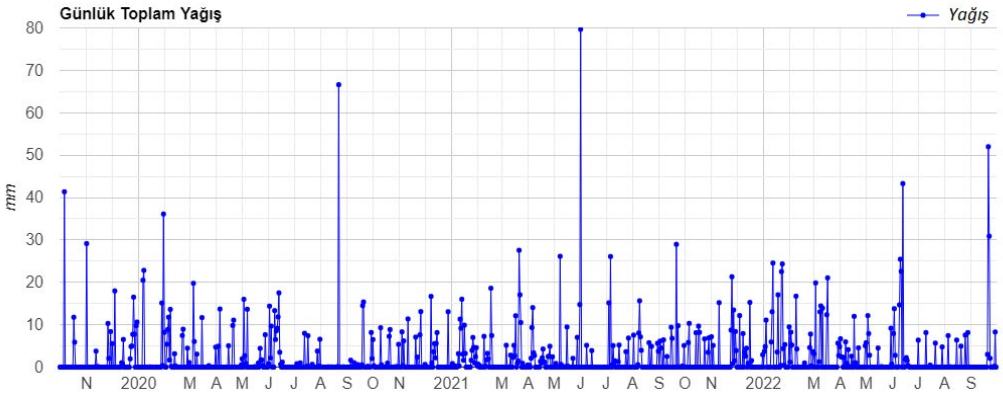

Şekil 3. Google Earth Engine Code Editor arayüzünde JavaScript betiği ile oluşturulan günlük toplam yağış grafiği.

```
// Havza Tanımlama
var aoi = ee.FeatureCollection('projects/assets/watershed');
// Havzayı Haritada Gösterme
Map.centerObject(aoi);
Map.addLayer(aoi, {}, 'Watershed');
// Veri kümesi ve zaman aralığı tanımlama
var startDate = '2019-10-01';
var endDate = '2022-10-01';
var precipitation = ee.ImageCollection('UCSB-CHG/CHIRPS/DAILY')
    .filterBounds(aoi)
    .filterDate(startDate, endDate)
    .select('precipitation');
// Grafik Çizdirme Fonksiyonu
var plotTimeSeries = function(collection, region, scale, title, yLabel){
  var timeSeries = ui.Chart.image.series({
    imageCollection: collection,
    region: region,
    reducer: ee.Reducer.mean(),
    scale: scale
  }).setOptions({
    title: title,
    vAxis: {title: yLabel},
    lineWidth: 1,
    pointSize: 3,
    series: {0: {color: '0000FF'}}
  });
  print(timeSeries);
};
// Grafiğin Çizdirilmesi
plotTimeSeries(precipitation, aoi, 5000, 'Günlük Toplam Yağış', 'mm');
```

Şekil 4. Google Earth Engine Code Editor arayüzünde kullanılan JavaScript betiği.

II. YÖNTEM

Derin öğrenme, yapay sinir ağları (ANN) kullanarak karmaşık veri setlerinden anlamlı bilgiler çıkaran bir makine öğrenme alt alanıdır. ANN'ler, biyolojik nöron sistemlerinin basitleştirilmiş modelleridir ve bilgiyi işleyen geniş paralel işlemcilerdir. Nöronlar katmanlar halinde düzenlenir ve sinir ağının mimarisi olarak adlandırılır. Nöronlar katmanlar halinde düzenlenir ve bu yapı sinir ağının mimarisini oluşturur. Her nöron, diğer nöronlarla iletişim bağlantıları aracılığıyla bilgi alışverişi yapar ve ağırlıklarla ilişkilendirilir [11]. Sinir ağları, katman sayısına, bilgi akış yönüne, düğümlerin çıkışlarını almak için kullanılan doğrusal olmayan denklemlere ve farklı katmanlardaki düğümler arasındaki ağırlıkları belirleme yöntemine göre sınıflandırılır [21].

Bir havzadaki hidrolojik modelin kavramsal yapısı ile süreçler arasındaki tutarlı anormallikler derin öğrenme modelleri tarafından daha iyi yakalanabilir. Bu modellerin yapı ve birçok gizli parametre seçimine bağlı olduğunu unutmamak önemlidir; bu özellikler, derin öğrenme modellerine eğitim verilerine uyum sağlama konusunda büyük bir esneklik kazandırır [6]. Derin öğrenme yötemlerinin, hidrolojik çalışmalarda, karmaşık yağış-akım ilişkisini simüle etmek için uygun olduğu bilinmektedir [20].

Çalışmada, (t) günündeki D22A002 numaralı AGİ'nin debi değerini [$Q_1(t)$] tahmin etmek için önceki günün yağış değeri [P(t-1)], D22A143 numaralı AGİ'nin debi değeri [$Q_2(t-1)$] ve D22A002 numaralı AGİ'nin debi değeri [$Q_1(t-1)$] kullanılmıştır (Tablo 2, Tablo 3). Tüm modellemeler için iterasyon değeri 100 olarak girilmiştir. Az girilen iterasyon, modelin eksik öğrenmesine neden olabilirken, çok fazla iterasyon aşırı öğrenmeye neden olabilir. En uygun olan iterasyon sayısı, modelin genel performansını dengelemek için önemlidir.

TABLO 2
RNN ve LSTM model yapılandırmaları.

Model	Girdiler	Nöron Sayısı	Çıktı	İterasyon (Epochs)
RNN	P(t-1), Q_2(t-1), Q_1(t-1)	50	Q_1(t)	100
LSTM	P(t-1), Q_2(t-1), Q_1(t-1)	50	Q_1(t)	100

TABLO 3
ANFIS model yapılandırması.

Kümeleme	Girdiler	Giriş üyelik fonksiyonu	Çıktı	Çıkış üyelik fonksiyonu	İterasyon (Epochs)
3 3 3	P(t-1), Q_2(t-1), Q_1(t-1)	gauss2mf	Q_1(t)	linear	100

RNN ve LSTM modelleri, Python programlama dili ve ilgili kütüphaneler kullanılarak oluşturulmuştur. Kullanılan kütüphaneler arasında TensorFlow ve Keras, derin öğrenme modelinin geliştirilmesinde temel kütüphaneler olarak öne çıkmaktadır. Pandas kütüphanesi, veri işleme ve analiz etmek için, Numpy kütüphanesi ise çok boyutlu diziler ve matrisler üzerinde matematiksel işlemler gerçekleştirmek için kullanılmıştır.

RNN modeli için Keras kütüphanesi içinde yer alan SimpleRNN katmanı, LSTM modeli için ise LSTM katmanı seçilmiş ve bu katmanlarda 50 nöron kullanılmıştır. Yapılan programlama işlemleri Anaconda dağıtım paketinde yer alan Jupyter Notebook ortamında geliştirilmiştir.

ANFIS modeli, MATLAB® R2013a programında çalıştırılmıştır. Programda bulunan MATLAB® Neuro-Fuzzy Designer uygulaması kullanılmıştır. Sugeno tipi bulanık çıkarım sistemi seçilmiştir. Üyelik fonksiyonu olarak giriş için iki gauss fonksiyonundan oluşan üyelik fonksiyonu (gauss2mf), çıkış için doğrusal üyelik fonksiyonu (linear) seçilmiştir [13]. Şekil 5'te Q_1(t) için oluşturulmuş 3 kümelemeli modelin yapısı verilmiştir.

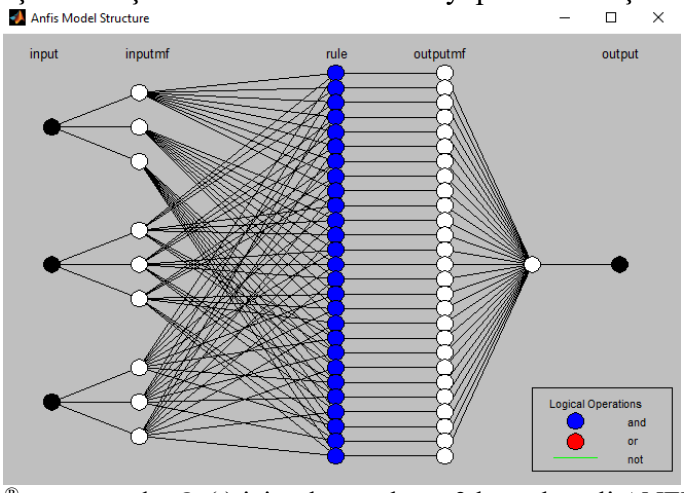

Şekil 5. MATLAB® arayüzünde, Q_1(t) için oluşturulmuş 3 kümelemeli ANFIS model mimarisi.

A. Tekrarlayan Sinir Ağı (RNN)

Tekrarlayan Sinir Ağları (RNN), sıralı veri işleme yetenekleri ile tanınan bir yapay sinir ağı (ANN) türüdür. RNN'ler, önceki adımların bilgilerini hatırlayarak ve bu bilgileri kullanarak sonraki adımları tahmin ederek çalışır. Bu yetenekleri, zaman serisi verilerinde doğrusal olmayan ilişkileri yakalamalarını sağlar. RNN'in temel yapı taşı, döngüsel bir bağlantıya sahip olan hücrelerdir. Hücreler, girdi verilerini ve önceki adımın çıktısını alarak güncel durumu hesaplar. Böylece, zaman içindeki bağımlılıkları modellemek mümkün olur [15]. RNN'in klasik mantığı, aşağıdaki (1) ve (2) numaralı denklemlerle ifade edilir [16]:

$$h_t = f_h(x_t, h_{t-1}) = \varphi_h(W^T h_{t-1} + U^T x_t) \quad (1)$$
$$\gamma_t = f_o(h_t, x_t) = \varphi_o(V^T h_t) \quad (2)$$

Denklemde x_t, (t) zamanındaki girişi, h_t gizli durumu ve γ_t çıkışı ifade eder. Alt indisler zaman değişkenini belirtir. İlk olarak, bir önceki zamandaki gizli durum (h_{t-1}) ile şu anki zamanın girdisi (x_t), kendi ağırlıkları W^T ve U^T ile birleştirilir. Denklem (1)'de, doğrusal olmayan bir fonksiyonla (genellikle tanh veya sigmoid) dönüştürülür ve yeni gizli durum (h_t) elde edilir. Denklem (2)'de, gizli durum (h_t), V^T ağırlığı ile çarpılarak bir doğrusal olmayan fonksiyonla işlenir ve nihayetinde sonuç (γ_t) olarak kabul edilir. Model, geçmişteki gizli durumları dikkate alarak kısa süreli bellek özelliği kazanır ve gelecekteki çıkışları tahmin eder. Önceki durumlar şu anki durumu etkileyerek, zaman serisi verilerinde etkili bir şekilde kullanılabilir.

RNN modellerinin karşılaşılan en büyük zorluklardan biri, uzun bağımlılıkların modellenmesinde zorluk çıkaran gradyan kaybolması problemidir [5]. Bu problemi aşmak için, daha ileri RNN türü olan LSTM gibi daha gelişmiş modeller üzerine çalışılmaktadır [15][23].

B. Uzun Kısa Süreli Bellek (LSTM)

Uzun Kısa Süreli Bellek (LSTM) ağları, tekrarlayan sinir ağlarının (RNN) bir çeşidi olup, uzun vadeli bağımlılıkları öğrenme kapasitesine sahip olacak şekilde tasarlanmıştır. Bu tasarımlarıyla, hidrolojik modellemede doğrusal olmayan ve karmaşık süreçleri öğrenme konusunda güçlü bir potansiyele sahiptir [26]. LSTM'ler, zaman serisi verilerinde geçmişteki önemli bilgileri unutmadan hatırlayabilen hücre yapıları içerir. Bu yapı, girdi, çıktı ve unutma kapıları ile kontrol edilir [16]. Aşağıdaki (3), (4), (5), (6), (7) ve (8) numaralı denklemlerle ifade edilir:

$$g_t = \sigma\left(U_g x_t + W_g h_{t-1} + b_f\right) \quad (3)$$
$$i_t = \sigma(U_i x_t + W_i h_{t-1} + b_i) \quad (4)$$
$$\tilde{c}_t = tanh(U_c x_t + W_c h_{t-1} + b_c) \quad (5)$$
$$c_t = g_t * c_{t-1} + i_t * \tilde{c}_t \quad (6)$$
$$o_t = \sigma(U_o x_t + W_o h_{t-1} + b_o) \quad (7)$$
$$h_t = o_t * tanh(c_t) \quad (8)$$

LSTM hücrelerinin işleyişi, çeşitli kapılar aracılığıyla önceki ve mevcut bilginin nasıl işlendiğine dayanmaktadır. Unutma kapısı (g_t), önceki hücre durumunun (c_{t-1}) unutulacağı kısmını belirler ve sigmoid fonksiyonu ile hesaplanır. Giriş kapısı (i_t), yeni bilginin hücre durumuna ne ölçüde ekleneceğini belirler ve yine sigmoid fonksiyonu ile hesaplanır. Giriş modülasyon kapısı ($\tilde{c}_t$), yeni bilginin aday değerlerini oluşturur ve tanh fonksiyonu ile -1 ile 1 arasında değer döner. Hücre durumu (c_t), unutma kapısı ve giriş kapısının çıktıları kullanılarak güncellenir. Çıkış kapısı (o_t), hücre durumundan hangi bilgilerin gizli duruma (h_t) dönüştürüleceğini belirler ve sigmoid fonksiyonu ile hesaplanır. Son olarak, gizli durum (h_t), çıkış kapısının değeri ve güncellenmiş hücre durumu kullanılarak tanh fonksiyonuyla elde edilir. Bu yapı, LSTM hücrelerinin zaman serisi verilerindeki uzun vadeli bağımlılıkları öğrenmesini sağlar.

Geleneksel bir RNN hücresinde, yalnızca bir iç durum (h_t) vardır (Şekil 6a), LSTM'de ise bilgi depolanabilecek ek bir hücre hafızası (c_t) ve hücresi içindeki bilgi akışını kontrol eden kapılar (Şekil 6b'deki üç yuvarlak harf) vardır [15].

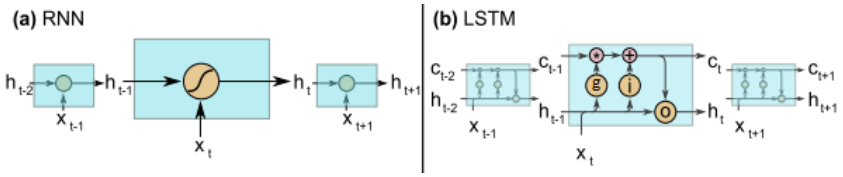

Şekil 6. (a) RNN hücresinin iç yapısı: h_t gizli durumu ve x_t zaman adımındaki girdi için kullanılır. (b) LSTM hücresinin iç yapısı: g unutma kapısını, i giriş kapısını, o çıkış kapısını, h_t gizli durumu ve c_t hücre durumunu zaman adımında temsil eder [19].

C. Uyarlamalı Ağ Tabanlı Bulanık Çıkarım Sistemi (ANFIS)

Uyarlamalı Ağ Tabanlı Bulanık Çıkarım Sistemi (ANFIS), bulanık mantık ve yapay sinir ağlarının (ANN) güçlü yönlerini birleştiren bir modeldir. Bu model, insan bilgisini ve veri setlerini kullanarak girdi-çıktı eşlemesi yapar. ANFIS, hibrit bir öğrenme prosedürü kullanarak doğrusal olmayan fonksiyonları modelleyebilir, kontrol sistemlerinde doğrusal olmayan bileşenleri tanımlayabilir ve kaotik zaman serilerini tahmin edebilir [17]. Bir tür yapay sinir ağı olan ANFIS, Takagi-Sugeno bulanık çıkarım sistemine dayanmaktadır [1]. Takagi-Sugeno bulanık model çıktısı, tüm kural çıktılarının ağırlıklı ortalamasıdır. Kural çıktıları, girdi değişkenlerin ve bir sabitin doğrusal kombinasyonudur. Aşağıda, üç girişli bir Takagi-Sugeno sistemi için EĞER-O ZAMAN (IF-THEN) kurallarının bir açıklaması bulunmaktadır [24].

Kural 1 - EĞER x, A_1 ise ve y, B_1 ise ve z, C_1 ise O ZAMAN $f_1=p_1\,x+q_1\,y+r_1z+s_1$.
Kural 2 - EĞER x, A_2 ise ve y, B_2 ise ve z, C_2 ise O ZAMAN $f_2=p_2\,x+q_2\,y+r_2z+s_2$.
Kural 3 - EĞER x, A_3 ise ve y, B_3 ise ve z, C_3 ise O ZAMAN $f_3=p_3\,x+q_3\,y+r_3z+s_3$.

Burada, kümedeki girdiler x, y, z olarak gösterilmiştir; dilsel etiketler A_i, B_i, C_i; sonuç parametreleri p_i, q_i, r_i ve çıktı bulanık üyelik fonksiyonları f_i ile temsil edilmiştir. Bağlantılı nöronlarının beş katmanı, benzer işleve sahip yapay sinir ağlarını gösteren tipik ANFIS tasarımını oluşturur. Şekil 7'de w_i nöronların ağırlıklarını, $\bar{w}_i$ ise normalleştirilmiş ağırlıklarını temsil eder [24].

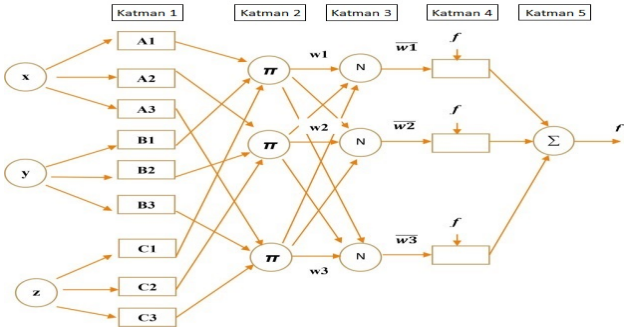

Şekil 7. ANFIS modelinin beş katmanlı yapısını göstermektedir [24].

Katman 1: Bu katmanda, her giriş değişkeni (x, y, z) üyelik fonksiyonlarına (A_i, B_i, C_i) dönüştürülür. Her düğüm, giriş değişkenlerinin bulanık değerlerini hesaplar ve bu değerler üyelik dereceleri olarak adlandırılır.

Katman 2: Bu katmandaki düğümler (π) giriş sinyallerini çarparak kuralın ağırlık nöronlarını (w_i) hesaplar.

Katman 3: Normalizasyon katmanı olarak bilinen bu katmanda, her bir kuralın ağırlık nöronları normalize edilir (N). Katmanındaki nöronlar sabittir ve bu katmandaki tüm nöronların ağırlıkları kullanılarak normalleştirilir.

Katman 4: Bu katmanda, normalize edilmiş ağırlık nöronları ve giriş değişkenleri kullanılarak kural çıktıları (f_i) hesaplanır. Her düğüm, bir kuralın sonucunu hesaplar ve bu

sonuçlar doğrusal kombinasyonlar şeklindedir.

Katman 5: Sonuç katmanıdır, tüm kural çıktıları toplanarak modelin çıktısı (f) bulunur.

D. Performans Metrikleri

Yapay sinir ağlarının (ANN) performansı, kullanılan verilerin ölçeklenmesine (normalizasyon) yakından bağlıdır [8]. Normalizasyon, veri setindeki dağılımı düzenler ve farklı birimlerdeki parametrelerin aynı ölçek ile değerlendirilmesini sağlar. Bu sayede, ANN'nin girdi setinde bulunan aşırı uç değerlerin tahmin performansını olumsuz etkilemesi önlenir ve ağın öğrenme süreci daha verimli hale gelir. Özellikle, ANN'lerin kesin değerlerle çalışması, 0 çarpanının ezberlenmesine ve sabit çıktı üretmesine yol açabilir. Yağış veri setinde çokça 0 değerinin olması sebebiyle, ağın ezberlemesini önlemek için veriler 0.1 – 0.9 aralığında ölçeklendirilmiştir. Normalizasyon işlemi için denklem (9) kullanılmıştır [27].

$$x' = 0.8 * \frac{x_i - x_{min}}{x_{max} - x_{min}} + 0.1 \tag{9}$$

Burada x' normalleştirilmiş değeri temsil eder, x_i ise orijinal veriyi ifade eder. x_{min} ve x_{max} sırasıyla veri setindeki minimum ve maksimum değerlerdir.

Hataların Karesinin Ortalamasının Karekökü (RMSE), model hatalarının büyüklüğünü ölçer. Düşük değerler, modelin tahminlerinin gözlemlenen değerlere yakınlığını gösterir. Formülü denklem (10)'da verilmiştir:

$$RMSE = \sqrt{\frac{1}{n}\sum_1^n (Q_{obs} - Q_{sim})^2} \tag{10}$$

Burada n veri adeti, Q_{obs} gözlemlenen debi ve Q_{sim} tahmin edilen debi değeridir.

Belirleme Katsayısı veya Pearson Korelasyon Katsayısının Karesi (R^2 veya r^2) iki değişken arasındaki doğrusal ilişkinin ne kadarının açıklanabildiğini gösterir. R^2 değeri 0 ile 1 arasında değişir. Formülü denklem (11)'de verilmiştir:

$$R^2 = \frac{\left(\sum(x-\bar{x})(y-\bar{y})\right)^2}{\sum(x-\bar{x})^2 \sum(y-\bar{y})^2} \tag{11}$$

Burada x ve y değişkenlerin değerleri, $\bar{x}$ ve $\bar{y}$ ise değişkenlerin ortalama değerleridir.

Nash-Sutcliffe Verimliliği (NSE), gözlemlenen değerlerin ortalamasına göre tahmin edilen değerlerin ne kadar iyi olduğunu gösterir. NSE değeri 1'e yaklaştıkça modelin uyumu artar. Formülü denklem (12)'de verilmiştir:

$$NSE = 1 - \frac{\sum_1^n (Q_{obs} - Q_{sim})^2}{\sum_1^n (Q_{obs} - \bar{Q}_{obs})^2} \tag{12}$$

Burada n veri adeti, Q_{obs} gözlemlenen debi, Q_{sim} tahmin edilen debi ve $\bar{Q}_{obs}$ gözlemlenen değerlerin ortalamasıdır.

Kling-Gupta Verimliliği (KGE), gözlemlenen ve tahmin edilen değerlerin benzerliğini ifade eder. KGE değeri 1'e yaklaştıkça, iyi kabul edilir. Formülü denklem (13)'te verilmiştir:

$$KGE = 1 - \sqrt{(r-1)^2 + (\alpha - 1)^2 + (\beta - 1)^2} \tag{13}$$

Burada r Pearson korelasyon katsayısı, α simüle edilen ve gözlemlenen veri setlerinin standart sapmalarının oranı, β ise ortalama değerlerin oranıdır.

III. BULGULAR

Bu çalışma kapsamında, Terme Çayı havzasında D22A002 numaralı AGİ için 01.02.2022-30.09.2022 tarihleri arasında gözlemlenen günlük ortalama debilerin (m^3/s) tahmin edilmesi için RNN, LSTM ve ANFIS derin öğrenme yöntemleri ile modeller oluşturulmuştur. Modellerde havzanın günlük toplam yağış miktarı ile D22A143 numaralı ve D22A002 numaralı AGİ'de ölçülen günlük ortalama debi veri setleri kullanılmıştır.

Modellerin girdi katmanında bulunan bir gün öncesinin (t-1) yağış verisi [P(t-1)], D22A143 numaralı AGİ'nin debi verisi [Q_2(t-1)] ve D22A002 numaralı AGİ'nin debi verisi [Q_1(t-1)] ile çıktı olarak istenilen D22A002 numaralı AGİ'ye ait (t) gününün debi verisi [Q_1(t)] arasındaki ilişkiyi gösteren korelasyon ısı haritası Şekil 8'de verilmiştir.

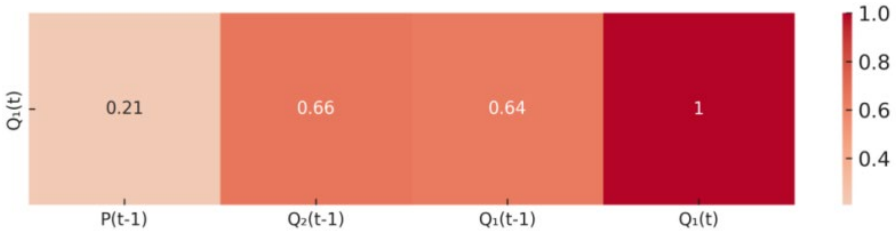

Şekil 8. Girdiler [P(t-1), Q_2(t-1), Q_1(t-1)] ile çıktı [Q_1(t)] veri seti arasındaki ilişkiyi gösteren korelasyon ısı haritası.

Isı haritası incelendiğinde, Q_1(t) ile Q_1(t-1) arasındaki korelasyon 0.64, Q_1(t) ile Q_2(t-1) arasındaki korelasyon 0.66 olarak belirlenmiştir. Bu durum, önceki gün debi değerlerinin güncel debi üzerinde etkili olduğunu, iki ardıl istasyonun hidrolojik olarak birbirleriyle ilintili olduğunu ve bir istasyondaki debi değişimlerinin diğer istasyondaki değişimleri tahmin etmede kullanılabileceğini göstermektedir. Q_1(t) ile P(t-1) arasındaki korelasyon 0.21 olup, bu da önceki günün yağış miktarının güncel debi üzerindeki etkisinin sınırlı olduğunu göstermektedir.

Modeller sonucunda çıktı olarak D22A002 numaralı AGİ için günlük ortalama debi (m^3/s) değerleri üretilmiştir. Bu üretilen tahminler için, performans metrikleri hesaplanmış ve görseller oluşturulmuştur. Hesaplanan performans metrikleri Tablo 4'te, oluşturulan görseller ise Şekil 9'da ve Şekil 10'da verilmiştir.

TABLO 4
Hesaplanan performans metrikleri.

	RNN	LSTM	ANFIS
RMSE	12.811	12.731	11.109
R^2	0.623	0.628	0.604
NSE	0.555	0.561	0.588
KGE	0.481	0.489	0.590

Tablo 4 incelendiğinde, RMSE değerleri modellerin tahminlerinde belirli bir hata payı olduğunu ve iyileştirilmeleri gerektiğini göstermektedir. En düşük RMSE değerine sahip model ANFIS'tir. R^2 değerlerinde, LSTM modeli veri varyansının %63'ünü açıklarken, RNN modeli de benzer bir performans sergilemektedir. ANFIS modelinin R^2 değeri diğerlerinden düşüktür. NSE değerlerine göre, ANFIS modeli gözlemlenen verilerle daha uyumludur, ancak performansı iyileştirilebilir. KGE değerlerine göre, ANFIS modeli genel performans açısından en iyi sonucu vermiştir.

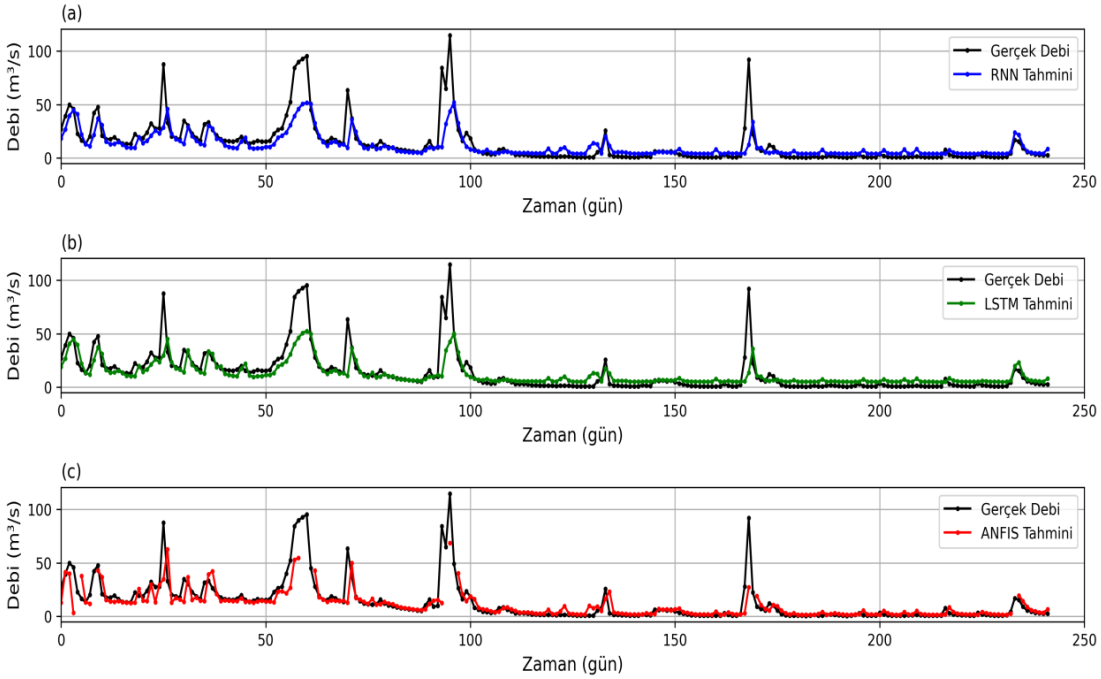

Şekil 9. (a) RNN, (b) LSTM ve (c) ANFIS modellerinin, zaman içerisindeki debi (m^3/s) değişimlerini nasıl yakaladıklarını gösteren zaman serisi grafikleri.

RNN (Şekil 9a) ve LSTM (Şekil 9b) modellerinin zaman serisi grafikleri incelendiğinde, her iki modelin de genel trende uyum sağladığı ve düşük ile orta debi değerlerinde gerçek değerlere yakın sonuçlar verdiği görülmüştür. Ancak, ani yükselme noktalarında tahmin performansları düşmektedir. RNN, kısa vadeli bellek yapısı nedeniyle ani değişimleri yakalamakta zorlanırken, LSTM dalgalanmaları daha iyi yakalamakta fakat bazı hatalar yapmaktadır. ANFIS modelinin zaman serisi grafiği (Şekil 9c) ise debi değişimlerini en iyi yakalayan modeldir ve özellikle düşük ve orta debi değerlerinde yüksek doğrulukla tahminler yapmaktadır. Yüksek debi değerlerinde de diğer iki modele göre daha iyi sonuçlar vermektedir. Değerlendirme sırasında ANFIS modelinin anormal değerleri (9 adet) temizlenmiştir.

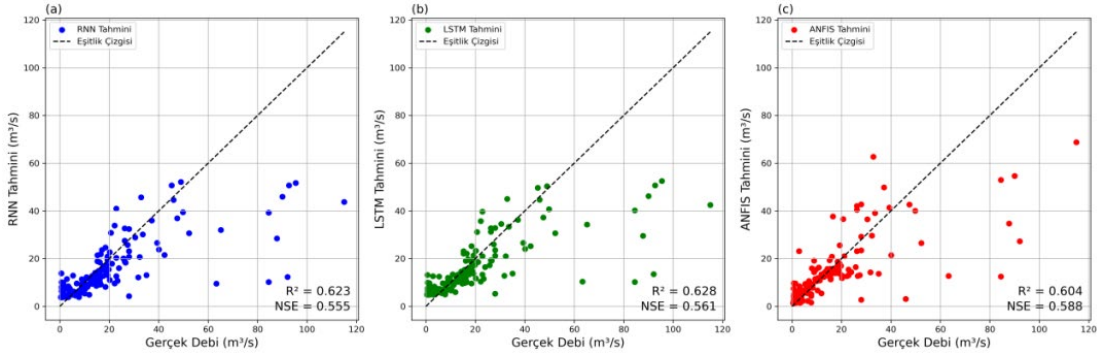

Şekil 10. (a) RNN, (b) LSTM ve (c) ANFIS modelleri için gerçek ve tahmin edilen debilerin (m^3/s) dağılımını gösteren saçılım grafikleri.

RNN (Şekil 10a) ve LSTM (Şekil 10b) modellerinin saçılım grafikleri, düşük debi değerlerinde (0-40 m^3/s) başarılı tahminler ürettiklerini, ancak orta ve yüksek debi değerlerinde (40 m^3/s ve üzeri) tahmin hatalarının arttığını göstermektedir. Özellikle 60 m^3/s ve üzeri değerlerde tahminler gerçeğin altında kalmıştır. LSTM modeli RNN modelinden biraz daha iyi performans gösterirken, yüksek debi değerlerinde her iki modelin de iyileştirilmesi gerekmektedir. ANFIS modelinin saçılım grafiği (Şekil 10c) düşük debi

değerlerinde çok başarılı, orta debi değerlerinde genel olarak doğru tahminler yaptığını, yüksek debi değerlerinde ise tahmin hatalarının arttığını ancak RNN ve LSTM modellerine göre daha düşük seviyelerde olduğunu göstermektedir. ANFIS modelinin performans metrikleri, modelin genel olarak iyi performans gösterdiğini ve yüksek debi değerlerinde diğer modellere göre daha tutarlı tahminler yaptığını ortaya koymaktadır.

IV. SONUÇ VE ÖNERİLER

Korelasyon analizi, debi tahminlerinde önceki dönem debi değerlerinin önemli olduğunu, yağışın etkisinin ise daha sınırlı kaldığını göstermiştir; yağış veri seti korelasyonunun düşük olması, ham CHIRPS veri seti kaynaklı olabileceği belirlenmiştir.

RNN modeli, düşük ve orta debi değerlerinde başarılı tahminler yapmış, ancak yüksek debi değerlerinde performansı düşmüştür; performans metrik değerleri, RNN modelinin orta seviyede bir performans sergilediğini göstermektedir. LSTM modeli, genel olarak RNN modeline göre daha iyi performans göstermiştir; düşük ve orta debi değerlerinde başarılı tahminler yapmış, ancak yüksek debi değerlerinde bazı sapmalar göstermiştir. Performans metrik değerleri, LSTM modelinin veri varyansını daha iyi açıkladığını ve gözlemlenen verilerle daha uyumlu olduğunu göstermektedir. ANFIS modeli, diğer iki modele kıyasla en yüksek performansı sergilemiştir; düşük, orta ve yüksek debi değerlerinde en tutarlı ve doğru tahminleri yapmıştır. Performans metrik değerleri, ANFIS modelinin tahminlerinin en az hata içerdiğini, veri varyansını iyi açıkladığını ve gözlemlenen verilerle en uyumlu model olduğunu göstermektedir.

ANFIS modelinin en yüksek NSE değerine sahip olmasına rağmen en düşük R^2 değerine sahip olması, modelin genel olarak gözlemlenen verilerle iyi bir uyum sağladığını, ancak doğrusal ilişkileri yakalamada yetersiz kalabileceğini göstermektedir. Ayrıca, NSE metriği ekstrem değerleri daha fazla dikkate aldığı için ANFIS modelinin ekstrem değerlerdeki performansının diğer modellere göre daha iyi olduğunu ortaya koymaktadır.

Sonuçlar, çalışmada kullanılan ANFIS yönteminin gelecekteki debi tahminlerinde uygulanabilir olduğunu ortaya koymuştur. Ayrıca, RNN ve LSTM modellerinin de geliştirilmesi durumunda önemli bir potansiyele sahip olduğu gösterilmiştir. Sonuçlar, CHIRPS veri setinin, yağış ölçümleri için yeterli yer istasyonu bulunmayan bölgelerde kullanılabileceğini, ancak mümkün olduğunca yerel yağış ölçüm verileri ile kalibre edilmesi gerektiğini göstermektedir.

Bu çalışmanın bulgularına dayanarak, derin öğrenme yöntemleriyle debi tahmin modellerinin performansını artırmak ve su kaynakları yönetiminde daha etkili kararlar almak için daha geniş zaman aralıklarını (örneğin 10 yıllık, 30 yıllık) ve daha kapsamlı veri setlerini (örneğin sıcaklık, buharlaşma, nem) kullanarak modellerin performansının artırılabileceği söylenebilir. Modellerde yüksek debi değerlerinde tahmin hatalarının arttığı gözlemlenmiştir, bu nedenle ekstrem olayların eğitim süreçlerinde daha fazla dikkate alınması ve model yapılandırmalarının bu doğrultuda optimize edilmesi gerekmektedir. Mevsimsel ve bölgesel farklılıkların dikkate alınması da model performansına olumlu etkisi olacaktır.

Gelecekteki debi tahminlerini iyileştirmek için, ara katmanlar ve nöron sayısı gibi model yapılandırmalarının yanı sıra, iterasyon miktarı, üyelik fonksiyonları ve algoritmaların da değiştirilmesi mümkündür. Çalışmada kullanılan modellerin her biri farklı güçlü yönlere sahiptir ve hibrit modellerin kullanılması ile elde edilen sonuçların çeşitli performans kriterleriyle değerlendirilmesi, daha başarılı sonuçlar sağlayan modellerin belirlenmesine yardımcı olabilir.

KAYNAKLAR

[1] Anusree, K., & Varghese, K. O. (2016). Streamflow Prediction of Karuvannur River

Basin Using ANFIS, ANN and MNLR Models [Elsevier B.V.]. In Procedia Technology (Vol. 24).
[2] Asaad, M. (2021). Aylık Ortalama Akım Verilerinin Yapay Sinir Ağları Kullanılarak Tahmin Edilmesi. In Doctoral dissertation, Necmettin Erbakan University (Turkey).
[3] Assem, H., Ghariba, S., Makrai, G., Johnston, P., Gill, L., & Pilla, F. (2017). Urban water flow and water level prediction based on deep learning. In Machine Learning and Knowledge Discovery in Databases: European Conference, ECML PKDD 2017, Skopje, Macedonia, September 18–22, 2017, Proceedings, Part III 10, Springer International Publishing.
[4] Bayazıt, M. (2011). Hidroloji. Birsen Yayınevi.
[5] Bengio, Y., Simard, P., & Frasconi, P. (1994). Learning long-term dependencies with gradient descent is difficult. IEEE transactions on neural networks, 5(2), 157-166.
[6] Beven, K. (2020). Deep learning, hydrological processes and the uniqueness of place. In Hydrological Processes (Vol. 34, Issue 16).
[7] Beven, K. J. (2012). Rainfall-runoff modelling: the primer. In John Wiley & Sons.
[8] Chakraborty, G., & Chakraborty, B. (2000). A Novel Normalization Technique for Unsupervised Learning in ANN (Vol. 11, Issue 1). IEEE transactions on neural networks, 11(1), 253-257.
[9] Cigizoglu, H. K. (2003). Estimation, forecasting and extrapolation of river flows by artificial neural networks. In Hydrological Sciences Journal (Vol. 48, Issue 3).
[10] de Oliveira-Júnior, J. F., da Silva Junior, C. A., Teodoro, P. E., Rossi, F. S., Blanco, C. J. C., Lima, M., de Gois, G., Correia Filho, W. L. F., de Barros Santiago, D., & dos Santos Vanderley, M. H. G. (2021). Confronting CHIRPS dataset and in situ stations in the detection of wet and drought conditions in the Brazilian Midwest. In International Journal of Climatology (Vol. 41, Issue 9).
[11] Dibike, Y. B., & Solomatine, D. P. (2001). River flow forecasting using artificial neural networks. In Physics and Chemistry of the Earth, Part B: Hydrology, Oceans and Atmosphere, 26(1), 1-7.
[12] Funk, C., Peterson, P., Landsfeld, M., Pedreros, D., Verdin, J., Shukla, S., Husak, G., Rowland, J., Harrison, L., Hoell, A., & Michaelsen, J. (2015). The climate hazards infrared precipitation with stations — a new environmental record for monitoring extremes [Scientific data, 2(1).].
[13] Gemici, E., Ardıçlıoğlu, M., & Kocabaş, F. (2013). Akarsularda debinin yapay zekâ yöntemleri ile modellenmesi. In Erciyes Üniversitesi Fen Bilimleri Enstitüsü Dergisi (Vol. 29, Issue 2).
[14] Girma, D., & Berhanu, B. (2021). Evaluation of the Performance of High-Resolution Satellite Based Rainfall Products for Stream Flow Simulation. In Research Article (Vol. 11, Issue April).
[15] Hochreiter, S., & Schmidhuber, J. (1997). Long short-term memory. Neural computation, 9(8).
[16] Hu, Y., Yan, L., Hang, T., & Feng, J. (2020). Stream-Flow Forecasting of Small Rivers Based on LSTM.
[17] Jang, J. S. (1993). ANFIS: adaptive-network-based fuzzy inference system (Vol. 23, Issue 3). IEEE transactions on systems, man, and cybernetics.
[18] Kişi, Ö. (2007). Streamflow Forecasting Using Different Artificial Neural Network Algorithms. In Journal of Hydrologic Engineering (Vol. 12, Issue 5).
[19] Kratzert, F., Klotz, D., Brenner, C., Schulz, K., & Herrnegger, M. (2018). Rainfall-runoff modelling using Long Short-Term Memory (LSTM) networks. In Hydrology and Earth System Sciences (Vol. 22, Issue 11).
[20] Kwak, J., Han, H., Kim, S., & Kim, H. S. (2022). Is the deep-learning technique a completely alternative for the hydrological model?: A case study on Hyeongsan River

Basin, Korea. In Stochastic Environmental Research and Risk Assessment (Vol. 36, Issue 6).

[21] Lohani, A. K., Kumar, R., & Singh, R. D. (2012). Hydrological time series modeling: A comparison between adaptive neuro-fuzzy, neural network and autoregressive techniques [Elsevier B.V.]. In Journal of Hydrology (Vols. 442–443, Issue January).

[22] Rivera, J. A., Marianetti, G., & Hinrichs, S. (2018). Validation of CHIRPS precipitation dataset along the Central Andes of Argentina [Elsevier B.V]. In Atmospheric Research (Vol. 213).

[23] Sahoo, B. B., Jha, R., Singh, A., & Kumar, D. (2019). Long short-term memory (LSTM) recurrent neural network for low-flow hydrological time series forecasting [Springer International Publishing]. In Acta Geophysica (Vol. 67, Issue 5).

[24] Sareen, K., Panigrahi, B. K., & Shikhola, T. (2023). A Short-term solar irradiance forecasting modelling approach based on three decomposition algorithms and Adaptive Neuro-Fuzzy Inference System. In Expert Systems with Applications, 120770.

[25] Sulugodu, B., & Deka, P. C. (2019). Evaluating the Performance of CHIRPS Satellite Rainfall Data for Streamflow Forecasting [Water Resources Management]. In Water Resources Management (Vol. 33, Issue 11).

[26] Xu, W., Jiang, Y., Zhang, X., Li, Y., Zhang, R., & Fu, G. (2020). Using long short-term memory networks for river flow prediction. In Hydrology Research (Vol. 51, Issue 6).

[27] Yavuz, S., & Deveci, M. (2012). İstatistiksel normalizasyon tekniklerinin yapay sinir ağın performansına etkisi. Erciyes Üniversitesi İktisadi ve İdari Bilimler Fakültesi Dergisi, (40), 167-187.

Self-Gravitational Solitary Potential in Degenerate Quantum Plasmas

Muhammad Asaduzzaman

azaman@phy.kuet.ac.bd, ORCID: 0009-0002-7632-045X
Department of Physics, Khulna University of Engineering and Technology, Khulna-9203, Banglades

Abstract: A rigorous theoretical investigation has been made on the nonlinear propagation of self-gravitational perturbation (SGP) mode in a degenerate quantum plasma system consisting of ultra-relativistic degenerate electrons and extremely heavy nuclei. The well-known reductive perturbation technique has been used to examine the propagation of this perturbation mode. The nonlinear dynamics of the SGP mode in planar geometry is governed by the Korteweg-de Vries (K-dV) equation with negative dispersion coefficient. The solution of the K-dV equation has been obtained and has also been analysed numerically to identify the salient features of self-gravitational solitary waves (SGSWs) that may form in such a plasma system. The implications of our results in astrophysical compact objects like white dwarfs and neutron stars, where degenerate quantum plasma exists, are briefly discussed.

Keywords: *Solitary waves, Self-gravitational perturbation, Degenerate quantum plasma, Relativity*

I. INTRODUCTION

Classical plasmas are those in which the quantum nature of the constituent particles does not affect the macroscopic dynamics of the plasma. Classical plasmas behave macroscopically and obey the laws of classical mechanics. Classical plasmas enter into the regime of quantum plasma when the particle number density of classical plasma increases or its temperature decreases and in this case the quantum nature of the constituent particles starts to affect its macroscopic properties and dynamics.

Under extremely high pressure, ordinary matter undergoes degenerate matter which are supported mainly by quantum mechanical effects. In physics, if two states have the same energy and are thus interchangeable then the states are known as degenerate states. When the quantum degeneracy of matter becomes significant [1] due to Pauli's exclusion principle then the plasma system becomes degenerate quantum plasma. White dwarfs and neutron stars are the examples of degenerate quantum plasma, where the number density is very high [2-8]. Neutron star is a mixture of electrons, nucleons, and extremely heavy nuclei/element [9-11]. Self-gravitational pressure counterbalances the degenerate pressure of electrons for astrophysical compact objects like white dwarfs and neutron stars.

The pressure balance equation for ultra-relativistic limit [2-4] can be written as $P_e = K_e n_e^{\gamma}$, where $\gamma = 4/3$ and $K_e = 3\hbar c/4$; P_e is the degenerate pressure of electrons; n_e is the number density of degenerate electrons; K_e is the constant of proportionality.

A significant number of authors [12-21] have been studied the propagation of electrostatic waves in degenerate quantum plasma. Marklund and Brodin [12] examined the response (linear) of the quantum plasma in an electron-ion system. Their results are applicable for both solid density plasma and astrophysical plasma. Shukla and Eliasson [13] examined the dark

solitons and vortices in quantum electron plasmas. Their results are applicable for the transport of information at quantum scales in microplasmas. Mahmood *et al.* [17] investigated the nonlinear propagation of ion acoustic wave in a homogeneous magnetized electron-positron-ion plasma. Michael *et al.* [19] studied ion-acoustic (IA) shock waves in a magnetized, five component cometary plasma consisting of positively and negatively charged oxygen ions, kappa described hydrogen ions, hot solar electrons and slightly colder cometary electrons. Manfredi [21] illustrated several mathematical models to describe the dynamics of a quantum plasma in the collision-less regime.

To the best of the authors knowledge, no investigation has been made of nonlinear waves associated with the self-gravitational solitary potential by considering a degenerate quantum plasma system consisting of non-inertial ultra-relativistic degenerate electrons and inertial heavy nuclei. Therefore, in this communication, we are interested in examining the SGSWs by considering a degenerate quantum plasma system containing inertial heavy nuclei and ultra-relativistic degenerate electrons.

The manuscript is organized in the following fashion: Section II contains the Governing equations. Subsection II*A* contains K-dV equation and its solution. Section III includes the results and finally section IV represents conclusion.

II. GOVERNING EQUATIONS

We consider the SGSWs propagating in a plasma system consisting of non-inertial ultra-relativistic degenerate electrons and inertial heavy nuclei. At equilibrium, the electron number density (n_{e0}) and the heavy nuclei number density (n_{h0}) make the relation $n_{e0} = Z_h n_{h0}$.

The dynamics of the ultra-relativistic degenerate electrons and the dynamics of the inertial heavy nuclei can be expressed as

$$K_e \frac{\partial n_e^{4/3}}{\partial x} = -m_e n_e \frac{\partial \psi}{\partial x}, \tag{1}$$

$$\frac{\partial n_h}{\partial t} + \frac{\partial}{\partial x}(n_h u_h) = 0, \tag{2}$$

$$\frac{\partial u_h}{\partial t} + u_h \frac{\partial u_h}{\partial x} = -\frac{\partial \psi}{\partial x}, \tag{3}$$

$$\frac{\partial^2 \psi}{\partial x^2} = 4\pi G[m_h(n_h - n_{h0}) + m_e(n_e - n_{e0})]. \tag{4}$$

In the above equations, the self-gravitational potential is defined by ψ; the nucleus fluid speed is expressed by u_h; the electron number density is defined by n_e; the heavy nucleus number density is denoted by n_h; the rest mass of electron and heavy nucleus are defined by m_e and m_h respectively; the space variable and time variables are expressed by x and t respectively; $K_e = 3\hbar c/4$; G is the universal gravitational constant; n_h and n_e are the unperturbed number densities of nondegenerate heavy nuclei and degenerate electrons, respectively.

In the abovementioned plasma model, the ultra-relativistic degenerate electrons provide the restoring force and the heavy nuclei provides the inertia. The continuity and momentum balance equation for electron is unnecessary because we get the value of n_e directly from Eq. (1).

A. K-dV Equations and its Solution

We consider the stretched coordinates [23-24]

$$\left.\begin{aligned}\xi &= \epsilon^{1/2}(x - V_p t),\\ \tau &= \epsilon^{3/2} t,\end{aligned}\right\} \tag{5}$$

where ϵ is a smallness parameter measuring the weakness of the amplitude or dispersion ($0 < \epsilon < 1$); V_p is the phase speed of the SGSWs. Now expanding the dependent variables in power series of ϵ, we obtain

$$\left.\begin{aligned}n_h &= n_{h0} + \epsilon n_h^{(1)} + \epsilon^2 n_h^{(2)} + \cdots\cdots\cdots,\\ n_e &= n_{e0} + \epsilon n_e^{(1)} + \epsilon^2 n_e^{(2)} + \cdots\cdots\cdots,\\ u_h &= 0 + \epsilon u_h^{(1)} + \epsilon^2 u_h^{(2)} + \cdots\cdots\cdots,\\ \psi &= 0 + \epsilon\psi^{(1)} + \epsilon^2\psi^{(2)} + \cdots\cdots\cdots\cdots.\end{aligned}\right\} \tag{6}$$

Substituting Eqs. (5) and (6) into Eqs. (1) - (4), we obtain various equations in various powers of ϵ. Now, taking the coefficient of lowest order in ϵ, we have

$$u_h^{(1)} = \frac{\psi^{(1)}}{V_p}, \tag{7}$$

$$n_h^{(1)} = \frac{n_{h0}}{{V_p}^2}\psi^{(1)}, \tag{8}$$

$$n_e^{(1)} = -\frac{3\,{n_{e0}}^{2/3}}{K}\psi^{(1)}, \tag{9}$$

$$V_p = \sqrt{\frac{m_h n_{h0} K}{3 m_e\,{n_{e0}}^{2/3}}}, \tag{10}$$

where $K = \frac{4K_e}{m_e}$.

If we take the coefficient of ϵ for the next higher order we get the following equations

$$\frac{\partial n_e^{(2)}}{\partial\xi} - \frac{6{n_{e0}}^{1/3}}{K^2}\psi^{(1)}\frac{\partial\psi^{(1)}}{\partial\xi} + \frac{3\,{n_{e0}}^{2/3}}{K}\frac{\partial\psi^{(2)}}{\partial\xi} = 0 \tag{11}$$

$$\frac{\partial n_h^{(1)}}{\partial\tau} - V_p\frac{\partial n_h^{(2)}}{\partial\xi} + \frac{\partial}{\partial\xi}\left[n_{h0}u_h^{(2)} + n_h^{(1)}u_h^{(1)}\right] = 0 \tag{12}$$

$$\frac{\partial u_h^{(1)}}{\partial\tau} - V_p\frac{\partial u_h^{(2)}}{\partial\xi} + u_h^{(1)}\frac{\partial u_h^{(1)}}{\partial\xi} + \frac{\partial\psi^{(2)}}{\partial\xi} = 0, \tag{13}$$

$$\frac{\partial^2\psi^{(1)}}{\partial\xi^2} - 4\pi G\left[m_h n_h^{(2)} + m_e n_e^{(2)}\right] = 0\,. \tag{14}$$

Now, using Eqs. (7) – (14) and by performing some mathematical calculation, we deduce the Korteweg-de Vries (K-dV) equation with the negative dispersion term in the form

$$\frac{\partial\psi^{(1)}}{\partial\tau} + A\psi^{(1)}\frac{\partial\psi^{(1)}}{\partial\xi} + B\frac{\partial^3\psi^{(1)}}{\partial\xi^3} = 0, \tag{15}$$

where A and B are nonlinear coefficient and dispersion coefficient respectively, which are given by

$$A = \left[\frac{3}{2V_p} + \frac{12\pi G m_e {n_{e0}}^{1/3}{V_p}^3}{K^2\omega_{jh}^2}\right], \tag{16}$$

$$B = -\frac{{V_p}^3}{2\omega_{jh}^2}, \tag{17}$$

with $\omega_{jh}^2 = 4\pi G m_h n_{h0}$.

The stationary localized solution of Eq. (15) for a moving frame moving with a speed u_0 can be written as

$$\psi^{(1)} = \psi^0 \, Sec^2\left(\frac{\zeta}{\Delta}\right), \tag{18}$$

where the amplitude ψ^0 and the width Δ are given by

$$\psi^0 = 3u_0/A \;\text{ and }\; \Delta = \sqrt{\frac{4B}{u_0}}. \tag{19}$$

Equation (18) discloses that the self-gravitational positive potential of amplitude $\psi^0 = 3u_0/A$ and width $\Delta = \sqrt{\frac{4B}{u_0}}$ exist only when $u_0 > 0$. It is observed that the amplitude ψ^0 of the SGSWs increases as shock speed (u_0) increases while the width Δ decreases. The numerical analysis of Eq. (15) is displayed in Figs. 1 – 5.

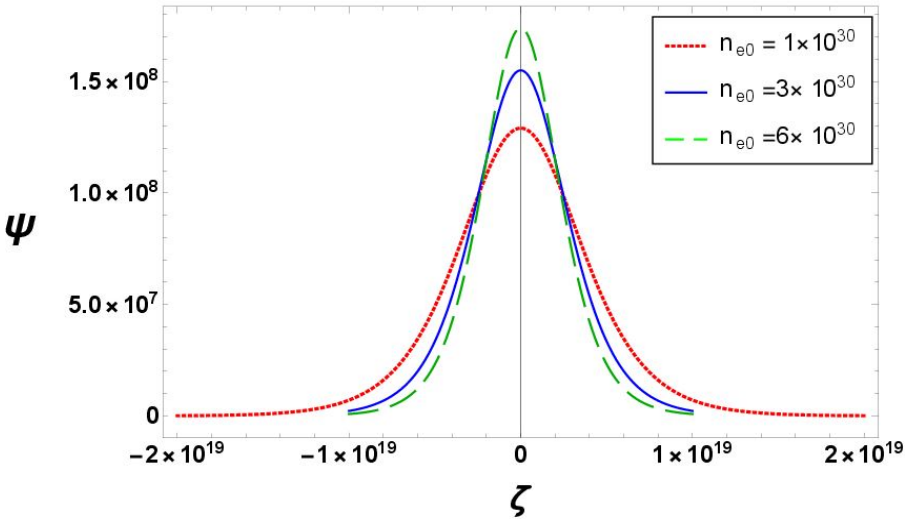

Fig. 1: Variation of the solitary profile for different values of n_{e0}. The other parameters are fixed at u_0 = 0.05 cm/sec, Z_h =37, and $M_h = 85m_p$ (m_p represents the mass of proton).

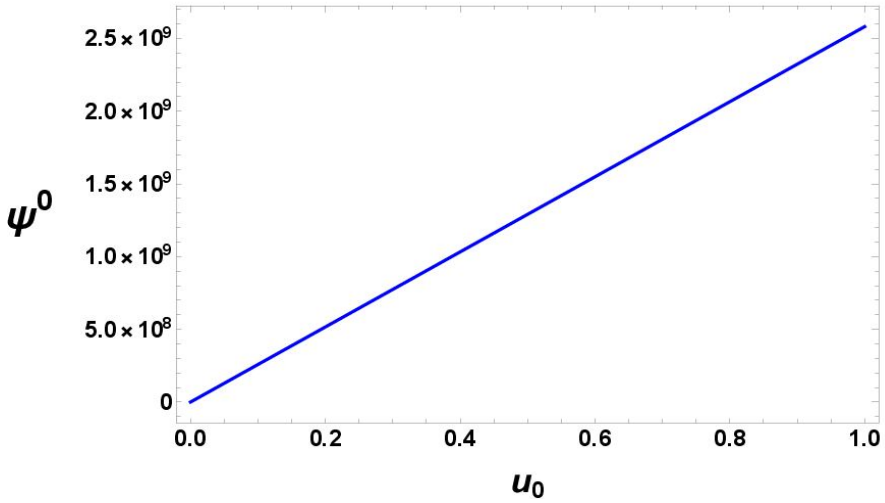

Fig. 2: Variation of the amplitude ψ^0 with the solitary speed u_0. The other parameters are fixed at $n_{e0} = 10^{30} cm^{-3}$, Z_h =37, and $M_h = 85m_p$.

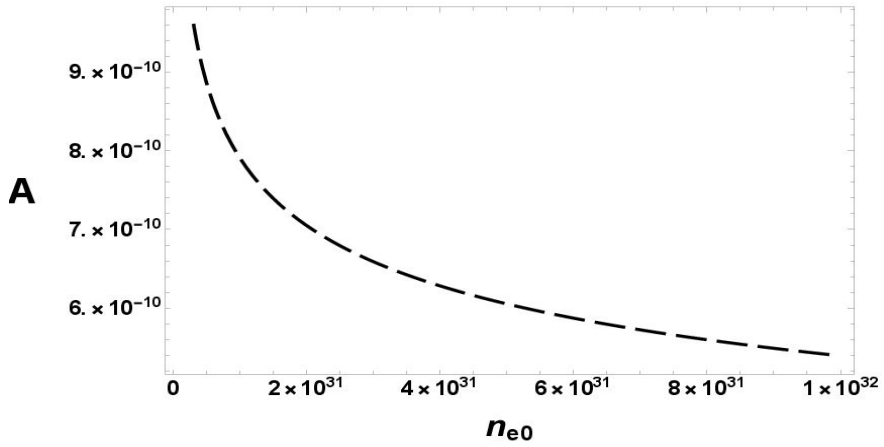

Fig. 3: Variation of the nonlinear coefficient A with electron number density n_{e0} for Z_h =37, and $M_h = 85m_p$.

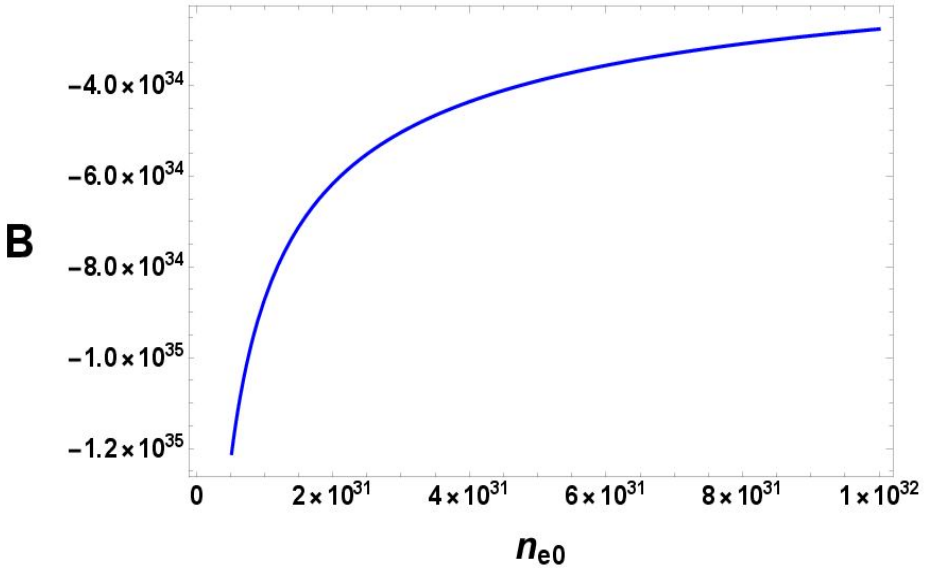

Fig. 4: Dispersion coefficient B versus n_{e0} curve with Z_h =37, and $M_h = 85m_p$.

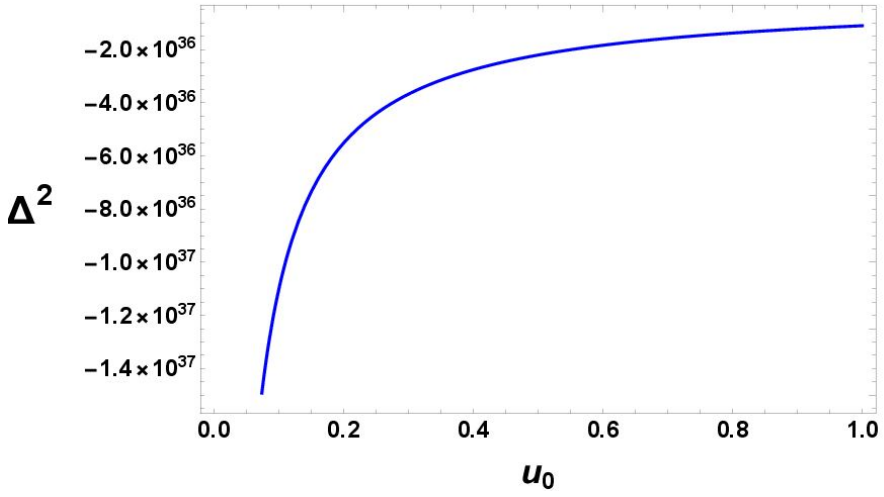

Fig. 5: Variation of Δ^2 with solitary speed u_0 with $n_{e0} = 10^{30} cm^{-3}$.

III. RESULTS

The results obtained from our current investigation can be pinpointed as follows:

i) when $u_0 > 0$, the SGSWs have positive potential only. .

ii) the amplitude of the SGSWs increases as the electron number density increases.

iii) the width of the SGSWs decreases as the electron number density increases.

iv) the amplitude of the SGSWs has linear relation with u_0.

v) the nonlinear coefficient varies inversely with the electron number density.

vi) the width of the SGSWs negatively increases with the solitary speed.

vii) the dispersion coefficient B increases as the electron number density decreases.

iv. CONCLUSION

We have studied the propagation of the solitary waves associated with the self-gravitational potential in a degenerate quantum plasma system consisting of ultra-relativistic inertialess degenerate electrons and inertial nondegenerate heavy nuclei. We have obtained the solution of K-dV equation and have also numerically analyzed to found the basic properties of SGSWs. We expect that our findings will be useful in understanding the salient features of the solitary self-gravitational potential in degenerate quantum plasmas, which exist in astrophysical compact objects like white dwarfs and neutron stars.

REFERENCES

[1] Yu. O. Tyshetskiy, S. V. Vladimirov and R. Kompaneets, "Unusual physics of quantum plasmas," *Voprosy Atomnoj Nauki i Tekhniki*, Vol. 46, pp. 76-80, 2013.

[2] S. Chandrasekhar, "The density of white dwarf stars", *The London, Edinburgh, and Dublin Philosophical Magazine and Journal of Science,* Vol. 11, no. **70**, pp. 592-596, Feb. 1931.

[3] S. Chandrasekhar, "The maximum mass of ideal white dwarfs", *Astrophysical Journal,* Vol. **74**, pp. 81, Jul. 1931.

[4] S. Chandrasekhar, "The highly collapsed configurations of a stellar mass", *Monthly Notices of the Royal Astronomical Society,* Vol. 91, pp. 456-466, Mar. 1931.

[5] S. Chandrasekhar, "An Introduction to the study of stellar structure", *Ciel et Terre,* Vol. 55, pp. 412, 1939.

[6] S. Chandrasekhar, "Dynamical instability of gaseous masses approaching the Schwarzschild limit in general relativity," *Physical Review Letters,* Vol. **12**, no. 15, pp. 437-438, Jan. 1964.

[7] S. Chandrasekhar and R. F.Tooper, "The Dynamical instability of the white-dwarf configurations approaching the limiting mass," *Astrophysical Journal, Vol.* **139**, pp. 1396, May. 1964.

[8] A. A. Mamun, "Self-gravito-acoustic shock structures in a self-gravitating, strongly coupled, multi-component, degenerate quantum plasma system," *Physics of Plasmas*, Vol. **24**, no. 10, Oct. 2017.

[7] S. A. Ema, M. R. Hossen and A. A. Mamun, "Planar and nonplanar shock waves in a degenerate quantum plasma," *Contributions to Plasma Physics,* Vol. **55**, no. 7, pp. 551-559, Aug. 2015.

[8] W. F. El-Taibany and A. A. Mamun, "Nonlinear electromagnetic perturbations in a degenerate ultrarelativistic electron-positron plasma,"*Physical Review E-Statistical, Nonlinear, and Soft Matter Physics,*Vol. **85**, no. 2, pp. 026406, Feb. 2012.

[9] A. A. Mamun and P. K. Shukla, "Solitary waves in an ultrarelativistic degenerate dense plasma," *Physics of Plasmas*, Vol. 17, no. 10, pp. 104504, Oct. 2010.

[10] A. A. Mamun and P. K. Shukla, "Arbitrary amplitude solitary waves and double layers in an ultra-relativistic degenerate dense dusty plasma," *Physics Letters A*, Vol. 374, no. 41, pp. 4238-4241, Sep. 2010.

[11] S. L. Shapiro and S. A. Teukolsky, Black Holes, White Dwarfs, and Neutron stars, "The Physics of Compact Objects," *Wiley, New York*, 19832, pp. 119-123, 1983.

[12] M. Marklund and G. Brodin, "Dynamics of spin-1 2 quantum plasmas,"*Physical Review Letters,* Vol. **98**, no. 2, pp. 025001, Jan. 2007.

[13] P. K. Shukla and B. Eliasson, "Formation and dynamics of dark solitons and vortices in quantum electron plasmas," *Physical Review Letters,* Vol. **96**, no. 24, pp. 245001, Jun. 2006.

[14] F. Haas, "Variational approach for the quantum Zakharov system," *Physics of Plasmas,* Vol. **14**, no. 4, pp. 042309, Apr. 2007.

[15] M. A. Hossen and A. A. Mamun, "Nonlinear ion-acoustic waves in a degenerate plasma with nuclei of heavy elements," *Physics of Plasmas,* Vol. **22**, no. 10, pp. 102710, Oct. 2015.

[16] M. R. Hossen and A. A. Mamun, "Electrostatic solitary structures in a relativistic degenerate multispecies plasma," *Brazilian Journal of Physics,* Vol. **44**, pp. 673-681, Dec. 2014.

[17] S. Mahmood, A. Mushtaq and H. Saleem, "Ion acoustic solitary wave in homogeneous magnetized electron-positron-ion plasmas," *New Journal of Physics,* Vol. **5**, no. 1, pp. 28, Apr. 2003.

[18] B. Hosen, M. Amina and A. A. Mamun, "Korteweg-de Vries-Burgers equation in a multi-component magnetized plasma with nuclei of heavy elements," *Journal of the Korean Physical Society,* Vol. **69**, pp. 1762-1770, Dec. 2016.

[19] M. Michael, A. Varghese, N. T. Wilington, S. Sebastian, D. E. Savithri, G. Sreekala and C. Venugopal, "Oblique io-acoustic shock waves in a magnetized, multi-species plasma," *In Journal of Physics: Conference Series,* Vol. **836**, no. 1, pp. 012007, Apr. 2017.

[20] A. P. Misra and S. Samanta, "Quantum electron-acoustic double layers in a magnetoplasma," *Physics of Plasmas,* Vol. **15**, no. 12, pp. 123307, Dec. 2008.

[21] G. Manfredi, "How to model quantum plasmas," *Fields Inst. Commun.*, Vol. 46, pp. 263- 287, Apr. 2005.

[22] A. P. Misra, S. Banerjee, P. K. Shukla and L. P. G. Assis, "Temporal dynamics in the one-dimensional quantum Zakharov equations for plasmas," *Physics of Plasmas,* Vol. **17**, no. 3, pp. 032307, Mar. 2010.

[23] P. K. Shukla and M. Y. Yu, "Exact solitary ion acoustic waves in a magnetoplasma," *Journal of Mathematical Physics,* Vol. **19**, no. 12, pp. 2506-2508, Dec. 1978.

[24] H. Washimi and T. Taniuti, "Propagation of ion-acoustic solitary waves of small amplitude," *Physical Review Letters,* vol. **17**, no. 19, pp. 996, Nov. 1966.

Effects of Different Nitrogen Levels on Some Agronomical Characteristics of *Echinacea purpurea* L. Moench.

Amir Soltanbeigi[1], Hasan Maral[2*]

[*] hasmaral@kmu.edu.tr ORCID: 0000-0001-9074-1109
[1]*Department of Basic Pharmaceutical Sciences, Faculty of Pharmacy, Afyonkarahisar Health Sciences University, Afyonkarahisar, Türkiye*
[2] *Karamanoğlu Mehmetbey University, Vocational School of Technical Sciences, Karaman, Türkiye*

Abstract: This study was carried out to determine the agronomic response of *Echinacea purpurea* L. Moench to different levels of N (urea) and foliar application of some macro and micronutrients in Afyonkarahisar Province, Türkiye. The experimental treatments were N_0: without any application as the control, N_1: 75 kg ha^{-1}, N_2: 150 kg ha^{-1} of N and N_3: 75 kg ha^{-1} of N + foliar fertilizer). While the highest values of all properties examined were obtained at the N_2 treatment, the lowest values were observed in the control group. According to the results of all five cuttings, the highest and lowest values of some yield components were as follows: number of stem (43 and 20 no plant^{-1}), number of buds (20 and 8 no plant^{-1}), number of flower (37 and 18 number plant-1), essential oil ratio (0.22 and 0.16%), fresh bud weight (17 and 7 g plant^{-1}), dry bud weight (3.6 and 1.6 g plant^{-1}), fresh flower weight (257 and 114 g plant^{-1}), dry flower weight (60 and 27 g plant^{-1}), fresh leaf weight (352 and 146 g plant^{-1}), dry leaf weight (82 and 35 g plant^{-1}), fresh stem weight (351 and 152 g plant^{-1}), dry stem weight (115 and 50 g plant^{-1}), fresh herb weight (979 and 423 g plant^{-1}), dry herb weight (262 and 114 g plant^{-1}). Also, the total yield of the plant in the 2nd (1st cutting in 2nd year) and 4th cuttings (1st cutting in 3rd year) was superior to other cuttings.

Keywords: *Echinacea, Foliar fertilizer, Nitrogen, Yield*

I. INTRODUCTION

Medicinal and aromatic plants have been used since ancient times to prevent and cure diseases. In addition, while these plants were used as incense in religious ceremonies and medicines in treatment in the past, today they are much more diversified and energized in aromatherapy, pharmaceutical drugs, aromatherapy, herbal dyeing, landscape, perfume industry, shampoos, detergents, soaps, candles, softeners, it is included in creams and lotions, so everything we want it to smell good [1].

Asteraceae, which is the richest family of flowering plants, is represented by around 1000 genera and 20.000 species on earth.134 genera and 1156 species belonging to this family are grown in Türkiye. One of the members of this family, which has great economic importance, is Echinacea species [2].

Echinacea (*Echinacea purpurea* L. Munch) is a medicinal and perennial herb which is widely used in the pharmaceutical industry, especially in Europe and the United States [3]. The genus Echinacea has 11 species, of those 3 species (*E. angustifolia* DC var. *Angustifolia*, *E. pallida* Nutt and *E. purpurea* L. Moench) are used pharmaceutically. The most valuable parts of *E. angustifolia* and *E. pallid* are their roots, while the whole of *E. purpurea* has medicinal uses [3].

The plant parts used in medicinal plants vary according to the species. In some species, all herbs, in others, special plant parts such as root, flower and leaf are used. *Echinacea* is one of the medicinal plants whose above and underground parts are used depending on the species, and the quality of the drug varies according to the parts on the plant. The market of the plant will be the whole plant herb according to its intended use, and there are also buyers who demand only special parts such as leaves, flowers and roots. Quality is important in order to benefit from medicinal and aromatic plants effectively. In medicinal and aromatic plants, the amount of substances in the composition of the plant is as important [4]. For this reason, it is important to determine the stages such as growing medicinal and aromatic plants, harvest time, drying, extraction and where the bioactive components of the plant are found more. The type and amount of bioactive components contained in *Echinacea* vary depending on various factors [4, 5]. Medicinal and aromatic plants are strongly affected by environmental factors. These factors influence the fresh and dry weight, as well as active substances of herbs. In this respect, the use of chemical fertilizers and their different forms can increase the yield of active substances and the main components of medicinal plants [6].

Nitrogen is an important factor affecting the quantity and quality of medicinal plants. Numerous studies indicated that increased nitrogen can improve water use efficiency and reduce the negative impacts of drought stress on plant growth in arid areas. However, nitrogen nutrition is associated with drought stress tolerance and increasing nitrogen supply, the physiological state and plant growth will be improved in response to reduced water availability in the soil [7]. On the other hand, if the available nitrogen is less or higher than the optimum amount for the plant growth rate, it will disrupt the vital and qualitative processes of the medicinal plants, which may reduce or stop the reproductive growth [8]. The use of more fertilizers leads to increased waste and, finally, pollution of living resources and the decreased quality of medicinal plants by increasing the accumulation of nitrate in herbal products and soil nitrate pollution.

Current study was carried out to determine the response of fresh and dry parts of *Echinacea* to nitrogenous fertilizer and foliar fertilizer applied in different doses under Afyonkarahisar conditions.

II. MATERIALS AND METHODS

Plant Material

The plant material used in the experiment consisted of young seedlings obtained from Echinacea seeds, which have 85% germination capability and 100% purity. Echinacea seeds were sowed in the greenhouse on 1 March 2016 in germination trays consisting of soil and peat (1:1) and irrigated regularly. The first germinations were observed on 17 March 2016.

Experimental Location and Conditions

The experiment was conducted in the research area of Afyonkarahisar Medicinal and Aromatic Plants Centre/Turkey (38° 46' N, 30° 30' E). The climate of this region is harsh and moderately rainy. Most precipitation occurs in winter and spring. Summers are hot and dry and winters are cold and snowy. Some meteorological data about the region are given in Table 1.

TABLE 1
Some local Meteorological data during 2016 to 2018

Month/Year	Temperature (°C)								
	Minimum			Maximum			Mean		
	2016	2017	2018	2016	2017	2018	2016	2017	2018
January	-2.8	-5.6	-1.4	5.7	1.2	7.3	1.1	-2.4	2.2

February	2.4	-1.9	2.1	14.1	7.8	11.7	7.7	2.6	6.4
March	2.1	2.3	5	13.5	13.5	15.8	7.5	7.6	9.8
April	6.8	3.9	6.7	21.3	16.8	21.5	14	10.3	14.3
May	8.8	9.0	11.3	21.2	20.8	23.3	14.8	14.6	16.9
June	14.2	12.7	13.5	28.2	26	26.1	21.4	19.4	19.5
July	15.7	16.9	15.8	31.6	31.8	29.7	23.6	24.5	22.7
August	16.3	15.9	16.2	31	29.9	30.2	23.4	22.6	23.1
September	11.3	13.0	12.4	25.5	29.3	26	18.2	21	19.1
October	8.1	6.4	7.7	20.6	18.3	20.5	13.9	11.9	13.4
November	1.2	2.0	3.2	14.2	12.8	13.1	7.2	6.6	7.7
December	-4	0.6	-0.5	3.1	10	5.8	-0.8	4.5	2.5

Month/Year	Rain (mm)			Average Relative Humidity (%)			Insolation (h)		
	2016	2017	2018	2016	2017	2018	2016	2017	2018
January	63	39.7	37.1	71.6	78.2	75.4	86.2	64.1	92.8
February	12.5	1.3	19.7	63.3	68	69.4	140	102.6	73.2
March	48.2	29.2	45.3	59.3	58.9	58.1	142.1	135.7	129.6
April	31.5	43.9	15.5	49.7	55.8	47.8	241.4	178.3	228.4
May	60.1	0.6	80.1	60.5	64.8	60.1	185.5	123.7	161
June	13.8	32.2	131.4	48.8	61	60.1	277.7	200.4	196.9
July	28.2	4.4	11.9	46.0	44.2	51.9	312.2	275.3	281.1
August	29.7	59.1	7.8	53.1	52.6	50.2	271.4	255.7	262.3
September	30.4	7.1	1.5	54.6	38.9	51	228.4	228.2	234.4
October	6.7	38.3	37.2	57.9	60.3	65	179.9	153.1	182.4
November	28.1	28.5	44.7	58.2	68.8	70.1	152.6	127.3	107.1
December	42.5	24.7	84.1	74.8	73.6	82	74.8	95.2	57.1
Total	394.7	309	516.3						

Source: Regional Directorate of State Meteorology

Treatments and Design

To carry out the field experiment, the field was plowed and soil samples were taken from 30 and 60 cm depths and analyzed (Table 2). The experimental design was arranged by using a randomized complete block design with three replications. In the experiment, 4 different fertilizer levels N_0: 0 fertilizer/control, N_1: 75 kg ha^{-1}, N_2: 150 kg ha^{-1} of N fertilizer and N_3: 75 kg ha^{-1} + foliar fertilizer was applied. The source of nitrogen fertilizer was 46% N. The contents of the chemical characteristics of the foliar fertilizer were given in Table 3. When Echinacea seedlings reached a certain level (with 8-10 leaves), they were transferred to the field on May 16, 2016, with 50 × 60 cm plant density. Simultaneously with planting the seedlings 2/3 of the N was applied at a depth of 5 cm to the root area. The remaining fertilizer (1/3 N) was applied when the first buds appeared. In following years, half of N was applied at the beginning of the growing season until the 1st cutting (½ at the end of winter and ½ at the beginning of the budding stage) and the other half was added after the 1st cutting (½ immediately after cutting and ½ at the beginning of the budding stage). A drip irrigation system was installed to ensure that all parcels receive equal amounts of water after planting.

The first foliar fertilizer was applied 77 days after planting and repeated two more times at 14-day intervals until cutting. Thus, the spraying of foliar fertilizer was done 3 times in each cutting. Control of weeds was done by mechanical methods during the study.

TABLE 2
Physico-chemical properties of experimental field soil at depth 30 and 60 cm

Properties	30 cm	60 cm	Elements	30 cm	60 cm
Organic matter (%)	0.34	0.27	Ca (ppm)	3952	4999
Total N (%)	0.10	0.08	Mg (ppm)	624	747
Sand (%)	52.99	48.61	K (ppm)	344	307
Clay (%)	32.70	32.89	Na (ppm)	50	838
Dust (%)	14.31	18.50	Fe (ppm)	1.07	1.08
Lime (%)	1.88	2.01	P (ppm)	73	49
EC (mS cm^{-1})	0.15	0.17	Cu (ppm)	0.75	0.62
pH	8.44	8.74	Zn (ppm)	1.12	0.86
			Mn (ppm)	6.03	3.50

Soil class: sandy clay-loam

TABLE 3
The contents of chemical characteristics of the foliar fertilizer

Element	(% v w^{-1})
Total N	9.2
Nitrate nitrogen (N)	4.4
Ammonium nitrate (N)	1.4
Urea nitrogen (N)	3.4
Water-soluble phosphorus pentoxide (P_2O_5)	6.8
Water-soluble potassium oxide (K_2O)	18.2
B	0.10
Cu* (EDTA chelated)	0.021
Fe** (EDTA chelated)	0.05
Mn* (EDTA chelated)	0.02
Mo	0.005
Zn* (EDTA chelated)	0.051
* pH range that chelate is stable:	pH 2-11
** pH range that chelate is stable:	pH 2-6.5

Harvesting

During this 3-year trial, a total of 5 cuttings were realized (Table 4). The cuttings were done at the flowering stage of the plants. The plants were cut from 8-10 cm soil surface and weighed for yield calculation. Then leaves, stems, flowers and buds were separated and weighed again. Primary and secondary branches, flowers and buds were dried in a cabinet type drying cabinet at 37 °C for 96 hours and weighed and recorded again.

TABLE 4
Cutting and foliar fertilizer application dates

Replication	1st year (2016)	2nd year (2017)		3rd year (2018)		Dosage
	1st Cutting	2nd Cutting	3rd Cutting	4th Cutting	5th Cutting	
1	1 Aug	22 May	28 Aug	7 May	20 Aug	300 ml 100 lt^{-1}
2	15 Aug	5 Jun	11 Sep	21 May	3 Sep	300 ml 100 lt^{-1}
3	29 Aug	19 Jun	25 Sep	4 Jun	17 Sep	300 ml 100 lt^{-1}
Cuttings Date	24 Oct	31 Jul	30 Oct	17 Jul	10 Nov	

Isolation of Essential Oils

To isolate the essential oil of samples, 200 g of dried and powdered flowers were extracted with 2000 ml of distilled water by a neo-Clevenger type apparatus. Hydro-distillation was performed for 3 hrs. The obtained essential oils were dried over anhydrous sodium sulphate and stored in amber vials at +4 ºC [9].

Statistical Analysis

The obtained data were analyzed using the MSTAT-C computer software program. The means of the applications were compared using the Least Reliable Difference method at the 0.05 probability level. Variance analysis was performed on the samples to determine the variation of the fertilizer effects and cuttings number.

III. RESULTS AND DISCUSSIONS

Results of variance analysis for growth and yield parameters and essential oil content are shown in Tables 5, 6 and 7. The influence of all the treatments was significant on every growth parameter (Tables 5, 6 and 7).

Fresh and Dry Herb Weight

The effects of nitrogen doses on fresh plant weight were significant and positive. The highest fresh herb weight was obtained at N_2 nitrogen dose (979 g plant^{-1}). This value is 43.20% higher than control parcels. Although 9% less fresh herb weight was obtained at the N_3 dose compared to the N_2 dose, it was included in the same statistical group. The number of cuttings also significantly affected the fresh plant weight. While the highest fresh plant weight was obtained in the 2nd cutting with 1313 g plant^{-1}, this value was 21.93% higher than the 3rd cutting with the lowest fresh plant weight (288 g plant^{-1}) (Tables 5).

Dry herb weights results were similar to that of fresh herb weights. The highest dry herb weight was observed at the N_2 nitrogen dose with 262 g plant^{-1}. The lowest weight was also obtained in control plots. The value obtained is 49.13% less than the highest value. Looking at the number of cuttings, it is seen that the highest dry herb yield was 387 g plant^{-1} in the 2nd cutting, and the lowest weight was 63 g plant^{-1} in the 3rd cutting (Table 6). When Tables 5 and 6 are examined, it is seen that fresh and dry herb weights reach the highest value in the first cutting of the 2nd and 3rd year. Dry herb weight is directly related to fresh herb weight so similar results were obtained for fresh and dry herb weight.

Kizil and Toncer [6] reported that the fresh herb weight of Echinacea ranged between 187.6-264.3 g plant^{-1} and the dry weight varied between 76.2-106.6 g plant^{-1}. Tansi et al. [10], in a study they conducted for 2 years, reported that the average weight of fresh herb in Echinacea was 754.0-798.9 g plant^{-1} and the average dry herb was 240.1-245.4 g plant^{-1}. Fresh herbage weight 664.4 g plant^{-1} and dry herb weight were reported as 164.81 g plant^{-1} by Kucukali [11]. The findings of the present study were higher than the mentioned researchers. This situation is thought to be due to the fact that plant herb weight is significantly affected by fertilization, harvest year, irrigation and the ecological region where it is grown.

Fresh and Dry Stem Weight

The effects of nitrogen doses on fresh and dry stem weight were significant. The highest fresh stem weight was obtained as 351 g plant^{-1} at N_2 dose. The N_3 dose followed the N_2 dose with 326 g plant^{-1} and was included in the same group. The lowest fresh weight (152 g plant^{-1}) was obtained in the control plots and the value obtained is 43.30% less than the highest value. Cuttings numbers had a significant effect on fresh and dry stem weight. The second cutting with the highest fresh stem weight was 539 g plant^{-1}, followed by the 4th cutting with 476 g

plant^{-1}. The lowest fresh stem weights were obtained from 3rd and 5th cuttings 52 and 57 g, respectively (Table 5).

The highest dry stem weight was again taken at the N_2 dose, followed by the N_3 dose. The lowest dry weight was obtained in the control plots. The highest and lowest dry stem weight difference is 43.47%. When Table 6 is examined, it is seen that the highest dry stem weight is obtained in the 2nd cutting with 188 g plant^{-1}, while the lowest dry weight is obtained in the 3rd cutting with 11 g plant^{-1}.

In the second cuttings, with decreasing photoperiod, temperature, light quality and day-night temperature difference may cause the vegetative growth of plants to slow down and thus yield to decrease (Yilmaz, 2018 12). In this study to the lowest fresh and dry stem weight was obtained from 3rd and 5th cuttings. 3rd and 5th cuttings are the second cuttings of the 2nd and 3rd years (Tables 6). There has been no previous study on fresh and dry stem weight.

Fresh and Dry Leaf Weight

Nitrogen doses positively affected the fresh and dry leaf weight. The highest fresh leaf weight was obtained at the dose of N_2 with 352 g plant^{-1}. 310 g plant^{-1} of fresh leaves were obtained at the N_3 dose and it was in the same group with the N_2 dose. The lowest fresh leaf weight with 146 g plant^{-1} was taken from the control plots. The highest and lowest difference in fresh leaf weight is 41.47%. The highest fresh leaf weights were obtained in the 2nd and 4th cuttings as 386 and 385 g plant^{-1} respectively. The lowest fresh leaf weight was taken in 1st cutting and the value obtained was 35.49% less than the highest value (Table 5).

The highest dry leaf weight results were obtained at the N_2 dose, as was the fresh leaf weight. The highest value obtained is 42.68% higher than the lowest value. Considering the effects of the number of cuttings on dry leaf weight, it is seen that the highest weight was taken in the 2nd cutting with 99 g plant^{-1}, and the lowest in the 1st cutting with 28 g plant^{-1} (Table 6).

In the first cuttings, increasing the sunshine duration positively affects the development of the plant, increasing the leaf area and dry matter accumulation. It has been reported that dry herb and dry leaf yield increase with increasing sunshine duration or light intensity (Fernandes et al., [13]. Our study supports the mentioned literature. Because the highest leaf weights were obtained from the first cutting of the 2nd and 3rd years (Table 6).

Fresh and Dry Flower Weight

The effects of nitrogen doses on fresh and dry flower weight were significant. The highest fresh flower weight was obtained at N_2 nitrogen dose (257 g plant^{-1}). This value is 44.35% higher than control parcels. The number of cuttings also significantly affected the fresh flower weight. The highest fresh flower weight was obtained in the 4th cutting with 364 g plant^{-1}, followed by the 2nd cutting with 271 g plant^{-1}. The lowest weight was obtained with 34 g plant^{-1} in 3rd cutting (Table 5).

As seen in Table 2, dry flower weight was taken from the highest N_2 dose and the lowest from the control plots. These values varied between 27-60 g plant^{-1}. The difference between the highest and the lowest value is 45%. Looking at the effects of the number of cuttings on dry flower weight, it is seen that the highest values were obtained in the 2nd and 4th cuttings 97 and 82 g plant^{-1} respectively. The lowest values were taken as 7 and 9 g plant^{-1} in 3rd and 5th cuttings, respectively (Table 6).

The most active ingredient ratio of *Echinacea purpurea* L. used in the pharmaceutical industry is its flowers [14]. Especially, caffeic acid derivatives found in flowers are important raw materials of the pharmaceutical industry [15]. Therefore, flower yield values are important. Kizil and Toncer 2013 6 reported that fresh flower weight varied between 35.9-66 g plant^{-1} in their study. Kucukali [11] reported that fresh flower yield of *E. purpurea* was 214.82 g plant^{-}

[1]. Chen et al., [16] determined that flower yield per plant ranged from 25.61 to 51.19 g plant^{-1}. Kucukali [11] reported that average of dry flower weight was 54.3 g plant^{-1}. Shalby et al., [17] indicated that dry flower weight was 45 g plant^{-1}. Chen et al., [18] dry flower weight varied from 26.08 to 31.60 g plant^{-1}. The highest values of fresh and dry flower weights obtained in our study are higher than the results of the researchers above. The lowest dry flower weight values are lower. Chen et al., [16] *E. purpurea* is a cross-pollinated plant and tends to be self-incompatible. Therefore, the large variability in its morphological and agronomic traits is not unexpected. Tillering occurred in the second year and thalamus was formed per each branch. Therefore, an increase in flower yields was observed in the 2nd and 3rd years. However, there was a decrease in yields in the second cuttings of the 2nd and 3rd years.

Fresh and Dry Bud Weight

The highest fresh and dry bud weight was observed in the N_2 and N_3 treatments at the same statistical group. N_1 and N_0 treatments were also placed at the lower ranks. The highest (N_2) and lowest (Control) bud weight difference is 41.17%. The application of nitrogen element amounts and its simultaneous consumption with foliar application of essential elements for plant growth showed its additive effect in improving bud weight. The effect of cutting numbers on bud weight was found to be significant. While the highest fresh and dry bud weights were obtained from 1st and 4th cuttings, the lowest values were obtained from 5th cutting (Table 5 and 6). Tansı et al. 2015 10 reported that the average fresh bud weight ranged from 26.2-32.1 g plant^{-1} and dry weight varied between 14.1-16.3 g plant^{-1} in their study for 2 years. Our results are lower than the results of the mentioned researcher. This may be due to the fact that the study areas are located in different ecological regions and applied cultural techniques.

Number of Stems Per Plant

The number of main and secondary stems per plant has changed significantly depending on the applications. While the highest number of branches was obtained from N_2 application with 43 number plant^{-1}, 37 number plant^{-1} were obtained from the N_3 application and they were included in the same group. The control group with the lowest number of branches is 46.51% less than the highest number of branches (Table 7). In this study, the number of branches per plant obtained when the data were examined, it was seen that Echinacea responded positively to nitrogenous fertilizers applied in high doses.

Yaldiz et al., [19] found that number of branch per plant was 13 per plant, Yeşil and Kan [20] reported that number of branches of *E. purpure* arranged from 9.5 to 26.6 per plant, Yarnia et al., [20] determined number of branches values as 13.4 per plant. Kucukali [11] also reported that the average of number of branch of *E. purpurea* was 9.20 per plant. Ault [22] reported that well-drained, deep-structured, pH-neutral and alkaline soils will increase branching in Echinacea. Mengel [23] reported that the soil properties of the plant, especially the organic matter in the soil and the available nutrients and water will affect the number of branches. When the soil analysis results of the area where the study was conducted are examined, it is seen that the soil structure is alkaline (pH, 8.44 at 30 cm depth and 8.74 at 60 cm depth) (Table 2).

Number of Buds Per Plant

Treatments made significantly affected the number of buds per plant. While N_2 application reaches the highest number of buds with 20 number plant^{-1}, this value is 40% more than the lowest number of buds (Control group). N_1 dose was also in the same group with N_0 dose with 9 number plant^{-1}. The number of cuttings also had a significant effect on the number of buds per plant. The highest numbers of buds were obtained in the 2nd and 4th cuttings as 21 and 18

number plant^{-1} respectively. The lowest number of buds was recorded from the 5th cutting with 7 number plant^{-1} (Table 7). While the highest bud numbers were obtained from the first cuttings of the 2nd and 3rd years, the lowest numbers were obtained from the second cuttings of the same years. The application of nitrogen element amounts and its simultaneous consumption with foliar application of essential elements for plant growth showed its additive effect in improving bud number. In the research of Isazadeh Hajagha et al., [24] the number of buds increased with the addition of different sources of fertilizer. Tansı et al., [10] reported in their study that the number of buds varied between 19.7-27.4 number plant^{-1}.

Number of Flowers Per Plant

Significant differences were determined between nitrogen doses for number of flower. While the highest number of flowers (37 number plant^{-1}) was obtained at the N_2 dose, the N_3 dose followed it with 33 number plant^{-1} number plants and was included in the same statistical group. The lowest number of flowers per plant was obtained from control parcels and the value obtained is 48.64% less than the highest value (Table 7).

Küçükali [11] reported that the number of flowers per plant in Echinacea ranged from 31.00 to 13.03 unit/plant. Kizil and Toncer [6] reported the number of flowers between 12.8 and 17.7 in their study. Tansı et al., [10] reported that the number of flowers per plant varied between 27.2-30.4 in their study for 2 years. The results of the number of flowers per plant we obtained as a result of this study are similar to Tansı et al., [10], one of the mentioned researchers, but higher than the others. In Echinacea, the number of branches and flowers are directly related to each other. It can be said that these parameters are affected by pre-flowering climatic data, available water and nutrients in the soil. As a matter of fact, when Table 1 is examined, it is seen that in 2018 when the highest number of flowers was obtained (4th cutting), there was a lot of rainfall in May and June, which is the period before flowering, compared to other years. It can be said that this situation has positive effects on the number of flowers.

Essential Oil Content

The essential oil ratios of the plants cutting in full bloom ranged from 0.16-0.22%. While the highest essential oil ratio was obtained at the N_2 dose, the lowest ratio was obtained from the control plots. Considering the effects of the cutting numbers on the essential oil ratio, it is seen that in the first cutting of the 2nd and 3rd years, the higher essential oil content was obtained compared to the second cuttings (Table 7).

Yeşil and Kan [20] found that the essential oils of Echinacea ranged from 0.25-0.36%. Satı [25] found the highest rate of essential oil as 0.16% and the lowest rate of essential oil as 0.10% in the first trial year and reported the highest rate of essential oil as 0.15% in the second trial year. Özcan [26] in a study conducted for two years, reported that the highest essential oil ratio was obtained from plants harvested in full bloom in both the 1st and 2nd year (0.119% and 0.101%, respectively). *Echinacea purpurea* essential oil ratio is reported to vary between 0.08-0.32% [27, 28]. The essential oil ratios we obtained from the experiment are similar to the rates determined by the WHO and ESCOP monographs.

TABLE 5
Fresh weight per plant of different plant parts of Purple coneflower (g plant^{-1})

Treatments	Fresh Weight of Bud	Fresh Weight of Flower	Fresh Weight of Leaf	Fresh Weight of Stem	Fresh Weight of Herb
			Nitrogen levels		
N_0 (Control / 0 N)	7 b	114 d	146 c	152 c	423 c
N_1 (75 kg/ha)	10 b	169 c	216 b	202 b	599 b

N_2 (150 kg/ha)	17 a	257 a	352 a	351 a	979 a
N_3 (75 kg/ha + F)	16 a	223 b	310 a	326 a	882 a
Probability level	P≤0.05	P≤0.01	P≤0.01	P≤0.01	P≤0.01
LSD (% 5)	4.183	24.05	54.05	46.66	117.4
Cutting no					
1st Cut. (1st year)	16 a	140 b	137 c	165 c	459 b
2nd Cut. (2nd year)	12 ab	271 a	386 a	539 a	1313 a
3rd Cut. (2nd year)	11 ab	34 c	190 b	52 d	288 c
4th Cut. (3rd year)	15 a	364 a	385 a	476 b	1247 a
5th Cut. (3rd year)	8 b	46 c	184 bc	57 d	296 c
Probability level	P≤0.05	P≤0.01	P≤0.01	P≤0.01	P≤0.01
LSD (% 5)	5.086	29.79	47.86	58.82	131.4

TABLE 6
Dry weight per plant of different plant parts of Purple coneflower (g plant^{-1})

Treatments	Dry Weight of Bud	Dry Weight of Flower	Dry Weight of Leaf	Dry Weight of Stem	Dry Weight of Herb
Nitrogen levels					
N_0 (Control / 0 N)	1.6 b	27 d	35 c	50 b	114 c
N_1 (75 kg/ha)	2.7 b	41 c	51 b	66 b	161 b
N_2 (150 kg/ha)	3.6 a	60 a	82 a	115 a	262 a
N_3 (75 kg/ha + F)	3.4 a	52 b	71 a	104 a	232 a
Probability level	P≤0.01	P≤0.01	P≤0.01	P≤0.01	P≤0.01
LSD (% 5)	0.9037	6.892	11.64	15.93	31.01
Cutting no					
1st Cut. (1st year)	3.3 a	29 c	28 c	49 c	110 c
2nd Cut. (2nd year)	2.9 ab	97 a	99 a	188 a	387 a
3rd Cut. (2nd year)	2.0 bc	7 d	42 b	11 d	63 d
4th Cut. (3rd year)	3.4 a	82 b	90 a	158 b	334 b
5th Cut. (3rd year)	1.6 c	9 d	41 b	14 d	67 d
Probability level	P≤0.01	P≤0.01	P≤0.01	P≤0.01	P≤0.01
LSD (% 5)	1.104	7.57	11.45	17.98	35.09

TABLE 7
Essential oil content and numbers of stem, bud and flower of *Purple coneflower*

Treatments	Number of Stems number plant^{-1}	Number of Buds number plant^{-1}	Number of Flowers number plant^{-1}	Essential Oil Content %
Nitrogen levels				
N_0 (Control / 0 N)	20 b	8 c	18 c	0.16 d
N_1 (75 kg/ha)	25 b	9 c	25 b	0.17 c
N_2 (150 kg/ha)	43 a	20 a	37 a	0.22 a
N_3 (75 kg/ha + F)	37 a	16 b	33 a	0.20 b
Probability level	P≤0.01	P≤0.01	P≤0.01	P≤0.01
LSD (% 5)	10.46	3.443	5.610	0.0009
Cutting no				
1st Cut. (1st year)	165 c	10 b	14 b	0.17 e
2nd Cut. (2nd year)	539 a	21 a	55 a	0.21 a
3rd Cut. (2nd year)	52 d	9 b	7 c	0.18 d
4th Cut. (3rd year)	476 b	18 a	58 a	0.19 b

5th Cut. (3rd year)	57 d	7 b	8 bc	0.18 c
Probability level	P≤0.01	P≤0.01	P≤0.01	P≤0.01
LSD (% 5)	58.82	5.051	6.204	0.0008

IV. CONCLUSION

Echinacea is an important medicinal plant that has the potential for future consumption in Türkiye. It is an advantage that disease and pest problems are not encountered in Echinacea cultivation and that it is easy to grow. However, considering the harvest and post-harvest processes of the plant, a conscious culture should be done. It was determined that different fertilizer treatments had significant effects on plant growth parameters. According to the results of this study carried out with Echinacea under Afyonkarahisar conditions, it can be suggested that as an alternative medicinal and aromatic plant in Afyonkarahisar and similar ecologies, irrigation can be done in irrigated agricultural areas depending on the annual rainfall.

REFERENCES

[1] L.E. Craker, "Reprinted from: Issues in new crops and new uses." J. Janick. Medicinal and Aromatic Plants- Future Opportunities. 2007, pp. 248-257.

[2] R.V. Soldamli, "Echinacea (*Echinacea purpurea* (L.) moench.) plant harvested at different times determination of antioxidant activities of extracts." University of Bozok, Institute of Natural and Applied Sciences, Field Crops Department, Yozgat, 2016, 54 pp.

[3] M.J. Sheshbahreh, M.M. Dehnavi, A. Salehi, B. Bahreininejad, "Effect of irrigation regimes and nitrogen sources on biomass production, water and nitrogen use efficiency and nutrients uptake in coneflower (*Echinacea purpurea* L.)." Agricultural Water Management, 2019, 213: pp. 358–367.

[4] S. S. Percival, "Use of *Echinacea* in medicine." Biochem. Pharmacol., 2000, 60: 155-158.

[5] N.B. Perry, E.J. Burgess, V.L. Glennie "*Echinacea* Standardization: Analytical Methods for Phenolic Compounds and Typical Levels in Medicinal species." Journal of Agricultural and Food Chemistry, 2001, 49:1702-1706.

[6] S. Kizil and O. Toncer, "Effects of different nitrogen forms on some agronomical characteristics of *Echinacea purpurea* in semi-arid conditions of Turkey." Scientific Papers. Series A. Agronomy, 2013, Vol. LVI.

[7] R.E. Drenovsky, A. Khasanova, J.J. James, 2012, "Trait convergence and plasticity among native and invasive species in resource poor environments." Am. J. Bot. 2012, V 99, pp. 629–639.

[8] K. Rios-Gonzalez, L. Erdei, S.H. Lips, "The activity of antioxidant enzymes in maize and sunflower seedlings as affected by salinity and different nitrogen sources." Plant Sci. 2002, V. 162, pp. 923–930.

[9] A. Soltanbeigi, H. Maral, "Agronomic yield and essential oil properties of purple coneflower (*Echinacea Purpurea* L. Moench) with different nutrient applications." Chilean J. Agric. Anim. Sci., 2022, V. 38, pp. 164-175.

[10] L.S. Tansi, S. Karaman, O. Toncer, S. Gedik,. The effects of plant density and year on yield of purple coneflower (*Echinacea purpurea* (L.) Moench)." Turkish Journal of Field Crops, 2015, V. 20(2), pp. 174-178.

[11] K. Kucukali, "The effect of different sowing density and harvest times on yield and quality of purple coneflower (*Echinacea purpurea* (L.) Moench) in Çukurova ecological conditions." Çukurova University Institute of Natural and Applied Sciences Field Crops Department, 2012, Msc Thesis, Adana.

[12] K. Yilmaz, "Determination of yield and quality characteristics of clones and cultivars of *Mentha piperita* L. species grown under Isparta conditions." Süleyman Demirel

University, Faculty of Agriculture, Field Crops Department, Master Thesis, 2018 Isparta. 59 p.

[13] V.F. Fernandes, L.B. Almeida, E.V.R.S. Feijó, D.C. Silva, R.A. Oliveira, M.S. Mielke, L.C.B. Costa, "Light intensity on growth, leaf micromorphology and essential oil production of *Ocimum gratissimum*." Brazilian Journal of Pharmacognosy, 2013, v. 23 (3), pp. 419-424.

[14] A. Mat, *Echinacea* Species. 14. Herbal Medicine Raw Materials Meeting, Proceedings, 29-31 May, Eskişehir, Eds. Baser, K.H.C. and Kirimer, N. Publication date on the web: 2004 ISBN 975-94077-2-8. İ.Ü., Faculty of Pharmacy, Department of Pharmacognosy, 34452 İstanbul.

[15] I. Mistrikova and S. Vaverkova, "Patterns of variation in lipophilic and hydrophilic constituents in flower developmental stages of *Echinacea purpurea* L. Moench cultivated in Slovakia." Plant Soil Environ., 2009, v. 55(2), pp. 70-73.

[16] C.L. Chen, S.C. Chang, J.M. Sung, "Biomass and caffeoyl phenols production of *Echinacea purpurea* grown in Taiwan." Expl. Agric., 2008, v. 44, pp. 497–507.

[17] A. Shalaby, S. El. Gengaihi, E. Agina, A. El-Khayat, S. Hendawy, "Growth and yield of *Echinacea purpurea* L. as influenced by planting density and fertilization." Journal of Herbs, Spices and Medicinal Plants, 1997, v. 5, pp. 69-76.

[18] C.L. Chen, S.C. Zhang, J.M. Sung, "Caffeoyl phenols and alkamides of cultivated *Echinacea purpurea* and *Echinacea atrorubens* var. *paradoxa.*" Pharmaceutical Biology, 2009, v. 47(9), pp. 835–840.

[19] G. Yaldiz, S.M. Kara, N. Sekeroglu, "Adaptation of different *Echinacea* species (*Echinacea* spp.) to Rize ecological conditions." Symposium on Medicinal and Aromatic Plants, 2012, pp. 250-254.

[20] R, Yesil, Y. Kan, "The effects of applications of organic and inorganic fertilizers in different doses on yield and components of essential oil of Echinacea species (*E. pallida* and *E. purpurea*) cultivated in Konya ecological conditions." Selcuk Journal of Agriculture and Food Sciences, 2013, v. 27(1), pp. 14-23.

[21] M. Yarnia, M. Farzanian, V. Rashidi, V. Javanshir, N. Aliasgharzad, "Effects of microelement fertilizers and phosphate biological fertilizer on some morphological traits of *Purple coneflower* in water stress condition." African Journal of Microbiology Research, 2012, v. 6(22), pp. 4825-4832.

[22] J.A. Ault, "Coneflower - *Echinacea* species. In: N.O. Anderson (ed.), Flower breeding and genetics." Springer, 2007, pp. 801-824.

[23] K. Mengel, B. Hutsch, Y. Kane, "Nitrogen fertilizer application rates on cereal crops according to available mineral and organic soil nitrogen." European Journal of Agronomy, 2006, v. 24, pp. 343–348.

[24] R. Isazadeh Hajagha, S. Kirici, L. Tabrizi, A. Asgharzadeh, A. Hamidi, "Evaluation of growth and yield of Purple coneflower (*Echinacea purpurea* L.) in response to biological and chemical fertilizers." Journal of Agricultural Science, 2017, v. 9(3), pp. 160-171.

[25] M. Sati, "The effect different plant density on some agricultural and quality characteristics of *Echinacea purpurea* L." University of Ege, Institute of Natural and Applied Sciences, Field Crops Department, 2012, Konya, 52 p.

[26] I.I. Ozcan, "The effect of different cultural applications on yield and quality of Echinacea species (*Echinacea* spp.)." University of Aydın Menderes, Institute of Natural and Applied Sciences, 2014, Aydın,173p.

[27] Escop Monographs, "The scientific foundation for herbal medicinal products, 2nd Ed. Exeter, United Kingdom: European Scientific Cooperative on Phytotherapy." 2003, pp. 126-140.

[28] World Health Organization, "WHO Monographs on Selected Medicinal Plants" 1999, v. 1, pp. 125-144.

Effect Of Fumed Silica on Cutting Carrying Performance of Spud Type Drilling Muds

Onur Eser Kök

oeser.kok@iste.edu.tr, ORCID: 0000-0002-7061-2921
Department of Petroleum and Natural Gas Engineering, Iskenderun Technical University, Hatay, Turkey

Abstract In this study, effect of fumed silica on cutting carrying performance in spud type drilling muds was investigated as detailed. Initially, characterization studies of materials were conducted. Then, spud type drilling muds were prepared with different fumed silica added (wt. 0.50-2.5%). After this, borehole portion was designed and measurements and calculations were conducted with dial readings (300 and 600 rpm), plastic viscosity, yield point, power law consistency factor and flow behavior index. Finally, cutting carrying index of the muds were calculated and fumed silica effect was evaluated. According to the results, it was determined that fumed silica has positive effect on cutting carrying performance on spud type drilling muds.

Keywords: *Fumed Silica, Cutting Transport, Drilling Fluids, Drilling*

I. INTRODUCTION

Drilling of petroleum, natural gas and geothermal water is most important methods achieve to energy sources among primary energy production. There are many drilling methods, however rotary drilling is come to front due to common usage. The rotary drilling method consists of many parameters for the successful production of these energy sources. Among the many parameters such as drilling bit, borehole design and formation structure, drilling mud is one of the mainly parameters for drillings because of cost and impact on all of drilling period [1,2].

Drilling muds are varying according to usage areas. However, the mainly ones are water-based, oil-based and air-based. Water-based drilling muds are the most common in drilling operations. In a general drilling well from beginning to end, differ type water-based drilling muds such as spud, lignosulfonate and polymer are used according to progress and plan of drilling [3].

Spud type drilling mud is used in beginning of drilling operations and contains basic and economic additive materials. Mainly tasks of additive materials are stabilizing to flow properties and cleaning to wellbore. In other words, wellbore cleaning is the most important task of drilling muds and quite important for drilling operations [4-6].

Having optimum flow properties of spud mud, ensure clean hole and cutting transport. Cutting transport ability of spud muds are evaluated with cutting carrying performance (CCP) calculation [7]. CCP is affected several factors such as pump parameters, flow diameters, well depth and additive materials. Thus, all parameters are must evaluated for CCP evaluation [8,9].

Fumed silica is produced from silicon tetrachloride and quartz powder with flame pyrolysis and electric arc in high temperature. It has quite low bulk density and extremely high specific surface area [10]. Particle size of FS varies from 5-50 nm and specific surface area from 25-500 m^2/g. Also, density is range from 150-200 kg/m^3. It has viscosity increasing effect and enhance thixotropic behavior in solutions with these properties [11].

In this study, effect of fumed silica on cutting carrying performance in spud type drilling muds was investigated as detailed. Initially, characterization studies of materials were conducted. Then, spud type drilling muds were prepared with different fumed silica added (wt. 0.50-2.5%). After this, borehole portion was designed and measurements and calculations were conducted with dial readings (300 and 600 rpm), plastic viscosity, yield point, power law consistency factor and flow behavior index. Finally, cutting carrying index of the muds were calculated and fumed silica effect was evaluated.

II. MATERIALS AND METHODS

A. Materials

The Spud type drilling muds were prepared in different amounts (poung per barrel, ppb) with the basic components bentonite, caustic soda (NaOH), soda ash (Na_2CO_3) and chromium-free lignosulfonate (CFL). Bentonite was obtained from CANBENSAN as suitable for drilling, fumed silica and others were obtained as commercial technical products.

In preparing the mud samples, bentonite was used as 25 ppb, NaOH was 0.25 ppb, Na_2CO_3 was 0.2 ppb and CFL was 0.15 ppb. The base sample consist of these materials and compositions. Then, fumed silica was added at different amounts as wt. 0.5, 1.0, 1.5, 2.0 and 2.5%. In a total, six samples were prepared for experimental studies.

B. Characterization Studies

Characterization of the bentonite were applied by X-ray fluorescence spectroscopy (XRF) for determining to contains. Also, digital microscope (DM) was used to determining to surface morphologies of the fumed silica and bentonite.

C. Measurements and Calculations

Dial reading (DR) measurements of the drilling muds were obtained by using OFITE Model 800 rotary viscometer. Plastic viscosity (PV) and yield point (YP) values were calculated according to Eq. 1-2.

For evaluate the cutting carry performance, cutting carrying index (CCI) of the muds was calculated. Also, a borehole portion (see Fig. 1) was designed with standard drilling equipments and Eq. 3-5 were used for the calculations. Annular velocity (AV) values of the system were calculated according to Eq. 6. Also, mud weight (MW) value was applied as 8.75 ppg (pound per gallon) for all calculations. Flow rate was calculated using pump circulation conditions from well desing.

$$PV = \theta_{600} - \theta_{300} \quad (1)$$

$$YP = \theta_{300} - PV \quad (2)$$

$$CCI = (k \times AV \times MW) / 400{,}000 \quad (3)$$

$$k = (511)^{1-n} \times (PV + YP) \quad (4)$$

$$n = 3.322 \times \log (\theta_{600} / \theta_{300}) \quad (5)$$

$$AV = (\text{Flow Rate} \times 1029.4) / (D_h^2 - D_p^2) \quad (6)$$

In the equations 'k' is the Power Law consistency factor ($lb/100ft^2$); AV is annular velocity (ft/min), 'n' is the flow behavior index; θ_{600} and θ_{300} are the dial reading of viscometer at 600 and 300 rpm shear rate respectively. Also, D_h is inside diameter of casing; D_p is outside diameter of pipe. AV unit is ft/min and flow rate unit is bbl/min.

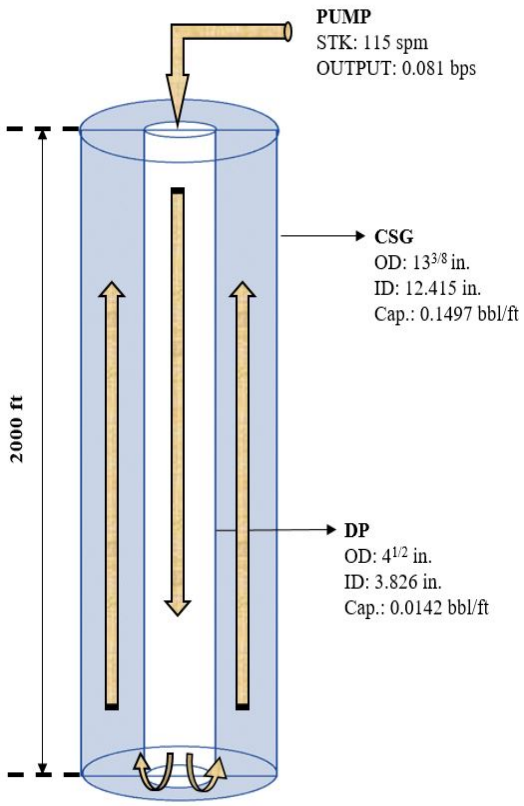

Figure 1. Borehole Design for Circulation

RESULTS AND DISCUSSION

D. *Characterization Results*

XRF result of the bentonite is given in Table I. According to the results, type of the bentonite was determined as mix type (Na/Ca bentonite) by calculated MR values ($Na_2O+K_2O/CaO+MgO$) [12].

Table I. XRF Results of the Bentonite

	SiO_2	Al_2O_3	Fe_2O_3	Na_2O	MgO	CaO	K_2O	TiO_2	Others	MR
Bentonite	%									
	64.71	17.51	7.99	2.17	2.38	1.99	0.67	0.17	2.41	0.649

Figure 2. DM images of Bentonite and Fumed Silica

DM images were obtained from bentonite and fumed silica sampled as differ magnification values range from 200-1000x and the images are given in Fig. 2. According to images, bentonite showed impurities but it was homogenous structure. Fumed silica showed cloudy and bulkly structure. Impurities were seen some areas. Also, agglomeration was seen due to atmosphere moisture.

E. Determination of Flow Parameters

Determination of flow properties of the drilling muds were obtained from rotary viscometer measurements according to designed for drilling muds. The measurements were conducted according to American Petroleum Institute (API) spec. 13B-1 standard. The results are given in Table II.

Table II. Measurement Results of the Flow Parameters

Samples	**Concentration**	**MW (ppg)**	**600 rpm (cP)**	**300 rpm (cP)**	**PV (cP)**	**YP (lb/100ft²)**
S-0 (Base Mud)	Bentonite – 25 ppb NaOH – 0.25 ppb Na_2CO_3 – 0.2 ppb CFL – 0.15 ppb	8.75	42	32	10	22
S-1	Base Mud + Fumed Silica (wt. 0.5%)		44	34	10	24
S-2	Base Mud + Fumed Silica (wt. 1.0%)		48	37	11	26
S-3	Base Mud + Fumed Silica (wt. 1.5%)		55	42	13	29
S-4	Base Mud + Fumed Silica (wt. 2.0%)		59	45	14	31
S-5	Base Mud + Fumed Silica (wt. 2.5%)		67	51	16	35

F. Evaluation of CCI

The parameters of the CCI equation were determined with the mud samples with calculations. The 'n' and 'k' results are given in Table III. In addition, AV was calculated as 71.6538 ft/min according to the designed borehole properties.

Table III. 'n' and 'k' Values of the Muds

Sample	**n**	**k**	**AV**
S-0	0.392	1415.752	71.6538
S-1	0.372	1707.772	
S-2	0.376	1817.874	
S-3	0.389	1896.519	
S-4	0.391	2009.957	
S-5	0.394	2237.487	

According to 'n' and 'k' values, it was determined that the values differ by adding fumed silica. The highest 'n' value was calculated from S-5 coded sample as 0.394 and the lowest 'n' value was calculated from S-1 coded sample as 0.372. In generally, results showed that fumed silica increased 'n' values after wt. 1.5% addition rate comparison with base mud. Also, the highest 'k' value was calculated from S-5 coded sample as 2237.487 and the lowest value was calculated from S-1 coded sample as 1707.772 in fumed silica added muds. All of the fumed silica added samples are higher than base mud. For improve the cutting carrying capability 'k' value should be increased. Thus, results showed that the 'k' values increased with addition of fumed silica.

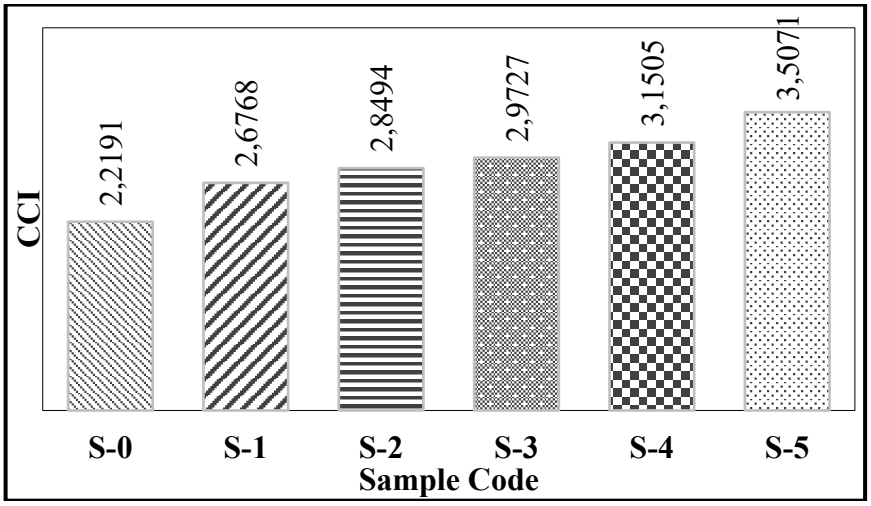

Figure 3. The CCI Values of the Drilling Mud Samples

CCI values of the mud samples were given in Fig. 3. According to the figure, it was determined that the CCI value increased with fumed silica addition and rate. In addition, higher CCI value indicated more effective cutting transport performance. Thus, it was determined that the fumed silica has positive effect for cutting transport in the muds. The highest CCI value was obtained from S-5 coded sample as 3.5071. This situation occured due to interaction of fumed silica particles with other additive particles.

III. CONCLUSION

In the drilling operations, cutting transport has vitaly important due to both economically and drilling ongoing. Thus, borehole cleaning is important. Flow properties of drilling fluids should be controlled frequently and tested according to drilling conditions.

This study reported that usability of fumed silica in spud type drilling muds as cutting transport performance increasing material. Results showed that fumed silica shows positive effect on cutting transport. Also, results indicated that fumed silica can be use in spud muds for low depth such as 0-3000 ft drilling operations.

REFERENCES

[1] Jamali, S., Wittig, V., Börner, J., Bracke, R., & Ostendorf, A. (2019). Application of high powered Laser Technology to alter hard rock properties towards lower strength materials for more efficient drilling, mining, and Geothermal Energy production. Geomechanics for Energy and the Environment, 20, 100112.

[2] Wang, X., Jin, W., Li, Y., Liu, S., Xu, J., Liu, J., ... & Long, T. (2024). Treatment advances of hazardous solid wastes from oil and gas drilling and production processes. Chemical Engineering Journal, 154182.

[3] Gao, C. H. (2023). Drilling fluids for shale fields: case studies and lessons learnt. Unconventional Resources, 100070.
[4] Erdoğan, Y., Demir, M. H., & Kök, O. E. (2021). Investigation and prediction of viscosity of spud type drilling muds added barite, calcium carbonate and olivine by artificial neural networks with limiting data.
[5] Jaiswal, A., & Verma, A. (2018). Comparative studies of using aphron drilling mud versus spud mud. International Journal of Management, IT and Engineering, 8(10), 74-81.
[6] Wang, Z., Sun, B., & Ke, K. (2014). Pre-Spud mud loss flow rate in steeply folded structures. Oil & Gas Science and Technology–Revue d'IFP Energies nouvelles, 69(7), 1269-1281.
[7] Al-Kayiem, H. H., Ismail, M. Z. A., Zaki, N. M., & Elfeel, M. E. (2010). Simulation of the cuttings cleaning during the drilling operation. American Journal of Applied Sciences, 7(6), 800-806.
[8] Khalil, A. A., & Adnan, M. S. (2020). Effect of mud rheology on cuttings' transport in drilling operations. In *IOP Conference Series: Materials Science and Engineering* (Vol. 671, No. 1, p. 012067). IOP Publishing.
[9] Busch, A., & Johansen, S. T. (2020). Cuttings transport: On the effect of drill pipe rotation and lateral motion on the cuttings bed. Journal of Petroleum Science and Engineering, 191, 107136.
[10] Flörke, Otto W.; Graetsch, Heribert A.; Brunk, Fred; Benda, Leopold; Paschen, Siegfried; Bergna, Horacio E.; Roberts, William O.; Welsh, William A.; Libanati, Cristian; Ettlinger, Manfred; Kerner, Dieter; Maier, Monika; Meon, Walter; Schmoll, Ralf; Gies, Hermann; Schiffmann, Dietmar (15 April 2008). "Silica". Ullmann's Encyclopedia of Industrial Chemistry: a23_583.pub3.
[11] Zhou, Shengxiong; Li, Siqi; Yan, Chuanqi (2023-09-15). "Influence of fumed silica nanoparticles on the rheological and anti-aging properties of bitumen". Construction and Building Materials. **397**: 132388.
[12] Karagüzel, C., Çetinel, T., Boylu, F., Çinku, K., & Çelik, M. S. (2010). Activation of (Na, Ca)-bentonites with soda and MgO and their utilization as drilling mud. Applied Clay Science, 48(3), 398-404.

Kentsel Geri Dönüşüm Atık Yönetimi için Belirsiz Talepler Altında Araç Rotalama Problemine Yönelik Matematiksel ve Sezgisel Çözüm Yaklaşımları

Mathematical and Heuristic Solution Approaches to the Vehicle Routing Problem Under Uncertain Demands for Urban Recycling Waste Management

Zehra Kamışlı Öztürk[*,1], Mert Erdinç[2], Beyza Nur Erdinç[3]

[*]zkamisli@eskisehir.edu.tr, ORCID: 0000-0003-3156-6464
[1]*Endüstri Mühendisliği Bölümü, Eskişehir Teknik Üniversitesi, Eskişehir, Türkiye*
[2,3]*Tedarik Zinciri Optimizasyonu, Solvoyo, Kocaeli, Türkiye*

Özet: Sanayileşmenin hızla artması, günümüzdeki tüketim alışkanlıklarını köklü bir şekilde değiştirmiştir. Bu süreçte, artan tüketim düzeyleri, hem evsel hem de endüstriyel atıkların miktarının hızla yükselmesine yol açmıştır. Giderek büyüyen atık hacmi, kentsel atık yönetim süreçlerinin önemini artırmış ve bu alanda etkili çözümler geliştirilmesi gerekliliğini ortaya koymuştur. Kentsel atık yönetimi, yalnızca bir yönetim aracı olmanın ötesine geçerek, çevresel sürdürülebilirlik ve halk sağlığı açısından zorunlu bir ihtiyaç haline gelmiştir. Bu nedenle, atıkların toplanması, geri kazanımı ve bertarafı üzerine yapılan araştırmalar daha sistematik ve derinlemesine bir şekilde incelenmektedir. Bu bağlamda, bir belediye için kentsel geri dönüşüm atıklarının belirsiz talepler altında kapasiteli araç rotalama problemi ele alınmıştır. Çalışmada matematiksel ve sezgisel çözüm yaklaşımları üzerinde durulmuş ve geliştirilen karma tamsayılı programlama temelli matematiksel model aracılığıyla ilçenin tüm atık yönetim süreci için makul bir sürede etkili bir sonuç elde edilemediği gözlemlenmiştir. Bu durum, söz konusu problemin NP-Zor sınıfında yer alması ve kesin yöntemlerle çözüm sağlamanın zorluğu ile ilişkilidir. Bu zorluğun üstesinden gelmek amacıyla, çözüm sürecinde metasezgisel algoritmalardan biri olan Karınca Kolonisi Algoritması kullanılmıştır. Ayrıca, taleplerdeki gerçek hayattaki dalgalanmaları göz ardı etmemek için Bulanık Küme Teorisi'nden yararlanılmıştır. Bu yöntem, belirsizliklerin ve değişkenlerin etkisini göz önünde bulundurarak daha gerçekçi bir modelleme sunmaktadır. Problemin çözümü için Python dilinde kodlanmış bir görsel program oluşturulmuş ve bu program aracılığıyla atık yönetimi süreçlerine dair yenilikçi bir bakış açısı geliştirilmiştir. Sonuç olarak, bu çalışma, belirsiz talepler altında ayrıt tabanlı araç rotalama problemi için yeni ve etkili yaklaşımlar sunarak, kentsel atık yönetimi alanında önemli katkılar sağlamayı hedeflemektedir. Bu tür araştırmalar, sürdürülebilir şehirler yaratma çabalarına önemli bir katkı sunmaktadır.

Anahtar Kelimeler: *Ayrıt Tabanlı Kapasiteli Araç Rotalama Problemi, Bulanık Küme Teorisi, Karınca Kolonisi Optimizasyonu, Kentsel Geri Dönüşüm Atık Yönetimi*

Abstract The rapid increase in industrialization has fundamentally changed consumption habits today. During this process, rising levels of consumption have led to a rapid increase in the amount of both household and industrial waste. The growing volume of waste has heightened the importance of urban waste management processes and highlighted the need for effective solutions in this area. Urban waste management has become a necessity for

environmental sustainability and public health, going beyond being just a management tool. Therefore, research on the collection, recovery, and disposal of waste is being conducted in a more systematic and in-depth manner. In this context, the capacity-based vehicle routing problem under uncertain demands for urban recycling waste has been addressed for a municipality. The study focuses on mathematical and heuristic solution approaches, and it has been observed that an effective result could not be achieved within a reasonable timeframe for the entire waste management process of the district through the developed mixed-integer programming-based mathematical model. This situation is related to the classification of the problem as NP-Hard and the difficulty of providing solutions using exact methods. To overcome this challenge, one of the metaheuristic algorithms, the Ant Colony Algorithm, has been utilized in the solution process. Additionally, to account for real-life fluctuations in demands, Fuzzy Set Theory has been employed. This method offers a more realistic modeling by considering the effects of uncertainties and variables. A visual program coded in Python has been created to solve the problem, leading to the development of an innovative perspective on waste management processes. As a result, this study aims to provide new and effective approaches to the vehicle routing problem under uncertain demands, contributing significantly to the field of urban waste management. Such research plays a vital role in efforts to create sustainable cities.

Keywords: *Edge Based Capacity Vehicle Routing Problem, Fuzzy Set Theory, Ant Colony Optimization, Urban Recycling Waste Management*

I. GİRİŞ

Dünyada her gün tonlarca atık üretilmektedir. Bu atıkların yönetiminde karşılaşılan üç büyük problem toplama, depolama ve ayrıştırma işlemleridir ve bu süreçler doğru yönetilemediğinden dünyamız için büyük bir tehdit yaratmaktadır. Bu işlemler ile atıkların türlerine göre geri dönüştürülmesi veya bertaraf tesislerine gönderilmesi sürekli bir döngü içinde gerçekleşmektedir. Bu döngü büyük maddi kaynağa ihtiyaç duymasının yanı sıra, insan sağlığı ve doğayı da tehdit etmektedir. Atık yönetimi için yapılan yatırımların yaklaşık %70-80'inin de toplama işlemleri için harcandığı bilinmektedir. Atık yönetiminde "0 Atık" konusunda çalışmalar yürütülse de tüketim var olduğu sürece atık yönetimi bu üç işlemden meydana gelecektir.

Atıklar kaynaklarına göre incelendiğinde evsel atıklar, inşaat (hafriyat) atıkları, tehlikeli atıklar, tıbbi atıklar, ambalaj atıkları, atık pil ve akümülatörler, atık yağlar ve elektronik atıklar olarak sınıflandırılabilir. Bu atıkların doğada yok olma süreleri göz önünde bulundurulduğunda, büyük ölçüde çevreye zarar vermeleri kaçınılmazdır. Ancak, yayınlanan raporlardan, sadece ambalaj atıklarının en fazla %4' ünün toplandığı bilinmektedir. Bu konuda, insan temasını azaltmak veya daha sağlıklı koşullar oluşturmak için çözüm önerileri sunmak hem yenilikçilik hem de sürdürülebilir kalkınma için önemli bir adım olacaktır. Atık yönetiminde ayrıştırma süreçleri ele alındığında ise yapılan tüm iyileştirmeler her yıl cam, metal ve plastik hammaddesi tasarrufu sağlamaktadır. Ayrıca kağıt atıklarının geri dönüştürülmesinin önemine de dikkat çekilmektedir [1].

Atık yönetiminde ayrıştırma süreçleri ele alındığında ise yapılan tüm iyileştirmeler her yıl cam, metal ve plastik hammaddesi tasarrufu sağlamaktadır. Toplanacak kağıtlar ile de daha fazla ağacın kesilmesi engellenecektir. Geri dönüştürülebilir atıkların tekrar kullanımı elektrik enerjisi tasarrufu sağlanmasını da sağlamaktadır.

Bu çalışma kapsamında atık yönetiminin atık toplam süreci ele alınmıştır. Atık toplama araçlarının en az maliyetle rotalanması için bir sistem önererek, araçların yakıt tüketimini azaltmak ve buna bağlı olarak karbon ayak izinin azalmasına katkı sağlamak hedeflenmiştir. Ayrıca, etkin araç rotalarının oluşturulması ile geri dönüştürülebilir atıkların düzenli bir şekilde

toplanacak olması çevre kirliliğini azaltacak, daha sağlıklı bir yaşam ortamı yaratacaktır.

Çalışmanın izleyen bölümlerinde önce literatür taraması, sonraki bölümlerde sırasıyla problemin tarifi, geçmiş dönemlere ait veri analizi ve çözüm için önerilen matematiksel model ile karınca kolonisi algoritması ve sayısal sonuçlar verilmiştir. Çalışma sonuç ve öneriler ile sonuçlanmıştır.

II. LİTERATÜR TARAMASI

Araç rotalama problemi (ARP), bir veya daha fazla aracın dağıtma, toplama veya her ikisini birden yapacak şekilde nasıl bir rota izlemesi gerektiğinin belirlenmesidir. Rota, aracın bir merkezden yola çıkıp birkaç noktaya uğradıktan sonra tekrar başladığı yere dönmesi ile oluşan turdur. ARP problemleri düğüm tabanlı ve ayrıt tabanlı olmak üzere iki temel sınıfta ele alınabilir. Çalışma konusu ayrıt tabanlı ARP'yi ele aldığından bu bölümde özellikle ayrıt tabanlı literatür araştırması verilmiştir.

Ayrıt tabanlı araç rotalama problemi, dağıtım ve/veya toplama yapılacak yerlerin serimde ayrıtlar üzerinde konumlanmış olması hâlinde ortaya çıkar. Dolayısıyla bir ayrıttan geçen bir araç, o ayrıt üzerindeki bütün noktalara uğrayacaktır. Sayaç okuma, kar küreme, tuz serpme ve yol bakımı ile polis devriyelerinin ve mektup dağıtım araçlarının rotalanması bu problemin uygulamalarına örnek olarak verilebilir [2]. Ayrıtların yönsüz olduğu durumlar yönsüz Çinli postacı problemi olarak adlandırılır. Örneğin, polis devriye araçları için bir uygulama yönsüz postacı problemi olarak ele alınabilir. Emel ve Taşkın [3] bir polis merkezine bağlı 10 mahalleye hizmet veren devriye araçları için problemi en kısa mesafeli eşleştirme yöntemi ile ele almıştır. Ayrıtlar arasında öncelik olması halinde ise hiyerarşik postacı problemi kullanılmaktadır. Bir başka çalışmada, karayolları bakım çalışması için kullanılan araçların güzergahlarının belirlenmesi için problemi hiyerarşik çinli postacı problemi olarak ele almıştır [4]. Problemin boyutu makul sürede en iyi çözüm elde elde edilemeyecek kadar büyük olduğundan, çözümü için klasik bir sezgisel algoritma olan en yakın komşuluk sezgiseli kullanılmıştır. Topuk vd. [5], Ege bölgesindeki illerde kapasite kısıtlı araç rotalama problemini ele almış, tasarruf algoritması ve süpürme sezgiselini kullanarak problemi çözmüştür. Eryavuz ve Gencer [6] çalışmalarında, bir personel servisinin tasarruf algoritması ile rotasını oluşturmuş; ardından tur geliştirici sezgiseller ile bu rota için %28'lik iyileşme sağlamıştır. Yılmaz [7] çok depolu araç rotalama problemlerinin çözümü için Karınca Kolonisi Optimizasyonu (KKO) kullanmıştır. En iyi sonucu bilinen problemler incelendiğinde, bilinen en iyi sonuca %7-%15 yaklaşan sonuçlar elde etmiştir.

Literatürde atık toplama problemini araç rotalama problemi temelinde ele alan çeşitli çalışmalar bulunmaktadır. Beltrami ve Bodin, New York ve Washington belediyelerinde çeşitli taşıt türlerini dikkate alarak kentsel atık toplama uygulamaları için araç rotalama problemini ele alan ilk araştırmacılardır. Çalışmada, Clarke ve Wrigh algoritması ile çözüm aranmıştır [8]. Türkiye'de de farklı örnekler bulunmaktadır. Örneğin, Eskişehir Odunpazarı ilçesinde evsel atık toplama ağını dört mahalle kapsamında tasarlanmış [9], Erzurum kentinin ambalaj atıkları geri dönüşüm sistemi tersine lojistik temelinde bir ARP olarak ele alınmıştır [10]. Çözüm için farklı olarak belirli bir dizi kural kullanılarak atık toplama rota sisteminin manuel analizine dayanan sezgisel bir model oluşturulmuştur. Önerilen güzergahların uygulanması ile kat edilen toplam mesafe yüzde 18,7 oranında azaltılmıştı [11].

Kentsel atık toplama problemi için en uygun güzergahı oluştururken Coğrafya Bilgi Sistemi uygulaması üzerinde de çalışılmaktadır [12]. Coğrafi Bilgi Sistemi temelli bir diğer çalışma da Fan vd. [13] tarafından yapılmıştır. Bu çalışmada, toplama yollarını en iyilemek için genetik algoritma simülasyonu entegre yöntemini benimsemiş ve Coğrafi Bilgi Sistemi tabanlı bir karar destek sistemi geliştirmiştir. Apaydın vd. [14] de çalışmalarında katı atık toplama işlemini Coğrafi Bilgi Sistemi ve RouteView Pro ™ yazılımını kullanarak en iyilemişlerdir.

Rota uzunluğu %20 ve harcanan zaman da %30 oranında azaltılmıştır. Kentsel katı atık toplama sisteminin tasarlanması için bir metodoloji önerilen çalışmada ise mevcut katı atık toplama sistemi geliştirilirken toplama süresini, işletme ve nakliye maliyetlerini en aza indirmek için kombinatoryal optimizasyon, tamsayı programlama ve Coğrafik Bilgi Sistemi araçları kullanılmıştır ve Santiago'da bir bölge için uygun toplama yolları oluşturulmuş, yeterli bir araç filosu boyutu belirlenmiştir [15]. Güney İtalya'da ortaya çıkan gerçek hayattaki bir ARP çalışmasında ise toplam maliyette yaklaşık %8'lik bir azalma sağlamak için Küme-Birinci Rota-İkinci Yöntemini kullanılmış; toplanacak atık miktarında belirsizlik olduğundan rotaların arzdaki değişikliklere duyarlılığını incelenmiş ve yaz mevsiminde arzdaki azalmanın etkisi değerlendirilmiştir [16].

Kentsel katı atık yönetiminde önemli bir konu da taleplerin yani atık miktarlarının belirsiz olmasıdır. Tirkolaee vd. [17], belirsiz talepler altında çok yönlü kapasiteli araç yönlendirme problemi için bir melez arttırılmış Karınca Kolonisi Algoritması (KKA) önermiştir. KKA literatürde, atık yönetimi ağ tasarımı çalışmalarında sıklıkla kullanılmaktadır. Atık yönetiminde kapasiteli ARP başka bir çalışmada da en küçük turu bulmak ve toplam mesafeyi en küçüklemek için Karınca Koloni Optimizasyonuna göre eşleştirilmiş en kısa yol ve ara depoları kullanmış ve yaklaşık %40 iyileştirme sağlanmıştır [18]. Gyamfi [19] çalışmasında atık yönetimi ağ tasarımı için kamyon güzergahlarının belirlenmesinde KKO kullanmıştır. Toplam maliyetin %35 azaltılması KKO' nun verimlilik açısından üstün performansını ortaya koymuştur.

Gerçek hayatta sokaklardan çıkan ambalaj atığı miktarı sabit ve belirli değildir. Literatürde bu durumu dikkate alan çalışma sayısı, atık toplama ağ tasarımı çalışmaları içinde görece oldukça azdır. Bu çalışmada gerçek hayat dalgalanmalarını göz önüne almak amacıyla sokaklardan çıkacak ambalaj atığı miktarının tahmin edilebilmesi için Bulanık Küme Teorisi kullanılmıştır. Yine literatür taraması sonucu görülmüştür ki KKA atık toplama ağ tasarımı için verimli ve sık kullanılan bir algoritmadır. Algoritmanın başarısı nedeniyle bu çalışmada da geri dönüştürülebilir ambalaj atıklarının toplanma ağı tasarımı için KKA kullanılmıştır.

III. MATERYAL VE YÖNTEM

A. Problemin Tarifi

Çalışma kapsamında, geri dönüşüm atıklarının toplandığı bir büyükşehre ait belediye ele alınmıştır. Mevcut durumda, belli bir döneme kadar anlaşmalı bir firma ile atıkları toplayan belediye, firma ile anlaşmasını yenilememiştir. Bu noktada, belediyede yeni bir atık toplama yönetim sistemi oluşturulmaktadır. Yönetimin aldığı karara göre her eve geri dönüştürülebilir atıklarını ayrı toplamaları için poşet dağıtılacak, bu poşetler belirli zamanlarda belirlenen noktalara bırakılacak ve belediyenin ilgili birimi de bu poşetleri toplayacaktır. Şekil 1'de 38 mahalle ve yaklaşık 4000 sokaktan oluşan belediye haritası verilmiştir.

Şekil 1. Belediyeye ait bölge.

Belediyenin toplama için beş adet aracı bulunmaktadır. Bunların dört tanesinin kapasitesi 4

ton, bir tanesinin ise 8 tondur. Marketlerden kaliteli ambalaj atığı çıktığından, 8 ton kapasiteli araç yalnızca marketleri dolaşacaktır. Geriye kalan diğer araçlar ise 38 mahalledeki sokak ve caddeleri dolaşarak poşetleri toplayacaktır.

Çalışmada ele alınan bu gerçek hayat probleminde taleplerin, yani evlerden çıkacak geri dönüştürülebilir atık miktarlarının, belirsiz olması çözüme yansıtılmıştır. Dolayısıyla, belirsiz talepler altında, belirli zamanlarda çıkarılan atıkları toplamak üzere kapasiteli araç rotalama problemi tanımlanmış ve matematiksel ve sezgisel çözüm yaklaşımları önerilmiştir.

B. Veri Toplama ve Analizi

Atık toplama problemini olabildiğince gerçekçi bir şekilde ele alabilmek için, geçmiş dönemlere ait toplanan ambalaj atığı miktarları kullanılarak gelecek dönemler için tahmin çalışması, mevsimsellik ve trend analizleri yapılmıştır.

Belediyeden alınan 2021, 2022 ve 2023 yıllarına ait toplanan ambalaj atıkları verileri incelenerek doğrusal ve mevsimsel tahminler değerlendirilmiştir. Tablo I' de geçmiş dönemlere ait veriler bulunmaktadır.

TABLO I
GEÇMİŞ DÖNEMLERE AİT TOPLANAN AMBALAJ ATIĞI MİKTARLARI (KG)

Periyot	2021	Miktar	Periyot	2022	Miktar	Periyot	2023	Miktar
1	Ocak	835	13	Ocak	693	25	Ocak	686
2	Şubat	779	14	Şubat	632	26	Şubat	634
3	Mart	953	15	Mart	749	27	Mart	705
4	Nisan	928	16	Nisan	775	28	Nisan	686
5	Mayıs	1.055	17	Mayıs	865	29	Mayıs	770
6	Haziran	1.068	18	Haziran	876	30	Haziran	696
7	Temmuz	1.009	19	Temmuz	841	31	Temmuz	729
8	Ağustos	1.009	20	Ağustos	785	32	Ağustos	721
9	Eylül	796	21	Eylül	752	33	Eylül	472
10	Ekim	773	22	Ekim	750			
11	Kasım	706	23	Kasım	663			
12	Aralık	693	24	Aralık	695			

Bu verilerden hareketle, doğrusal tahmin ve mevsimsel tahmin çalışmaları yapılmış, sonuçlar Tablo II'de verilmiştir. Bu veriler analiz edilerek grafik üzerinde okunur hale getirilmiş ve Şekil 2 ile gösterilmiştir. Grafik üzerinde artan ve azalan talep dalgalanmalarının kök nedenleri araştırılarak Pareto analizi çalışması yapılmıştır.

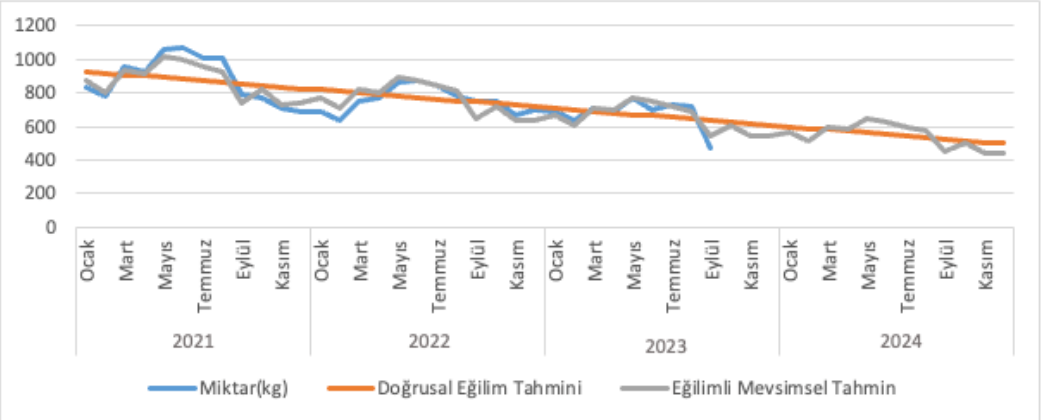

Şekil 2. Ambalaj atığı miktarları analizi.

TABLO II
TAHMİNİ AMBALAJ ATIĞI MİKTARLARI (KG)

Periyot	Yıl	Ay	Doğrusal Eğilim Tahmini	Eğilimli Mevsimsel Tahmin
34	2023	Ekim	626,15	610,372
35		Kasım	617,03	540,663
36		Aralık	607,91	540,064
37	2024	Ocak	598,79	565,689
38		Şubat	589,67	514,551
39		Mart	580,55	596,269
40		Nisan	571,43	582,513
41		Mayıs	562,31	645,438
42		Haziran	553,19	623,168
43		Temmuz	544,07	598,733
44		Ağustos	534,95	574,088
45		Eylül	525,83	453,236
46		Ekim	516,71	503,693
47		Kasım	507,59	444,771
48		Aralık	498,47	442,842

Şekil 2' de doğrusal azalma ile mevsimsellik görülmektedir. Yaz aylarında artış gösteren ambalaj atıklarının nedeni daha fazla hazır gıda tüketimi olarak görülebilir. Bu da çıkan ambalaj atığı miktarının artmasına neden olmuştur. Grafik üzerinde artan ve azalan talep dalgalanmalarının kök nedenlerini araştırmak üzere bir Pareto analizi çalışması yapılmıştır. Belediyeyle birlikte yapılan görüşmeler sonucu bu azalmaya sebep olabilecek altı farklı neden belirlenmiştir:

Bu nedenler,

A: Bağımsız toplayıcılar
B: Atık toplama konusundaki bilinçsizlik
C: Ambalaj atıklarının etkilerinin hemen gözlenmemesi
D: İnsanların atık yönetimine güvenmemesi
E: İnsanların evlerindeki atıkları ayrıştıramamaları
F: Konuyla ilgili bir kanun olmaması

olmak üzere altı başlık altında incelenmiştir. Pareto analizi sonucu bu sorunun neredeyse %80'ini bağımsız toplayıcılar ve atık toplama konusundaki bilinçsizliğin sonucu olduğu Şekil 3' te görülmektedir. Dolayısıyla, özellikle belediyenin kendi atık toplama sistemine ihtiyacı tekrar vurgulanmıştır.

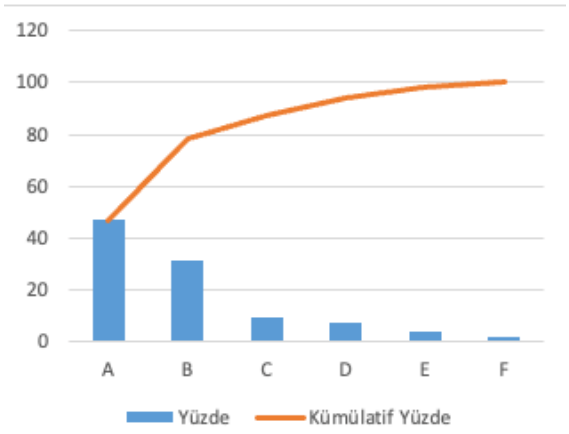

Şekil 3. Pareto analizi sonucu.

C. Önerilen Matematiksel Model

Atık toplama araçlarına ait en iyi rotaları bulmak ve toplam katedilen mesafeyi en küçüklemek amacıyla Tirkolaee vd.'nin [17] geliştirdiği matematiksel model temel alınarak, ilgili belediyeye özgü ayrıt tabanlı karma tamsayılı programlama modeli geliştirilmiştir. Modele ait indis, parametre ve karar değişkenleri izleyen sırada verilmiştir.

Küme ve indisler:

i, j, p: *düğüm noktaları* $i, j, p = 1, \ldots, n$
K: *araçlar kümesi* $\forall\, k \in K$
E_R: *kullanılan ayrıtlar kümesi* $\forall e\,(i,j) \in E_R$
T: *tüm düğümler kümesi* $\forall i, \forall j, \forall p \in T$

Parametreler:

c_{ij} : *(i,j) ayrıtının uzunluğu*
d_{ij} : *(i,j) ayrıtının talebi*
W_k: *k. aracın kapasitesi*

Karar Değişkenleri:

$$y_{ijk} = \begin{cases} 1\,; & k \text{ aracı } (i,j) \text{ ayrıtının talebini karşılarsa} \\ 0\,; & d.d \end{cases}$$

$x_{ijk} = (i,j)$*ayrıtından k aracı ile geçilme sayısı*

$$\sum_{p \in T} x_{ipk} = \sum_{p \in T} x_{pik} \qquad \forall i \in T \;\; \forall k \in K \qquad (1)$$

$$y_{ijk} \leq x_{ijk} \qquad \forall\, e(i,j) \in E_R \; \forall k \in K \qquad (2)$$

$$\sum_{e(i,j) \in E_R} d_{ij} y_{ijk} \leq W_k \qquad \forall k \in K \qquad (3)$$

$$\sum_{e(j,p) \in E_R} x_{jpk} \leq \mathrm{M} \sum_{e(i,j) \in E_R} x_{ijk} \qquad \forall k \in K \qquad (4)$$

$$y_{ijk} + y_{jik} \geq 1 \qquad \forall\, e(i,j) \in E_R \forall (i,j,k) \qquad (5)$$

$$x_{ijk} \geq 0 \qquad \forall\, (i,j,k), \;\; y_{ijk} = 0{,}1 \;\; \forall (i,j,k) \qquad (6)$$

kısıtları altında

$$Enk\; Z = \sum_{e(i,j) \in E_R} \sum_{k \in K} c_{ij} x_{ijk} \qquad (7)$$

Modelde yer alan (1) numaralı eşitlik akışı sağlayan süreklilik kısıtıdır. Kısıt grubu (2) ile k. aracın atıkları toplamak için bir başka sokağa gitmek için hizmet etmediği bir sokaktan geçebilmesi sağlanır. Araç kapasitelerinin aşılmaması kısıt grubu (3) ile garantilenir. Kısıt grubu (4), alt tur engelleme kısıtlarıdır. Kısıt grubu (5), her ayrıttan herhangi bir yönde en az bir kez geçilmesini sağlar. İşaret kısıtı, kısıt grubu (6) ile gösterilmiştir. Amaç fonksiyonu olan eşitlik (7) katedilen mesafeyi en küçüklemeyi hedefler.

Belediye, 38 mahalleden ambalaj atığı toplamaktadır. Bu mahallelerde yaklaşık 4000 sokak bulunmaktadır. Araçlar tüm mahallelerin sokaklarını dolaşmaktadır. Dolayısıyla problem boyutu büyümekte, karmaşıklığı artmaktadır. Önerilen matematiksel modelin doğrulaması için bir mahalleden seçilen beş sokak ile oluşturulan problem çözülmüştür. Çözüm için

optimizasyon yazılımı GAMS kullanılmıştır. Sokakların konumları serim üzerinde örnek olarak Şekil 4' te verilmiştir. Mevcut araç sayısının üç ve her birinin kapasitesinin de 400 kilogram olduğu varsayılmıştır. Araçların herhangi bir düğümden yola çıkması ve 1 numaralı düğüme dönerek turunu tamamlaması istenmiştir.

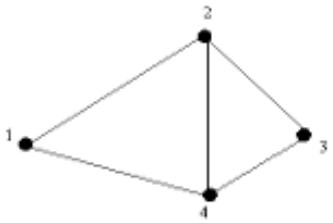

Şekil 4. Serim üzerinde örnek sokak gösterimi

Sokakların uzunlukları metre cinsinden, sokaklardan çıkacak ambalaj atığı miktarları yani talepler ise kilogram cinsinden Tablo III ile verilmiştir.

TABLO III
SOKAK UZUNLUKLARI VE SOKAKLARDAN ÇIKACAK TAHMİNİ ATIK MİKTARLARI

Ayrıt	Uzunluk (m)	Talep (kg)
1-2	150	60
1-4	100	11
2-3	120	76
2-4	100	10
3-4	60	52

Sonuçlar Tablo IV ile gösterilmiştir. Bu sonuca göre Araç 1 ayrıtları 1-2-3-4-1 şeklinde dolaşacak ve tesiste turunu tamamlayacak, diğer araç ise 2-4 ayrıtındaki talebi karşılayacak ve tesise dönerek turunu tamamlayacaktır. Bu durumda amaç fonksiyonu, 630 metre değerini almıştır. Ayrıca, mevcut durumda üç araç kullanılabilir durumda iken en iyi sonuçta sadece iki araç kullanılmıştır.

TABLO IV
ÖRNEK PROBLEM İÇİN SOKAK ARAÇ ATAMALARI

	Atanan Araç	
Ayrıt	Araç 1	Araç 2
1-2	1	
2-3	1	
2-4		1
3-4	1	
4-1	1	

Taleplerin belirsiz olması, araçların kapasite kısıtının bulunması gibi kısıtlar ile 4000 adet yol üzerinden toplama yapılacak olması problemin kesin olarak çözülebilmesini çok zor hale getirmektedir. Bu kısıtlar altındaki problemlerin genelde sezgisel ve metasezgisel yaklaşımlar ile çözülmeye çalışıldığı görülmüştür. Problem ilk olarak matematiksel model kurularak GAMS ile çözülmüştür. Problem boyutu arttırıldığında belirlenen zaman içerisinde GAMS ile uygun bir çözüm elde edilememiştir. Bu sebeple problemin çözümünde meta sezgisel çözüm yöntemlerinden olan KKA kullanılmıştır. Taleplerdeki belirsizlik ve gerçek hayattaki dalgalanmalar da göz önünde bulundurularak Bulanık Küme Teorisinden faydalanılmıştır.

D. Önerilen Sezgisel Yöntem-Karınca Kolonisi Algoritması (KKA)

Karıncaların yiyecek arama prensipleri ilk olarak Dorigo tarafından karıncaların yiyecek arama prensipleri incelenmiştir [20]. Karıncalar besinleri küçük parçalar halinde yuvalarına taşımaktadır. Dolayısıyla besin ve yuva arasında bir toplama ağı oluştururlar. Karıncaların bu yiyecek arama süreci birçok eniyileme probleminin çözümünde kullanılmıştır. Karınca kolonisi sistemi gezgin satıcı ve iş çizelgeleme gibi problem türlerinde geliştirilip kullanılmaktadır. Karıncalar, yuvalarından uzaktaki besin kaynağını görme duyularını kullanmadan da bulabilirler. Dışarıdan gelen bazı etkilerin sonucunda karıncaların kullandıkları yol artık en kısa yol değilse, karıncalar kullanabilecekleri en kısa yolu belirleyebilmektedirler. Bunu salgıladıkları feromon kimyasal salgısı ile yapmaktadırlar. Karıncalar tarafından salgılanan feromon salgısı, karıncaların birbirleri ile iletişim içerisinde olmasını sağlamaktadır. Feromon seviyesindeki artış karıncaların yol seçimini belirler. Yoldan her geçen karınca bu salgıdan bırakır, salgı seviyesi ne kadar çoksa karıncalar bu yolu tercih eder. Zamanla, tercih edilmeyen yoldaki feromon seviyesi azalır. Karıncalar bu salgı ile kullandıkları yolun en kısa yol olduğu bilgisini birbirlerine aktarmaktadırlar. Karıncalar hangi yoldan gideceğine bu şekilde karar verir ve en iyi rotaya ulaşır.

Şekil 5' te görüldüğü gibi, ilk olarak karıncaların yuvalarından uzaktaki besin kaynağına ulaşmada düz bir yolu takip ettikleri görülmektedir. İkinci adımda ise yuva ve besin kaynağı arasına bir engel konulmuştur. Bu engel ile karıncalar rassal olarak bir yolu seçerek besin kaynağına ulaşmaktadırlar. Birim zamanda kısa olan yoldan geçen karınca sayısı, uzun olan yoldan geçen karınca sayısından fazla olacaktır. Kısa olan yolun bilgisi ise karıncalar arasında feromon kimyasal salgısı ile iletilmiş olacaktır. KKA, karınca kolonilerinden esinlenilerek oluşturulduğundan bu sisteme Karınca Sistemi denilmektedir. Algoritmanın ismi ise Karınca Kolonileri Algoritması olarak adlandırılmaktadır.

Büyük boyutlu problemlerde kullanılan meta sezgisel bir çözüm yöntemi olan KKA çözüm uzayında daha geniş bir arama yaparak istenen iterasyon sayısında veya belirlenen süre içerisinde en iyiye yakın çözümü bize hızlı bir şekilde vermektedir. Karıncaların bir sonraki adımda hangi yola gideceğini belirleyen olasılık değeri eşitlik (8) yardımı ile hesaplanır.

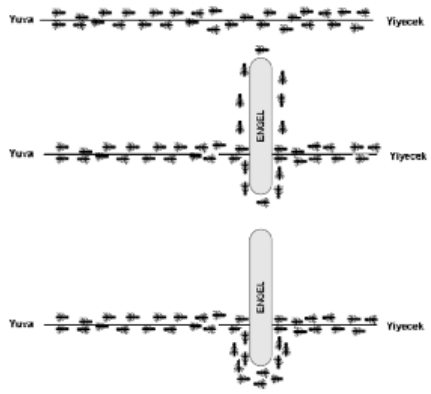

Şekil 5. Karınca sistemi çalışma prensibi.

$$P_{ij}^{k} = \frac{[\tau_{ij}]^{\alpha}[n_{ij}]^{\beta}}{\sum_{k \in N_i^k}[\tau_{ik}]^{\alpha}[n_{ik}]^{\beta}} \qquad \text{eğer } j \in N_i^k \tag{8}$$

$\in N_i^k$: k. karıncanın gidebileceği tüm j noktaları
$k \in N_i^k$: i. noktada bulunan bütün karıncalar
P_{ij}^{k} : k. karıncanın i. noktanın j. noktaya geçme olasılığı

τ_{ij} : i ve j noktaları arasındaki feronom seviyesi
n_{ij} : i ve j noktaları arasındaki görünürlük değeri
α : feronom katsayısı
β : görünürlük katsayısı
i : karıncanın bulunduğu nokta
j : karıncanın henüz gitmediği nokta
N : noktalar kümesi

Her tur sonrasında yollardaki feromon seviyeleri eşitlik (9) ile güncellenir.

$$\tau_{ij}(t+1) = p\tau_{ij}(t) + \Delta\tau_{ij} \tag{9}$$

$(1-p)$ yoldaki feromonun buharlaşma miktarıdır. $\Delta\tau_{ij}^{k}$ k. karıncanın i ve j noktaları arasında bıraktığı feromon miktarıdır. Eşitlik (10) yardımı ile hesaplanır.

$$\Delta\tau_{ij}^{k} = \begin{cases} \frac{Q}{L_k} & i-j\ yolu\ kullanılırsa \\ 0 & diğer\ durumda \end{cases} \tag{10}$$

Q : feromon sabiti
L_k : k. karıncanın tur uzunluğu

Karıncaların izleyeceği yolu seçmesi için eşitlik (11) kullanır:

$$j = \begin{cases} \arg\max u \in N_i^K \{[\tau_{iu}]^{\alpha}[n_{iu}]^{\beta}\} & q > q_0 \\ j & diğer\ durumda \end{cases} \tag{11}$$

q rassal bir sayı, q_0 ise sabittir. q_0 değeri bir güven seviyesini gösterir. Yapılan uygulamada bu değerler semtlerin sosyoekonomik ve demografik yapıları incelenerek belirlenecektir.

E. Bulanık Küme Teorisi

Bir problemin parametreleri gerçek dünya koşullarına göre dalgalanıp belirsizliğe yol açtığında olasılık dağılımını tahmin etmek zorlaşır. Bulanık küme teorisi, bir elemanın bir kümeye kısmi üyeliğine olanak tanır. Üyelik derecesi 0 ile 1 arasında değerler alır. Kümeye tamamen aitliği 1; 0 ise kümeye kesinlikle ait olmamayı ifade eder.

Zadeh (1965) tarafından geliştirilen Bulanık Küme Teorisi, yıllar içinde farklı araştırma konularında kullanılmıştır. Liu (2004), bulanıklık küme teorisi güvenilirlik seviyesini geliştirmiştir. Bulanık bir olayın güvenilirliği, olasılık ve gerekliliğinin ortalaması olarak tanımlanır [17]. Şekil 6' daki gibi üçgensel klasik bir küme tanımlanabilir. Ayrıtlarda oluşacak belirsiz talepler d_1 ile d_3 arasında değerler alır; d_2 ise en makul değerdir.

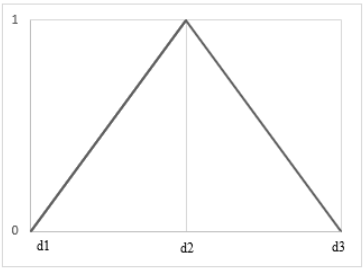

Şekil 6. Üçgensel bulanık küme.

Üçgensel bulanık küme üyelik fonksiyonu eşitlik (12) ile gösterilir.

$$\mu_{\tilde{D}}(x) = \begin{cases} \frac{(x-d_1)}{(d_2-d_1)} & d_1 \le x \le d_2 \\ 1 & x = d_2 \\ \frac{(d_3-x)}{(d_3-d_2)} & d_2 < x \le d_3 \end{cases} \quad (12)$$

Rassal sayı d_1 ve d_3 arasında ise üyelik derecesi eşitlik (12) ile belirlenir. Ancak d_1 ve d_3 aralığında değil ise üyelik derecesi sıfırdır. Bulanık bir olayın güvenilirliği ise eşitlik (13) yardımıyla hesaplanır. r rassal sayı olmak üzere;

$$Cr\{\tilde{D} \ge r\} = \begin{cases} 1 & r > d_1 \\ \frac{2d_2-d_1-r}{2(d_2-d_1)} & d_1 \le r \le d_2 \\ \frac{d_3-r}{2(d_3-d_2)} & d_2 \le r \le d_3 \\ 0 & diğer\ durumda \end{cases} \quad (13)$$

IV. KARINCA KOLONİSİ ALGORİTMASI VE PYTHON UYGULAMALARI

Belirsiz talepler altında geri dönüştürülebilir evsel atıkların en düşük maliyet ve en düşük karbon salınımı ile toplanması amacıyla önerilen KKA genel sözde kodu Şekil 7'de verilmiştir. Kod, elde edilen araç rotalarının gerekli koordinatlar ile harita üzerinde görselleştirilmesini de verecektir.

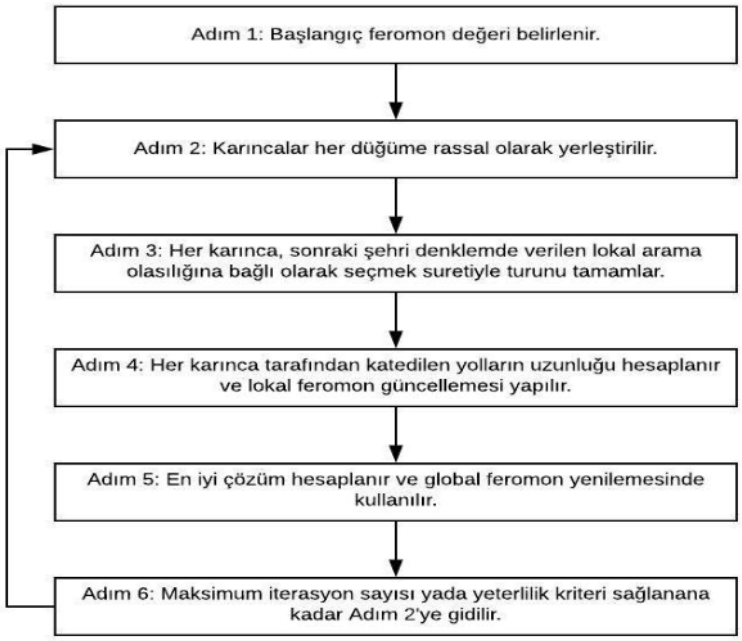

Şekil 7. KKA sözde kodu.

Karınca Yolu Programı adı verilen program, açık kaynak kod olması sebebi ile Python yazılım dili ile kodlanarak çalıştırılmıştır. Ayrıca, sırasıyla sokak ve kavşaklara karşı gelen ayrıt ve düğümlerin koordinat bilgilerinin, araç sayıları ile araç kapasitelerinin girilebilmesi ve rotaların izlenebilmesi için görselleştirme yapılmıştır. Böylece, programı kullanacak kişilerin de herhangi bir programlama bilgisine sahip olmasına gerek kalmayacaktır.

Uygulama, ilçeye ait üç mahallenin verileri ile gerçekleştirilmiştir. Harita kullanılarak sokakların koordinatları programa girilmiştir. Bulanık küme teorisi kullanılarak oluşacak

taleplerde gerçek hayat dalgalanmaları göz önüne bulundurulmuştur. Rotalara ait çıktı Şekil 8'de verilmiştir. Yapılan örneğe göre 100 sokağa atanan 4 araç 10 farklı rotada turlarını tamamlayacaktır.

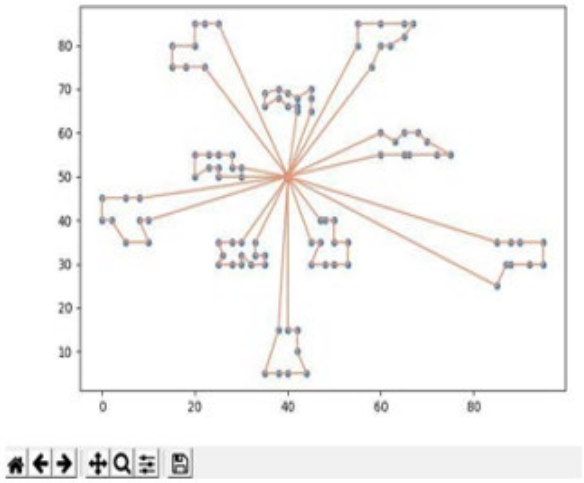

Şekil 8. KKA program çıktısı

V. SONUÇ VE ÖNERİLER

Sanayileşmenin ve dolayısıyla tüketimin de artmasıyla evsel ve endüstriyel atıklardan kaçınmak neredeyse imkânsız hale gelmiştir. Dolayısıyla daha sağlıklı bireyler ve çevre için kentsel atık yönetimi, yerel yönetimlerin ele alması gereken bir konudur.

Çalışmada, bir ilçeye ait sokak ve caddeler üzerindeki evlerden çıkan geri dönüştürülebilir atıkların en etkin şekilde toplanması amacıyla ayrıt tabanlı rotalama problemi ele alınmıştır. Problem için öncelikle bir matematiksel model geliştirilmiştir. 4000 sokak ile problem boyutu çok büyük olduğundan, beş sokaklı küçük bir alan için matematiksel model GAMS optimizasyon yazılımında çalıştırılmış ve en iyi sonuç elde edilmiştir. Ancak, 10 sokak için belirlenen zaman içinde uygun bir çözüm bulunamamış, çözüm için sezgisel bir algoritmaya ihtiyaç ortaya konmuştur. Bu sebeple, çözüm için bir karınca kolonisi algoritması geliştirilmiş, uygun rotalar elde edilmiştir.

Çalışmanın diğer önemli katkısı, taleplerin yani evlerden çıkan geri dönüştürülebilir atık miktarlarının belirsiz olması durumunu dikkate almasıdır. Bulanık Küme Teorisinden yararlanılarak, olabildiğince gerçek hayat problemini yansıtan bir çözüm algoritması geliştirilmiştir. Çalışmada ayrıca, çözümü elde etmek için önerilen KKA'nın kullanılabilmesi için herhangi bir kullanıcı bilgisi gerektirmeyen yazılım da geliştirilmiştir. Böylece kullanıcılar sokak, cadde, araç sayısı ve araç kapasitesi gibi parametreleri girilebilecek, sonuçları da görsel olarak harita üzerinden inceleyebilecektir.

Mevcut durumda ilçe belediyesinin atıkları toplamak için kullandığı sistematik bir yaklaşım bulunmamaktadır. Dolayısıyla, çalışma ile geliştirilen çözüm yaklaşımı ile herhangi bir teknik kullanım bilgisi gerektirmeyen görsel yazılım ile etkin araç rotaları elde edilecektir.

KAYNAKLAR

[1] S. Karahan, "En az beş yıllık olan depolanmış atık ofis kâğıtlarının geri dönüşüm olanaklarının araştırılması," Gümüşhane Üniversitesi Fen Bilimleri Enstitüsü Dergisi, vol. 10, no. 2, pp. 366-373, 2020.

[2] A. Khajepour, M. Sheikhmohammady, and E. Nikbakhsh, "Field path planning using capacitated arc routing problem," Computers and Electronics in Agriculture, vol. 173, pp.105401, 2020.

[3] A. G. Emel and Ç. Taşkın, "Yönsüz çinli postacı problemi polis devriye araçları için bir uygulama," Anadolu Üniversitesi Sosyal Bilimler Dergisi, vol. 3, no. 1, pp. 0–0, 2003.

[4] M. Yılmaz, "Karayolları bakım çalışmasında kullanılan araçların güzergahlarının hiyerarşik çinli postacı problemi kullanılarak düzenlenmesi," Iğdır Üniversitesi Fen Bilimleri Enstitüsü Dergisi, vol. 8, no. 4, pp. 107-115, 2018.

[5] N. Topuk, O. Özyeşil, ve T. Keskintürk, "Araç rotalama problemleri ile çözüm yöntemlerinin sınıflandırılması," İşletme Bilimi Dergisi, vol. 3, no. 2, pp. 77-107, 2015.

[6] M. Eryavuz, ve C. Gencer, "Araç rotalama problemine ait bir uygulama," Süleyman Demirel Üniversitesi İktisadi Ve İdari Bilimler Fakültesi Dergisi, vol. 6, no. 1, pp. 139-155, 2001.

[7] Ş. Yılmaz, "Çok depolu araç rotalama probleminin karınca kolonisi optimizasyonu ile modellenmesi ve bir çözüm önerisi,"*Fen Bilimleri Enstitüsü, Endüstri Mühendisliği Bölümü, Yüksek Lisans Tezi*, 2008.

[8] G. Ghiani, F. Guerriero, G. Improta, and R. Musmanno, "Waste collection in Southern Italy: Solution of a real-life arc routing problem," International Transaction in Operational Research, vol. 12, no. 2, pp. 135-144, 2005.

[9] H. Aydın, D. Başoğlu, M. Demirel, A. Güleç, E. Palaoğlu, A. Şimşek, ve B. Kara, "Evsel atık toplama ağı tasarımı ve geri kazanım süreçlerini iyileştirilmesi," Endüstri Mühendisliği, vol. 19, no. 3, pp. 2-16, 2008.

[10] Ü. Şengül, ve S. Kaçtıoğlu, S., "Erzurum kenti ambalaj atıkları geri dönüşümü için tersine lojistik ağı tasarımı ve bir karma tamsayılı programlama modeli,". Atatürk Üniversitesi İİBF Dergisi, vol. 24, no. 1, pp. 89-112, 2011.

[11] R. Ronen, A. Kellerman, and M. Lapidot, "Improvement of a solid waste collection system: the case of Givatayim, Israel," Applied Geography, vol. 3, pp. 133-144, 1983.

[12] A. Forghani, and A. Farahbakhsh, 2019. "Sustainable location and route planning with GIS for waste sorting centers, case study: Kerman, Iran," Waste Management & Research, vol. 37, pp. 287-300, 2019.

[13] X. Fan, M. Zhu, X. Zhang, Q. He, and A. Rovetta, 2010. "Solid waste collection optimization considering energy utilization for large city area," ICLSIM, Harbin, China, pp. 1905-1909, 2010.

[14] Ö. Apaydın, E. Arslankaya, Y. Avsar, and M. Gönüllü, 2004. "GIS supported optimization of solid waste collection in Trabzon," Sigma Journal of Engineering and Natural Sciences, vol. 4, pp. 249-254, 2004.

[15] C. A. Arribas, 2010. "Urban solid waste collection system using mathematical modelling and tools of geographic information systems," Waste Management & Research, vol. 28, no. 4, pp. 355-363, 2010.

[16] G. Ghiani, Improta, G., and Laporte, G., 2001. "The capacitated arc routing problem with intermediate facilities," Networks, vol. 37, pp. 134-143, 2001.

[17] Babaee Tirkolaee, E., Mahdavi, I., Seyyed Esfahani, M. M., & Weber, G. W. "A hybrid augmented ant colony optimization for the multi-trip capacitated arc routing problem under fuzzy demands for urban solid waste management," Waste management & Research, vol. 38, no. 2, pp. 156-172, 2020.

[18] D. Otoo, 2012. "Capacitated arc routing problem: collection of solid waste at Kwadaso Estate, Kumasi," (Doctoral dissertation), 2012.

[19] M. Gyamfi, 2012. "Sequential ordering of routes for trucks for efficient garbage collection. scase study of Sekondi –Takoradi Metropolitan Assembly," American Based Research Journal, vol. 2, no. 9, pp. 22-30, 2012.

[20] Dorigo, M. (2007). "Ant colony optimization," Scholarpedia, vol. 2, no. 3, pp. 1461, 2007.

A Hybrid DEA-AHP Approach for Assessing the Calorific Efficiency of Softwoods

Hilal Singer*,[1]

*hilal.singer@hotmail.com, ORCID: 0000-0003-0884-2555
[1]*Department of Industrial Engineering, Bolu Abant Izzet Baysal University, Bolu, Turkey*

Abstract Energy is one of the most important elements of a country's economic and social development. The demand for natural resources and energy is increasing day by day due to the rise in trade and production activities driven by population growth, industrialization, urbanization, and globalization. Softwood trees are valuable biomass resources that can provide clean energy for a variety of applications, ranging from household heating to large-scale power generation. Evaluating the calorific efficiency of different parts of softwood tree species is crucial in determining and improving their performance. This study proposes a two-stage decision-making approach to evaluate the calorific efficiencies of wood and bark samples obtained from the trunks and branches of various softwood tree species. Firstly, the wood and bark samples are compared based on their ash content, volatile matter content, and fixed carbon content using the data envelopment analysis. A total of 196 mathematical models are established to obtain efficiency comparison results. The analytic hierarchy process is applied to generate precise efficiency ranking indexes for the samples. According to the results, scots pine exhibits the highest calorific efficiency among the trunk wood and branch bark samples. Furthermore, black pine ranks first in the efficiency ranking of the branch wood and trunk bark samples. In the final phase of the study, the ranking results are examined through a comparative analysis. This study represents an important step in analyzing the calorific value of softwood trees. The results of the study present a roadmap for decision-makers in terms of considering the utilization of softwood trees in efficient energy production and evaluating their potential for other industrial applications.

Keywords: *Analytic Hierarchy Process, Calorific Efficiency, Data Envelopment Analysis, Softwood*

I. INTRODUCTION

Energy is one of the most important elements of a country's economic and social development. The demand for natural resources and energy is increasing day by day due to the rise in trade and production activities driven by population growth, industrialization, urbanization, and globalization. A large portion of the world's energy demand is met through fossil fuels such as coal, natural gas, and oil. However, due to various issues such as environmental pollution and economic concerns associated with fossil resources, there has been an increased interest in renewable energy sources. The commonly used renewable energy sources worldwide are solar energy, hydraulic energy, geothermal energy, biomass energy, and wind energy [1].

Softwood trees are valuable biomass resources that can provide clean energy for a variety of applications, ranging from household heating to large-scale power generation. Efficiency evaluation is a critical aspect of determining and enhancing the performance of these energy sources. The efficiency evaluation process entails analyzing the output(s) and inputs to identify how resources can be used most efficiently. Evaluating the calorific efficiency of different parts

of softwood tree species can aid in selecting the most suitable species for efficient energy production. In the literature, there are many research papers focusing on the topics of biomass-related efficiency evaluation [2], [3], [4], [5], [6], [7], [8], [9], [10]. Unlike the previous studies conducted in the literature, this problem will be treated as a complex decision-making problem and will be solved via an integrated data envelopment analysis (DEA) and analytic hierarchy process (AHP) approach.

The DEA method is a linear programming-based non-parametric decision support tool that measures the efficiency of homogeneous decision-making units (DMUs) with multiple input and output variables. It is based on observed values and does not require any functional relationship. DEA modeling is performed for comparable DMUs that carry out similar tasks and produce similar outputs using the same inputs [11]. The number of studies employing the DEA method in different disciplines has exponentially increased. The DEA method has been applied to solve various decision problems such as efficiency measurement of public expenditures [12], hospital sustainability assessment [13], scale elasticity measurement [14], evaluation of safety performance in construction projects [15], university department evaluation [16], comparison of railway passenger stations [17], portfolio optimization [18], modeling of business partnerships [19], and airport performance measurement [20]. The traditional DEA method evaluates DMUs in two categories: efficient and inefficient, and assigns a score of 1 to all efficient DMUs. While ranking results are obtained for inefficient DMUs, efficient DMUs cannot be prioritized among themselves. The AHP method can overcome this disadvantage of the DEA method.

The AHP method is a decision support tool that analyzes complex problems by taking into account the knowledge, experience, and intuition of decision-makers. This method enables decision-making processes to be conducted in light of rational data and models decision problems with a hierarchical structure that shows the relationships between criteria and alternatives. The importance of decision elements is determined through pairwise comparisons [21]. The popularity of the AHP method stems from its features such as simplicity, flexibility, ease of use, and ease of interpretation [22]. The AHP method has brought new insights into the solution of many problems such as surface roughness evaluation [23], softwood species selection [24], hospital site selection [25], metallic biomaterial assessment [21], landfill site selection [26], shrimp farming site selection [27], university laboratory safety evaluation [28], soil erosion susceptibility mapping [29], and beach quality assessment [30].

The calorific efficiency of a particular softwood tree species is related to the amount of energy that can be released when the material is burned. This efficiency is an important factor in determining the potential use of species as fuel. This study focuses on developing a decision-making model to evaluate the calorific efficiencies of wood and bark samples from various softwood tree species. In this study, the DEA method is first employed to make pairwise comparisons of the wood and bark samples based on their ash content, volatile matter content, and fixed carbon content. Then the AHP method is applied to generate precise efficiency ranking indexes for the samples. In the final phase, the study's results are examined through a comparative analysis.

II. MATERIALS AND METHODS

A. Data Envelopment Analysis

The DEA method is a non-parametric decision support tool used to estimate the efficiency of a set of DMUs. This method examines complex and/or unknown relationships between multiple inputs and outputs based on the principles of linear programming and carries out performance assessments by measuring the distance of each DMU from the efficiency frontier. The fundamental principle in the DEA is that all DMUs share common objectives and generate identical outputs using identical inputs. Efficiency measurement helps understand how effectively and efficiently resources are being utilized [11].

The DEA method indicates the efficiency of DMUs through values in the range [0-1]. DMUs with an efficiency score less than 1 are labeled as inefficient. At the end of the DEA process, evaluations are made regarding what needs to be done for inefficient DMUs, and potential improvement actions are identified. The DEA method uses frontier-based estimation for input or output orientation in the initial modeling stage. Subsequently, the output and input ratios of DMUs are compared on the efficient frontier, and efficiency scores are determined. The mathematical computation for the technical efficiency of each DMU is explained below [12], [31].

Symbols

e_k: Efficiency score,
y_{rj}: Amount of output r produced by DMU_j,
x_{ij}: Amount of input i utilized by DMU_j,
u_r: Weight of output r,
v_i: Weight of input i,
n: Number of DMUs,
t: Number of outputs,
m: Number of inputs.

$$e_k = max \sum_{r=1}^{t} u_r y_{rj} \tag{1}$$

subject to:

$$\sum_{i=1}^{m} v_i x_{rj} = 1 \tag{2}$$

$$\sum_{r=1}^{t} u_r y_{rj} - \sum_{i=1}^{m} v_i x_{rj} \leq 0 \tag{3}$$

$$u_r \geq 0, r = 1,\ldots,t \tag{4}$$

$$v_i \geq 0, i = 1,\ldots,m \tag{5}$$

B. Analytic Hierarchy Process

The AHP is a multicriteria decision-making method that solves complex problems based on the opinions of decision-makers. In the first step of the AHP method, the decision problem and objective are defined. In the second step, the AHP hierarchy is constructed with objectives, criteria, and alternatives. In the third step, pairwise comparisons are made for each level of the AHP hierarchy. Then a mathematical process is initiated to determine the priorities of decision elements [32].

Pairwise comparison matrices are used to compare decision elements with each other. When creating these matrices, a decision-maker assigns a performance score to each decision element. The diagonal values of each matrix are set to 1 because there is no priority between two identical decision elements. The values below the diagonal in the matrix are the inverses of the values above the diagonal. Pairwise comparisons are generally conducted using the Saaty scale, which ranges from 1 (equal importance) to 9 (absolute importance) [23].

In the final phase of the AHP, several series of mathematical operations are performed to prioritize decision elements. The normalized matrix is obtained by dividing each element by the sum of its matrix column. Then the importance vector is obtained by dividing the row sums of the normalized matrix by the number of decision elements. This vector represents the weights of decision elements. The sum of these weights is always 1 [33].

C. Hybrid DEA-AHP Approach

The hybrid DEA-AHP approach is a two-stage ranking method based on efficiency measurement. In the first phase of this method, DEA modeling is performed to make pairwise comparisons between DMUs. In the second phase, the decision matrix obtained in the first

phase is subjected to AHP modeling to rank DMUs. The DEA-AHP method combines two popular decision-making methods and incorporates the advantages of these methods [34]. The DEA-AHP procedure follows the following steps for solving decision problems [31], [35]:

Step 1: Pairwise comparison matrices for decision elements (k and $\grave{k}=1,\ldots,n$) are constructed by employing the DEA method. Comparison results ($e_{k,\grave{k}}$) are obtained according to the following linear programming model:

$$e_{k,\grave{k}} = max \sum_{r=1}^{t} u_r y_{rk} \tag{6}$$

subject to:

$$\sum_{i=1}^{m} v_i x_{rk} = 1 \tag{7}$$

$$\sum_{r=1}^{s} u_r y_{rk} - \sum_{i=1}^{m} v_i x_{rk} \leq 0 \tag{8}$$

$$\sum_{r=1}^{s} u_r y_{r\grave{k}} - \sum_{i=1}^{m} v_i x_{r\grave{k}} \leq 0 \tag{9}$$

$$u_r \geq 0, r = 1,\ldots,t \tag{10}$$

$$v_i \geq 0, i = 1,\ldots,m \tag{11}$$

Step 2: Matrix components are determined.

$$a_{k,\grave{k}} = \frac{e_{k,\grave{k}}}{e_{\grave{k},k}} \tag{12}$$

Step 3: To obtain a normalized matrix, each value in matrix columns is divided by the sum of its corresponding column values.

$$\dot{a}_{k,\grave{k}} = \frac{a_{k,\grave{k}}}{\sum_{k=1}^{n} a_{k,\grave{k}}} \tag{13}$$

Step 4: Column vector elements are obtained by summing matrix rows.

$$\ddot{a}_{k,\grave{k}} = \sum_{k=1}^{n} \dot{a}_{k,\grave{k}} \tag{14}$$

Step 5: The column vector undergoes a normalization process to determine the priority value of each decision element.

$$\ddot{a}_{k,\grave{k}} = \frac{\ddot{a}_k}{\sum_{k=1}^{n} \ddot{a}_k} \tag{15}$$

III. APPLICATION

A. Efficiency Measurement with the DEA-AHP Approach

This study proposes a two-stage decision-making approach to evaluate the calorific efficiencies of wood and bark samples obtained from the trunks and branches of various softwood tree species. In the first stage, the DEA method is used for pairwise comparisons of the samples. The DEA results are then transferred to pairwise comparison matrices. In the second stage, the calculation procedure of the AHP method is applied to the obtained matrices. Thus, precise efficiency ranking indexes are revealed to prioritize the samples. These methods have certain limitations when used independently. The DEA method divides DMUs into two groups: efficient and inefficient. The AHP method models the subjective judgments of decision-makers to rank DMUs. In the DEA-AHP approach, the results of efficiency comparisons in DEA analysis are subjected to AHP analysis to prioritize all DMUs. This way, both the limitation of the DEA method (ranking of DMUs) and the limitation of the AHP method (subjective influence) are eliminated. Fig. 1 presents the structure of the proposed decision-making framework.

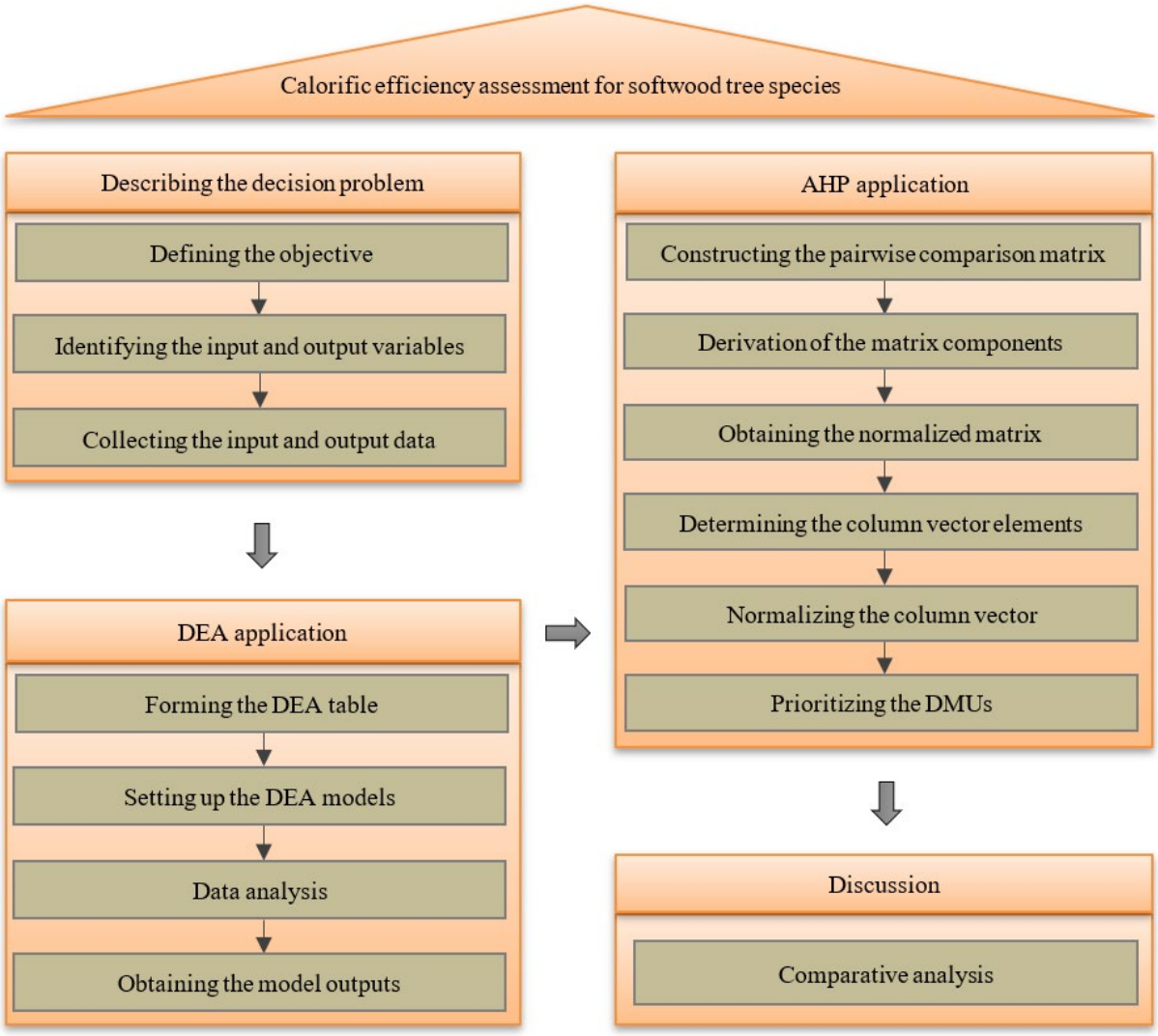

Fig 1. Structure of the proposed decision-making framework.

The decision elements of the model and the datasets for these elements are determined based on a previous report [36]. Seven softwood tree species native to Turkey are selected as the materials for this study. The calorific efficiencies of their wood and bark samples are analyzed based on variables such as ash content, volatile matter content, and fixed carbon content. The softwood tree species considered in the study are as follows: scots pine (*Pinus silvestris* L.), black pine (*Pinus nigra* A.), red pine (*Pinus brutia* T.), cypress (*Cupressus sempervirens* L.), cedar (*Cedrus libani* B.), fir (*Abies bornmülleriana* M.), and spruce (*Picea orientalis* L.).

In the decision models, the inputs are the ash content, volatile matter content, and fixed carbon content, while the output is the calorific value. The input variables are represented as percentage (%) changes, and the output variable is measured in units of cal/g. The datasets, which include the experimental results, are presented in Table 1. For detailed information on the experimental procedure, please refer to the literature [36].

TABLE I
INPUT AND OUTPUT DATA FOR THE DEA-AHP ANALYSIS [36]

Trunk wood				
Species	Calorific value (cal/gr.)	Ash (%)	Volatile matter (%)	Fixed carbon (%)
Scots pine	5274	0.19	76.85	12.60
Black pine	5266	0.26	76.33	12.85
Red pine	5096	0.26	78.61	12.12
Cypress	5010	0.34	77.00	13.14
Cedar	4933	0.39	77.04	13.58
Fir	4803	0.25	78.39	14.60
Spruce	4758	0.39	71.78	17.67
Branch wood				
Species	Calorific value (cal/gr.)	Ash (%)	Volatile matter (%)	Fixed carbon (%)
Scots pine	5181	0.36	78.98	13.48
Black pine	5266	0.28	75.35	14.16
Red pine	5067	0.35	75.51	14.04
Cypress	4933	0.45	73.60	16.09
Cedar	4898	0.41	74.39	14.50
Fir	4981	0.35	74.40	15.92
Spruce	4796	0.68	71.23	18.94
Trunk bark				
Species	Calorific value (cal/gr.)	Ash (%)	Volatile matter (%)	Fixed carbon (%)
Scots pine	5310	1.20	64.90	23.78
Black pine	5252	0.90	64.72	23.25
Red pine	5087	1.49	62.26	25.58
Cypress	4410	6.19	67.49	16.93
Cedar	4561	4.03	63.58	22.61
Fir	4772	2.83	65.55	20.76
Spruce	4913	2.69	59.42	26.34
Branch bark				
Species	Calorific value (cal/gr.)	Ash (%)	Volatile matter (%)	Fixed carbon (%)
Scots pine	4989	1.94	69.87	17.34
Black pine	5227	1.30	67.89	19.56
Red pine	4531	5.12	65.88	18.47
Cypress	4250	7.52	67.29	16.11
Cedar	4456	5.31	67.83	16.98
Fir	4969	2.93	69.47	18.09
Spruce	4602	4.54	66.46	18.71

The traditional DEA method evaluates any given DMU simultaneously with all other DMUs. All DMUs with an efficiency score of 1 are labeled as efficient. This situation prevents the ranking of efficient units among themselves. Therefore, in the current study, the DEA method equipped with the AHP method is used. After obtaining the input and output data, the calorific performances of the wood and bark samples are compared in pairs by employing the modified DEA method. A total of 196 ($4 \times (7 \times 7)$) mathematical models are established to obtain efficiency comparison results. The generated models are solved using the GAMS 24.1.3 optimization software. The initial comparison matrices consist of the outputs of the mathematical models. Therefore, the matrix components required for the AHP analysis are determined using (12). The final matrices are presented in Table 2.

TABLE II
MATRIX COMPONENTS

Trunk wood							
	SS1	SS2	SS3	SS4	SS5	SS6	SS7
SS1	1	1	1	1.055	1.072	1.120	1.035
SS2	1	1	1	1.060	1.077	1.054	1.041
SS3	1	1	1	1	1.012	1.020	1
SS4	0.948	0.943	1	1	1.016	1	1
SS5	0.933	0.928	0.988	0.984	1	1	1
SS6	0.893	0.949	0.980	1	1	1	1
SS7	0.966	0.961	1	1	1	1	1
Branch wood							
	SS1	SS2	SS3	SS4	SS5	SS6	SS7
SS1	1	1	1	1	1	1	1
SS2	1	1	1.030	1.043	1.061	1.044	1.038
SS3	1	0.970	1	1.001	1.019	1.002	1
SS4	1	0.959	0.999	1	1	1	1
SS5	1	0.942	0.981	1	1	1	1
SS6	1	0.958	0.998	1	1	1	1
SS7	1	0.963	1	1	1	1	1
Trunk bark							
	SS1	SS2	SS3	SS4	SS5	SS6	SS7
SS1	1	1	1.001	1	1.107	1	1
SS2	1	1	1	1	1.120	1	1
SS3	0.999	1	1	1	1	1	1
SS4	1	1	1	1	1	1	1
SS5	0.903	0.893	1	1	1	0.985	1
SS6	1	1	1	1	1.015	1	1
SS7	1	1	1	1	1	1	1
Branch bark							
	SS1	SS2	SS3	SS4	SS5	SS6	SS7
SS1	1	1	1.038	1.091	1.087	1	1.031
SS2	1	1	1.089	1.013	1.018	1	1.086
SS3	0.963	0.918	1	1	1	0.962	0.997
SS4	0.917	0.987	1	1	1	0.960	1
SS5	0.920	0.982	1	1	1	0.955	1
SS6	1	1	1.040	1.041	1.047	1	1.033
SS7	0.970	0.920	1.003	1	1	0.968	1

SS1: scots pine, SS2: black pine, SS3: red pine, SS4: cypress, SS5: cedar, SS6: fir, SS7: spruce

After obtaining the matrix components, four decision matrices are normalized using (13). The efficiency scores of the wood and bark samples are calculated by applying (14) and (15), respectively, to the normalized matrices. Subsequently, the samples are prioritized in descending order of the efficiency scores. The results obtained through the DEA-AHP approach are presented graphically in Fig. 2.

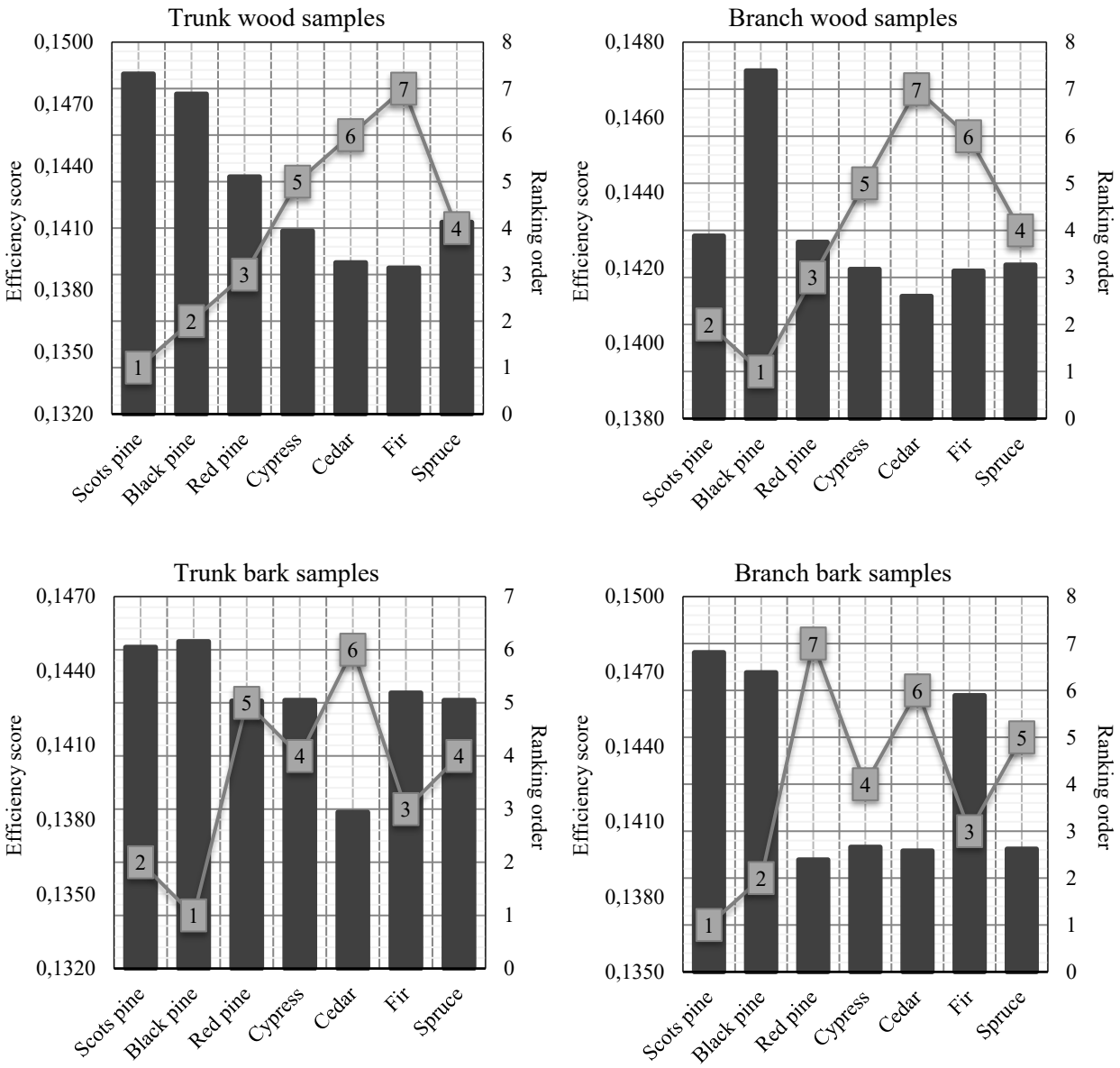

Fig. 2. DEA-AHP results.

The calorific efficiency of the trunk wood samples varies between 0.139 and 0.149. Scots pine has the highest efficiency score, followed by black pine. Red pine, spruce, and cypress are ranked in the middle of the efficiency ranking. Fir has a lower efficiency score compared to the other species. The results obtained for the branch wood samples show that black pine has the highest efficiency score of 0.147, ranking first. However, scots pine and red pine also achieved high efficiency scores, ranking second and third, respectively. Fir and cedar rank sixth and seventh, respectively. In the measurements conducted on the trunk bark samples, black pine has the highest efficiency score and ranks first. Scots pine ranks second. Cedar has the lowest efficiency score and takes last place. Among the branch bark samples, scots pine and black pine have the highest calorific efficiency scores and rank first and second, respectively. Cedar and red pine have the lowest efficiency scores and rank sixth and seventh, respectively.

The rankings vary for different types of samples. However, it is generally observed that scots pine and black pine have the highest calorific efficiency. Ash content, volatile matter content, and fixed carbon content are important factors that determine combustibility properties. These factors affect the amount of energy generated during combustion. For example, a high ash content has a negative impact on the combustion process and leads to less energy production. Therefore, an analysis that takes into account the factors mentioned above allows us to better

understand the combustibility performance of biomass and makes the results more meaningful. This study presents a roadmap for decision-makers in terms of considering the utilization of softwood trees in efficient energy production and evaluating their potential for other industrial applications.

B. Comparative Analysis

The DEA method measures the efficiency of DMUs that produce similar outputs. It utilizes various models for solving decision problems. The input-oriented DEA model involves examining changes in input quantities while keeping output quantities constant. The output-oriented DEA model investigates how much output can be achieved with a specific input combination [37]. In this study, the input-oriented DEA model is preferred due to our higher control power over the inputs. Different mathematical models are established based on ash content, volatile matter content, fixed carbon content, and calorific value. These established mathematical models are solved to determine the efficiency scores of the wood and bark samples. According to the comparative analysis results presented in Table 3, the priority rankings produced by the DEA and DEA-AHP methods are very similar. The DEA method detects several DMUs with the same ranking position, whereas the DEA-AHP approach yields a distinct ranking among the DMUs. The DEA-AHP approach integrates the weighting procedure of the AHP into the DEA. This allows for clearer differentiation among the DMUs and a more effective capture of the complex relationships within the datasets.

TABLE III
COMPARISON TABLE FOR THE DEA AND DEA-AHP METHODS

Species	Trunk wood			Branch wood			Trunk bark			Branch bark		
	DEA score	DEA ranking	DEA-AHP ranking	DEA score	DEA ranking	DEA-AHP ranking	DEA score	DEA ranking	DEA-AHP ranking	DEA score	DEA ranking	DEA-AHP ranking
Scots pine	1.000	1	1	1.000	1	2	1.000	1	2	1.000	1	1
Black pine	1.000	1	2	1.000	1	1	1.000	1	1	1.000	1	2
Red pine	1.000	1	3	0.967	2	3	0.996	2	5	0.906	6	7
Cypress	0.943	3	5	0.959	4	5	1.000	1	4	0.917	3	4
Cedar	0.928	4	6	0.942	6	7	0.890	4	6	0.916	4	6
Fir	0.889	5	7	0.958	5	6	0.973	3	3	0.978	2	3
Spruce	0.961	2	4	0.963	3	4	1.000	1	4	0.910	5	5

IV. CONCLUSION

Softwood trees are important energy sources. These trees are typically fast-growing, making them ideal for biomass production. Softwood trees also tend to have high energy content, which makes them effective sources of fuel. Analyzing the calorific efficiency of different parts of softwood tree species is very important as it contributes to maximizing the efficiency and effectiveness of the utilization of this energy source. In this study, the calorific efficiencies of wood and bark samples from various softwood tree species are evaluated using an integrated DEA and AHP approach. Firstly, the wood and bark samples are compared based on their ash content, volatile matter content, and fixed carbon content using the DEA method. Then the AHP method is applied to generate precise efficiency ranking indexes for the samples. The priority ranking obtained for the trunk wood samples is scots pine - black pine - red pine - spruce - cypress - cedar - fir. The sequence of the branch wood samples is determined as follows: black pine - scots pine - red pine - spruce - cypress - fir - cedar. The ranking of the trunk bark samples is obtained as black pine - scots pine - fir - cypress = spruce - red pine - cedar. Lastly, the branch wood samples are ranked as scots pine - black pine - fir - cypress - spruce - cedar - red pine.

This research endeavor differs from the previous studies. The current study focuses on evaluating the calorific values of the woods and barks of softwood tree species as a complex decision-making problem. The DEA and AHP methods are hybridized to conduct a detailed and comprehensive multicriteria analysis of the problem. The DEA method is complemented by the AHP method to enhance its disaggregation power. The DEA-AHP approach reveals the precise efficiency ranking indexes of the wood and bark samples. The proposed evaluation framework provides a novel way to assessing the thermal performance of different materials and serves as a roadmap for identifying the most efficient materials in energy production.

This study is an important step in analyzing the caloric efficiency of tree parts. The results of the study can be useful for decision-makers intending to use trees as energy sources. Additionally, this study can serve as a foundation for future research. The current study can be expanded by incorporating different variables, increasing the number of alternatives, and incorporating expert opinions into the decision-making process. Furthermore, various performance evaluation methods can be included in the methodology.

REFERENCES

[1] C. Gökoğlu, "Determination of fuel properties of the wood pellet's made from Turkish red pine (Pinus Brutia L.) forests harvesting residues," MSc Thesis, Muğla Sıtkı Koçman University, Turkey, 2016.

[2] N. Vertregt and F. W. T. Penning de Vries, "A rapid method for determining the efficiency of biosynthesis of plant biomass," *Journal of Theoretical Biology*, vol. 128, no. 1, pp. 109–119, 1987, doi: 10.1016/S0022-5193(87)80034-6.

[3] M. J. Prins, K. J. Ptasinski, and F. J. J. G. Janssen, "More efficient biomass gasification via torrefaction," *Energy*, vol. 31, no. 15, pp. 3458–3470, 2006, doi: 10.1016/j.energy.2006.03.008.

[4] X. He *et al.*, "Efficient preparation of biomass-based mesoporous carbons for supercapacitors with both high energy density and high power density," *Journal of Power Sources*, vol. 240, pp. 109–113, 2013, doi: 10.1016/j.jpowsour.2013.03.174.

[5] J. S. Kuzmina, L. B. Director, A. L. Shevchenko, and V. M. Zaichenko, "Energy efficiency analysis of reactor for torrefaction of biomass with direct heating," *Journal of Physics: Conference Series*, vol. 774, no. 1, pp. 1–7, 2016, doi: 10.1088/1742-6596/774/1/012138.

[6] S. Cheng, I. DCruz, M. Wang, M. Leitch, and C. Xu, "Highly efficient liquefaction of woody biomass in hot-compressed alcohol-water co-solvents," *Energy and Fuels*, vol. 24, no. 9, pp. 4659–4667, 2010, doi: 10.1021/ef901218w.

[7] C. A. Barcelos *et al.*, "High-efficiency conversion of ionic liquid-pretreated woody biomass to ethanol at the pilot scale," *ACS Sustainable Chemistry and Engineering*, vol. 9, no. 11, pp. 4042–4053, 2021, doi: 10.1021/acssuschemeng.0c07920.

[8] T. Hammar, J. Stendahl, C. Sundberg, H. Holmström, and P. A. Hansson, "Climate impact and energy efficiency of woody bioenergy systems from a landscape perspective," *Biomass and Bioenergy*, vol. 120, pp. 189–199, 2019, doi: 10.1016/j.biombioe.2018.11.026.

[9] M. ; C. Han G.-W.; Kim, Y.; Koo, B.-C., "Bioethanol production by Miscanthus as a lignocellulosic biomass: focus on high efficiency conversion to glucose and ethanol," *Bioresources*, vol. 6, pp. 1939–1953, 2011.

[10] F. Frombo, R. Minciardi, M. Robba, F. Rosso, and R. Sacile, "Planning woody biomass logistics for energy production: a strategic decision model," *Biomass and Bioenergy*, vol. 33, no. 3, pp. 372–383, 2009, doi: 10.1016/j.biombioe.2008.09.008.

[11] R. Rostamzadeh, O. Akbarian, A. Banaitis, and Z. Soltani, "Application of DEA in benchmarking: a systematic literature review from 2003–2020," *Technological and*

Economic Development of Economy, vol. 27, no. 1, pp. 175–222, 2021, doi: 10.3846/tede.2021.13406.
[12] R. F. Lavado and E. C. Cabanda, "The efficiency of health and education expenditures in the Philippines," *Central European Journal of Operations Research*, vol. 17, no. 3, pp. 275–291, 2009, doi: 10.1007/s10100-009-0095-1.
[13] Y. M. Pederneiras, M. A. Pereira, and J. R. Figueira, "Are the Portuguese public hospitals sustainable? A triple bottom line hybrid data envelopment analysis approach," *International Transactions in Operational Research*, vol. 30, no. 1, pp. 453–475, 2023, doi: 10.1111/itor.12966.
[14] A. Amirteimoori, B. K. Sahoo, and S. Mehdizadeh, "Data envelopment analysis for scale elasticity measurement in the stochastic case: with an application to Indian banking," *Financial Innovation*, vol. 9, no. 1, pp. 1–36, 2023, doi: 10.1186/s40854-022-00447-1.
[15] J. Li, A. Alburaikan, and R. de Fátima Muniz, "Evaluation of safety-based performance in construction projects with neutrosophic data envelopment analysis," *Management Decision*, vol. 61, no. 2, pp. 552–568, 2023, doi: 10.1108/MD-02-2022-0237.
[16] D. B. Mirasol-Cavero and L. Ocampo, "Fuzzy preference programming formulation in data envelopment analysis for university department evaluation," *Journal of Modelling in Management*, vol. 18, no. 1, pp. 212–238, 2023, doi: 10.1108/JM2-08-2020-0205.
[17] S. L. Fadaei Foroutan and S. Bamdad, "Efficiency measurement of railway passenger stations through network data envelopment analysis," *Research in Transportation Business and Management*, vol. 46, pp. 1–15, 2023, doi: 10.1016/j.rtbm.2021.100767.
[18] M. M. Hosseinzadeh, S. Ortobelli Lozza, F. Hosseinzadeh Lotfi, and V. Moriggia, "Portfolio optimization with asset preselection using data envelopment analysis," *Central European Journal of Operations Research*, vol. 31, no. 1, pp. 287–310, 2023, doi: 10.1007/s10100-022-00808-2.
[19] G. R. Amin and M. Ibn Boamah, "Modeling business partnerships: a data envelopment analysis approach," *European Journal of Operational Research*, vol. 305, no. 1, pp. 329–337, 2023, doi: 10.1016/j.ejor.2022.05.036.
[20] J. Cifuentes-Faura and U. Faura-Martínez, "Measuring Spanish airport performance: a bootstrap data envelopment analysis of efficiency," *Utilities Policy*, vol. 80, pp. 1–9, 2023, doi: 10.1016/j.jup.2022.101457.
[21] H. Singer and T. Över Özçelik, "Metallic biomaterial assessment via a risk-based decision-making approach," *Journal of the Faculty of Engineering and Architecture of Gazi University*, vol. 37, no. 2, pp. 641–654, 2022, doi: 10.17341/gazimmfd.935288.
[22] H. Singer and Ş. Özşahin, "Applying an interval-valued Pythagorean fuzzy analytic hierarchy process to rank factors influencing wooden outdoor furniture selection," *Wood Mater Sci Eng*, vol. 18, no. 1, pp. 322–333, 2023, doi: 10.1080/17480272.2021.2025427.
[23] H. Singer and Ş. Özşahin, "Employing an analytic hierarchy process to prioritize factors influencing surface roughness of wood and wood-based materials in the sawing process," *Turkish Journal of Agriculture and Forestry*, vol. 42, no. 5, pp. 364–371, 2018, doi: 10.3906/tar-1801-138.
[24] Ş. Özşahin, H. Singer, A. Temiz, and İ. Yildirim, "Selection of softwood species for structural and non-structural timber construction by using the analytic hierarchy process (AHP) and the multiobjective optimization on the basis of ratio analysis (MOORA)," *Balt. For.*, vol. 25, no. 2, pp. 281–288, 2019, doi: 10.46490/vol25iss2pp281.
[25] T. Şahin, S. Ocak, and M. Top, "Analytic hierarchy process for hospital site selection," *Health Policy and Technology*, vol. 8, no. 1, pp. 42–50, 2019, doi: 10.1016/j.hlpt.2019.02.005.
[26] F. Abdelouhed, A. Ahmed, A. Abdellah, B. Yassine, and I. Mohammed, "GIS and remote sensing coupled with analytical hierarchy process (AHP) for the selection of appropriate sites for landfills: a case study in the province of Ouarzazate, Morocco," *Journal of*

Engineering and Applied Science, vol. 69, no. 1, pp. 1–23, 2022, doi: 10.1186/s44147-021-00063-3.

[27] H. B. Akdeniz, S. Yalpir, and S. Inam, "Assessment of suitable shrimp farming site selection using geographical information system based analytical hierarchy process in Turkey," *Ocean and Coastal Management*, vol. 235. p. 106468, 2023. doi: 10.1016/j.ocecoaman.2022.106468.

[28] C. Guan, Y. Yang, C. Chen, and J. Feng, "Design and application of university laboratory safety evaluation system based on fuzzy analytic hierarchy process and back propagation neural network," *International Journal of Applied Decision Sciences*, vol. 16, no. 1, pp. 114–128, 2023, doi: 10.1504/IJADS.2023.10050866.

[29] F. Mushtaq, M. Farooq, A. S. Tirkey, and B. A. Sheikh, "Analytic hierarchy process (AHP) based soil erosion susceptibility mapping in Northwestern Himalayas: a case study of Central Kashmir Province," *Conservation*, vol. 3, no. 1, pp. 32–52, 2023, doi: 10.3390/conservation3010003.

[30] H. Li, J. Wang, and C. Zhu, "Assessment and application of beach quality based on analytic hierarchy process in Yangkou Beach, Qingdao," *Journal of Ocean University of China*, vol. 22, no. 1, pp. 151–160, 2023, doi: 10.1007/s11802-023-5414-y.

[31] B. D. Rouyendegh, A. Oztekin, J. Ekong, and A. Dag, "Measuring the efficiency of hospitals: a fully-ranking DEA–FAHP approach," *Annals of Operations Research*, vol. 278, no. 1–2, pp. 361–378, 2019, doi: 10.1007/s10479-016-2330-1.

[32] P. Madzík and L. Falát, "State-of-the-art on analytic hierarchy process in the last 40 years: literature review based on Latent Dirichlet Allocation topic modelling," *PLoS ONE*, vol. 17, pp. 1–31, 2022, doi: 10.1371/journal.pone.0268777.

[33] H. U. Khan and S. Nazir, "Assessing the role of AI-based smart sensors in smart cities using AHP and MOORA," *Sensors*, vol. 23, no. 1, pp. 1–14, 2023, doi: 10.3390/s23010494.

[34] P. Kecman, P. Jovanović, and M. Bugarinovic, "Evaluating and ranking infrastructure manager strategies using the combined AHP/DEA method," in *5th International Scientific Conference "Theoretical and Practical Issues in Transport,"* Pardubice, Czech Republic, 2010, pp. 318–323.

[35] B. D. Rouyendegh, "DEA-ANP sequential hybrid algorithm for multiple-criteria decision-making process, a long with an application," PhD Thesis, Gazi University, Turkey, 2009.

[36] P. Erten and S. Önal, "Determination of calorific value of native species woods and barks," *Turkish Forest Research Institute Publications*, vol. 31, no. 62, pp. 90–110.

[37] S. T. Xaba, N. Marwa, and B. Mathur-Helm, "Efficiency evaluation of agricultural cooperatives in Mpumalanga: an empirical study using the DEA approach," *African Journal of Economic and Management Studies*, vol. 11, no. 1, pp. 51–62, 2020, doi: 10.1108/AJEMS-10-2018-0291.

Towards Intelligent Industry: Optimizing Processes through AI and Blockchain Integration

Al Mothana Al Shareef[*,1], Serap Seçkiner[2]

[*]engr1st@gmail.com, ORCID: 0009-0004-5279-3900
[1]*Industrial Engineering Department, Gaziantep University (UoG), Gaziantep, Türkiye*
[2]*Industrial Engineering Department, Gaziantep University (UoG), Gaziantep, Türkiye*

Abstract This study explores opportunities to optimize industrial processes through the integration of AI and Blockchain as new approach, aiming at benefits such as industrial manufacturing efficiency, enhancing product quality, and achieving sustainability in an increasingly competitive modern industrial world. We provide a brief introduction to AI and Blockchain technologies, which will serve as a basis to further strengthen our argument. Furthermore, we introduce significant application areas of each technology and further elaborate on their advantages and challenges in the modern industrial space. Hence, we introduced a general overview of the operations and systematic steps of an Industrial Processes System to open new doors for our discussions. This paper further builds on AI and its subsets, including Machine Learning (ML), which has been credited as a significant contributor in reducing human workforce and its benefits on optimizing manufacturing processes. Moreover, various applications in AI have been discussed to further outline its major contributions in the industry. Our paper suggests significant solutions to supply chain management by introducing Blockchain and AI as key technologies. Furthermore, we propose our conceptual and comprehensive model, providing key insights to the exploration of AI and Blockchain in the optimization process. Our framework illustrates the steps in a detailed manner in combination with AI and Blockchain inputs, from the initial stage of raw materials to the output stage of the product itself, further finalizing the process with logistics and distribution. Combined with both technologies, our findings based on our framework suggests that AI-driven analytics can provide significant optimizations to the production process, such as enhanced decision-making, scheduling production, and arranging quality control processes. Meanwhile, Blockchain provides data integrity and opens doors for ease in regulatory compliance. Finally, the integration of AI and Blockchain led to sustainable industrial processes, which encourages the implementation of sustainable business practices as well. Our study underscores the numerous advantages both technologies provide for the industrial sector, opening doors for further research and achieve smart, innovative, and autonomous industrial processes. Overall, our paper maintains a strong stance to indicate that the integration of Blockchain and AI is inevitable towards maintaining operational excellence in manufacturing processes, promote partnerships between stakeholders, and improve overall efficiency in industrial processes.

Keywords: *Artificial Intelligence, Blockchain Technology, Industrial Optimization, Machine Learning, Industrial Processes*

I. INTRODUCTION

Industries are transforming rapidly with the latest revolution of Industry 4.0. It changed the course of industrial production, and diverse technologies are shown to be effective in industrial performance rather than conventional methods [1]. However, this raises questions of

optimizing industrial processes in diverse sectors [2], such as healthcare, agriculture, energy, and big data. Moreover, it is set to transform manufacturing processes today and fast-forward to the future. Challenges arise when industrial processes are not optimized, such as sustainability issues, technical downsides, system downtime, and regulatory compliance [3]. More specifically, cost of integration, significant energy usage, data management, and environmental hazard are a few to mention. However, those challenges can be overcome if the integration process is carried out smoothly. The systematic approach to various issues lies on the aspects of the system that is being implemented.

The "flow" of manufacturing processes is determined by the efficiency of the system. Thus, an optimized system will be fully efficient and sustainable. Reducing the time of manufacturing and delivering products is a significant reason why optimization is greatly needed. For this reason, different manufacturing techniques and systems are being proposed [4]. According to the National Association of Manufacturing (NAM) [5], $2.33 trillion was added to the US economy, while the cost of production averaging on a range between half a million to several million US dollars. The report had been published in the first quarter of 2020, and it was stated that raw material prices and product prices would increase, which adds to the cost of manufacturing.

Blockchain technology and Artificial Intelligence (AI) are used in different sectors in today's world, ranging from healthcare, supply chain and logistics, finance, retail and e-commerce, energy, manufacturing and Industry 4.0, agriculture, and automotive. While Blockchain technology is a unique approach to handle large amounts of data, AI enhances user experience by providing optimized automated processes. Blockchain technology mainly operates under smart contracts to achieve functionality, so every transaction occurs on the user side. Conversely, AI provides a more seamless ecosystem to the user by carrying operations smoothly. Unequivocally, industrial processes are slow, inefficient, and resource-consuming with traditional technologies. However, Blockchain and AI serve as the basis of a new industrial standard in terms of optimization. While Blockchain achieves scalability and decentralization, AI focuses on improving automated processes drastically, by implementing deep algorithms. Traditional technologies handling industrial processes will hardly achieve optimization. The main advantage Industry 4.0 brings is its sole focus on efficiency and smart automation for industrial processes, which are areas Blockchain technology and AI are equipped with naturally. IoT puts an enterprise forward when integrating with manufacturing processes [6].

However, optimization in industrial processes through AI and Blockchain technology integration still remains in its early stages where very few researches were conducted and needs to be explored deeply. Modern industrial systems require the collective benefits of both AI and Blockchain to achieve full automation. For instance, scalability appears as a common issue in industrial processes that we have to simultaneously use the properties of both technologies. Otherwise, a concept of a fully optimized manufacturing process cannot be imagined. How can the costs that arise from integrating heavy technologies like AI and Blockchain be lowered? How can we achieve sustainability within the whole process of manufacturing using AI and Blockchain? Is it possible to introduce a renewable energy model where sustainability is achieved within the manufacturing process?

Although significant advancements in the application of both technologies have been made, several research gaps remain. Specifically using Blockchain technology and AI to optimize industrial processes is a relatively scarce topic. Most studies focus on Blockchain and AI individually; they do not specifically research on the combination of AI and Blockchain, opportunities, and challenges in the industrial sector. As such, there one single research that builds on both promising technologies—AI and Blockchain—together to optimize industrial processes. For instance, authors in [7] explored the integration of AI and Blockchain in Industry 4.0 but it lacks a well-rounded framework that brings together AI and Blockchain to enhance various industrial processes, with little emphasis on improving overall efficiency and

sustainability. Consequently, the need for a novel concept to optimize typical industrial process systems that exist today is one of the main goals of this paper. An enormous potential is observed among the scientific community regarding AI and Blockchain technology, even if most research focus on them individually. Latest applications in Blockchain and AI highlight the importance of these concepts for the future of industry and manufacturing. Moreover, no research has introduced a conceptual and comprehensive model that actively uses both Blockchain technology and AI combined for a typical industrial processing system for future use. Both the benefits of AI and Blockchain technology outweigh the disadvantages greatly. A lack of research effort about this matter highlights why starting to close the research gap as our first attempt to emphasize solutions based on a comprehensive and conceptual framework for optimizing industrial processes is introduced. Therefore, our paper will be the first to visualize the effectiveness of optimizing industrial processes by combining AI and Blockchain.

The main contribution of this paper can be summed up as follows:
We briefly introduce the Industrial Process System, and Blockchain and AI technologies as the key concepts to optimize industrial processes. We first start by providing a brief introduction by explaining the basics of AI and Blockchain with their optimization potentials and challenges in their respective areas, highlighting their application areas and each technology's benefits in the industrial sector. Finally, we propose our conceptual framework exploring AI and Blockchain integration opportunities in optimizing industrial processes. Our paper provides a unique model that explains how the combination of AI and Blockchain can optimize industrial processes and shift it toward smarter industries.

II. LITERATURE REVIEW

1. Industrial Process System

An industrial process system refers to the whole systematic approach in which a combination of machinery or equipment, technologies, and procedures are used to create a certain product. This approach can be similar to a cycle, where it can be applied over and over again. The main goal of the system is to create a finished product using a series of instructions; the process can

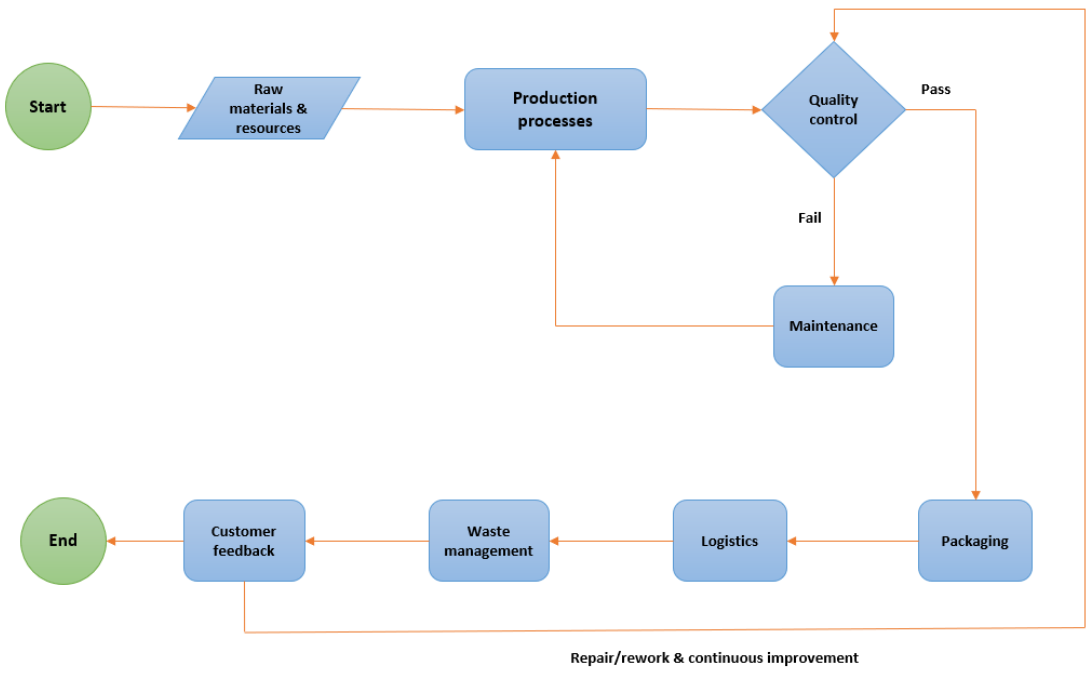

Fig. 1. Main industrial processes.

be mechanical, chemical, or physical. A typical industrial process from the start to the end serves as the foundation of a production and delivery. The need for a framework arose to visualize the steps. As in Fig. 1, The industrial processes mainly can be divided into 8 components: (1) Raw materials & resources input, (2) Production Stage, (3) Quality Control and Inspection stage, (4) Maintenance Stage, (5) Packaging Stage, (6) Logistics Stage, (7) Waste Management and (8) Customer Feedback Stages.

1.1. Raw Materials and Resources

The Input Stage serves as readying the necessary resources of the manufacturing process and bring them together. To start the whole process, raw materials are required to transform them into a product.

The importance of raw materials has been recognized long ago with the initial industrial process system [8]. The final product consists of which raw materials? Raw materials are basic materials that are required for production (e.g., plastics, metals, food ingredients, chemicals). Moreover, energy sources to power the manufacturing process should be collected (e.g., oil, gas, and electricity). A skilled workforce to ensure that the manufacturing process passes through successfully and manage equipment is needed. Moreover, to observe the production process from the beginning to the end requires equipment, which makes it possible to create the product.

1.2. Production Stage

After the completion of gathering the necessary resources for our production, production process must begin. It is the actual stage that converts resources gathered to an actual product. Nevertheless, this stage is the most comprehensive stage in the industrial process as a whole. The production environment should adhere to the relevant product's properties in the best possible way [9]. During the production phase, significant amounts of energy is consumed, which can lead to high costs and environmental issues. Transitioning to a renewable energy model will not only foster growth, but also cut costs and reduce environmental impacts drastically.

1.2.1. Design and Planning

During the design stage, the details of the main product that will be manufactured will be specified in this stage (e.g., materials that will be used, dimensions, functionality). Then, the Manufacturing Planning stage answers the question of, "how will this product be manufactured?" (e.g., the order of the equipment it will go through, equipment, and the specific time of the production) [10].

1.2.2. Acquisition and Resource Management

During the Acquisition stage, raw materials, product components, and resources from suppliers are purchased. [11]. Then, acquired products are managed to avoid any shortage or excess production during the Resource Management stage.

1.2.3. Processing

The Transporting Materials stage is when the raw materials are purchased from the supplier, they should be transferred to a place suitable to establish initiate production. They can be transported using automated systems or forklifts. Secondly, the Essential Processes stage involves the transformation of raw materials into shape parts by using basic machinery methods, such as molding, cutting, and forming them into essential parts for further shaping [12]. The Essential Processes stage provided with the basic shaping to further integrate the parts to form the product. Finally, in the Further Shaping step we apply further processes to the parts into their respective locations in the product.

1.2.4. Assembly and Advanced Production

In a typical industrial processes system, a challenge might occur when unexpected machinery

errors happen, which reduces efficiency and increases production time, which might have economic impacts as well. As a result, this reduces productivity and interferes with operations. In this stage, manual interference may be required to ensure errorless production due to complexity, which may result in inefficiency, errors, and slow production processes.

Combining parts before the main assembly or completing the products fully assembled and delivered to the Quality Control department occurs in the Pre-Assembly and Assembly Line process [13]. After that, last touches to the product using Essential Shaping or Further Shaping can be applied namely Automation Processes. Moreover, packaging the product is established and a non-stop production or batch production can be established. For example, if the product is cars and electronics, then batch production will be established as these products require high precision of manufacturing.

1.3. Quality Control

Quality Control checks are made to ensure the product meets industry standards. Checks such as reliability, durability, and longevity are tested. While examination or inspection are made to the parts of the product to detect any errors or non-compliant parts. Eventually, tests are carried out such as stress, safety, or durability tests are performed to ensure the quality of the product [14].

However, Quality Control checks might be challenging due to slow manual checks, resulting in diverse subjective product qualities. However, ensuring that the product meets industry standards and regulations is essential to ensure positive customer experience. If the product is detected to be defective, then it is sent to the maintenance department.

1.4. Maintenance and Machinery Checks

Preventive and predictive maintenance is applied to ensure that the manufacturing equipment runs smoothly and fully operational at all times. Also, to ensure that manufacturing machinery is fully operational by predicting failure moments using AI and IoT and scheduling regular periods for maintenance. Ultimately, a machine lifecycle method will track equipment status used in manufacturing to ensure they are replaced with new ones when required.

1.5. Packaging and Labeling

At this stage, automated packaging is involved for efficient shipment while the products are sealed and packaged to ready them for shipment. Meanwhile, unique identification numbers are assigned to products for tracking purposes which is known as labelling as well.

1.6. Logistics and Distribution

The distribution of products is an essential stage in the industrial processes system. Nevertheless, some challenges arise when arriving to this stage. For example, the lack of transparency in the warehousing process may result in fraud, lost shipments, and delays. This can affect logistics management greatly and hinder processes. There might be errors when managing products in the inventory, if poor management skills exist. This results in further costs and inefficiencies, so balancing in the inventory level is essential to ensure everything runs smoothly [15].

The process starts with manufactured products being sent to warehouses and awaited to be shipped to distributors or customers. Next, the products are loaded onto vehicles (e.g., trucks, cargo planes, ships) to be transported to their destinations. Moreover, the entire process from raw material acquisition to product delivery can be improved to ensure timely delivery and cost-effective logistical operations.

1.7. Waste Management and Recycling

A business model cannot thrive without sustainability. It is simply natural that industrial systems produce a considerable amount of waste, which can lead to environmental issues. Achieving waste reduction and recycling are essential for a sustainable business.

To reduce effort, it is essential to research novel methods and implement technologies that leads to significant waste reduction during the manufacturing process [16]. Commonly, the end of any manufacturing process will indeed have excess parts of raw materials that are not used. Recycling those materials will be beneficial to reuse them later in production. Nevertheless, not all materials will be recyclable. For this reason, we have to ensure that non-recyclable materials are disposed in an environmental-friendly way, ensuring compliance with regulations.

1.8. Customer Feedback and Assistance

After-sale, robust customer feedback involves with collecting feedback from customers about issues encountered, or if any improvements can be made to the product [17]. Also, warranties, maintenance services, and technical support offered to customers will be beneficial to ensure customer satisfaction. However, if a wide issue affecting a huge number of products are detected, then they are recalled back to maintain brand reputation.

Additional challenges such as data security and tracking are significant concerns regarding the whole industrial processing system, as industrial processes often require maintaining data integrity and security. Protecting manufacturing, product, and customer data is a must to maintain trust and credibility. Moreover, establishing partnerships and deals between the brand and different stakeholders can be challenging, as concerns arise for cyberattacks and data integrity. In conclusion, protecting data is a top priority for a brand to secure deals.

2. Optimization with Blockchain Technology

Blockchain was first introduced in 2008 by Satoshi Nakamoto, who developed the initial Bitcoin software and brought cryptocurrency to public attention. Unlike traditional systems managed by central authorities, such as central banks, Blockchain operates as a decentralized and distributed ledger technology (DLT) that eliminates the need for intermediaries in digital transactions. It is open-source and functions across a peer-to-peer network [18]. As in Fig. 2, Blockchain is a decentralized system where transactions are stored in interconnected, locked blocks. Blockchain's anonymity, security, and data integrity make it widely adopted across industries. It secures data using cryptographic hashes and consensus mechanisms, ensuring tamper-proof information [19]. Smart contracts play a crucial role in securing transactions, deciding whether to permit or trigger activities on the Blockchain. There are four types: public, private, consortium, and hybrid Blockchains. Key features include eliminating intermediaries to enhance speed and reduce costs, ensuring immutable and secure records, providing transparency for easy auditability, validating only legitimate transactions, preserving user anonymity, and allowing for smart contract creation through flexible programming.

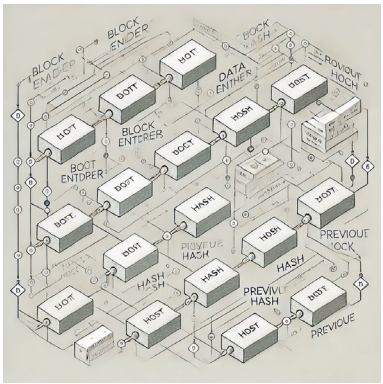

Fig. 2. A schematic representation of a Blockchain system illustrating the sequential linkage of blocks.

In the industrial domain, traditional methods of industrial processes are supported with traditional technologies to record data and facilitate production. However, Blockchain technology plays a significant role in optimizing industrial processes by providing transparency, efficiency, and security. Moreover, Blockchain technology is decentralized by nature, so no centralized authority can interfere with operations. The potential of Blockchain in transforming supply chain management is inevitable. It enables data security and assists with quality control (QC). According to [20], Blockchain technology has significant advantages, such as transparency and traceability, security and trust, immutable data, and smart contracts.

2.1. Supply Chain Transparency

Data on the ledger is immutable, meaning that everything recorded on the Blockchain is never subjected to change. Moreover, every transaction is recorded on the Blockchain, so data can be traced easily. For example, supply chain records such as product information and unique identification numbers securely. This provides benefits such as reduction in delays and improves legitimacy. The traditional process of sending requests of the customer side to the supplier is time-consuming [21].

2.2. Data Security

Blockchain's architecture is designed to ensure data security. Cryptographic keys and protocols such as smart contracts ensure that no one can access any data. The industrial processing system includes numerous sensitive data, such as product information, manufacturing processing parameters, machinery information, and distribution information. Also, Blockchain's architecture ensures that data is protected robustly, which greatly reduces the chances of cyberattacks. For instance, it is reported that hackers have to allocate at least 50% of their computing resources to break a Proof-of-Work consensus mechanism powered Blockchain [22]. Nevertheless, it is also important to note that a system regarding optimizing industrial processes should be secured with a secure technology, and Blockchain is the only and best choice to achieve it.

2.3. Smart Contracts

Smart contracts build on the trust and security of Blockchain. Those contracts are basically computer programs that function under the Blockchain [23]. They enable the execution of operations smoothly on the Blockchain, preventing unauthorized action. They automate processes, such as on-chain payments, delivery verification, or checks regarding compliance without third-party intermediaries. Smart contracts are an optimal way to reduce costs and speed up operations.

2.4. Asset Optimization & Partnerships

Another key topic regarding industrial processing systems is "Asset Management." Blockchain technology tracks data in real-time throughout the whole production process. Whenever a new production cycle is initialized, Blockchain will record manufacturing data. This will ensure that information is up-to-date and accurate. Moreover, we predict that the use of Blockchain will greatly reduce errors and costs. Since data recorded in the ledger is immutable, any partnerships established with the brand will establish a strong sense of trust and collaboration. The Blockchain will serve as a proof of verified information.

2.5. Quality Control (QC) & Regulatory Compliance

Product details are recorded under the Blockchain, and the industrial process system aims for improving the quality of the products as well. From the beginning to the end of the process, Blockchain technology records all the data. Indeed, this will establish a guarantee that the product will adhere to industry standards. If any defects found on the product, data recorded in the Blockchain will assist with the solution of the issue. Quality Control (QC) with Blockchain

will greatly optimize the quality of products. Blockchain contains every necessary data that is needed to be ready for regulatory compliance. For instance, if the brand's factory were to be subjected to audits, then we expect that the process would be carried out smoothly because data can be validated. Counterfeit products are rising in popularity in today's world. To prevent fake products to succeed, assigning a unique identification number is of extreme significance. In maintenance processes, Blockchain provides a record of past repairs, product adjustments, machinery optimization, and maintenance schedules.

2.6. Automation & Sustainability

Our main purpose with Blockchain integration is to achieve automation. With Blockchain, we do not need any administration unit within the factory to pull out records. Smart contracts are the main framework within Blockchain to automate processes, so they handle operations without a need of workforce. Sustainable business practices and compliance will be handled transparently with Blockchain technology, and it will ensure that environmental hazard is at the lowest possible. On the other hand, logistics and shipment details can be tracked via data recorded in the Blockchain, which reduces probability of mismanaging supply.

2.7. IoT and Blockchain

The combination of IoT with Blockchain offers real-time data transaction between interconnected devices. Data can be about machines, environmental conditions, and sensor readings. Also, critical data regarding system status can be observed at all times. In case of system errors, the issue can be swiftly found and resolved. A Blockchain-powered industrial Internet of Things (IoT) framework has been proposed in [24], named "ManuChain." A manufacturing permissioned Blockchain that stores data, and a custom consensus mechanism is proposed to synchronize data.

3. Optimization with Artificial Intelligence

Artificial Intelligence (AI), first proposed as a concept by John McCarthy in 1956, has evolved significantly, moving towards full system automation that enhances efficiency across sectors such as corporations, government agencies, and businesses. AI systems mimic human intelligence by comprehending, learning from experience, reasoning, and solving problems. AI's unique advantages include performing multiple tasks faster, simultaneously, and with fewer errors [25]. Modern AI, which adapts with insufficient knowledge and resources [26], has led to advancements like machine learning (ML)—a critical subset of AI that uses algorithms and vast datasets to improve its predictive and decision-making capabilities. As illustrated in Table 1, ML approaches are divided into supervised, unsupervised, semi-supervised, and reinforcement learning [27], with applications in areas such as natural language processing, computer vision, and information retrieval. In the energy sector, AI's integration with Blockchain supports demand-side management and fully autonomous energy systems [28], while an IoT platform enhances AI's ability to manage smart devices and streamline industrial management processes.

TABLE I
OVERVIEW OF MACHINE LEARNING APPROACHES AND THEIR DESCRIPTIONS

Type of Learning	Description
Supervised Learning	Learns from labeled data with input-output pairs.
Unsupervised Learning	Identifies patterns in unlabeled data.
Semi-Supervised Learning	Combines labeled and unlabeled data.
Reinforcement Learning	Learns through rewards and actions in an environment.

3.1. Predictive Maintenance

Machine failures are common mishappens in industrial processes. Thus, intelligently predicting the time of machinery failures is what AI will achieve. For this, the AI intelligently captures past usage and detects failures by analyzing real-time data as well. This improves performance of machinery and reduces downtimes, thus eliminating repair costs and time waste.

3.2. Automation & Supply Chain Optimization

Real time control powered by machine learning applications can ensure that manufacturing machines process smoothly [29]. AI improves as production cycle continues; repetitive tasks become easier and faster to handle, eliminating human workers for complex tasks. In conclusion, automating processes increases overall productivity by ensuring repetitive tasks can be handled by AI. For instance, supply chain issues arise when management wrongly predicts processes. However, AI enhances processes by optimizing demand, supply, asset management, and power up supply chains. Moreover, AI can forecast potential disruptions that might occur during production process, and it builds the chain to be stronger by incorporating data. In [30], the authors offer a recent system that has been integrated across different industries: RFID technology establishes identification of IoT devices with Auto-ID, which creates an efficient system to track manufacturing processes.

3.3. Quality Control & Sustainability

Quality control is a common aspect in both Blockchain and AI. Thus, AI can monitor production lines during the manufacturing process and detect defects, if away from quality standards. AI contribution ensures that the product is delivered errorless and in a sustainable way. In modern industrial processes, achieving energy efficiency has become a real goal for corporations and factories across the globe. Integrating renewable energy models to production lines will enhance energy efficiency. Adjusting settings of energy consumption in real-time leads to reduction in energy costs and push sustainability goals forward by minimizing waste. Sustainability has been one of the common goals for both AI and Blockchain. Thus, if manufacturing processes are completed with high precision and consistency, sustainable production practices are implemented. As a result, hazardous waste and non-environmentally friendly materials can be eliminated as much as possible.

3.4. Demand Forecasting

Moreover, process optimization has become a need for overall production throughputs. As a result, making use of big data, integrating information technologies, and develop a unique product to meet the standards of intelligent manufacturing by integrating AI has become a goal [31]. AI intelligently identifies manufacturing inefficiencies and suggests real-time corrections. Optimizing throughput, reduce and increase overall efficiency in production cycles, and enhance operational performance are the tasks AI will tune by referencing to insights. A brand does not need to produce more than it is required, based on market demand. AI intelligently analyzes market trends and commands production line to manufacture based on demand. If a product is not trending or selling high figures, cutting overproduction would be a solution. In the end, AI will decide the production rate of the products. Moreover, generated analytics by AI can help identify patterns and anomalies for decision-makers. Also, AI will be a key role player in producing different variations of the product, by integration in production line.

3.5. Enhanced Safety

AI-powered equipment can perform complex shaping tasks such as welding, painting, and assembly with high precision, eliminating human error and enabling full automation. Safety in the factory and human workers is a top priority when integrating AI in industrial processes. Predicting dangers and hazardous happenings within the production line or factory will save lives and eliminates life-threatening dangers. Also, assigning unique IDs for workers within

the factory and tracking work fatigue can reduce the risk of accidents drastically.

In conclusion, Blockchain, AI, and IoT unifies the whole industrial processing system by optimizing the whole production process. Authors in [32] proposed a system model that combines Blockchain, IoT, and Artificial Intelligence in the food industry.

III. PROPOSED CONCEPTUAL FRAMEWORK

Optimizing the industrial processes is a key part of the strategy followed by industries to increase the efficacy of their operations, and the quality of the products, and be competitive in a fast-changing marketplace. AI and Blockchain technologies can jointly make ordering raw materials and delivering final goods leading to a new experience for manufacturing companies. Dissolving differences through strategic technology combination as a means of enhancing the operational efficiency of industrial processes, among others, is what we need to explore. With the integration of these technologies, the use of AI optimization techniques, and the speed earned from the low latency characteristic of Blockchain technologies, collaboration within the industry is likely to be much improved. Identifying new data-related economies will also be part of this because of the soaring capacity of the digital era to store information in a multitude of ways. As in Fig. 3, a conceptual framework for integrating AI and Blockchain with the industrial process for the purpose of optimizing the main industrial processes is proposed and explained in detail.

1. Raw Materials and Resources

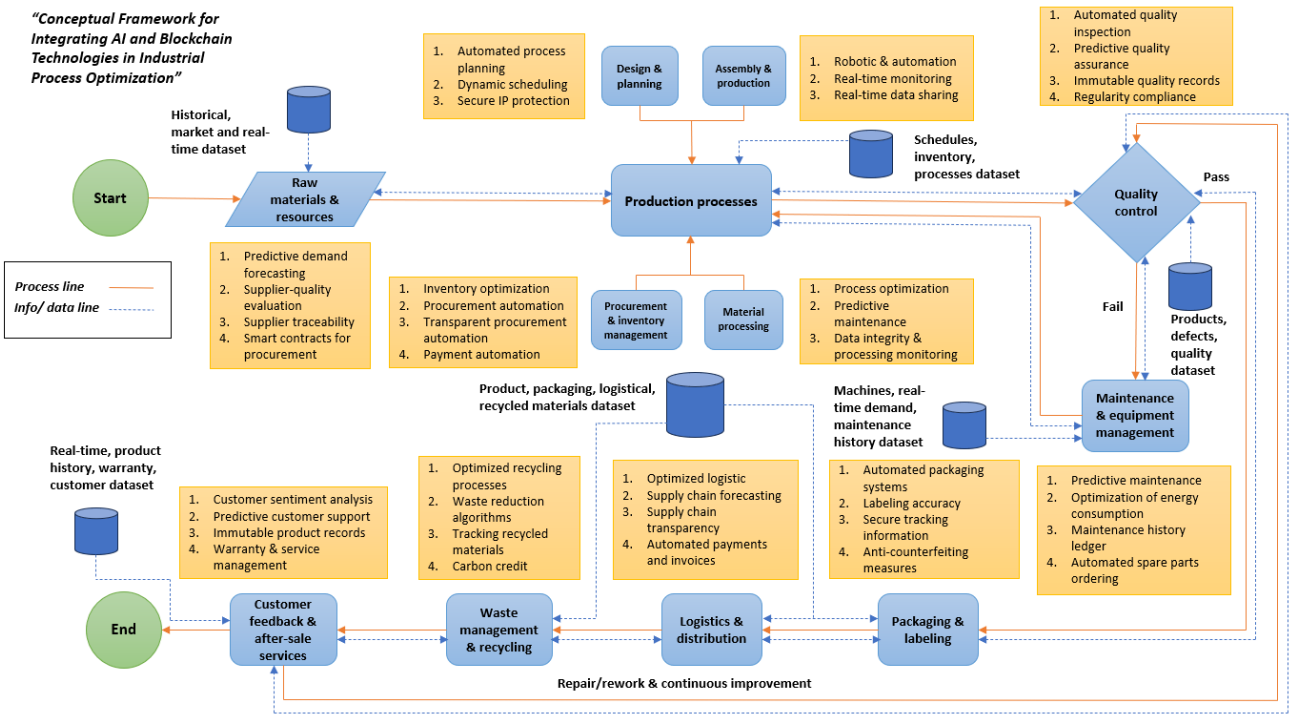

It starts from optimizing raw material management where AI helps through forecasting for predictive demand using methods like regression and Time Series. Factoring in historical sales data, businesses can adjust procurement to synchronize better with market conditions, potentially reducing overstocks and the cost associated. The benefit of Blockchain is that traceability is built into Distributed Ledger Technology (DLT), which has the potential to securely track material origins and accountability throughout a supply chain. Smart contracts also automate procurement through delivery or fulfillment confirmations which partitions the manual mode, offers efficiency and allows strengthened supplier relationships as a result. With

a centralized data repository, the analysis is done in real-time (less latency) and decision-making can be more realistic.

2. *Production Stage*

However, once we have raw materials locked in, the next question turns to how to make best of these materials. The use of AI-driven algorithms like genetic algorithms and linear programming allows for the optimization in production schedules dictated by real-time information ensuring machine availability, workforce capabilities, and possible constraints as scrutiny points to these optimized schedules. This makes things faster and removes bottlenecks. At the same time, Blockchain protects production data by providing an unalterable record and creating genuinely transparent data that meets international standards. When together, they provide a single version of the reliable production by using a central data repository that stores both AI insights and Blockchain records.

3. *Quality Control (QC)*

During production, quality control is very important, and using AI, this process can be automated by the exploitation of machine learning techniques, like computer vision and anomaly detection. With AI, we can increase the accuracy of defect detection by analyzing product images in real time and therefore reduce human error. The Blockchain inspects and verifies the data history data and boost security through decentralized ledger records. AI can forecast future quality errors, and Blockchain ensures the transparency and compliance that will improve trust in processes for consumers and regulators alike.

4. *Maintenance and Machinery Checks*

The AI-driven predictive maintenance cuts the downtime by analyzing performance data for predicting future equipment failure, hence enabling timely intervention. It does so by considerably reducing unplanned outages and enhancing efficiency in operations. This is further enhanced by Blockchain, safely recording history of maintenance, hence providing a transparent record of all maintenance activities. Each one thus complements the other: AI and Blockchain together provide full insight into machinery health and hence optimize maintenance management via predictive insights and by reliably keeping track of the maintenance schedules.

5. *Procurement and Inventory Management*

The use of demand forecasting models, such as moving averages and exponential smoothing in procurement and inventory management, allows AI to optimize inventory levels in such a way that material availability is assured at all times while holding costs are minimized. Machine learning dynamically rebalances inventory positions based on historical sales. This gets even more efficient with Blockchain, which makes procurement transactions secure and automated upon the confirmation of delivery, reducing fraud and building trust between parties. The data repository makes the AI forecast and the Blockchain locks the transactions, hence offering both efficiency and transparency in the supply chain.

6. *Material Processing*

Material processing is done with the goal of optimizing resource utilization, while AI algorithms analyze production data for energy consumption and waste reduction, meeting sustainability goals. AI further optimizes resource allocation and monitors quality processes to meet regulatory compliance. Meanwhile, Blockchain provides a fitting complement to such steps by tracking material handling for greater accountability and measuring variables for quality inconsistencies. A data repository reinforces the actionable insights of AI and the secure record of all material transactions in the Blockchain.

7. *Packaging and Labeling: Compliance and Efficiency*

As products near the packaging stage, AI-driven systems optimize packaging designs to

reduce waste and ensure safety, while also improving labeling accuracy and keeping up with regulatory changes. Blockchain secures labeling information, preventing counterfeiting and ensuring product authenticity. A data repository combines AI's analysis with Blockchain's secure record-keeping, ensuring compliance and efficiency throughout the packaging process.

8. Logistics and Distribution

Finally, after packaging, the products go into logistics and distribution, where AI-driven forecasting tools analyze demand from historical data, while delivery routes are optimized to reduce transportation costs. The AI algorithms adjust routes in real time according to the flow of traffic. The aim is the minimal consumption of fuel with further enhancement in the efficiency of deliveries. Blockchain provides the basis for transparency in the supply chain since all the stakeholders will, in real time, have insight into product movement and status. This is going to build trust and will help in resolving very key issues related to transaction costs and imbalance of information. It is also about the data repository, which has a very critical role in integrating AI analytics into Blockchain records for the delivery of accurate and timely information to all participants.

9. Customer Feedback and After-Sale Services: Building Relationships

The journey of optimization ends by accruing and analyzing customer feedback and after-sales service. AI conducts a sentiment analysis of the feedback from each touchpoint, enabling them to enhancing their products based on customers' insights. Blockchain secures the product record and warranty claims for completeness with full transparency and trust. Therefore, this allows the integration of feedback and warranty data by AI to spot trends and patterns, allowing for better service delivery and realizing consumer verification of authenticity and quality of products to enhance brand loyalty.

10. Waste Management and Recycling

Sustainability is an important issue in industrial processes. AI creates the opportunity to reduce waste by analyzing production data and presents more efficient ways of production with less environmental impact. Blockchain follows the materials that are being recycled and creates incentives for collecting waste. It therefore fosters accountability and traceability in the recycling processes. All these put together make transparent recycling programs possible and drive AI business strategy that centers on waste reduction.

IV. CONCLUSION

Artificial Intelligence integrated with Blockchain technology simply refurbishes industrial processes, speaking volumes about the realization of operational excellence and optimization in making operations efficient, more transparent, and sustainable, especially in the competitive environment that exists today. This is achieved through AI's capability to optimize decision-making and streamline processes while Blockchain will ensure data integrity by addressing fragmented data pieces and operational inefficiencies. In this respect, the proposed conceptual framework brings forth the contribution of predictive analytics and machine learning coming from AI for the betterment of raw material management, smoothing of production schedules, and automation of quality control toward high-quality products with operational efficiency. Furthermore, research in these areas should be continuous to see their fuller realization while enhancing ease regarding compliance issues with regulatory matters and more cooperation among partners and stakeholders across the supply chain. From predictive maintenance to procurement and inventory management, AI and Blockchain are in synergy, with AI-driven models further supported by secure, decentralized ledgers for better decision-making and resource utilization. The integration further emphasizes sustainability through the reduction of wastes from AI waste strategies and traceability through Blockchain that facilitates accountability and innovation in recycling practices. This eventually may lead to opportunities

for smart, innovative and optimal industrial processes, where most industries, after transforming various challenges into growth opportunities, will be encouraged in further process development.

REFERENCES

[1] L. S. Dalenogare, G. B. Benitez, N. F. Ayala, A. G. Frank, "The expected contribution of Industry 4.0 technologies for industrial performance," International Journal of production economics, ELSEVIER, 204, pp. 383-394, 2018.
[2] K. Salah, M. H. U. Rehman, N. Nizamuddin, and A. AlFuqaha, "Blockchain for AI: Review and Open Research Challenges," IEEE Access, 7th ed., pp. 10127–10149, 2019.
[3] S. C. C. Flores, A. A. R. Punzo, F. N. Rivera, "Applications of Multi-Objective Optimization to Industrial Processes: A Literature Review," Processes, 10th ed., vol. 1, pp. 133, 2022.
[4] L. Braccesi, M. Monsignori, P. Nesi, "Monitoring and Optimizing Industrial Production Processes," IEEE International Conference on Engineering of Complex Computer Systems, IEEE, 213-222, 2004.
[5] National Association of Manufacturers, (2020), "U.S. Manufacturing Competitiveness Report," National Association of Manufacturers.
[6] A. A. Khan, A. A, Laghari, M. A. Dootio, S. Karim, "The Collaborative Role of Blockchain, Artificial Intelligence, And Industrial Internet of Things in Digitalization of Small and Medium-Size Enterprises," Scientific Reports, 13th ed., vol. 1, pp. 1656, 2023.
[7] M. Soori, R. Dastres, B. Arezoo, "AI-Powered Blockchain Technology in Industry 4.0, A Review," Journal of Economy and Technology, ScienceDirect, 1st ed., pp. 222-241, 2023.
[8] E. A. Wrigley, "The Supply of Raw Materials in The Industrial Revolution. In The Causes of The Industrial Revolution," Routledge, pp. 97-120, 2017.
[9] S. Erkman, "Industrial Ecology: A New Perspective on the Future of the Industrial System," Swiss Medical Weekly, pp. 531-538, 2001.
[10] Y.-M. Deng, K. L. Edwards, "The Role of Materials Identification and Selection in Engineering Design," Materials & Design, ELSEVIER, 28(1), pp. 131-139, 2007.
[11] M. Sulgan, J. Sosedova, "Procurement of Materials and Components for Manufacturing Activity," ReseachGate, 16th ed., vol. 2, pp. 58-62, 2014.
[12] G. Ingarao, "Manufacturing Strategies for Efficiency in Energy and Resources Use: The Role of Metal Shaping Processes," Journal of Cleaner Production, 142nd ed., vol. 4, pp. 2872-2886, 2017.
[13] B. Micieta, P. Macek, V. Binasova, L. Dulina, M. Gaso, J. Zuzik, "Modular Intelligent Control System in the Pre-Assembly Stage," Electronics, MDPI, 13th, vol. 9, pp. 1609, 2024.
[14] M. S. N. Zadeh, F. Shoushtari, M. Talebi, "Optimization of Analytical Methods in Industrial Engineering: Enhancing Decision-Making in Process Design and Quality Control," International Journal of Industrial Engineering and Construction Management, 2(1), 2024.
[15] G. E. A. Gunasekaran, K-L, Choy, "Industrial Logistics Systems: Theory and Applications," International Journal of Production Research, 50, pp. 2377-2379, 2011.
[16] D. Li, M-Q. Wang, C. Lee, "The Waste Treatment and Recycling Efficiency of Industrial Waste Processing Based on Two-Stage Data Envelopment Analysis with Undesirable Inputs", International Journal of Production Research, pp. 242, 2020.
[17] E. Vaittinen, M. Martinsuo, "Industrial Customers' Organizational Readiness for New Advanced Services," International Journal of Production Research, 30th ed., vol. 7, 2019.
[18] S. Nakamoto, Bitcoin, A Peer-To-Peer Electronic Cash System, 2008. [Online]. Available: https://bitcoin.org/bitcoin.pdf32. N. Ramadani, E. Ramadani, F. Idrizi, V.

Misimi, "Blockchain: general overview of the Architecture, Security and Reliability". Journal of Natural Sciences and Mathematics of UT, vol. 3, No. 5-6, 2018.

[19] Z. Zheng, S. Xie, H. Dai, X. Chen, H. Wang, "Blockchain Challenges and Opportunities: A Survey," International Journal of Web and Grid Services, 14th ed., pp. 352-375, 2018.

[20] T. K. Vashishth, V. Sharma, K. K. Sharma, B. Kumar, S. Chaudhary, R. Panwar, "Intelligent Resource Allocation and Optimization for Industrial Robotics Using AI And Blockchain," AI and Blockchain Applications in Industrial Robotics, IGI Global, pp. 82-110, 2024.

[21] H. Yetis, M. Karakose, N. Baygin, "Blockchain-Based Mass Customization Framework Using Optimized Production Management for Industry 4.0 Applications," Engineering Science and Technology, an International Journal, 36th ed., 2022.

[22] B. Cao, X. Wang, W. Zhang, H. Song, Z. Lv, "A Many-Objective Optimization Model of Industrial Internet of Things Based on Private Blockchain," IEEE Network, 34th ed., vol. 5, pp. 78-83, 2020.

[23] G. Azhar, M. Ashar, W. Azeem, U. Farooq, "Enhanced and Optimized Industrial Processes Management Using Machine Learning (Ml) and Blockchain," Pakistan Journal of Scientific Research, 4th ed., vol. 1, pp. 27-39, 2024.

[24] J. Leng, et al., "Manuchain: Combining Permissioned Blockchain with A Holistic Optimization Model as Bi-Level Intelligence for Smart Manufacturing," IEEE Transactions on Systems, Man, and Cybernetics: Systems, 50th ed., vol. 1, pp. 182-192, 2019.

[25] C. Khanzode, R. Sarode, "Advantages and Disadvantages of Artificial Intelligence and Machine Learning: A Literature Review," International Journal of Library & Information Science (IJLIS), 9th ed., vol. 1, 2020.

[26] D. Monett, C. Lewis, K. Thorisson, "On Defining Artificial Intelligence," Journal of Artificial General Intelligence, 10th ed., vol. 2, pp. 1-37, 2019.

[27] M. Kang, N. Jameson, "Machine learning Fundamentals," Prognostics and health management in electronics: Fundamentals, Machine Learning, and Internet of Things, Willey Online Library, 2018.

[28] H. R. Rocha, I. H. Honorato, R. Fiorotti, W. C. Celeste, L. J. Silvestre, & J. A. Silva, "An Artificial Intelligence Based Scheduling Algorithm for Demand-Side Energy Management in Smart Homes," Applied Energy, 282, 116145, 2021.

[29] E. Carpanzano, D. Knüttel, "Advances in Artificial Intelligence Methods Applications in Industrial Control Systems: Towards Cognitive Self-Optimizing Manufacturing Systems," Applied Sciences, 12nd ed., vol. 21, 10962, 2022.

[30] A. Azizi, "Introducing A Novel Hybrid Artificial Intelligence Algorithm to Optimize Network of Industrial Applications in Modern Manufacturing," Complexity, 1, 2017.

[31] T. Yang, X. Yi, S. Lu, K. H. Johansson, T. Chai, T, "Intelligent Manufacturing for The Process Industry Driven by Industrial Artificial Intelligence," Engineering, 7th ed., vol. 9, pp. 1224-1230, 2021.

[32] P. W. Khan, Y. C. Byun, N. Park, "IoT-Blockchain Enabled Optimized Provenance System for Food Industry 4.0 Using Advanced Deep Learning," Sensors, 20th, vol. 10, 2020

Yüksek Sıcaklık Faktörünün Karbon Lif Katkılı Çimentolu Harçların Mekanik Özellikleri Üzerine Etkisi

Alim Berk Çağlayan[1], Murat Özturk[1]

*acaglayan@uludag.edu.tr, ORCID: 0000-0002-9131-4595
[1]*Bursa Uludağ Üniversitesi, Mühendislik Fakültesi, Bursa, Türkiye*

Özet Teknolojik gelişmeler ve artan insan ihtiyaçları, yapı malzemelerinin yalnızca temel işlevlerini yerine getirmekle kalmayıp, çok sayıda ek görev üstlenmesini zorunlu kılmaktadır. Geleneksel çimentolu kompozitlerin bu taleplere yanıt verememesi, alternatif malzemelere yönelimi hızlandırmıştır. Karbon lifler, çimentolu kompozitlere eklenerek elektriksel iletkenlik, mekanik dayanıklılık gibi özelliklerin iyileştirilmesini sağlamakta, bu sayede yapısal sağlık izleme gibi akıllı malzeme uygulamalarını mümkün kılmaktadır. Akıllı özellik performanslarının yanında, oluşturulan karbon lif takviyeli çimentolu karışımların, mekanik dayanım ve durabilite özelliklerinin ortaya konulması, söz konusu kompozitlerin pratik uygulamalara konu olabilmesi için önem arz etmektedir. Yüksek sıcaklık geleneksel betonda iç yapısal bozulmalara yol açarken, mekanik dayanımında azalmalara yol açmaktadır. Karbon lif takviyesinin, çimentolu kompozitlerin yüksek sıcaklık direncini arttıracağı düşünülmektedir. Bu çalışma kapsamında 3 farklı boyda (5 mm, 10 mm, 15 mm) kesikli karbon lif katkılı çimentolu harçlardan oluşan 40mmx40mmx160mm boyutlarındaki prizma numuneler, 28 günlük olgunluğa eriştiklerinde, maksimum sıcaklığı 600°C ve 800°C olan 2 farklı sıcaklık prosedürüne tabii tutulmuştur. Sıcaklık prosedürlerinin ardından prizma numuneler üzerinde 0.05 mm/s yükleme hızında 3 noktalı eğilme testi gerçekleştirilmiştir. Deneylerin sonucunda numunelere ait ortaya çıkan kırılma yükleri, kırılma durumundaki deplasmanlar, kırılma enerjileri ve eğilmede çekme dayanımları kıyaslanmıştır. Ayrıca, prizmalardan 3 noktalı eğilme deneyi sonunda ortaya çıkan kalıntı parçalar üzerinden harç basınç dayanımları belirlenmiştir. Sonuç olarak, çimentolu harçlara karbon lif takviye edilmesi durumunda yüksek sıcaklık durumunda eğilmede çekme dayanımının ve kırılma enerjisinin arttığı belirlenmiştir. Ayrıca, karışımda yer alan lif boyu 5 mm olan numunelerin, gözlenen mekanik özelliklerinin, hem sıcaklık prosedürü uygulandığında, hem de uygulanmadığı durumlarda diğer boylara göre daha yüksek olduğu belirlenmiştir. Buna paralel olarak, kesikli karbon lif boyunda yaşanan artışın, mekanik özellikleri olumsuz etkilediği sonucuna varılmıştır. Buna ek olarak yüksek sıcaklığa maruz kalan lifsiz harçlarda ortalama basınç dayanımında 600°C için %50, 800°C için ise %61 azalma gözlenmiştir.

Anahtar Kelimeler: *Yüksek Sıcaklık, Karbon Lif Katkılı Harç, Lif Boyu, Çimentolu Kompozitler*

Abstract Technological advancements and growing human needs necessitate that construction materials not only fulfill their basic functions but also undertake numerous additional tasks. The inability of traditional cement-based composites to meet these demands has accelerated the shift toward alternative materials. Carbon fibers, when added to cement-based composites, enhance properties such as electrical conductivity and mechanical durability, thereby enabling smart material applications like structural health monitoring. In addition to their smart applications characteristics, it is crucial to establish the mechanical strength and durability properties of the carbon fiber-reinforced cementitious mixtures for their practical applications.

High temperatures lead to internal structural degradation in traditional concrete, resulting in reductions in mechanical strength. It is hypothesized that carbon fiber reinforcement will increase the high-temperature resistance of cement-based composites. In this study, prismatic samples measuring 40mmx40mmx160mm, composed of cementitious mortars reinforced with three different lengths of discontinuous carbon fibers (5 mm, 10 mm, and 15 mm), were subjected to two different temperature procedures with maximum temperatures of 600°C and 800°C after achieving 28 days of curing. Following these temperature procedures, three-point bending tests were conducted on the prism samples at a loading rate of 0.05 mm/s. The results of the experiments were compared in terms of the fracture loads, displacements at failure, fracture energies, and tensile strengths in bending. Additionally, the compressive strengths of the mortars were determined from the residual fragments after the three-point bending tests. The results indicated that reinforcing cementitious mortars with carbon fibers leads to an increase in both tensile strength in bending and fracture energy under high-temperature conditions. Furthermore, it was found that the samples containing 5 mm long fibers exhibited higher mechanical resistance compared to other lengths, regardless of whether the temperature procedure was applied. Conversely, an increase in the length of the discontinuous carbon fibers was found to negatively affect the mechanical properties. Additionally, fiber free mortars exposed to high temperatures showed an average compressive strength reduction of 50% at 600°C and 61% at 800°C.

Keywords: *High Temperatura, Carbon Fiber Reinforced Mortar, Fiber Length, Cement-Based Composites*

I. GİRİŞ

Teknolojik ilerlemeye paralel olarak artan insan ihtiyaçlarının karşılanmasında, beşeri unsurların ana işlevlerinin yanında, farklı görevleri de yerine getirebilmesi beklenmektedir. Örneğin, taşıtlar, ilk ortaya çıktıklarında, yalnızca ulaştırma görevini yerine getirebilirken, günümüzde kullanılan taşıtlardan ulaştırma işlevini konforlu, güvenli, hızlı, minimum yakıt tüketimiyle seyahat edebilme gibi beklentiler bulunmaktadır. Geleneksel işlevi üzerine gelen yükleri ve çevresel etkileri servis ömrü boyunca güvenle karşılamak olan betonun, güncel teknolojik ilerleme hızına direnerek yalnızca ana işlevini yerine getiren bir malzeme olarak varlığını sürdürmesinin mümkün olmadığı düşünülmektedir. Bunun yanında, hâlihazırda çok-fonksiyonlu özelliklere sahip betonlar ve çimentolu malzemeler çeşitli araştırmalara ve uygulamalara konu olmaktadır.

Çimentolu kompozitlere çok-fonksiyonluluk özelliği kazandırılması, genellikle içerisine katılan çeşitli malzemeler ile elde edilmektedir. Örneğin, çimentolu kompozitler içerisine iletken liflerin katılması ile birlikte, kompozite elektriksel iletkenlik özelliği kazandırılabilmektedir. Kompozite elektriksel iletkenlik özelliği kazandırılmasıyla birlikte, yapı sağlığının izlenmesi, anlık gerilme, genleme, hasar durumunun tespiti, sıcaklık seviyesinin izlenmesi gibi akıllı malzeme uygulamaları gerçekleştirilebilmektedir. Çimentolu kompozitlere elektriksel iletkenlik özelliği kazandırılabilmesi için çelik, karbon, pirinç lif gibi malzemeler tercih edilmektedir. Bu malzemeler arasında karbon liflerin korozif direncinin, ağırlık/dayanım oranlarının, iletken ağ geliştirme etkinliğinin yüksek olması, karbon lifleri çimentolu kompozitlerde akıllı uygulamalar için bir adım öne çıkarmaktadır.

Kesikli karbon lif katkılı çimentolu kompozitler üzerine çalışmaların başlangıcı, 1990'lı yılların ortalarına dayanmaktadır. Birçok malzemeye kıyasla mekanik özelliklerinde üstünlükler bulunan karbon liflerin farklı sektörlere yayılması ile birlikte, malzeme inşaat mühendisliği uygulamalarına da konu olmuştur.

Kesikli karbon liflerin hacimce belirli miktarlarda çimentolu kompozitlerde yer alması durumunda, oluşturulan kompozitin çeşitli mekanik ve termal özelliklerinin görüntülenebilmesi mümkün olmaktadır [1]. Bu durum sensör, veri kayıt cihazı gibi herhangi

bir ataşmana ihtiyaç duyulmadan, elemanın kendi bünyesindeki elektriksel iletkenlik ve piezo-resistif potansiyelinin kullanılmasıyla, hasar tespiti, gerilme durumunun belirlenmesi gibi işlemlere olanak tanımaktadır. Ayrıca ataşman ihtiyacının eksiltilmesi ile birlikte, yapısal elemanlara gömülü halde bulunan bu ataşmanların oluşturacağı ilkel kusurların önüne geçilebilmektedir. Bunlara ek olarak çimentolu kompozitlerde karbon lif kullanımı durumunda kompozitin katodik korozif direncinin artmasıyla birlikte, kompozit içerisinde yer alabilecek çelik donatıların korozif direncine olumlu etkilerinin olduğu da ortaya konulmuştur [2], [3], [4].

Akıllı uygulamalara ek olarak, elektriksel iletkenliğin arttırılmasıyla birlikte, çimentolu kompozitlerin elektromanyetik dalga soğurma performansı da artmaktadır. Kesikli karbon lifler, çimentolu kompozitlere, elektromanyetik dalga soğurma performansının iyileştirilmesi amacıyla da katılabilmektedir [5], [6], [7].

Karbon liflerin oldukça yüksek dayanım/ağırlık oranına sahip olması, yüksek çekme mukavemetleri gibi avantajları sebebiyle, çimentolu kompozitler içerisinde doğrudan mekanik özellikleri iyileştirmeye yönelik çalışmalar da mevcuttur [8], [9], [10], [11]. Bu çalışmalardan elde edilen sonuçlar göz önünde bulundurulduğunda karbon lif katkısının, kompozitlerin eğilmede çekme dayanımını iyileştirdiği, basınç dayanımına gözle görülür bir olumlu etki yapmadığı söylenebilmektedir. Eğilmede çekme dayanımındaki iyileşmeler, liflerin çatlak yakalama potansiyeli ve çatlak gelişiminin önüne geçmesine dayandırılmaktadır.

Karbon lif katkılı çimentolu kompozitlerin durabilite özelliklerinin araştırıldığı çalışmalar sınırlı da olsa mevcuttur. Çimentolu kompozitlerde karbon lif katkısının kuruma büzülmesi davranışı, kompozitin su emme kapasitesi ve porozite üzerine etkileri, tartışılmıştır [12], [13].

Çimentolu kompozitlerin yüksek sıcaklığa maruz kalması durumunda bünyelerinde gelişen makro ve mikro boyutlu termal çatlakların, kompozit dayanımını büyük ölçüde etkilediği bilinmektedir [14]. Bu durum büyük ölçüde çimentolu kompozitleri oluşturan bileşenlerin termal genleşmeleri arasındaki farklılıktan kaynaklanan malzeme bünyesindeki mekanik çözülmelerden ileri gelmektedir. Bu durum literatürde termal uyumsuzluk olarak adlandırılmaktadır. Bu durumun sonucunda kompozit bünyesindeki çimento fazında çeşitli boyutlarda çatlaklar gelişir. Karbon lif katkılı çimentolu kompozitlerin termal etkiler sonrasında mekanik performansını inceleyen çalışmalar mevcuttur.

Drchalová vd. Tarafından gerçekleştirilen çalışmada, PAN (Poliakrilonitril) tipi ve Zift bazlı karbon lif katkılı çimentolu kompozitler, 3 farklı yüksek sıcaklık prosedürüne maruz bırakılmış, ardından doğrudan çekme dayanımları ve porozite özellikleri araştırılmıştır. Ancak bu çalışmada numuneler doğrudan hedef sıcaklığa getirilen fırınlar içerisine ya da ön-ısıtma işlemi uygulanıp bırakılmıştır. Ön-ısıtma işleminin seviyesine dair bir bilgiye çalışmada rastlanmamış olup yazarlar tarafından ön-ısıtmanın işleminin, mekanik özellikleri etkileyen en önemli parametre olduğu düşünülmektedir [15].

Çavdar tarafından gerçekleştirilen çalışmada farklı tipteki lifler içeren çimentolu kompozitlerin yüksek sıcaklık maruziyeti ardından mekanik dayanımları araştırılıp, mikro-yapılarında gelişen kimyasal reaksiyonlar incelenmiştir. Farklı hacimsel içeriklerde karbon lif kullanılarak numuneler kıyaslanmıştır [16].

Gerçekleştirilen çalışma kapsamında farklı boylarda (5 mm -10 mm – 15 mm) kesikli karbon lif içeren çimentolu harçların, 3 farklı sıcaklık prosedürüne maruz kalmasının ardından işlenebilirlik ve mekanik özellikleri araştırılıp elde edilen sonuçlar ortaya konulmuştur.

II. MATERYAL

Bu çalışma kapsamında karbon lif takviyeli 5 farklı özelliğe sahip çimentolu harç karışımdan oluşan prizma numuneler, Maksimum sıcaklığı 600°C ve 800°C olan 2 farklı sıcaklık prosedürüne tabii tutulup, ardından 3 noktalı eğilme testi ile, kırılma yükü, kırılma anındaki maksimum deplasmanı, kırılma enerjisi, eğilmede çekme dayanımları belirlenmiştir.

Hazırlanan karışımların tamamında agrega/bağlayıcı/karışım suyu oranı 2.75/1.00/0.485 sabit tutulmuştur. Karışımlar oluşturulurken kullanılan çimentoya ait bazı kimyasal ve fiziksel özellikler **Tablo 1**'de yer almaktadır.

Tablo 1: Çimento Özellikleri.

Çimento Sınıfı	CEM I 42.5 R
Yoğunluk (g/cm^3)	3.1
Özgül Yüzey Alanı (cm^2/g)	3600
28 günlük minimum dayanım (MPa)	42.5
Klorür Muhtevası	< % 0.1
Kızdırma Kaybı	<% 5.0

Karbon liflerin çimentolu kompozitler içerisinde kullanılması durumunda, taze haldeki karışımların işlenebilirliğini oldukça düşürdüğü bilinmektedir [17]. Ayrıca karbon liflerin, kompozit içerisinde homojen dağılımının dayanımı etkileyen önemli faktörlerden biri olduğu ortaya konmuştur [18], [19]. Tüm bunlara dayanılarak hazırlanan karışımlarda bağlayıcı malzeme miktarının %15'i, işlenebilirliği arttırdığı bilinen F sınıfı uçucu kül olarak seçilmiştir [20]. İşlenebilirliği arttırmasına ek olarak, kesikli karbon liflerin kompozit içerisindeki dağılımının iyileştirilebilmesi amacıyla polikarboksilik eter esaslı süperakışkanlaştırıcı beton katkısı karışımlarda bağlayıcı ağırlığının %0.40 oranında yer almıştır. Kullanılan süperakışkanlaştırıcı katkıya ait özellikler **Tablo 2**'de sunulmaktadır. Süperakışkanlaştırıcı oranına yapılan deneme karışımları sonucunda elde edilen yayılma çapları göz önünde bulundurularak karar verilmiştir.

Tablo 2: MasterGlenium ACE 30® Süperakışkanlaştırıcı Beton Katkısı Özellikleri.

Yoğunluk (g/cm^3)	1.05
Klorür Muhtevası	< % 0.10
Alkali Muhtevası	< % 3.00

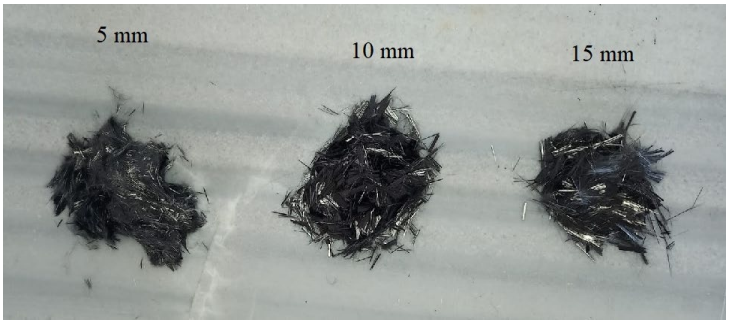

Şekil 1: Farklı boylardaki kesikli karbon liflere ait görünüm.

Çimentolu harç karışımlarda yer alan agregalar 0-4 mm tane boyutuna sahip, özgül yoğunluğu 2.65, kalkersi kökene sahiptir. Çalışma kapsamında kullanılacak kesikli karbon lifler 7 µm çapındadır ve bir demetinde 24 000 adet karbon lif bulunan yüzey polimerine sahip olmayan (*virgin*) sürekli yapıdaki karbon liflerin mekanik olarak kesilmesiyle elde edilmiştir. Karbon fiberlerin kökeni poliakrilonitril (PAN) olup, yoğunluğu 1.6 g/cm^3 kadardır. Oluşturulacak karışımlardaki karbon lif içeriği, Pratik uygulamalarda önerilen miktarlara uygun olacak şekilde sabit olarak hacimce %0.50 olarak seçilmiştir [21]. 3 Farklı boydaki kesikli karbon liflere ait görünüm **Şekil 1**'de sunulmaktadır.

Çalışma kapsamında incelenen karışımların özellikleri Tablo 3'te sunulmaktadır.

Tablo 3: Karbon Lif Takviyeli Harç Özellikleri.

Karışım Adı	Karbon Lif İçeriği (%V)	Karbon Lif Boyu (mm)	Uçucu Kül/Bağlayıcı Oranı	Su /Bağlayıcı Oranı
CTRL FA	0	-	0.15	0.485
CF05	0.50	5	0.15	0.485
CF10	0.50	10	0.15	0.485
CF15	0.50	15	0.15	0.485

III. YÖNTEM

Karbon lif takviyeli çimentolu kompozitlerde, liflerin performansını ortaya koyduğu etkili bir dayanım artışının gözlenebilmesi, lif dağılımının olabildiğince iyileştirilmesi, liflerin, matris içerisinde topaklanmasının önüne geçilmesinden ileri gelmektedir. Liflerin dağılımını iyileştirilebilmesinde literatürde uygulanan 3 farklı yaklaşım bulunmaktadır [22]. Bu çalışma kapsamında, karbon liflerin karışım suyu ve süperakışkanlaştırıcı katkıyla birlikte önceden solüsyon haline getirilip, karışımın katı fazına eklendiği metot olan ön-karıştırma yöntemi tercih edilmiştir. Farklı araştırmacılar tarafından bu karıştırma yönteminin literatürde yer alan diğer yöntemlere kıyasla avantajları ortaya konmuştur [22], [23], [24].

Karışımlar harç mikserinde sabit hızda (300 dev./dakika) 12 dakika boyunca karıştırılmış olup tüm karışımlarda birbirine yakın yayılma çapları (19±2 cm) ölçülmüştür. Karışımlar 40x40x160 mm^3 boyutlarındaki prizmatik kalıplara yerleştirildikten sonra, sarsma tablası yardımıyla sıkıştırılmıştır. 24 saat priz alma süresinin ardından elde edilen numuneler kalıplardan çıkarılıp 23±2ºC sabit sıcaklıktaki su içerisinde 28 günlük test yaşlarına kadar kür koşullarına maruz bırakılmıştır.

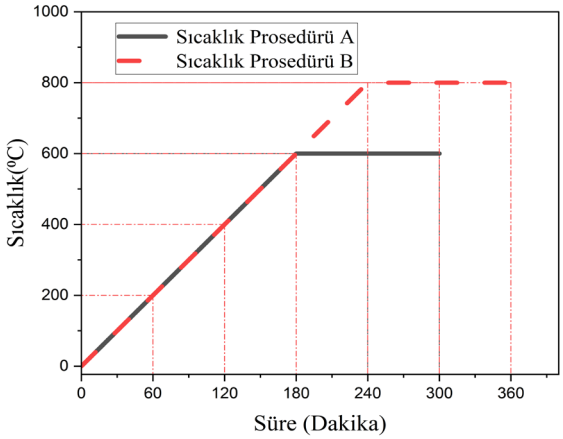

Şekil 2: Yüksek Sıcaklık Fırınında Uygulanacak Sıcaklık Prosedürleri.

28 günlük olgunluğa erişen numuneler, hem bünyelerinde yer alan nemi kaybetmeleri, hem de fırında sıcaklık prosedürlerine maruz kaldıklarında termal şok ile karşılaşmamaları amacıyla 50ºC sıcaklıkta 48 saat boyunca etüv içerisinde bekletilecektir. Fırında gerçekleştirilecek sıcaklık prosedürlerine ait sıcaklık zaman çizelgesi **Şekil 2**'de sunulmaktadır. A ile gösterilen sıcaklık prosedüründe fırın iç sıcaklığı sabit sıcaklık artış hızıyla (200ºC/saat) 600ºC hedef sıcaklığa ulaşıp bu sıcaklıkta 2 saat boyunca bekletildikten sonra fırına enerji girişi durmakta, fırın iç ortamı ve dolayısıyla hazırlanan numuneler serbest soğumaya bırakılmaktadır. B ile gösterilen sıcaklık prosedüründe ise fırın iç sıcaklığı sabit sıcaklık artış hızıyla (200ºC/saat) 800ºC hedef sıcaklığa ulaşıp bu sıcaklıkta 2 saat boyunca bekletildikten sonra fırına enerji girişi durmakta, fırın iç ortamı ve dolayısıyla hazırlanan numuneler serbest soğumaya

bırakılmaktadır. Fırında sıcaklık prosedürlerine maruz bırakılan numunelerin yanında, oda sıcaklığında bekleyen eşlenik numuneler de mevcuttur. Bu numuneler, fırın prosedürlerine maruz kalacak numuneler ile birlikte etüvde 48 saat boyunca bekletilmesinin ardından oda sıcaklığında bekletilmiştir. Artan sıcaklıkla birlikte çimentolu malzemelerde dayanım gelişiminin hızlandığı bilinmektedir. Bu uygulamada etüv içerisinde çimento dayanım kazandırıcı kimyasal reaksiyonlarının hızlanması ile ortaya çıkabilecek yanıltıcı sonuçların önüne geçilemesi hedeflenmiştir.

Yüksek sıcaklık prosedürlerine maruz bırakılan numuneler, fırın iç sıcaklığı, ortam sıcaklığına eriştiği anda, yüksek sıcaklık fırınından çıkarılarak 3 noktalı eğilme testine tabi tutulmuştur. 3 Noktalı eğilmede yükleme deplasman kontrollü olarak 0.5 mm/dakika hızında gerçekleştirilmiştir ve numunelere ait yük-deplasman ilişkisi yükleme çerçevesine entegre deplasman ölçer ve bilgiyar yardımıyla kayıt altına alınmıştır. Sıcaklık prosedürüne maruz bırakılmayan numuneler oda sıcaklığında iken test edilmiştir. 3 Noktalı eğilme deneyinden elde edilen veriler kullanılarak, numunelere ait, kırılma yükü, kırılma anındaki maksimum deplasman, kırılma enerjileri, eğilmede çekme dayanımları hesaplanmıştır.

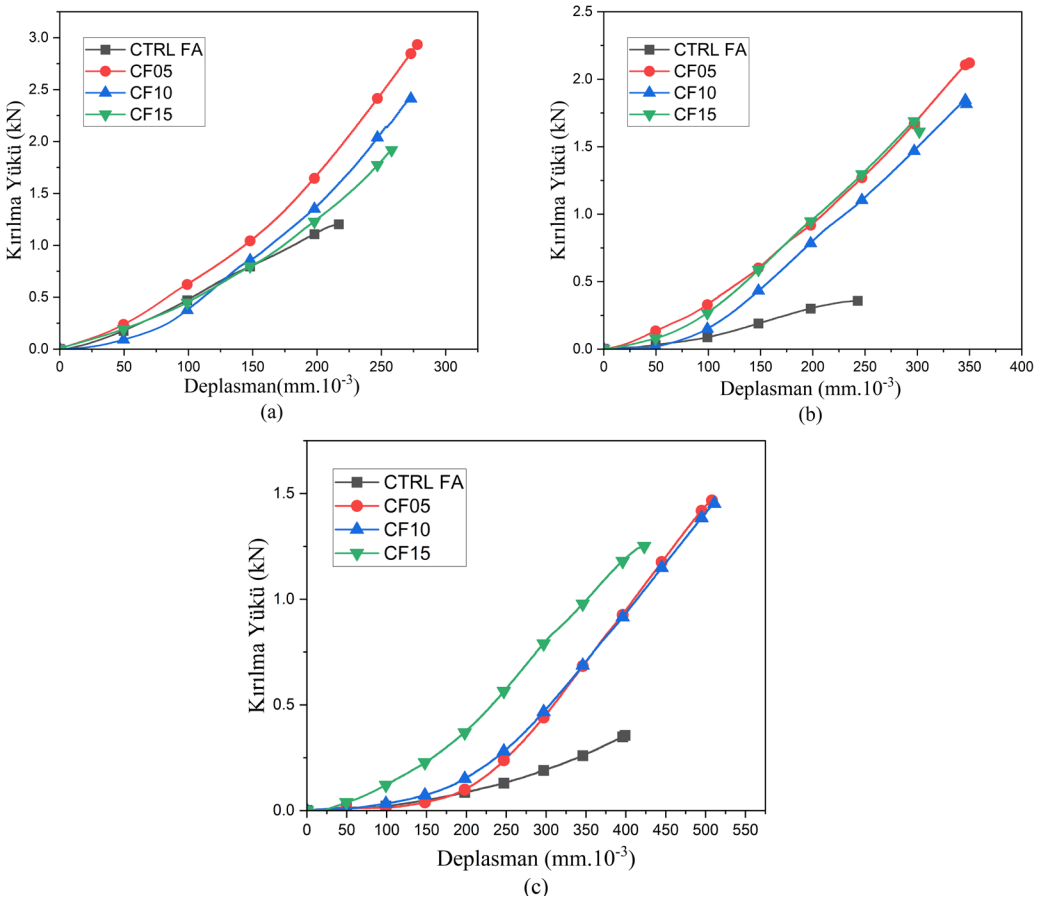

Şekil 3: Numunelere ait Yük-Deplasman İlişkileri. (a) Sıcaklık Prosedürüne maruz kalmamış, (b) 600ºC sıcaklık prosedürüne maruz kalmış, (c) 800ºC sıcaklık prosedürüne maruz kalmış numuneler.

3 noktalı eğilme deneyinde kırılan prizmatik numunelerin kalıntıları, 3N/s yükleme hızında basınç testine maruz bırakılarak, harçların basınç dayanımları da belirlenmiştir. Sıcaklık prosedürüne maruz bırakılmayan numuneler ile karşılaştırmalı analizler gerçekleştirilip, yüksek sıcaklığın ve karbon lif boyunun sıralanan parametreler üzerine etkisi değerlendirilmiştir.

IV. BULGULAR

Çimento esaslı malzemelerin, çoğu malzemeye kıyasla yangın ve yüksek sıcaklık etkisine karşı dirençli bir malzeme olduğu bilinmektedir [25]. Sıcaklık artışıyla birlikte çimento esaslı bileşenler içeren kompozitler bünyesinde çeşitli kimyasal reaksiyonlar ve fiziksel etkiler gelişmektedir. Sıcaklık arttıkça kompoziti oluşturan malzemelerin termal genleşme katsayıları farklı olduğundan, göreli genleşmeler gerçekleşecektir. Bu durum termal uyumsuzluk olarak bilinir ve kompoziti oluşturan malzemelerin birbirinden bağımsız davranışlar sergilemesine neden olur. Çimento pastası ve agrega ara yüzey özelliklerinin, dayanımı kontrol eden bir parametre olduğu bilinmektedir [25]. Termal uyumsuzluk durumunda arayüzey bölgesinde gerçekleşecek zayıflamalar, kompozit dayanımında etkili olacaktır. Çimento hidratasyonu ürünleri, bünyelerindeki serbest nemi 100ºC'de tamamen kaybetmektedir. 105ºC sıcaklıktan itibaren ise çimento hidratasyon ürünlerine bağlı olarak bulunan bünye suyu buharlaşmaya başlar, sıcaklık 400ºC'ye ulaştığında ise kimyasal olarak bağlı su tamamen kaybedilmiş olur, Kalsiyum hidroksit ($Ca(OH)_2$) bileşenleri CaO'ya dönüşür. Bu olay çimento fazında bir dayanım kaybına yol açmazken, poroziteyi arttırmaktadır. 400ºC'den yüksek sıcaklık seviyelerinde hidratasyon ürünleri ayrışmaya başlamakta ve çimentoda dayanım sağlayan ana unsur olan C-S-H jellerinin kimyasal yapısı bozulmaktadır. Çimento bünyesinde gelişen reaksiyonlar sürerken, 200ºC sıcaklığa kadar çimento-agrega arayüzünde herhangi bir mikro çatlak gelişimi yaşanmamaktadır [26], [27]. Bu sıcaklık seviyelerinden itibaren, mikro çatlak yoğunluğu, sıcaklık artışıyla birlikte artmaktadır. Sıralanan faktörlerin, kesikli karbon lif içeren çimentolu harçların mekanik dayanımları üzerine etkileri gerçekleştirilecek testler sonucunda kıyaslanacaktır.Gerçekleştirilen 3 noktalı eğilme deneyinden sonra elde edilen numunelere ait yük-deplasman ilişkileri **Şekil 3**'de sunulmaktadır.

Numunelere ait yük-deplasman verilerinden elde edilen Kırılma yükü, kırılma anındaki deplasman ve yük-deplasman grafiğinin altındaki alandan faydalanılarak hesaplanan kırılma enerjisi parametrelerine dair sütun grafikleri **Şekil 4**, **Şekil 5** ve **Şekil 6** 'da sunulmaktadır.

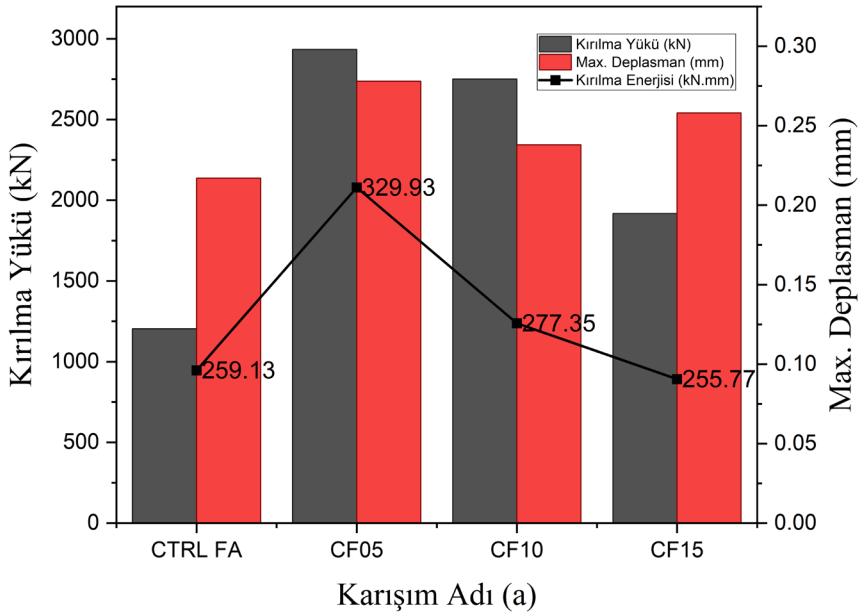

Şekil 4: Numunelere ait Kırılma yükü, Deplasman ve Kırılma enerjileri. (a) Sıcaklık Prosedürüne maruz kalmamış.

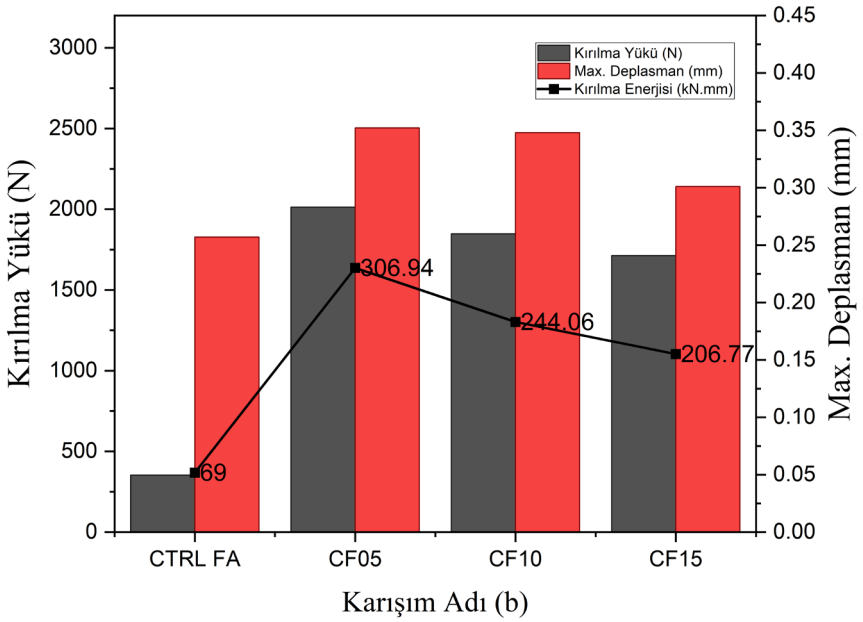

Şekil 5: Numunelere ait eğilmede çekme dayanımları. (b) 600ºC sıcaklık prosedürüne maruz kalmış.

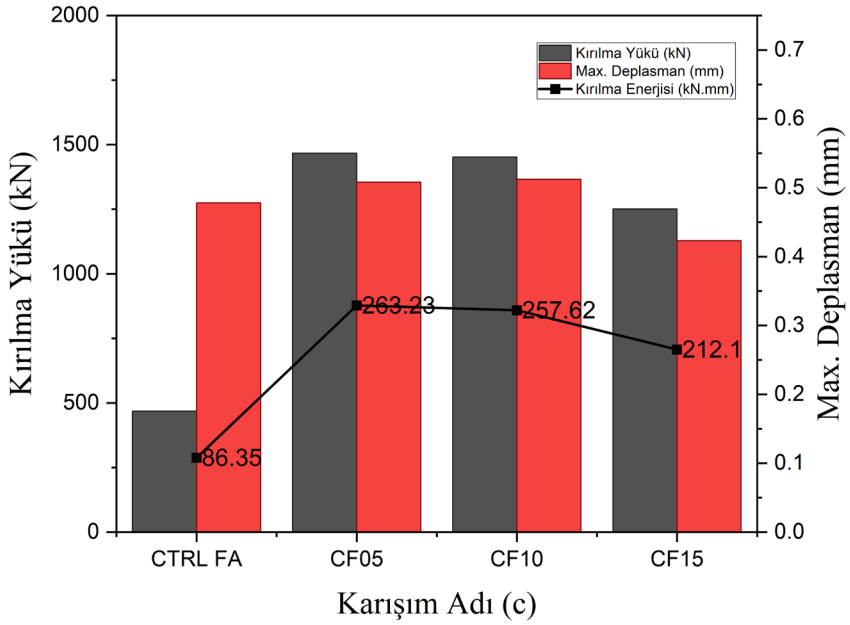

Şekil 6: Numunelere ait eğilmede çekme dayanımları. (c) 800ºC sıcaklık prosedürüne maruz kalmış.

Dikdörtgen kesite sahip numunelerde 3 noktalı eğilme deneyi için eğilmede çekme dayanımı Denklem (1) yardımıyla hesaplanabilmektedir. Karışımlara ait eğilmede çekme dayanımlarına ait sütun grafikleri **Şekil 7**'de sunulmaktadır.

$$\sigma_{tf} = \left(\frac{3}{2}\right)\frac{P.L}{b.h^2} \quad (1)$$

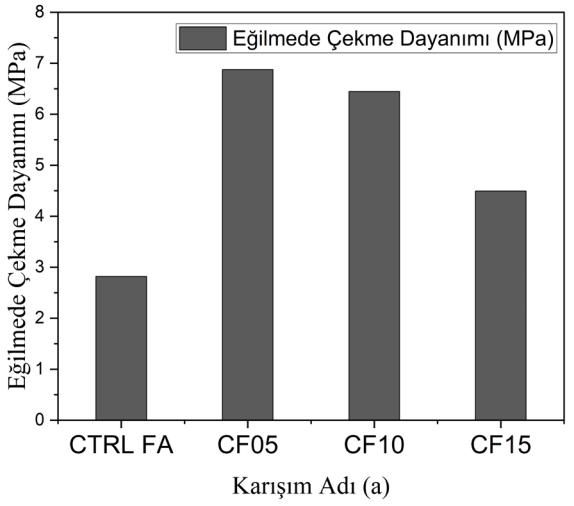

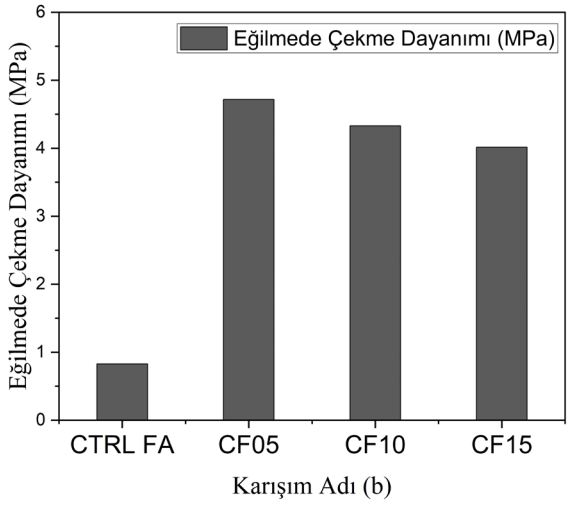

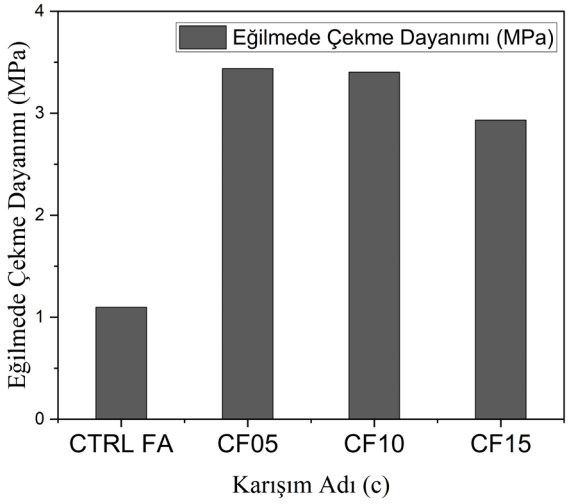

Şekil 7: Eğilmede Çekme Dayanımları. (b) 600ºC sıcaklık prosedürüne maruz kalmış, (c) 800ºC sıcaklık prosedürüne maruz kalmış numuneler.

3 Noktalı eğilme deneyinin ardından ortaya çıkan prizma kalıntıları, basınç testine tabi utulmuştur. Basınç dayanımlarına ait sütun grafikleri ve hesaplanan standart hata miktarlar **Şekil 8**'de sunulmaktadır.

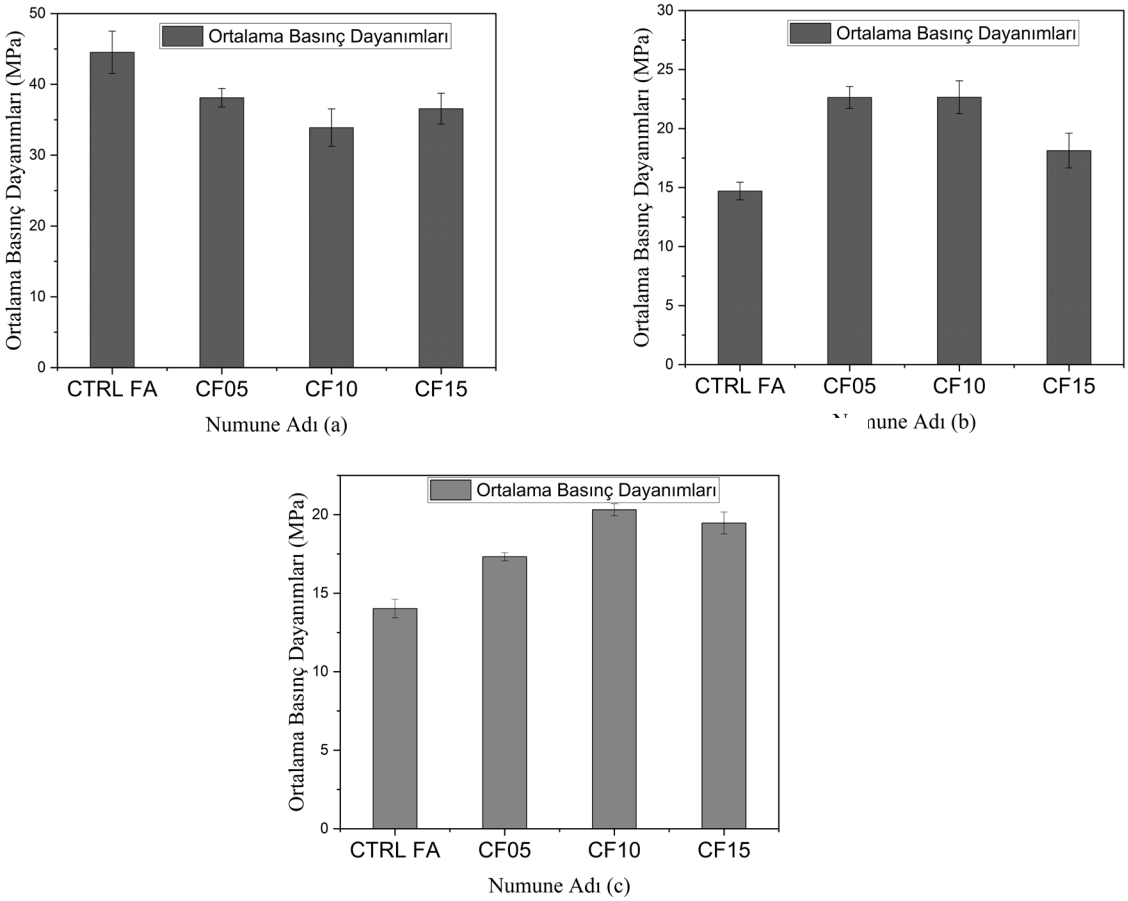

Şekil 8: Ortalama Prizma Basınç Dayanımları. a) Sıcaklık Prosedürüne maruz kalmamış, (b) 600ºC sıcaklık prosedürüne maruz kalmış, (c) 800ºC sıcaklık prosedürüne maruz kalmış numuneler.

V. SONUÇLAR

Kesikli karbon lif katkıları akıllı uygulamalar için çimentolu malzemeler ile birlikte kullanılabilmektedir. Bu biçimde oluşturulan kompozitlerin elektriksel özellikleri günümüzde ilgi konusu olsa da mekanik ve durabilite özelliklerinin araştırılması da bu tipteki kompozitlerin pratik uygulamalara konu olabilmesi için önem arz etmektedir. Gerçekleştirilen çalışma kapsamında yüksek sıcaklığa maruz bırakılmış kesikli karbon lif içeren çimentolu harçların, 3 noktalı eğilme deneyi sonucunda mekanik dayanımları ve karbon lif boyunun mekanik dayanımlar üzerine etkisi araştırılmıştır. Elde edilen bulgulardan yararlanılarak varılan sonuçlar şu şekilde sıralanabilir:

- Karbon lif boyunun artması, çimentolu harçlarda eğilmede çekme dayanımını azaltmaktadır. Bu durum sıcaklık faktöründen bağımsız olarak gelişmektedir.
- Sıcaklık faktörü lif içeren harçlarda eğilmede çekme dayanımını sınırlı düzeyde azaltırken, lif içermeyen kontrol harcında kayda değer azalımlar gözlenmiştir (600ºC için %50 ve 800ºC için %61 ortalama basınç dayanımı azalmıştır).
- Kırılma enerjisi lif boyundaki artışa paralel olarak azalmaktadır. Bu durum sıcaklık faktöründen bağımsız olarak gerçekleşmektedir.

- Karbon lif varlığının, prizma 3 noktalı eğilme deneyi sonrası kalıntılar üzerinde gerçekleştirilen basınç dayanımına kayda değer bir etkisi gözlenmemiştir.

KAYNAKLAR

[1] P. W. Chen ve D. D. L. Chung, "Carbon fiber reinforced concrete for smart structures capable of non-destructive flaw detection", *Smart Mater. Struct.*, c. 2, sayı 1, s. 22, Mar. 1993, doi: 10.1088/0964-1726/2/1/004.

[2] R. Brousseau, G. P.-A. materials journal, ve undefined 1997, "Proprietary and carbon fiber modified overlays in the cathodic protection of reinforced concrete", *scholar.archive.org*, c. 94, sayı 4, ss. 306–310, Erişim: 01 Ekim 2024. [Çevrimiçi]. Available at: https://scholar.archive.org/work/qjqvn63lonbnvm44lt3ey5w5di/access/wayback/https://nrc-publications.canada.ca/eng/view/accepted/?id=85e92856-383c-4c9d-8fc3-e29a255072ed

[3] J. Hou, D. C.-C. and concrete research, ve undefined 1997, "Cathodic protection of steel reinforced concrete facilitated by using carbon fiber reinforced mortar or concrete", *Elsevier*, Erişim: 01 Ekim 2024. [Çevrimiçi]. Available at: https://www.sciencedirect.com/science/article/pii/S0008884697000586

[4] F. Lee-Orantes, A. A. Torres-Acosta, M. Martínez-Madrid, ve C. López-Cajún, "Cathodic Protection in Reinforced Concrete Elements, using Carbon Fibers Base Composites", *ECS Trans.*, c. 3, sayı 13, ss. 93–98, Tem. 2007, doi: 10.1149/1.2721433/META.

[5] D. Y. Yoo, M. C. Kang, H. J. Choi, W. Shin, ve S. Kim, "Electromagnetic interference shielding of multi-cracked high-performance fiber-reinforced cement composites – Effects of matrix strength and carbon fiber", *Constr. Build. Mater.*, c. 261, s. 119949, Kas. 2020, doi: 10.1016/J.CONBUILDMAT.2020.119949.

[6] D. Wanasinghe, F. Aslani, ve G. Ma, "Electromagnetic shielding properties of carbon fibre reinforced cementitious composites", *Constr. Build. Mater.*, c. 260, s. 120439, Kas. 2020, doi: 10.1016/J.CONBUILDMAT.2020.120439.

[7] M. Ozturk ve D. D. L. Chung, "Enhancing the electromagnetic interference shielding effectiveness of carbon-fiber reinforced cement paste by coating the carbon fiber with nickel", *J. Build. Eng.*, c. 41, s. 102757, Eyl. 2021, doi: 10.1016/J.JOBE.2021.102757.

[8] Y. Zhao, J. Zhang, S. Qiang, H. Lu, ve J. Li, "Effect of carbon fibers and graphite particles on mechanical properties and electrical conductivity of cement composite", *J. Build. Eng.*, c. 94, s. 110036, Eki. 2024, doi: 10.1016/J.JOBE.2024.110036.

[9] S. Y. Ghanem ve J. Bowling, "Mechanical Properties of Carbon-Fiber–Reinforced Concrete", *Adv. Civ. Eng. Mater.*, c. 8, sayı 3, ss. 224–234, Kas. 2019, doi: 10.1520/ACEM20180089.

[10] W. Khalil, A. A.-E. and T. Journal, ve undefined 2011, "Mechanical properties of high performance carbon fiber concrete", *iasj.net*, c. 29, sayı 5, 2011, Erişim: 01 Ekim 2024. [Çevrimiçi]. Available at: https://www.iasj.net/iasj/download/3a5cd36b5b58adf6

[11] A. Katz ve A. Bentur, "Mechanical properties and pore structure of carbon fiber reinforced cementitious composites", *Cem. Concr. Res.*, c. 24, sayı 2, ss. 214–220, Oca. 1994, doi: 10.1016/0008-8846(94)90046-9.

[12] M. G. S. Mendonça, T. S. de Almeida, C. R. A. Daniel, ve L. S. Barreto, "Carbon fiber effect on the physico-mechanical and durability properties of a cement/coir pith composite", *Sustain. Mater. Technol.*, c. 25, s. e00187, Eyl. 2020, doi: 10.1016/J.SUSMAT.2020.E00187.

[13] Y. Ohama, M. Amano, M. E.-C. international, ve undefined 1985, "Properties of carbon fiber reinforced cement with silica fume", *concrete.org*, Erişim: 01 Ekim 2024. [Çevrimiçi]. Available at: https://www.concrete.org/publications/internationalconcreteabstractsportal/m/details/id

/9611
[14] Z. Bažant, M. Kaplan, ve Z. Bazant, "Concrete at high temperatures: material properties and mathematical models", 1996, Erişim: 01 Ekim 2024. [Çevrimiçi]. Available at: https://www.scholars.northwestern.edu/en/publications/concrete-at-high-temperatures-material-properties-and-mathematica
[15] J. Drchalová, E. Mňahončáková, R. Vejmelka, J. Kolísko, P. Bayer, ve R. Černý, "Hydric and mechanical properties of carbon fiber reinforced cement composites subjected to thermal load", *Constr. Build. Mater.*, c. 18, sayı 8, ss. 567–578, Eki. 2004, doi: 10.1016/J.CONBUILDMAT.2004.04.015.
[16] A. Çavdar, "A study on the effects of high temperature on mechanical properties of fiber reinforced cementitious composites", *Compos. Part B Eng.*, c. 43, sayı 5, ss. 2452–2463, Tem. 2012, doi: 10.1016/J.COMPOSITESB.2011.10.005.
[17] M. Safiuddin, G. Abdel-Sayed, ve N. Hearn, "Effects of Pitch-Based Short Carbon Fibers on the Workability, Unit Weight, and Air Content of Mortar Composite", *Fibers 2018, Vol. 6, Page 63*, c. 6, sayı 3, s. 63, Ağu. 2018, doi: 10.3390/FIB6030063.
[18] N. Ozyurt, T. O. Mason, ve S. P. Shah, "Correlation of fiber dispersion, rheology and mechanical performance of FRCs", *Cem. Concr. Compos.*, c. 29, sayı 2, ss. 70–79, Şub. 2007, doi: 10.1016/J.CEMCONCOMP.2006.08.006.
[19] C. Wang, K. Z. Li, H. J. Li, G. S. Jiao, J. Lu, ve D. S. Hou, "Effect of carbon fiber dispersion on the mechanical properties of carbon fiber-reinforced cement-based composites", *Mater. Sci. Eng. A*, c. 487, sayı 1–2, ss. 52–57, Tem. 2008, doi: 10.1016/J.MSEA.2007.09.073.
[20] S. Wen ve D. D. L. Chung, "A comparative study of steel- and carbon-fibre cement as piezoresistive strain sensors", *https://doi.org/10.1680/adcr.2003.15.3.119*, c. 15, sayı 3, ss. 119–128, May. 2015, doi: 10.1680/ADCR.2003.15.3.119.
[21] S. Wen ve D. D. L. Chung, "Seebeck effect in carbon fiber-reinforced cement", *Cem. Concr. Res.*, c. 29, sayı 12, ss. 1989–1993, Ara. 1999, doi: 10.1016/S0008-8846(99)00185-4.
[22] J. Gao, Z. Wang, T. Zhang, ve L. Zhou, "Dispersion of carbon fibers in cement-based composites with different mixing methods", *Constr. Build. Mater.*, c. 134, ss. 220–227, Mar. 2017, doi: 10.1016/J.CONBUILDMAT.2016.12.047.
[23] H. Zhu, H. Zhou, ve H. Gou, "Evaluation of carbon fiber dispersion in cement-based materials using mechanical properties, conductivity, mass variation coefficient, and microstructure", *Constr. Build. Mater.*, c. 266, s. 120891, Oca. 2021, doi: 10.1016/J.CONBUILDMAT.2020.120891.
[24] W. Chuang *vd.*, "Dispersion of carbon fibers and conductivity of carbon fiber-reinforced cement-based composites", *Ceram. Int.*, c. 43, sayı 17, ss. 15122–15132, Ara. 2017, doi: 10.1016/J.CERAMINT.2017.08.041.
[25] Q. Ma, R. Guo, Z. Zhao, Z. Lin, ve K. He, "Mechanical properties of concrete at high temperature—A review", *Constr. Build. Mater.*, c. 93, ss. 371–383, Eyl. 2015, doi: 10.1016/J.CONBUILDMAT.2015.05.131.
[26] W. M. Lin, T. D. Lin, ve L. J. Powers-Couche, "Microstructures of fire-damaged concrete", *Vol. 93, Issue 3, Pages 199 - 205*, c. 93, sayı 3, ss. 199–205, May. 1996, doi: 10.14359/9803.
[27] X. J. Li, Z. J. Li, M. Onofrei, G. Ballivy, ve K. H. Khayat, "Microstructural characteristics of HPC under different thermo-mechanical and thermo-hydraulic conditions", *Mater. Struct. 1999 3210*, c. 32, sayı 10, ss. 727–733, 1999, doi: 10.1007/BF02905069.

Bulut Servisi Sağlayıcı Seçiminde Çok Kriterli Karar Verme Yaklaşımları: AHS ve TOPSIS Uygulaması

Multi-Criteria Decision-Making Approaches in Cloud Service Provider Selection: Application of AHP and TOPSIS

Pınar Simay Ergün[*,1], Hasan Şahin[1]

[*]simayergun16@gmail.com, ORCID: 0000-0002-2391-4716
[1]*Endüstri Mühendisliği, Bursa Teknik Üniversitesi, Bursa, Türkiye*

Özet: Günümüzde bulut bilişim, işletmelerin dijital dönüşüm sürecinde hayati bir rol oynamakta olup, doğru bulut hizmet sağlayıcısının seçimi, organizasyonların operasyonel verimliliğini artırmada kritik bir faktördür. Ancak, bulut hizmet sağlayıcıları arasında çok sayıda kriter ve alternatifin bulunması, karar verme sürecini oldukça karmaşık hale getirmektedir. Bu çalışma, en uygun bulut hizmet sağlayıcısının belirlenmesi amacıyla gerçekleştirilmiştir. Bilgi teknolojileri alanında çalışan 6 uzman ile yapılan beyin fırtınası ve literatür taraması sonucunda, bulut hizmet sağlayıcısı seçiminde önemli olan 8 temel ölçüt belirlenmiştir: Maliyet, Sağlamlık, Ölçeklenebilirlik, Güvenlik, Hizmet Çeşitliliği, Yüksek Erişilebilirlik, Performans ve Esneklik. Analitik Hiyerarşi Süreci (AHS) kullanılarak her bir ölçütün ağırlıkları hesaplanmış ve TOPSIS yöntemiyle 5 alternatif sağlayıcı (AWS Cloud, Microsoft Azure Cloud, IBM Cloud, Google Cloud, Oracle Cloud) sıralanmıştır. Bu yöntemler sayesinde, en uygun bulut hizmet sağlayıcısı objektif bir şekilde tespit edilmiştir.

Anahtar Kelimeler: *Bulut Bilişim, Bulut Hizmet Sağlayıcıları, Bilgi Teknolojileri Hizmetleri, Çok Ölçütlü Karar Verme Metotları, AHS, TOPSIS*

Abstract: Currently, cloud computing plays a vital role in the digital transformation process of businesses, and the selection of the appropriate cloud service provider is a critical factor in enhancing organizations' operational efficiency. However, the presence of numerous criteria and alternatives among cloud service providers complicates the decision-making process significantly. This study aims to determine the most suitable cloud service provider. Through brainstorming sessions with six experts in the field of information technology and a comprehensive literature review, eight key criteria were identified as essential for the selection of a cloud service provider: Cost, Reliability, Scalability, Security, Service Variety, High Availability, Performance, and Flexibility. Using the Analytic Hierarchy Process (AHP), the weights of each criterion were calculated, and five alternative providers (AWS Cloud, Microsoft Azure Cloud, IBM Cloud, Google Cloud, Oracle Cloud) were ranked using the TOPSIS method. Through these methodologies, the most suitable cloud service provider was objectively identified.

Keywords: *Cloud Computing, Cloud Service Providers, Information Technology Services, Multi-Criteria Decision-Making Methods, AHP, TOPSIS*

I. GİRİŞ

Bulut bilişim, günümüzde işletmelerin dijital dönüşüm süreçlerinde önemli bir unsur haline gelmiş olup, doğru bulut hizmet sağlayıcısının seçimi, organizasyonların operasyonel verimliliği ve sürdürülebilirliği açısından kritik bir karar noktasıdır. Bulut hizmet sağlayıcıları, farklı özellikler ve performans düzeyleri sunmakta; bu da seçim sürecini karmaşıklaştıran çok sayıda kriter ve alternatifin değerlendirilmesini gerektirmektedir. İşletmeler için en uygun sağlayıcıyı seçerken maliyet, güvenlik, sağlamlık ve ölçeklenebilirlik gibi faktörlerin yanı sıra, hizmet çeşitliliği, yüksek erişilebilirlik, performans ve esneklik gibi kriterlerin de göz önünde bulundurulması gerekmektedir. Bu çalışmada, çok ölçütlü karar verme teknikleri kullanılarak, işletmelere en uygun bulut hizmet sağlayıcısının nasıl seçilebileceği incelenmiş ve bu doğrultuda Analitik Hiyerarşi Süreci (AHS) ve TOPSIS yöntemleri kullanılarak bir değerlendirme yapılmıştır.

Bu çalışmada, en iyi bulut hizmet sağlayıcısını seçmek amacıyla çok ölçütlü karar verme yöntemleri kullanılmıştır. İlk olarak, Analitik Hiyerarşi Süreci (AHS) yöntemiyle bulut hizmet sağlayıcısının seçiminde dikkate alınacak kriterlerin ağırlıkları belirlenmiştir. Ardından, TOPSIS yöntemi ile bu kriterler üzerinden alternatif sağlayıcılar sıralanmıştır.

Literatür taraması sonucunda, bulut hizmet sağlayıcısı seçiminde en yaygın kullanılan güvenlik, maliyet, sağlamlık, ölçeklenebilirlik, hizmet çeşitliliği, yüksek erişilebilirlik, performans ve esneklik gibi 8 ana kriter belirlenmiştir. Bu kriterler doğrultusunda, bilişim teknolojileri alanında uzman 6 kişi ile anket yapılmış ve anket sonuçlarının tutarlılığı kontrol edilmiştir. Tutarsız sonuçlar tekrar değerlendirilerek anketler tutarlı hale getirilmiştir.

Çalışmanın sonucunda, ilgili firma için en uygun bulut hizmet sağlayıcısı belirlenmiş ve AHS ile TOPSIS entegrasyonuna dayalı hesaplamalar yapılarak en uygun alternatif seçilmiştir.

II. BULUT BİLİŞİM TEKNOLOJİSİ

Bulut bilişim gelişmeye devam eden bir süreç olduğundan genel kabul görmüş bir tanım bulmak güçtür. Bilişim sektörü içerisindeki taraflar bulut bilişim için farklı tanımlar yapmaktadırlar [1]. Bu tanımlar şu şekilde açıklanabilir: Bulut, çok sayıda bilgisayarın birleşimi ile oluşan veri merkezlerini içeren, kullanıcıların kaynaklara internet üzerinden erişimine imkân tanıyan bir bilgi işlem ağıdır.

Bulut bilişim ise işlem ve depolama kaynaklarının dağıtımı için oluşturulmuş, kullanıcıların bilgiye internet üzerinden erişmesi, paylaşması ve bilgi üzerinde ortak işlem yapmasını sağlayan bir teknolojidir. Bulut bilişim, bir bilgisayar için gerekli görülen tüm programların, kurulumana ihtiyaç duyulmadan internet üzerinden erişilerek kullanılması fikrine dayanır. Bulut bilişim, bilgisayarların yeteneklerini genişleten, kullanıcıların bir dizi yazılım ve servise internet aracılığı ile erişimlerine imkan sağlayan bir teknolojidir [2]. Bulut bilişim bilgi teknolojileri servisleri için, internet tabanlı yeni bir destek ve dağıtım modelidir.

Bu model, uzak cihazlara ve sunucu hizmetlerine internet aracılığı ile kolaylıkla erişim sağlanması fikrinin bir ürünüdür. Tipik bulut bilişim, bir sunucu üstünde tutulan veri ve yazılımlara web servisi ya da web tarayıcı benzeri yazılımlarla erişilebilmesini sağlar {3]. Web'in ikinci büyük dalgası olarak isimlendirilen ve gelecekte iş dünyasına ışık tutacak en önemli kavramlardan biri olan bulut bilişim, internet üzerinden bir servis olarak sunulan bilgi teknolojileri kaynaklarının kullanımı ve geliştirimidir.

Bulut bilişim, gerçek zamanlı ve internet tabanlı teknoloji servis ve kaynaklarını içeren bir kavramdır [4]. Bulut bilişim, depolama ve veri işleme yükünü bilgisayarlar üzerinden alarak, uzak sunucular üzerine aktaran bir modeldir. Sunucular üzerinde bulunan veriler, ihtiyaç duyulduğu anda, internet üzerinden bilgisayarlara aktarılır. Verilere dünyanın herhangi bir yerinden ve internete bağlı olan herhangi bir cihaz üzerinden erişilebilmektedir.

III. ÇOK KRİTERLİ KARAR VERME YÖNTEMLERİ

Karar verme, bulunan bütün alternatifler arasından amaca en uygun ve olması en mümkün olan bir veya birkaç alternatifin seçilmesi sürecidir. Özellikle son zamanlarda yapılan bilimsel çalışmalar, karmaşıklık ve belirsizliğin yer aldığı bir karar ortamında bulunan karar verme gerekliliği olan karar vericinin, bilgi ve tecrübelerini sistematik bir biçimde değerlendirerek, en iyi sonuca nasıl ulaşabileceğine ilişkin yaklaşımlar getirmiştir. Bu sebeple de karar vericilerin yapması gereken, amaçlarını gerçekleştirecek farklı alternatifler arasından seçtiği kriterlere göre bir analiz yapmak ve birini seçmektir.

ÇKKV, karar bilimlerinin bir alt dalı olup, karar sürecinin belirlenen ölçütlere göre modellenmesi ve analiz edilmesi sürecine dayanmaktadır. Karar vericinin sayılabilir sonlu veya sayılamaz sayıda alternatiften oluşan bir küme içerisindeki en az iki kritere dayalı değerlendirmeler yaparak seçim yapılmasını sağlar. Bu sebeple de ÇKKV yöntemleri, karar vericinin topladığı verileri en iyi şekilde analiz ederek hedef ya da hedeflerini gerçekleştirecek alternatifleri çeşitli ölçütlere göre analiz edilmesine ve karar vericinin isteklerini karşılayacak en uygun alternatifin belirlemesine yardımcı olmaktadır [5].

Literatürde, birçok çok kriterli karar verme yöntemi önerilmiştir. Ayrıca, özelliklerinin ve performanslarının karşılaştırılmasına dayalı birçok makale de bulunmaktadır. Ancak, hangi yöntemin en uygun ve hangi yöntemin en etkili olduğuna kesin bir cevap vermek hala önemlidir. Bu nedenle, Stanujkić, D., Dordević, B., & Dordević, M. (2013), bazı çok kriterli karar verme yöntemlerini Sırbistan bankalarının sıralama örneğinde kullanmışlardır. Bu makalenin amacı, bankaları sıralamada hangi yöntemin uygun olduğunu belirlemek değildir. Makalenin amacı, farklı çok kriterli karar verme yöntemlerinin kullanılmasının bazen farklı alternatif sıralamalar yaratabileceğini vurgulamaktır. Farklı sonuçlara yol açan bazı sebepleri ortaya koymak ve farklı ÇKKV yöntemleriyle elde edilen farklı sonuçların rastgele bir olay olmadığını, tersine gerçekliği yansıttığını belirtmektedir [6].

Çok kriterli karar verme (ÇKKV), hem nicel hem de nitel yöntemdir. Bir problemin birden çok çözümü vardır, ancak çözümü bulmak ve çözüm ile ilgili uygun kararı almak ÇKKV'nin uygulanmasıdır. Bhole & Deshmukh (2018), tüm ÇKKV yöntemleri hakkında bilgi verir ve literatürdeki çeşitli alanlara ÇKKV yöntemlerinin uygulanmasını açıklar. Amaç, ÇKKV yöntemlerini ve uygulamalarını ortaya koymak ve çeşitli problemler için ÇKKV'nin doğasını anlamaktır. ÇKKV'nin diğer alanlara uygulanması, yeni araştırma alanları için bir fikir vermektedir. Çalışma, farklı araştırmacılar tarafından incelenen problemleri ve AHS, TOPSIS, MAUT gibi ÇKKV yöntemlerini kullanarak yorumladıkları çözümleri bulmaya yardımcı olmaktador. AHS, TOPSIS, MAUT en çok kullanılan yöntemler olmuştur ancak hibrit veya entegre yöntemler gibi çözümler konum, finans, atık su, iflas, köprü inşaatı gibi problemler için çözüm sağlar. Bu kombinasyon, ÇKKV tarihinde yeni bir çağın başlangıcını oluşturur [7].

IV. LITERATÜR TARAMASI: BULUT BILIŞIM VE ÇOK ÖLÇÜTLÜ KARAR VERME YÖNTEMLERI

Bulut bilişim, bilişim dünyasında önemli bir paradigma değişikliği yaratmıştır ve birçok çalışma bu konuda derinlemesine incelemeler sunmaktadır. Yıldız (2009) bulut bilişimin şirketler üzerindeki etkilerini ve denetim süreçlerini ele almıştır [1]. Rayport ve Heyward (2009) bulut bilişimin gelecekteki potansiyelini vurgulamışlardır [2]. Knorr ve Gruman (2008) ise bulut bilişimin gerçek anlamını ve bu teknolojinin iş dünyasında ne anlama geldiğini açıklamıştır [3]. Kocagüneli ve arkadaşları (2009), bulut bilişimde yazılım ölçümleme, hata analizi ve tahmin araçlarını tartışmıştır [4].

Çok ölçütlü karar verme (MCDM) yöntemleri, bulut hizmet sağlayıcıları gibi karmaşık seçim süreçlerinde kritik bir rol oynamaktadır. Chen ve Hwang (1992), bulanık çok ölçütlü karar verme yöntemlerinin temellerini atmıştır [5]. Stanujkić ve arkadaşları (2013) bazı öne çıkan MCDM yöntemlerini analiz ederek Sırp bankalarının sıralanmasına yönelik bir uygulama

yapmışlardır [6]. Bhole ve Deshmukh (2018), çok kriterli karar verme yöntemlerinin genel uygulamaları üzerine kapsamlı bir çalışma sunmuştur [7].

Saaty (1986), Analitik Hiyerarşi Süreci (AHS) metodunun aksiyomatik temellerini açıklamış ve bu yöntemin karar verme süreçlerinde nasıl kullanıldığını detaylandırmıştır [8]. Taş ve arkadaşları (2018), AHS ve TOPSIS yöntemlerinin entegrasyonunu kullanarak poliklinik değerlendirmeleri üzerine bir çalışma yapmıştır [9]. Asoğlu ve Eren (2018) ise benzer yöntemlerle bir işletmenin kargo şirketi seçimini incelemişlerdir [10]. Cheng ve arkadaşları (2002), AHS yönteminin hatalı kullanımında ortaya çıkan problemleri ele almışlardır [11].

Yurdakul ve İç (2005), üretim şirketleri için performans ölçüm modelleri geliştirmiş ve AHS ile TOPSIS yöntemlerini birleştirerek bu modelleri değerlendirmişlerdir [12]. Bu çalışmalar, bulut hizmet sağlayıcı seçimi gibi karmaşık karar süreçlerinde çok ölçütlü karar verme yöntemlerinin önemini ve etkinliğini ortaya koymaktadır.

Bu literatür çalışmaları, hem bulut bilişimin hem de çok ölçütlü karar verme yöntemlerinin kuramsal temellerini oluşturmakta ve pratik uygulamalarına yönelik çeşitli yöntemler sunmaktadır.

V. ANALİTİK HİYERARŞİ SÜRECİ (AHS)

Analitik Hiyerarşi Süreci (AHS), ilk olarak 1968'de Myers ve Alpert tarafından ortaya konmuş, daha sonra 1977'de Profesör Thomas Lorie Saaty tarafından geliştirilmiştir. AHS, alternatiflerin veya projelerin önceliklerini belirlemek için, birçok değişkenin dikkate alındığı karmaşık karar verme süreçlerinde kullanılan bir tekniktir. Bu yöntemin uygulanması, bir problemin daha etkili bir şekilde analiz edilmesi ve bağımsız olarak karşılaştırılabilmesi için ölçütlerin bir hiyerarşi şeklinde düzenlenmesiyle başlar. Hiyerarşi oluşturulduktan sonra, karar vericiler, her bir ölçüt için alternatifleri sistematik olarak değerlendirmek amacıyla ikili karşılaştırmalar yapmaktadırlar [8].

1. Adım: Problem tanımlanır. Karar için gerekli olan ölçütler belirlenerek, ölçüt öncelikleri tespit edilir.

2. Adım: Hiyerarşik yapı, en üstte ulaşılması gereken ana hedefin yer aldığı bir düzenle oluşturulmaktadır. Bu ana hedefin altında temel ölçütler ve alt ölçütler bulunmaktadır. Hiyerarşinin en alt seviyesinde ise alternatifler yer almaktadır. Hiyerarşinin aşama sayısı, problemin karmaşıklığı ve detay düzeyine bağlı olarak değişmektedir. Hiyerarşi oluşturulurken, aynı düzlemde bulunan seçeneklerin birbirinden tamamen bağımsız olduğu varsayılmaktadır [9].

3. Adım: İkili karşılaştırmalar matrisi oluşturulmaktadır. 1 ile 9 arasında değer alan bir önem derecesi ölçeği kullanılmaktadır. Önce temel ölçütler, varsa alt ölçütler ve son olarak tüm ölçütlerin dikkate alınarak ölçütlere göre karar seçeneklerinin karşılaştırıldığı matrisler oluşturulur. Karşılaştırma matrisleri köşegen elemanları 1 olan bir kare matristir. Önem değerlerine göre dilsel değerler Tablo 1.1'de gösterilmektedir.

Tablo 1.1 Önem Değerlerine Göre Dilsel Değerler

Önem Değerleri	Önem Değerleri
1	Eşit Önemde
3	Biraz Daha Önemli (Az Üstünlük)
5	Oldukça Önemli (Fazla Üstünlük)
7	Çok Önemli (Çok Üstünlük)
9	Son Derece Önemli (Kesin Üstünlük)
2,4,6 ve 8	Ara Değerler (Uzlaşma Değerleri)

4. Adım: Matristeki her eleman kendi sütun toplamına bölünerek, normalize edilir. Normalize edilmiş matrisin her bir sütun toplamı 1 olur.

5. Adım: Öncelik vektörü hesaplanır. Normalize edilmiş matrisin her bir satır toplamı, matrisin boyutuna bölünerek ortalaması alınır. Bulunan bu değerler her bir ölçüt için hesaplanan önem ağırlıklarıdır. Bu ağırlıklar, öncelik vektörünü oluşturur.

6. Adım: Tutarlılık oranı hesaplanır. İkili karşılaştırmalar yapıldıktan ve öncelikler belirlendikten sonra, karşılaştırma matrislerinin tutarlılığı değerlendirilmektedir. Bir A matrisinin tutarlı olup olmadığını belirlemek için "Tutarlılık İndeksi Katsayısı" gibi yöntemlerden biri kullanılır. Tutarlılığı değerlendirmek için "Rasgele İndeks" (RI) değeri de bilinmelidir. CI ve RI değerleri belirlendikten sonra, "Tutarlılık Oranı" hesaplanmaktadır [10].

7. Adım: Ölçütler için ikili karşılaştırma matrisi oluşturularak, karar seçeneklerinin öncelik vektörü hesaplanır. Bu öncelik vektörü, ölçütler için ağırlık vektörü olarak da tanımlanabilir.

8. Adım: Karar seçenekleri sıralanır. Ölçütler için elde edilen öncelik vektörleri birleştirilerek tüm öncelikler matrisi oluşturulmaktadır. Bu matris ile karar seçeneklerinin öncelik vektörü çarpılıp toplanarak sonuç vektörü elde edilmektedir. Sonuç vektöründe en yüksek ağırlığa sahip olan karar seçeneği, problemin çözümü için tercih edilmesi gereken seçenek olarak belirlenmektedir [11].

VI. TOPSIS METODU

TOPSIS, Hwang ve Yoon tarafından 1980 yılında geliştirilen bir çok kriterli karar verme (ÇKKV) yöntemidir. Bu yöntem, birçok alternatif arasından en iyi tercihin yapılmasını kolaylaştırarak karar vericilere yardımcı olmaktadır. TOPSIS, ÇKKV yöntemlerinde yaygın olarak kullanılan bir yöntemdir. Uygulama aşamalarının kolay ve anlaşılır olması, sonuçların yorumlanmasının zor olmaması sebepleri ile birçok karar alıcı tarafından tercih edilmektedir.

Karar matrisi m adet alternatif ile n adet ölçütlü karar verisinden oluşmaktadır. Burada A değerleri alternatifleri, x değerleri ise bu alternatiflerin ölçütlerini ifade etmektedir.

1.Adım: Standart karar matrisi, *A* matrisinin elemanlarından yararlanarak ve aşağıdaki formül kullanılarak hesaplanmaktadır.

$$r_{ij} = \frac{a_{ij}}{\sqrt{\sum_{i=1}^{m} a_{ij}^2}} \tag{1}$$

2. Adım: Öncelikle değerlendirme faktörlerine ilişkin ağırlık değerleri (Wi) belirlenmektedir. Daha sonra R matrisinin her bir sütunundaki elemanlar ilgili değeri ile çarpılarak V matrisi oluşturulmaktadır.

3. Adım: TOPSIS yöntemi, her bir değerlendirme faktörünün sabit artan veya azalan bir eğilime sahip olduğunu varsaymaktadır. Uygun çözüm setinin oluşturulabilmesi için V matrisindeki ağırlıklandırılmış değerlendirme faktörlerinin, yani sütun değerlerinin en büyükleri seçilmektedir. Uygun çözüm setinin bulunması aşağıdaki formülde gösterilmektedir.

$$A^{+} = \left\{ \left(\max_{i} V_{ij} \middle| \; j \in J \right), \left(\min_{i} V_{ij} \middle| \; j \in J' \right) \right\} \tag{2}$$

Negatif uygun çözüm seti, V matrisindeki ağırlıklandırılmış değerlendirme faktörlerinin, yani sütun değerlerinin en küçükleri seçilerek oluşturulmaktadır. Negatif uygun çözüm setinin belirlenmesi aşağıdaki formülde gösterilmektedir.

$$A^{-} = \left\{ \left(\min_{i} V_{ij} \middle| \; j \in J \right), \left(\max_{i} V_{ij} \middle| \; j \in J' \right) \right\} \tag{3}$$

Her iki formülde de fayda en büyüklenirken, kayıp ise en küçüklenme değerini göstermektedir. Hem uygun hem de negatif uygun çözüm seti, m elemandan oluşan değerlendirme faktörü sayısını içermektedir.

4. Adım: TOPSIS yönteminde, her bir karar noktasına ait değerlendirme faktör değerlerinin, uygun ve negatif uygun çözüm setlerinden sapmalarını bulmak için Öklid Uzaklık Yaklaşımı kullanılmaktadır. Elde edilen sapma değerleri, Uygun Ayırım (S_i+) ve Negatif Uygun Ayırım (S_i–) Ölçüsü olarak adlandırılmaktadır. Uygun Ayırım (S_i+) Ölçüsünün hesaplanma formülü ile Negatif Uygun Ayırım (S_i–) Ölçüsünün hesaplanması aşağıdaki formüllerle gösterilmektedir [12].

$$S_{i+} = \sqrt{\sum_{j=i}^{n} (V_{ij} - V_{J+})^2} \tag{4}$$

$$S_{i-} = \sqrt{\sum_{j=i}^{n} (V_{ij} - V_{J-})^2} \tag{5}$$

Burada hesaplanacak S_i+ve S_i–sayısı karar noktası sayısı kadar olacaktır.

5. Adım: Her bir karar noktasının uygun çözüme göreli yakınlığının (C_i) hesaplanmasında, uygun ve negatif uygun ayırım ölçülerinden faydalanılmaktadır. Burada, negatif uygun ayırım ölçüsünün toplam ayırım ölçüsü içindeki payı dikkate alınır. Uygun çözümün yakınlık değerinin hesaplanması aşağıdaki formülde gösterilmektedir.

$$C_i = \frac{S_{i-}}{(S_{i-} + S_{i+})} \tag{6}$$

Burada C_i değeri $0 \leq C_i \leq 1$ aralığında değer alır ve $C_i = 1$ ilgili karar noktasının uygun çözüme, $C_i = 0$ ilgili karar noktasının negatif uygun çözüme mutlak yakınlığını göstermektedir.

VII. ANALİZ VE BULGULAR

Bu çalışmada, bulut hizmet sağlayıcısı seçiminde çok ölçütlü karar verme yöntemlerinden Analitik Hiyerarşi Süreci (AHS) ve TOPSIS yöntemleri entegre bir yaklaşımla kullanılmıştır. Bilgi teknolojileri alanında uzman 6 kişi ile yapılan anketler sonucunda, bulut hizmet sağlayıcısı seçiminde en etkili 8 ana ölçüt belirlenmiştir: Maliyet, Sağlamlık, Ölçeklenebilirlik, Güvenlik, Hizmet Çeşitliliği, Yüksek Erişilebilirlik, Performans ve Esneklik. AHS yöntemi ile her bir ölçütün ağırlıkları hesaplanmış ve ardından TOPSIS yöntemiyle bu kriterler doğrultusunda belirlenen 5 alternatif bulut sağlayıcısı (AWS Cloud, Microsoft Azure Cloud, IBM Cloud, Google Cloud, Oracle Cloud) sıralanmıştır. Belirlenen ölçütler ve alternatiflerin yapısı, Şekil 1.1'de detaylı olarak sunulmaktadır.

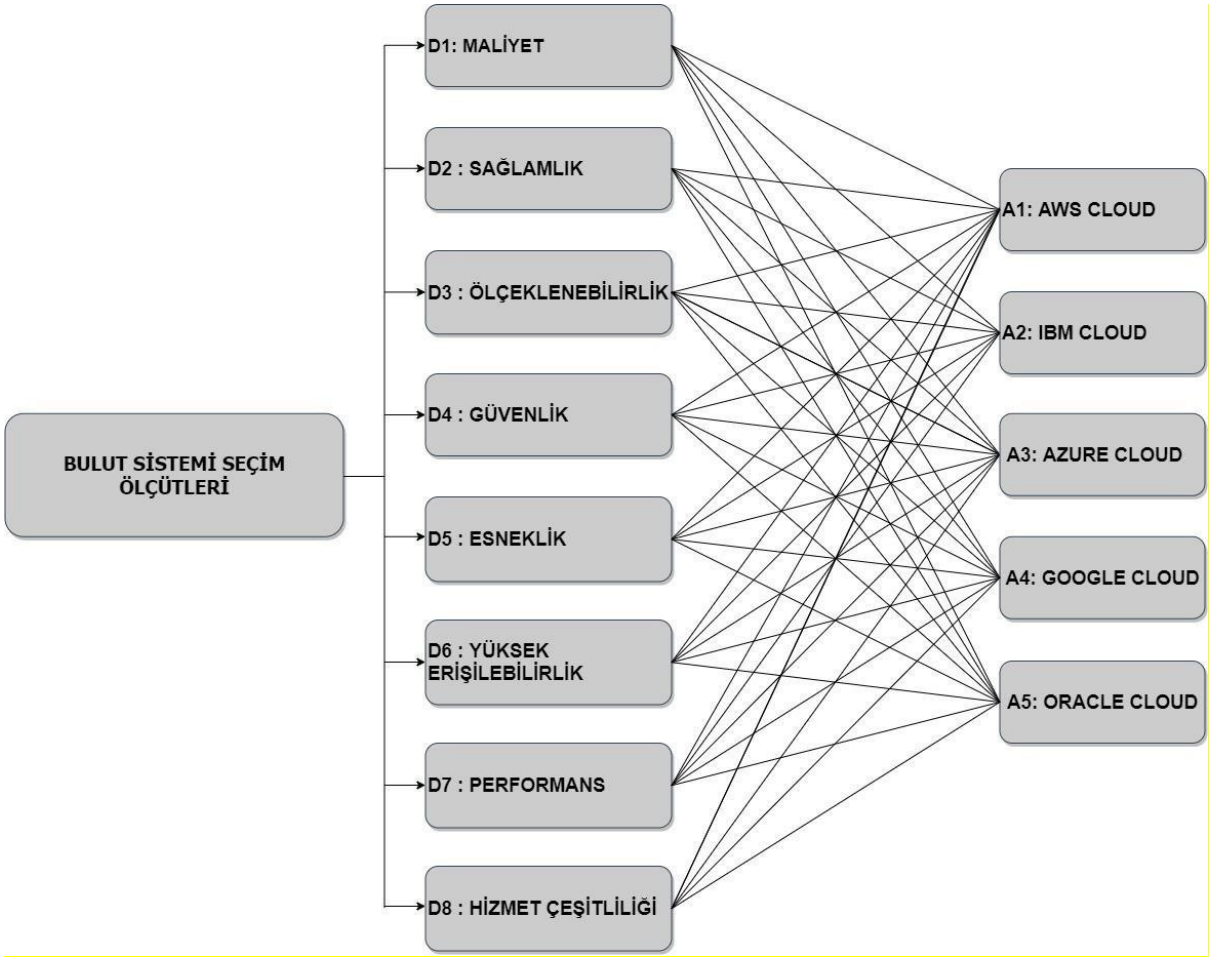

Şekil 1.1 Bulut Hizmet Sağlayıcısının Değerlendirilmesi İçin Hiyerarşik Yapı

Aşağıdaki çok ölçütlü karar verme yöntemlerinde kullanılacak olan ölçütlerin açıklamaları verilmiştir.

Tablo 1. 2 Ölçütlerin Açıklamaları

Ölçütler	**Açıklamalar**
D1: Maliyet	Bulut hizmet yapılandırmalarını ve iş yükünü hesaba katarak bulutta oluşabilecek hizmetlerin işletme maliyetidir.
D2: Sağlamlık	Uygulama çalıştırılırken müdahale edilmeden sorunsuz çalışıp çalışmadığı ve ne kadar uzun süre ayakta durabildiğidir.
D3:Ölçeklenebilirlik	Sistemin değişen iş yükü miktarına veya web uygulamasına gelen trafiğe uyarlanabilmesidir. Temel olarak, uygulama için kaynakların artırılması veya azaltılması, ölçeklendirme olarak adlandırılır.
D4: Güvenlik	Bulut bilgi işlem güvenliği olarak da adlandırılan bulut güvenliği, bulut bilişim ortamlarını, uygulamalarını, verilerini ve bilgilerini koruma disiplini ve uygulamasını ifade eder.

D5: Esneklik	Bulut çözümleri, verilerinize ve kaynaklarınıza dünyanın herhangi bir yerinden hızlı ve güvenli bir şekilde erişmenizi ve işlemenizi sağlayarak işletmelerinize ve çalışanlarına daha fazla esneklik sunar.
D6: Yüksek Erişilebilirlik	Bir sistemin kabul gören bir operasyonel performansla normalden uzun süre çalışmasını sağlamaya yönelik bir karakteristiktir.
D7: Performans	Bulut servisinin kolay yönetilebilmesi için gerekliolan yönetimsel araçlardır.
D8: Hizmet Çeşitliliği	Sistemde ihtiyaç olduğunda bu ihtiyacı karşılayabilmegücüdür.

Bu çalışmada, bulut hizmet sağlayıcısı seçiminde etkili olan ölçütler araştırılmıştır. Yapılan literatür taramaları ve uzman görüşleri doğrultusunda, bulut hizmet sağlayıcısı seçiminde belirleyici olan ölçütler 5 ana başlıkta toplanmıştır. Bu ölçütler, bilgi teknolojileri alanında deneyimli 6 uzman tarafından değerlendirilmiş ve ölçütlerin birbiriyle olan ilişkileri nedeniyle, çok kriterli karar verme yöntemlerinden Analitik Hiyerarşi Süreci (AHS) kullanılmıştır. Orta ölçekli şirketler için bulut hizmet sağlayıcısı seçiminde, AHS ile elde edilen kriter ağırlıkları dikkate alınarak bir değerlendirme yapılmıştır.

alışmada, en uygun bulut hizmet sağlayıcısının seçimi için AHS ile entegre edilen TOPSIS yöntemi kullanılmıştır. Bu süreçte, belirlenen kriterler doğrultusunda, 20 ila 30 yıllık deneyime sahip bulut mimarları ve uzmanlara anket uygulanmıştır. Ankete katılan uzmanlar, Cloud Solution Architect, Founder-Devopslogy, Senior Solution Architect ve Cloud Advocate gibi pozisyonlarda çalışmaktadır. Anketlerin tutarlılığı kontrol edilmiş ve gerekli düzenlemeler yapılmıştır.

AHS yöntemi kullanılarak kriterlerin ağırlıkları hesaplanmış ve şu sonuçlar elde edilmiştir: 0.22, 0.20, 0.11, 0.10, 0.10, 0.09, 0.09 ve 0.08. Bu ağırlıklar, TOPSIS yöntemi ile birleştirilmiş ve alternatif bulut hizmet sağlayıcıları sıralanmıştır. Sonuçlar, Tablo 1.3'te gösterilmiş olup, Azure, AWS, IBM, Google ve Oracle bulut hizmet sağlayıcıları arasında en uygun seçenek olarak Azure seçilmiştir.

Tablo 1. 3 ÇKKV Yöntemi Sonuçları Genel Gösterimi

Alternatifler	AHS&TOPSIS
AZURE	1
AWS	2
ORACLE	3
GOOGLE	4
IBM	5

TARTIŞMA

Bu çalışmada, bulut hizmet sağlayıcılarının seçiminde çok ölçütlü karar verme yöntemleri olan Analitik Hiyerarşi Süreci (AHS) ve TOPSIS yöntemlerinin entegrasyonu ele alınmıştır. Literatür taraması sonucunda, bulut bilişim ve çok ölçütlü karar verme yöntemleri üzerine

yapılan önceki çalışmaların kapsamı ile mevcut çalışma arasındaki benzerlikler ve farklılıklar belirlenmiştir.

Öncelikle, literatürdeki çalışmaların bulut bilişimin iş dünyasındaki rolü ve etkileri üzerine odaklandığı görülmektedir. Yıldız (2009) ve Knorr ile Gruman (2008), bulut bilişimin sağladığı avantajları ve işletmeler için kritik önemini vurgularken, bu çalışmada doğrudan bulut hizmet sağlayıcılarının seçiminde kullanılan kriterlerin belirlenmesi hedeflenmiştir. Bu bağlamda, literatürdeki bulgularla paralellik gösteren bir yaklaşım benimsenmiştir.

Ayrıca, çok ölçütlü karar verme yöntemlerinin uygulamaları üzerine yapılan araştırmalar, bu çalışmada benzer bir çerçevede değerlendirilmiştir. Özellikle, Stanujkić ve arkadaşlarının (2013) MCDM yöntemlerini kullanarak gerçekleştirdiği çalışmalar, yapılan araştırmanın somut bir örneği olarak öne çıkmaktadır. AHS ve TOPSIS yöntemlerinin entegrasyonu, literatürdeki mevcut çalışmalarla örtüşmekte ve bulut hizmet sağlayıcıları seçiminde uygulamalı bir katkı sağlamaktadır.

Uzman görüşleri ile belirlenen ölçütler, araştırmanın güvenilirliğini artırmakta ve literatürdeki benzer yaklaşımlarla tutarlılık göstermektedir. Bu çalışma, hem akademik literatürdeki teorik temellerle uyumlu bir şekilde bulut hizmet sağlayıcılarının seçiminde etkili olan kriterleri belirlerken, hem de sektöre özgü bir analiz sunarak pratik bir katkı sağlamaktadır.

Sonuç olarak, bu çalışma bulut hizmet sağlayıcılarının seçiminde kullanılan çok ölçütlü karar verme yöntemlerinin önemini ve etkinliğini ortaya koymaktadır. Elde edilen sonuçlar, işletmelerin doğru karar verme süreçlerini destekleyerek bulut bilişim alanındaki rekabetçiliklerini artırmalarına olanak tanımaktadır. Bu bağlamda, literatürdeki bilgi birikimini uygulamaya dönüştüren bu çalışma, hem akademik hem de pratik açıdan önemli bir katkı olarak değerlendirilmektedir.

VIII. SONUÇ VE ÖNERİLER

Bu çalışmada, bulut hizmet sağlayıcılarının seçiminde çok ölçütlü karar verme yöntemleri olan Analitik Hiyerarşi Süreci (AHS) ve TOPSIS yöntemlerinin entegrasyonu kullanılarak en uygun bulut hizmet sağlayıcısının belirlenmesi amaçlanmıştır. Çalışma sonucunda, güvenlik, maliyet, sağlamlık, ölçeklenebilirlik, hizmet çeşitliliği, yüksek erişilebilirlik, performans ve esneklik gibi kriterlerin önemine vurgu yapılmış ve bu kriterlere göre AWS, Microsoft Azure, IBM Cloud, Google Cloud ve Oracle Cloud alternatifleri arasında en iyi seçenek olarak Microsoft Azure belirlenmiştir.

Bu sonuçlar, bulut hizmet sağlayıcılarının seçiminde sistematik bir yaklaşımın ve analitik yöntemlerin önemini göstermektedir. Şirketlerin, karar verme süreçlerini daha verimli hale getirmek ve rekabet avantajı sağlamak için AHS ve TOPSIS gibi yöntemleri benimsemeleri önerilmektedir. Özellikle, karar vericilerin, kriterlerin ağırlıklarını belirlerken uzman görüşlerine dayanan anketlerin sonuçlarını dikkate alarak daha kapsamlı ve güvenilir kararlar alabilecekleri sonucuna varılmıştır.

Gelecek araştırmalar için öneriler, farklı sektörlerde bulut hizmet sağlayıcılarının seçiminde bu yöntemlerin uygulanması ve alternatif MCDM yöntemleri ile karşılaştırmalı çalışmalar yapılmasıdır. Ayrıca, bulut bilişim alanındaki gelişmelerin hızla değiştiği göz önünde bulundurularak, güncel kriterlerin sürekli olarak gözden geçirilmesi ve yeni bulut hizmet sağlayıcılarının eklenmesi önerilmektedir. Bu tür çalışmalar, işletmelerin karar verme süreçlerini destekleyerek daha etkili ve verimli bulut hizmet kullanımlarını teşvik edecektir.

Sonuç olarak, bulut hizmet sağlayıcılarının seçiminde çok ölçütlü karar verme yöntemlerinin entegrasyonu, işletmelerin dijital dönüşüm süreçlerine katkı sağlamakta ve rekabetçiliklerini artırmaktadır.

KAYNAKÇA

[1] Yıldız, Ö. R. (2009). Bilişim dünyasının yeni modeli: Bulut bilişim cloud computing ve denetim. Sayıştay Dergisi, (74), 5-23.
[2] Rayport, J. F., & Heyward, A. (2009). Envisioning the cloud: The next computing paradigm. International Journal of Database Management Systems (IJDMS), 1(1).
[3] Knorr, E., & Gruman, G. (2008). What cloud computing really means. InfoWorld, 7(20-20), 1-17.
[4] Kocagüneli, E., Tosun, A., Çağlayan, B., Bener, A., Aytaç, T., & Turhan, B. (2009). Bulutlarda akıllı bir yazılım ölçümleme, hata analiz ve tahmin aracı: Prest. Ulusal Yazılım Mühendisliği Sempozyumu-UYMS'09, 311-314.
[5] Chen, S. J., & Hwang, C. L. (1992). Fuzzy multiple attribute decision making methods. In Fuzzy multiple attribute decision making: Methods and applications (pp. 289-486). Berlin, Heidelberg: Springer Berlin Heidelberg.
[6] Stanujkić, D., Đorđević, B., & Đorđević, M. (2013). Comparative analysis of some prominent MCDM methods: A case of ranking Serbian banks. Serbian Journal of Management, 8(2), 213-241.
[7] Bhole, G. P., & Deshmukh, T. (2018). Multi-criteria decision making (MCDM) methods and its applications. International Journal for Research in Applied Science & Engineering Technology (IJRASET), 6(5), 899-915.
[8] Saaty, T. L. (1986). Axiomatic foundation of the analytic hierarchy process. Management Science, 32(7), 841-855.
[9] Taş, C., Bedir, N., Eren, T., Alağaş, H. M., & Çetin, S. (2018). AHP-TOPSIS yöntemleri entegrasyonu ile poliklinik değerlendirilmesi: Ankara'da bir uygulama. Sağlık Yönetimi Dergisi, 2(1), 1-17.
[10] Asoğlu, İ., & Eren, T. (2018). AHP, TOPSIS, PROMETHEE yöntemleri ile bir işletme için kargo şirketi seçimi. Yalova Sosyal Bilimler Dergisi, 8(16), 102-122.
[11] Cheng, E. W., Li, H., & Ho, D. C. (2002). Analytic hierarchy process (AHP): A defective tool when used improperly. Measuring Business Excellence, 6(4), 33-37.
[12] Yurdakul, M., & İç, Y. T. (2005). Development of a performance measurement model for manufacturing companies using the AHP and TOPSIS approaches. International Journal of Production Research, 43(21), 4609-4641.

Boşluklu Betonarme Kirişlerin Davranışı Üzerine Nümerik Bir Çalışma

A Numerical Study on the Behavior of Reinforced Concrete Beams with Web Openings

Serkan Sağıroğlu[*,1], İrem Şule Gülen[1], Gökhan Barış Sakcalı[1]

[*] serkansagiroglu@uludag.edu.tr, ORCID: 0000-0001-7248-3409
[1] *İnşaat Mühendisliği Bölümü, Bursa Uludağ Ünivesitesi, Bursa, Türkiye*

Özet: Betonarme yapılarda mekanik ve elektrik tesisatı için kullanılan boru ve kabloların projelerinde belirtilen şekilde döşeme ve kiriş alt yüzeyinden geçirilmesi gerekmektedir. Ancak net kat yüksekliğini azalttığı, enerji kaybına sebep olduğu ve birtakım estetik kaygılara yol açtığı gibi gerekçelerle iletim hatlarının kirişlerde imalat esnasında bırakılan veya üretimin tamamlanmasından sonra oluşturulan gövde boşluklarının içinden geçirildiği uygulamalarla sıklıkla karşılaşılır. Ancak gövde boşlukları kirişin yük taşıma kapasitesini, göçme tipini, enerji tüketme kapasitesini, kullanılabilirlik sınır durumlarını olumsuz yönde etkileyebilmektedir. Hâlihazırda imalat süreci tamamlanmış ve kiriş gövdesinde boşluk bulunduran yatay taşıyıcı elemanlara sahip yapıların sayısının azımsanmayacak kadar fazla olduğu unutulmamalıdır. Bu nedenle boşluklu betonarme kirişlerin dayanım ve davranışlarının irdelenmesi oldukça önemlidir.

Bu çalışma kapsamında gövde boşluklarının betonarme kirişlerin performansı üzerindeki etkisi araştırılmıştır. Bu amaçla yedi adet kolon kiriş birleşiminin nümerik modelleri oluşturulmuş ve monotonik yükleme etkisindeki davranışları incelenmiştir. Altı adet dikdörtgen gövde boşluğuna sahip kiriş ve karşılaştırma amacıyla bir adet boşluksuz referans kiriş analiz edilmiştir. Gövde boşluğunun sayısı, boşluğun kiriş yüksekliği boyunca olan konumu ve boşluk boyutu çalışmanın değişkenleri olarak belirlenmiştir. Kirişlerdeki boyuna donatı miktarları sabit tutulmuş ve boşluk çevresine ilave donatı yerleştirilmemiştir. Nümerik modelleri oluşturulan kirişlerin performansı yük taşıma kapasitesi ve enerji tüketme kapasitesi açısından değerlendirilmiştir. Değişen parametrelerin sonuçlar üzerindeki etkisi kıyaslamalar yapılarak sunulmuştur. Elde edilen sonuçlara göre kirişte etriye kaybına neden olan geniş gövde boşluğuna sahip numunede taşıyabileceği maksimum yükün ve enerji tüketme kapasitesinin referans numuneye göre önemli ölçüde azaldığı anlaşılmıştır. Elde edilen bulgulara göre monotonik yükleme altında kirişin çekme bölgesinde açılan boşluğun kiriş davranışında fark edilebilir bir değişikliğe sebep olmadığı, buna karşın basınç bölgesinde açılan boşluğun kirişin yük taşıma kapasitesi ve sünekliliğini azalttığı gözlenmiştir. Kiriş yüksekliğinin orta bölgesinde açılan deliklerin de basınç bölgesindeki delikler kadar olmasa da kirişin yük taşıma kapasitesi ve sünekliliğini azalttığı gözlenmiştir. Kiriş yüksekliğinin orta bölgesinde açılan deliklerin sayısının arttırılmasının (enine donatı kaybı olmadan) davranışı değiştirmediği gözlemlenmiştir. Ancak delik genişliğinin artması ve dolayısıyla enine donatı kaybının yaşanmasının davranışta görülecek olumsuz değişimde en büyük etkiye sahip olduğu bulunmuştur.

Anahtar Kelimeler: *Betonarme, boşluklu betonarme kirişler, kolon-kiriş birleşimi, sonlu elemanlar yöntemi,*

Abstract: In reinforced concrete structures, pipes and cables used for mechanical and electrical installations must be installed according to the project specifications, typically passing through the floor slab and the bottom surface of the beams. However, due to reasons such as reducing the floor height, causing energy loss, and raising aesthetic concerns, it is possible to see beams with web openings that are either left in the beams during manufacturing or created after the completion of production. However, the use of these beams with web openings can negatively affect the load-carrying capacity of the beam, the failure type, ductility and the usability limits. It should not be forgotten that there are a significant number of structures with beams that have openings. Therefore, investigating the strength and behavior of beams with web openings is of considerable importance.

This study investigates the effects of web openings in the beam on the performance of reinforced concrete beams. To this end, numerical models of seven beam-column joints were created, and their behavior were examined under displacement control technique. Six beams with rectangular web openings and one reference beam without any web openings were analyzed for comparison. The number of web openings, the location of the web openings along the beam height, and the size of the web openings were determined as the variables of the study. The amount of longitudinal reinforcement in the beams was kept constant, and no additional reinforcement was placed around the web openings.

The performance of the beams with numerical models was evaluated in terms of load-carrying capacity, failure load, and ductility. The effects of the varying parameters on the results were compared and presented. According to the results, in the beam with a large rectangular web opening close to the support (BRC-6), it was found that the maximum load it could carry, its energy dissipation capacity, and the failure load significantly decreased. Based on the findings, it was observed that the presence of a web opening in the tensile region under push down loading did not cause a noticeable change in the beam's behavior, whereas a web opening in the compression region reduced the beam's load-carrying capacity and ductility. Web openings located in the middle section of the beam height also decreased the beam's load-carrying capacity and ductility, though not as much as web openings in the compression region. It was observed that increasing the number of web openings in the middle section of the beam height did not change the behavior. However, an increase in the web opening width had the most significant negative impact on the behavior.

Keywords: *Reinforced concrete, beams with opennings, beam-column joints, finite element method*

I. GİRİŞ

Bir yapının mekanik ve elektrik tesisatının doğru şekilde projelendirilmesi ve yerleştirilmesi taşıyıcı sisteme ait elemanların projelendirilmesi ve üretimi kadar önemlidir. Yapı içerisinde yer alması zorunlu ve kullanım amacına göre ihtiyaç duyulabilecek ısıtma ve soğutma sistemleri, havalandırma kanalları, sıhhi tesisat boruları, elektrik tesisatına ait iletim kanalları gibi yapının mekanik ve elektrik tesisatı elemanlarının projelerine uygun şekilde konumlandırılmadığı örneklerle sık şekilde karşılaşılmaktadır. Kat net yüksekliğinin korunması, maliyetin azaltılması, enerji kaybının önüne geçilmesi ve estetik kaygılar sebebiyle kirişe denk gelen iletim hatlarının kiriş alt yüzünden geçirilmesinden kaçınılır. Bu gibi nedenlerle kiriş imalatı sırasında veya sonrasında iletim hatlarının geçebileceği boşluklar oluşturulur. Kiriş açıklığı ve yüksekliği boyunca kare, dikdörtgen veya dairesel geometrili, farklı boyutlara sahip gövde boşlukları ile karşılaşılabilmektedir.

Literatür incelendiğinde bugüne kadar kiriş gövde boşluklarının geometrisinin, konumunun, boyutlarının kiriş dayanım ve davranışına etkisinin incelendiği birçok deneysel ve nümerik çalışmanın yapıldığı görülmektedir.

Mansur, Lee, Tan ve Lee yaptıkları çalışmada büyük gövde boşluklarına sahip, boyuna donatı miktarları ve düzenleri eş betonarme kirişlerin dayanım ve davranışlarını deneysel

olarak incelemişlerdir. Çalışmada boşluk boyutu, kiriş açıklıklarının sayısı ve boşluğun açıklıktaki konumunun kirişlerin göçme şeklini nasıl etkilediği araştırılmıştır. Boşluk genişliği ve derinliğinin artmasıyla kiriş mukavemetinin ve rijitliğinin yanında göçme yükünün de azaldığı belirlenmiştir. İncelenen kirişlerde boşluk konumunun çatlama yükü üzerinde neredeyse hiçbir etkisinin olmadığı anlaşılmıştır. Boşlukların, momentin büyük olduğu bölgelerde yer alması durumunda deformasyonları arttığı ve kirişin daha erken göçmesine neden olduğu anlaşılmıştır [1].

Tan, Mansur ve Wei [2] çalışmalarında ACI-318 [3] yönetmeliğinin dairesel gövde boşluklarına sahip betonarme kirişlerin kesme dayanımı için ortaya koyduğu yaklaşımın yeterliliğini incelemektedir. Gövde boşluğuna sahip T kesitli betonarme kirişlerin negatif moment bölgesindeki davranışının anlaşılması amacıyla kirişler ters şekilde test edilmiştir. Yapılan deneyler, boşluk çevresinin yönetmelikte belirtilen şekilde donatılandırılmasıyla kirişin nihai dayanımının korunabileceği ve çatlakların kontrol altında tutulabileceğini göstermiştir. Boşluk etrafına yerleştirilen diyagonal donatı çubuklarının kiriş basınç bölgesindeki gerilmeleri azaltarak betonun erken ezilmesinin önüne geçtiği belirlenmiştir [2].

Mansur, Tan ve Wei [4] T kesitli betonarme kirişlerle ilgili yaptığı çalışmada, var olan yapı elemanlarında delik açılmasının sonuçlarını incelemektedir. Çalışmada dikkate alınan ana parametreler boşluk boyutu ve konumudur. Kirişlerin mesnet bölgelerine yakın açılan deliklerin kiriş dayanımını ve rijitliğini önemli ölçüde azalttığı belirlenmiştir. Kiriş rijitliğinin, kiriş enine donatılarına zarar verilmeden açılan boşluklardan minimum oranda zarar gördüğü tespit edilmiştir. Kiriş gövdesinde açılan delikleri harçla doldurulmuş kirişlerin, kirişin boşluksuz durumundaki eğilme rijitliğine yaklaşmakta yetersiz kaldığı belirtilmiştir [4].

Tan, Mansur ve Huang [5] çalışmalarında büyük gövde boşluklarına sahip T kirişleri pozitif veya negatif moment etkisinde test etmişlerdir. Birden çok boşluğa sahip kirişlerin dayanım ve kullanılabilirlik yönünden tek boşluklu kirişlerden daha iyi performans gösterdiği belirlenmiştir [5].

Mansur ve Paramasivam [6] imalat esnasında bırakılan küçük gövde boşluğuna sahip bir kirişin burulma ve eğilme etkisi altındaki dayanımının belirlenebilmesi için analiz yöntemi sunmuştur. Kiriş dayanımlarının çeşitli göçme modlarında belirlenebilmesi için denklemler de türetilmiştir ve bu denklemlerin deneylerden elde edilen sonuçlarla uyumlu olduğu gözlenmiştir. Boşluk boyutu ve konumunun yanında boşluk çevresi için önerilen ilave donatıların boyut ve yerleşimini de çalışma parametreleri olarak kullanılmıştır. Yapılan deneylerde ilave köşe donatılarının çatlak genişliğini sınırlamada etriyeden daha etkin olduğunu göstermiştir.

Mansur, Tan ve Lee [7] çalışmalarında eğilme ve kesme etkisinde büyük dikdörtgen gövde boşluğuna sahip betonarme kirişlerin tasarlanması için bir yöntem önermektedir. Test sonuçları önerilen yöntemin başarısını ortaya koymuştur. Çalışmada ana parametreler boşluğun boyutu, derinliği, konumu, dışmerkezliği, boşluk çevresindeki donatıların miktarı ve düzenidir. Köşe donatısı olarak kullanılan diyagonal donatıların çatlak genişliği ve sehim kontrolünde kiriş enine donatısından daha etkili olduğu belirlenmiştir. Boşluklu kirişlerin kesme dayanımının %75'inin diyagonal donatılar tarafından karşılandığı belirlenmiştir [7].

Ashour ve Rishi [8] çalışmalarında boyuna donatı oranları ve geometrileri aynı olan gövde boşluğuna sahip betonarme kirişleri test etmiştir. Boşluk boyutu ve konumu deneyin ana değişkenleridir. Sabit tutulan değişkenler sebebiyle boşluk konumuna bağlı olarak 2 farklı göçme modu ile karşılaşılmıştır. Kiriş kapasitesinde boşluk çevresine yerleştirilen dikey donatıların yatay olarak yerleştirilenlerden daha etkili olduğu belirlenmiştir [8].

Berk [9], betonarme kiriş üzerinde açılan tek bir noktadaki boşluğun sebebiyet vereceği gerilme yığılmaları için çözümler araştırmış ve kiriş boyunca bırakılan düzenli boşluklar sayesinde gerilmelerin tüm kirişe yayılması amaçlamıştır. Daire ve kare şeklinde gövde boşluğuna sahip betonarme kirişler kiriş boyutu ve boşluk konumu değiştirilmeden deneye tabi tutulmuştur. Boyuna donatı oranı, boşluk geometrisi, boşluklar arası dikmelerde etriye kullanımı ve çapraz donatı kullanımı değişen deney parametreleridir. Deney sonuçlarına göre değişen parametrelerin kiriş sünekliliğine, kesme davranışına, kiriş dayanımına ve rijitliğine

etkileri araştırılmıştır. Boyuna donatı miktarı fazla olan kirişlerden biri hariç diğer tüm deney elemanları çok sünek davranmıştır. Deney numunelerinin çoğunda yapılan uygulamalar sayesinde referans kirişlerden elde edilen süneklik değerlerinin 1.5-2 katına ulaşılmıştır. Kiriş numunelerinin kesme kırılması yerine eğilmeden göçtüğü belirlenmiş, bir noktada gerilme yığılmalarını önlemek amacıyla düzenli boşluk oluşturulması fikrinin işe yaradığı görülmüştür. Dairesel boşluklu elemanların süneklik, rijitlik ve dayanım değerlerinin kare boşluklu elemanlardan daha yüksek olduğu belirlenmiştir [9].

Aykaç ve Yılmaz [10] çalışmalarında daire veya üçgen şeklinde düzenli büyük boşluklara sahip betonarme kirişlerin düzgün yayılı yük altındaki davranışlarını deneysel olarak araştırmıştır. Düzenli ve kiriş boyunca devam eden boşluklar sayesinde gerilmelerin kirişe dağılacağı bir noktada yığılmayacağı düşünülmüştür. Deney değişkenleri olarak boşluk geometrisi ve çekme bölgesindeki donatı oranı seçilmiştir. Normal ve az çekme donatısına sahip kirişlerin yeterli dayanım gösterdiği belirlenmiştir. Çok donatılı boşluklu kirişler taşıma güçlerini aniden yitirmiş bunun sonucunda çok donatılı kirişlerde istenilen başarının elde edilemediği farklı bir donatı düzenine ihtiyaç duyulduğuna karar verilmiştir. Daire şeklinde boşluklara sahip kirişler üçgen şeklinde boşluklulara göre daha sünek olduğu belirlenmiştir. Bunun yanında dairesel kesitli numunelerin dayanımı daha yüksektir [10].

Kahraman [11] çok sayıda kare gövde boşluğuna sahip betonarme kirişlerin eğilme davranışlarını incelemiştir. Çalışma kapsamında referans boşluksuz kirişler ile boşluklu betonarme kirişlerin sonlu eleman modelleri oluşturulmuş ve bu modellerin analiz sonuçlarıyla literatürdeki deney sonuçları kıyaslanmıştır. Nümerik sonuçlarla deneysel sonuçların yakın ve uyumlu olduğu anlaşılmıştır. Ardından boşluk çevresinde farklı donatı düzenlemeleri yapılmış ve yapılmamış düzenli kare gövde boşluklarına sahip kirişlerin çekme donatısı oranlarının kirişlerin eğilme davranışı, yük taşıma kapasiteleri ve başlangıç rijitliklerinde meydana gelen değişimler üzerindeki etkileri araştırılmıştır [11].

Deifalla ve Elzeiny [12] çalışmalarında gövde boşluğunun betonarme bir kolon kiriş birleşiminin deprem davranışı üzerindeki etkisi araştırmıştır. Boşluk çevresine yerleştirilen ilave donatıların davranışa olan katkısının belirlenebilmesi için ilave donatısız ve ilave donatılı kirişler deneye tabi tutulmuştur. Oluşturulan kolon-kiriş birleşimlerinin çevrimsel yükleme altındaki rijitlikleri, taşıyabildikleri maksimum yük ve buna karşılık gelen deplasman değerleri incelenmiştir. Gövde boşluğunun boyutlarındaki artışın betonarme birleşimin sünekliliğini ve dayanımını azalttığı belirlenmiştir. İlave donatının yerleştirildiği numunelerin davranışlarında iyileşme gözlemlenmiştir [12].

Saleh, Hamad, Elzeny, Elwan ve Deifalla [13] çevrimsel yükleme etkisindeki betonarme bir kolon-kiriş birleşiminde gövde boşluklarının çatlama tipi, göçme modu, rijitliği, yük deplasman eğrileri, dayanım ve süneklik üzerindeki etkileri deneysel olarak incelenmiştir. Gövde boşluklarının boyutları ve kiriş üzerindeki konumu deney parametreleridir. Genel bir sonuç olarak, gövde boşluğuna sahip kolon-kiriş birleşimlerinin yük taşıma kapasitelerinin, deplasmanlarının ve rijitliklerinin azaldığı sonucuna varılmıştır [13].

Bu çalışmada bir adet boşluksuz referans kirişin ve altı adet gövde boşluğu içeren kirişin aşağı yönlü artımsal yükleme etkisinde nümerik analizleri gerçekleştirilmiştir. Kullanılan boşluksuz referans kirişin boyutu ve donatıları [13] tarafından kullanılan referans kiriş numunesiyle aynı seçilmiştir.

II. MALZEME VE MATERYAL

Çalışmada incelenen tüm kirişler bir kolon kiriş birleşim bölgesinin konsol şeklindeki kiriş bölgeleridir. Kolon kiriş birleşimleri T kesitli bir kiriş ve dikdörtgen geometrili bir kolondan oluşmaktadır. T kesitli kirişler 400 mm yüksekliğe ve 150 mm gövde genişliğine sahiptir. Kirişlerin başlık derinliği ve genişliği sırasıyla 60 mm ve 350 mm' dir. Kirişlerin net uzunluğu 1500 mm' dir. Kolon kesiti 350x250 mm boyutlarında ve 2000 mm uzunluğundadır. Kiriş alt ve üst donatıları 16 mm çapında olup başlık içerisinde 10 mm çapında 4 adet boyuna donatı (döşeme donatısı) bulunmaktadır. Kiriş uzunluğu boyunca 120 mm aralıklarla 8 mm çapında

enine donatılar yerleştirilmiştir. Kiriş başlığında 8 mm çapında ilave enine donatılar kullanılmıştır. Numune boyutları ve donatı detayları Şekil 1(a)' da sunulmaktadır. Şekil 1(b)-(g)' de ise incelenen delikli kirişlere ait bilgiler sunulmuştur.

Modelleme aşamasında geometrinin referans alındığı çalışmada [13] yer alan ve malzeme deneylerinden elde edilen veriler kullanılmıştır. Deneysel çalışmada kullanılan betonun 28 günlük silindir basınç dayanımı 20 MPa' dır. Boyuna donatıların akma ve çekme dayanımı sırasıyla 384 MPa ve 570 MPa' dır.. Bu değerler 8 mm çapındaki enine donatı için sırasıyla 282 MPa ve 413 MPa' dır.

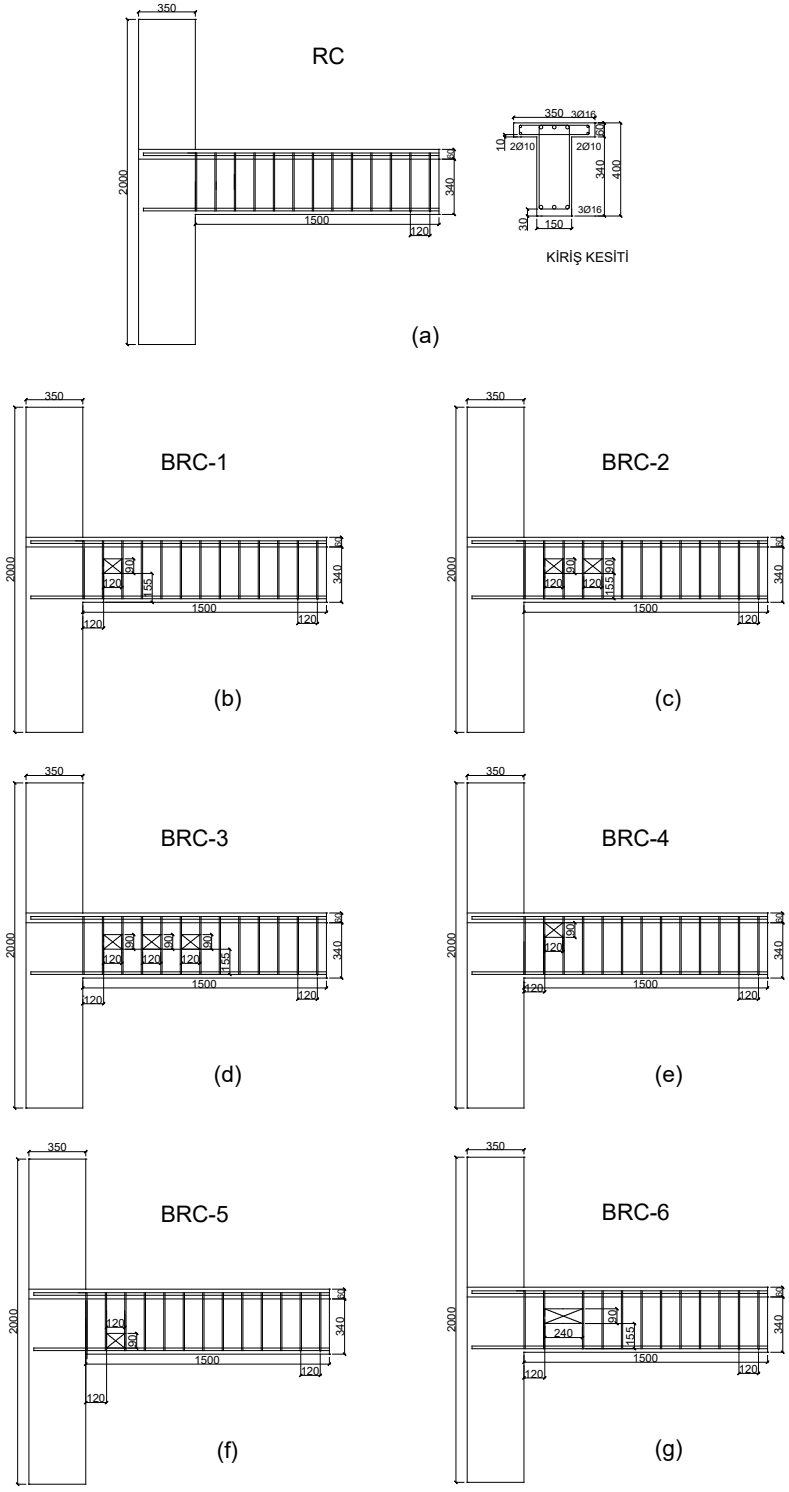

Şekil 1. Kirişlerin geometri ve donatı detayları.

Şekil-1(a)' da görüldüğü gibi kontrol numunesi olarak modellenen referans kirişte (RC) gövde boşluğu bulunmamaktadır. BRC-1 kolon yüzünden 120 mm uzaklıkta 90x120 mm boyutlarında bir adet dikdörtgen geometrili gövde boşluğuna sahiptir (Şekil-1(b)). Sırasıyla BRC-2 ve BRC-3 gövde boşlukları arasında bir enine donatı aralığı 120 mm olacak şekilde 2 ve 3 adet gövde boşluğuna sahiptir (Şekil1-(c) ve(d)). Bu numuneler boşluk sayısındaki değişimin kirişin yük taşıma kapasitesi üzerindeki etkisi için oluşturulmuştur. BRC-4 numunesi kiriş başlığının hemen altında (Şekil-1 (e)) ve BRC-5 numunesi kiriş alt boyuna donatıların hemen üzerinde kolon yüzünden 120 mm uzaklıkta 1 adet boşluğa sahiptir (Şekil 1(f)). Bu iki numunede kiriş gövdesi üzerinde boşluk konumunun etkilerinin araştırılması için kullanılmıştır. Son olarak boşluk boyutlarının değişiminin yarattığı olumsuzlukların anlaşılabilmesi için BRC-6 numunesine 90x240 mm boyutlarında dikdörtgen geometrili bir boşluk yerleştirilmiştir (Şekil 1(g)). Yalnızca BRC-6 numunesinde boşluk ortasına denk gelen enine donatı kaldırılmıştır. Boşluk çevresinde ilave donatı hiçbir numunede kullanılmamıştır.

III. SONLU ELEMANLAR MODELLERİNİN OLUŞTURULMASI

Çalışma kapsamında oluşturulan modellerin analizleri ABAQUS[14] sonlu elemanlar programı kullanılarak yapılmıştır. Kolon-kiriş birleşiminden meydana gelmiş betonarme yapı elemanlarının aşağı yönlü artımsal yükleme etkisinde doğrusal olmayan analizi gerçekleştirilmiştir. Bir adet boşluksuz referans kiriş ve 6 adet dikdörtgen geometrili boşluğa sahip kiriş modellenmiştir. Programa biri doğrusal elastik olmak üzere 2 adet beton malzemesi tanımlanmıştır. Kolonda hasar meydana gelmeyeceği öngörülerek doğrusal elastik malzeme tanımlaması yapılmıştır.

Betonun basınç ve çekme etkisindeki hasar mekanizmalarının tanımlanmasında CDP (Concrete Damage Plasticity) kullanılmıştır. Yapı çeliği için pekleşmeli üç doğrulu malzeme modeli kullanılmıştır.

Beton 3 boyutlu katı (solid) eleman olarak, donatı çubukları çubuk eleman (truss) olarak modellenmiştir. Beton modelinin oluşturulmasında; 3 serbestlik dereceli, 8-düğümlü ve azaltılmış integrasyon noktalı (C3D8R) eleman tipi kullanılmıştır. Donatı elemanları ise eksenel doğrultuda tek serbestlik dereceli, 2-düğüm noktalı, doğrusal (T3D2) eleman tipi kullanılarak modellenmiştir. Beton ve donatı çubukları arasındaki etkileşim tanımlanırken tam aderans kabulü yapan gömülü (embedded) etkileşim kullanılmıştır. Nümerik modeller için oluşturulacak mesnetler [13] çalışmasında deneyleri yapılan numunelerdeki mesnet yerleri ve koşulları dikkate alınarak çizgisel olarak tanımlanmıştır. Kiriş uç noktasından belirli bir mesafeye konumlandırılan yükleme noktası da çizgisel olarak tanımlanmıştır. Yapılan duyarlılık/yakınsama testleri sonucunda mesh aralığı 50 mm olarak belirlenmiştir.

Kolon kiriş birleşimleri için uygulanan tüm analizlerde kolonlar alt ve üst ucundan kayıcı mesnetlerle tutulu şekilde modellenmiştir. Ayrıca kolonun düzlem içi eğilme davranışı da kolonun sağ ve sol uçlarına yerleştirilen kayıcı mesnetlerle engellenmiştir. Kirişler serbest uçlarından aşağı yönlü deplasman kontrollü olarak yüklenmişlerdir.

Şekil 2'de nümerik modeli oluşturulan boşluksuz referans kiriş gösterilmektedir.

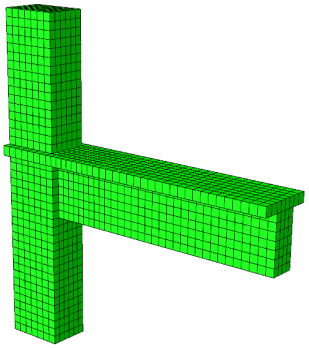

Şekil 2. Oluşturulan referans kiriş (RC) modeli.

IV. BULGULAR

Çalışma kapsamında modellenen yedi adet betonarme kolon kiriş birleşimi için elde edilen yük-deplasman grafiği Şekil 3' te sunulmuştur. Çalışmada incelenen her bir kiriş için nihai yükleme anındaki basınç ve çekme etkilerindeki hasar parametre kontur görselleri Şekil 4-17 arasında sunulmuştur.

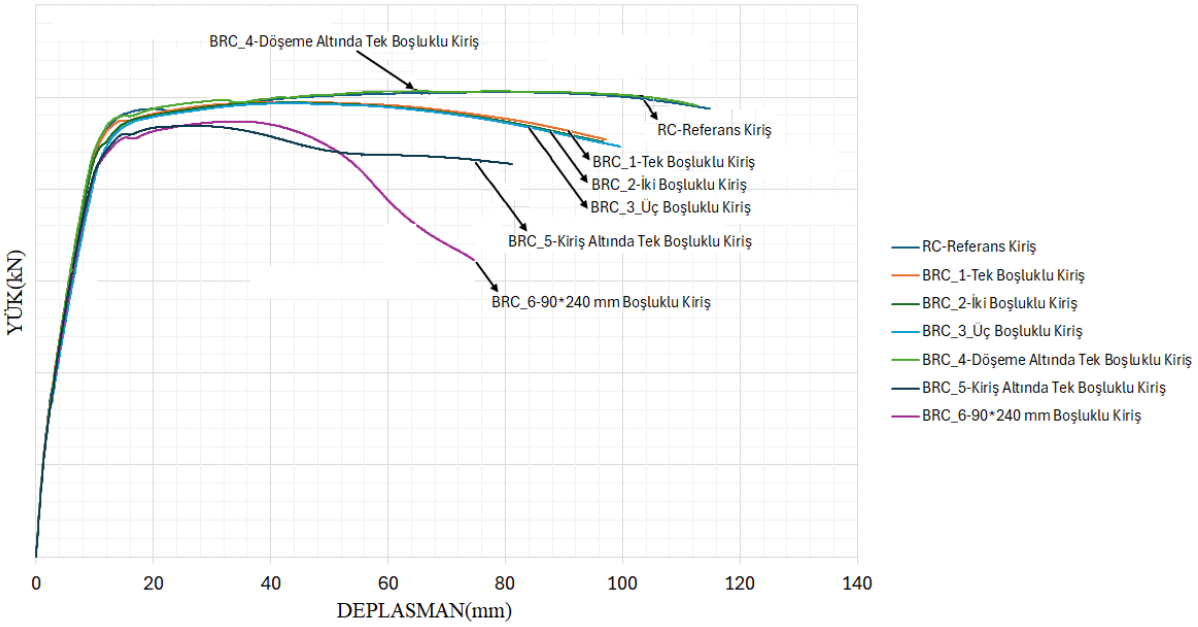

Şekil 3. İncelenen kirişlere ait yük-deplasman grafikleri.

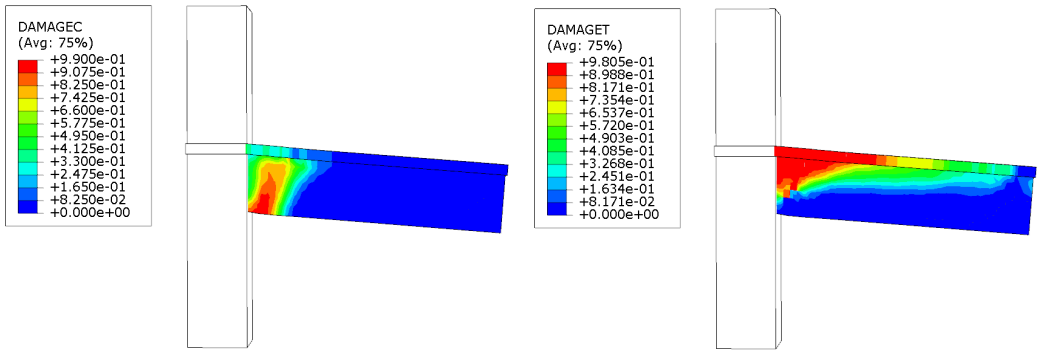

Şekil 4. RC Referans kirişinin basınç ve çekme etkisindeki hasar durumu.

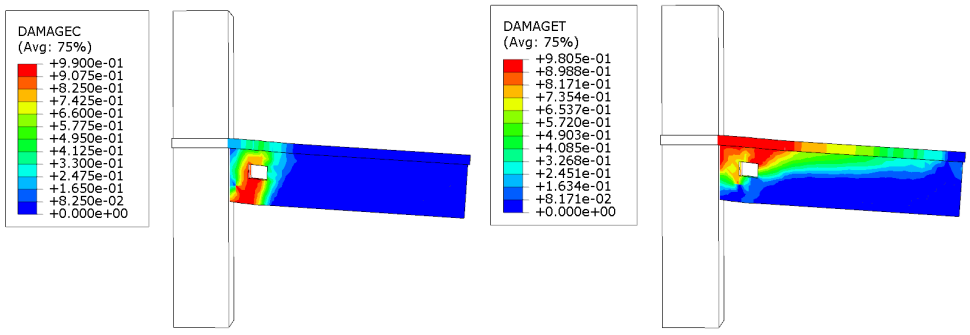

Şekil 5. BRC-1 kirişinin basınç ve çekme etkisindeki hasar durumu.

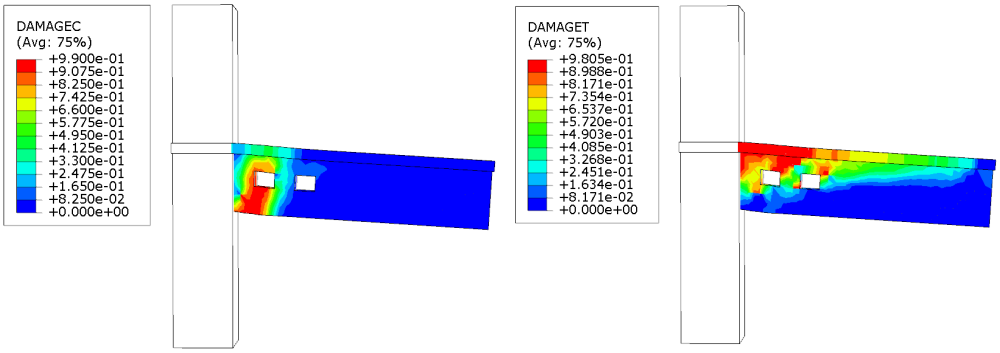

Şekil 6. BRC-2 kirişinin basınç ve çekme etkisindeki hasar durumu.

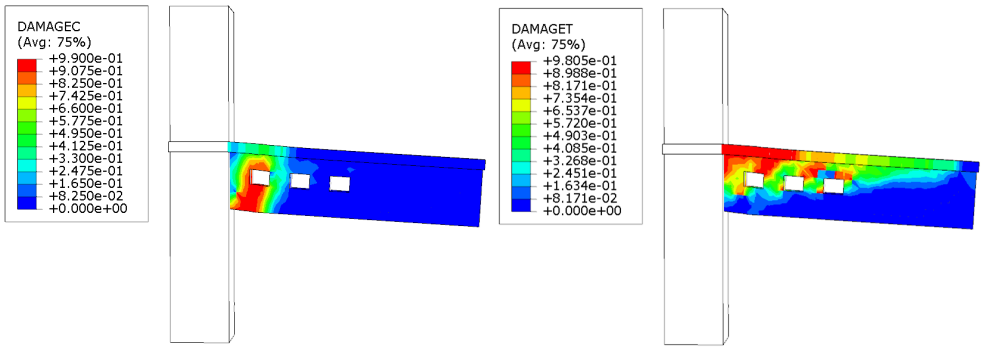

Şekil 7. BRC-3 kirişinin basınç ve çekme etkisindeki hasar durumu.

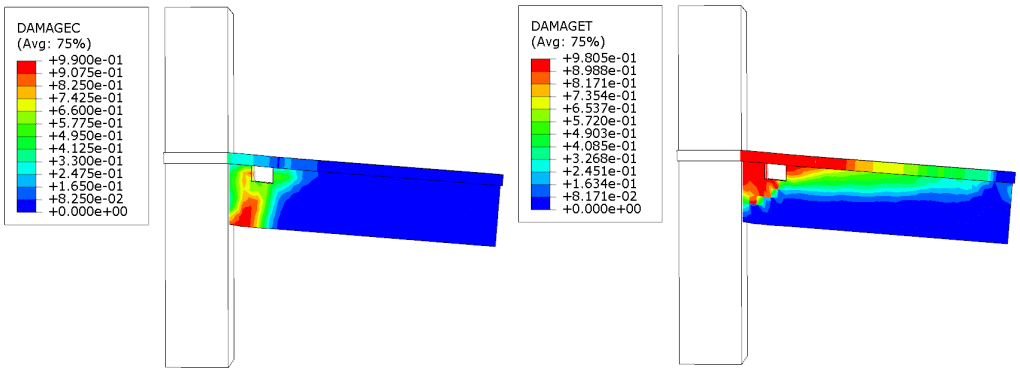

Şekil 8. BRC-4 kirişinin basınç ve çekme etkisindeki hasar durumu.

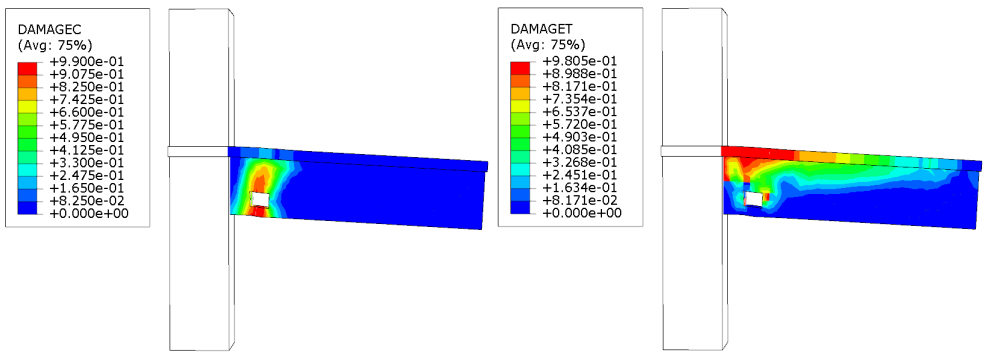

Şekil 9. BRC-5 kirişinin basınç ve çekme etkisindeki hasar durumu.

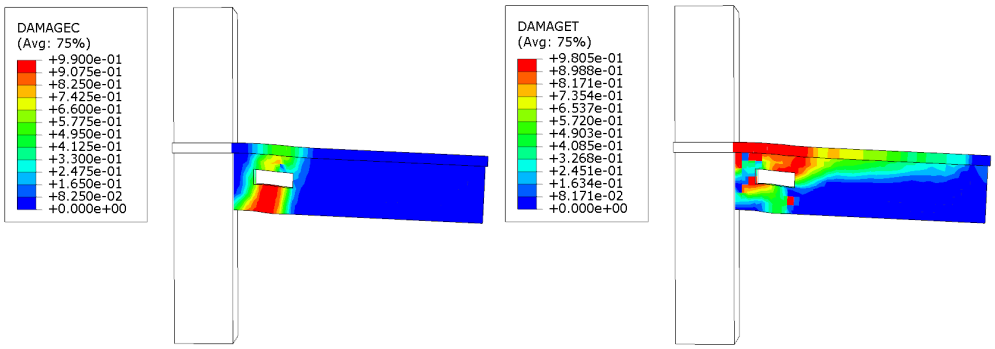

Şekil 10. BRC-6 kirişinin basınç ve çekme etkisindeki hasar durumu.

V. SONUÇLAR

Bu çalışma kapsamında gövde boşluğunun betonarme kirişlerin yük taşıma ve enerji tüketme kapasitelerini ne yönde etkilediği nümerik analizler ile araştırılmıştır.
Yaklaşık olarak kiriş yüksekliğinin yarısı yükseklikte (orta bölgede) bırakılan boşlukların kiriş boyunca sayısının artmasının kirişlerin başlangıç rijitlikleri ve akma yükleri üzerindeki etkisinin oldukça az olduğu görülmüştür. Ancak gövde boşluklarının kirişin enerji tüketme kapasitesini azalttığı sonucuna varılmıştır.

Kiriş derinliği boyunca boşluğun konumunun değiştirilmesiyle kiriş dayanım ve davranışının nasıl değiştiğinin araştırılması için kullanılan kirişler incelendiğinde boşluğun kirişin çekme veya basınç bölgesinde yer almasının farklı sonuçlar ortaya çıkardığı anlaşılmıştır. Kirişin yükleme protokolü nedeniyle basınç bölgesi alt taraftadır. Kiriş gövdesinde yer alan boyuna donatıların hemen üzerinde bir adet gövde boşluğuna sahip BRC-5 numunesinin basınç bölgesindeki beton alanının azalması sebebiyle kirişin yük taşıma kapasitesinin ve enerji tüketme kapasitesinin azaldığı görülmüştür. Kiriş başlığının (döşemenin) hemen altında 1 adet 90x120 mm gövde boşluğuna sahip BRC-4 numunesinin yük taşıma kapasitesinin kiriş alt bölgesinde gövde boşluğu bulunduran BRC-5 numunesinden daha iyi olması kirişin çekme bölgesinde beton katkısının ihmal edilebilecek kadar küçük olmasından kaynaklandığı sonucuna varılmıştır.

Yük deplasman grafikleri incelendiğinde en büyük gövde boşluğuna sahip olan kolon kiriş birleşiminde yer alan enine donatılarından birinin boşluk içerisine denk geldiği için kaldırılması ve boşluk boyutunun diğer numunelerden daha büyük olması sebebiyle yük taşıma kapasitesi ve enerji tüketme kapasitesi diğer numunelerden daha fazla olumsuz yönde etkilenmiştir.

KAYNAKLAR

1] M. A. Mansur, Y. F. Lee, K. H. Tan, And S. L. Lee, "Tests On Rc Continuous Beams With Openings," *J. Struct. Eng.*, Vol. 117, No. 6, Pp. 1593–1606, Jun. 1991, doi: 10.1061/(ASCE)0733-9445(1991)117:6(1593).

[2] K. H. Tan, M. A. Mansur, And W. Wei, "Design Of Reinforced Concrete Beams With Circular Openings," *Struct. J.*, Vol. 98, No. 3, Pp. 407–415, May 2001, doi: 10.14359/10229.

[3] "ACI Code-318-19(22): Building Code Requirements For Structural Concrete And Commentary (Reapproved 2022)." Accessed: Mar. 07, 2024. [Online]. Available: https://www.Concrete.Org/Store/Productdetail.Aspx?Itemıd=318u19&Language=English&Units=Us_Units

[4] M. A. Mansur, K. H. Tan, And W. Wei, "Effects Of Creating An Opening İn Existing Beams," *Struct. J.*, Vol. 96, No. 6, Pp. 899–905, Nov. 1999, doi: 10.14359/785.

[5] K. H. Tan, M. A. Mansur, And L. M. Huang, "Reinforced Concrete T-Beams With Large Web Openings İnpositive And Negative Moment Regions," *Struct. J.*, Vol. 93,

No. 3, Pp. 277–289, May 1996, doi: 10.14359/9687.
[6] M. A. Mansur And P. Paramasivam, "Reinforced Concrete Beams With Small Opening İn Bending And Torsion," *J. Proc.*, Vol. 81, No. 2, Pp. 180–185, Mar. 1984, doi: 10.14359/10677.
[7] M. A. Mansur, K. H. Tan, And S. L. Lee, "Design Method For Reinforced Concrete Beams With Large Openings," *J. Proc.*, Vol. 82, No. 4, Pp. 517–524, Jul. 1985, doi: 10.14359/10364.
[8] A. F. Ashour And G. Rishi, "Tests Of Reinforced Concrete Continuous Deep Beamswith Web Openings," *Struct. J.*, Vol. 97, No. 3, Pp. 418–426, May 2000, doi: 10.14359/4636.
[9] D. Berk, "Düzenli Boşluklara Sahip Betonarme Kirişlerin Davranış Ve Dayanımı," Gazi Üniversitesi Fen Bilimleri Enstitüsü, Ankara, 2008.
[10] S. Aykaç And Ve M. C. Yılmaz, "Düzenli Üçgen Veya Dairesel Boşluklara Sahip Betonarme Kirişlerin Davranış Ve Dayanımı," *J. Fac. Eng. Archit. Gazi Univ.*, Vol. 26, No. 3, Pp. 711–718, Feb. 2013, Accessed: Mar. 07, 2024. [Online]. Available: Https://Dergipark.Org.Tr/En/Pub/Gazimmfd/İssue/6689/88780
[11] E.Kahraman, "Çekme Donatı Oranının Düzenli Kare Boşluklu Betonarme Kirişlerin Eğilme Davranışına Etkisi," T.C. Kırıkkale Üniversitesi Fen Bilimleri Enstitüsü, Kırıkkale, 2018.
[12] A. F. Deifalla And Sherif Elzeiny, "Effect Of Reınforcement Around Web Openıng On The Effect Of Reınforcement Around Web Openıng On The Cyclıc Behavıor Of Exterıor Rc Beam-Column Joınts Cyclıc Behavıor Of Exterıor Rc Beam-Column Joınts Mostafa Hamad," *Futur. Eng. J.*, Vol. 2, No. 1, P. 3.
[13] A. Saleh, M. Hamad, S. Elzeny, S. K. Elwan, And A. Deifalla, "The Behavior Of Rc Exterior Beam-Column Joint With Nearby Beam Unreinforced Web Opening Under Cyclic Loading-Experimental Study," *Iosr J. Mech. Civ. Eng. E-ISSN*, Vol. 14, No. 4, Pp. 22–30, doi: 10.9790/1684-1404072230.
[14] "Abaqus Finite Element Analysis | Sımulıa - Dassault Systèmes." Accessed: Mar. 14, 2024. [Online]. Available: https://Www.3ds.Com/Products/Simulia/Abaqus

Arbitrary Amplitude Solitary Potential in Ultra-Relativistic Degenerate Plasma

Muhammad Asaduzzaman

azaman@phy.kuet.ac.bd, ORCID: 0009-0002-7632-045X
Department of Physics, Khulna University of Engineering and Technology, Khulna-9203, Bangladesh

Abstract: The nonlinear propagation of arbitrary amplitude solitary potential (associated with the self-gravitational field), which are found to exist in a degenerate plasma system consisting of inertial heavy nuclei and non-inertial ultra-relativistic degenerate electron species, have been investigated by employing the pseudo-potential approach. The nonlinear analysis shows that the considered plasma model can support solitary waves with negative potential only. The magnitude of amplitude of the solitary potential first increases and then decreases with the increase of propagation speed. The width of the solitary waves changes linearly with the propagation speed. The implications of our results to some astrophysical plasma systems are briefly mentioned.

Keywords: *Pseudo-potential, Solitary waves, Self-gravitational perturbation, Degenerate pressure, Relativity*

I. INTRODUCTION

Degenerate matter, which are supported mainly by quantum mechanical effects, exist in the cores of dead stars. In physics, "degenerate" refers to two states that have the same energy and are thus interchangeable. Degenerate matter is supported by the Pauli exclusion Principle, which prevents two fermionic particles from occupying the same quantum state. Unlike regular plasma, degenerate plasma expands little when heated, because there are simply no momentum states left. Consequently, degenerate stars collapse into very high densities. More massive degenerate stars are smaller, because the gravitational force increases, but pressure does not increase proportionally. Electron-degenerate matter is found inside white dwarf and neutron stars.

The degenerate quantum plasmas occurring in high densities or low temperatures are those, which obey the laws of quantum mechanics and in which the mean inter-particle distance becomes comparable to the mean de Broglie wavelength of the lightest plasma particles, and the effects of degeneracy become significant. The most common examples of degenerate quantum plasmas are white dwarfs and neutron stars, where the particle number density is extra-ordinarily high [1-6]. The constituents of neutron star are mainly electrons, nucleons, and extremely heavy nuclei/element [7-9]. In the dense stars like white dwarfs and neutron stars, the self-gravitational attraction counterbalances the degenerate pressure to keep the dense star from further gravitational shrinking or collapse.

For ultra-relativistic limit, the pressure balance equation given by Chandrashekhar [2-4] is $P_e = K_e n_e^{4/3}$, where $K_e = 3\hbar c/4$; P_e represents the electron degenerate pressure; n_e represents the electron number density and K_e is the constant of proportionality.

The propagation of nonlinear waves in degenerate quantum plasma have been studied by many authors [10-19]. Mahmood *et al.* [15] studied the propagation of nonlinear wave in a magnetized electron-positron-ion plasma. Michael *et al.* [17] examined ion-acoustic waves in

a magnetized, five component cometary plasma. Manfredi [19] illustrated several mathematical models to describe the dynamics of a quantum plasma in the collision-less regime.

The physics of nonlinear self-gravitational perturbation, which has not been studied by the above authors, is very important for understanding the salient features of astrophysical compact objects like white dwarfs and neutron stars. Therefore, in our present work, we have investigated the nonlinear propagation of arbitrary amplitude solitary potential structures associated with the self-gravitational field in a degenerate quantum plasma system consisting of non-inertial ultra-relativistic degenerate electrons and inertial heavy nuclei.

The manuscript is organized in the following fashion: Section II contains the Governing equations. Subsections II*A* and II*B* contains derivation of Pseudo-potential and analysis of arbitrary amplitude solitary potential structures, respectively. Section III includes the results and finally section IV represents conclusion.

II. GOVERNING EQUATIONS

We consider a self-gravitating, super dense degenerate quantum plasma system consisting of non-inertial ultra-relativistic degenerate electrons and inertial heavy nuclei. At equilibrium, we have $n_{e0} = Z_h n_{h0}$, where n_{e0} is the electron number density at equilibrium and n_{h0} is the heavy nuclei number density at equilibrium.

The dynamics of arbitrary amplitude self-gravitational solitary potential in the plasma system under consideration can be expressed as

$$\frac{K_e}{m_e N_e}\frac{\partial N_e^{4/3}}{\partial X} + \frac{\partial \Psi}{\partial X} = 0\,, \tag{1}$$

$$\frac{\partial N_h}{\partial T} + \frac{\partial}{\partial X}(N_h U_h) = 0, \tag{2}$$

$$\frac{\partial U_h}{\partial T} + U_h\frac{\partial U_h}{\partial X} = -\frac{\partial \Psi}{\partial X}\,, \tag{3}$$

$$\frac{\partial^2 \Psi}{\partial X^2} = \omega_{jh}^2\left[\left(\frac{N_h}{n_{h0}} - 1\right) + \beta\left(\frac{N_e}{n_{e0}} - 1\right)\right], \tag{4}$$

where the self-gravitational potential is defined by Ψ; the nucleus fluid speed is expressed by U_h; the electron number density is defined by N_e; the heavy nucleus number density is denoted by N_h; the rest mass of electron and heavy nucleus are defined by m_e and m_h respectively; the space variable and time variables are expressed by X and T respectively; $K_e = 3\hbar c/4$; $\omega_{jh}^2 = 4\pi G m_h n_{h0}$; c is the speed of light; G is the universal gravitational constant; N_h and N_e are the unperturbed number densities of nondegenerate heavy nuclei and degenerate electrons, respectively.

In the abovementioned plasma model, the ultra-relativistic degenerate electrons provide the restoring force and the heavy nuclei provides the inertia. The continuity and momentum balance equation for electron is unnecessary because we get the value of N_e directly from Eq. (1).

The explanation for the validity of Eqs. (1) - (4) describing the dynamics of arbitrary amplitude solitary potential in the considered plasma system is given below:

(i) Equation (1) is the pressure balance equation, where gravitational shrinking (inward pull due to self-gravitational attraction) counterbalances the outward degenerate electron pressure.

(ii) Equation (2) is the continuity equation for inertial heavy nuclei/element.

(iii) The momentum balance equation for heavy nuclei is presented in Eq. (3).

(iv) The Poisson's equation for the self-gravitational potential is expressed in Eq. (4) which is obtained from the equation $\frac{\partial^2 \Psi}{\partial X^2} = 4\pi G[m_h(N_h - n_{h0}) + m_e(N_e -$

$n_{e0})]$, where N_h and N_e are the unperturbed number densities of the heavy nuclei and degenerate electrons, respectively.

The normalized forms of Eqs. (1) – (4) can be written as

$$n_e = (1-\alpha\psi)^3 \tag{1a}$$

$$\frac{\partial n_h}{\partial t} + \frac{\partial}{\partial x}(n_h u_h) = 0, \tag{2a}$$

$$\frac{\partial u_h}{\partial t} + u_h \frac{\partial u_h}{\partial x} = -\frac{\partial \psi}{\partial x}, \tag{3a}$$

$$\frac{\partial^2 \psi}{\partial x^2} = \gamma[(n_h - 1) + \beta(n_e - 1)], \tag{4a}$$

where $n_h = \frac{N_h}{n_{h0}}$, $n_e = \frac{N_e}{n_{e0}}$, $\psi = \frac{\Psi}{C_q^2}$, $u_h = \frac{U_h}{C_q}$, $C_q = \sqrt{\frac{\pi\hbar^2 n_{e0}^{2/3}}{m_e^2}}$, $L_q = \frac{\pi\hbar}{m_e c}$, $x = \frac{X}{L_q}$, $t = \frac{T}{(L_q/C_q)}$, $\gamma = \frac{\omega_{jh}^2 L_q^2}{C_q^2}$ and $\alpha = \frac{L_q n_{e0}^{1/3}}{3}$.

A. Derivation of the Pseudo-potential

To examine the fundamental characteristics of arbitrary amplitude solitary potential structures in the considered degenerate quantum plasma system, we assume that the dependent variables in the governing equations depend only on a single variable [8]

$$\xi = x - Mt, \tag{5}$$

where M is the speed of propagation of the solitary potential structure.

Substituting Eqs. (5) into Eqs. (2a) and (3a), and applying the boundary conditions, viz., $\psi \to 0$, $u_h \to 0$ and $n_h \to 1$ at $\xi \to \pm\infty$, we obtain the number density of heavy nuclei in the stationary frame as

$$n_h = \frac{1}{\sqrt{1-\frac{2\psi}{M^2}}}. \tag{6}$$

Now, substituting Eqs. (1a), (5) and (6) into Eq. (4a), we obtain

$$\frac{d^2\psi}{d\xi^2} = \gamma\left[\left(\frac{1}{\sqrt{1-\frac{2\psi}{M^2}}} - 1\right) + \beta\{(1-\alpha\psi)^3 - 1\}\right]. \tag{7}$$

Multiplying both sides by $\frac{d\psi}{d\xi}$, integrating once and applying the boundary conditions, viz., $\psi \to 0$, $\frac{d\psi}{d\xi} \to 0$ at $\xi \to \pm\infty$, we obtain

$$\frac{1}{2}\left(\frac{d\psi}{d\xi}\right)^2 + V(\psi) = 0. \tag{8}$$

The above equation is the energy integral for the self-gravitational potential ψ and $V(\psi)$ is the Pseudo-potential which is given by

$$V(\psi) = \gamma M^2\left[\sqrt{1-\frac{2\psi}{M^2}} - 1\right] + \gamma(1+\beta)\psi + \frac{\beta\gamma}{4\alpha}[(1-\alpha\psi)^4 - 1]. \tag{9}$$

According to McLaurin series expansion, the Pseudo-potential $V(\psi)$ can be written as

$$V(\psi) = -\frac{1}{2}A_2\psi^2 - \frac{1}{2}A_3\psi^3 - \frac{1}{2}A_4\psi^4 - \cdots, \quad (10)$$

where

$$A_2 = \left(\frac{\gamma}{M^2} - 3\alpha\beta\gamma\right), A_3 = \left(\frac{\gamma}{M^4} + 2\alpha^2\beta\gamma\right), A_4 = \left(\frac{5\gamma}{4M^6} - \frac{\alpha^3\beta\gamma}{2}\right).$$

Near $\psi \approx 0$, Eq. (10) becomes

$$V(\psi) \approx -\frac{1}{2}A_2\psi^2 - \frac{1}{2}A_3\psi^3. \quad (11)$$

The existence of solitary potential structures (SPSs) in the parametric regime can be investigated by introducing the convexity requirement, which is given by $\frac{d^2V(\psi)}{d\psi^2}\Big|_{\psi=0} \leq 0$. We can get one limit of M (say M_1) from the convexity requirement for the existence of solitary structures. From Eq. (11), we found that $V(0) = 0$ and $\frac{dV(\psi)}{d\psi}\Big|_{\psi=0} = 0$. The energy integral defined by Eq. (8) provides SPSs if $\frac{d^2V(\psi)}{d\psi^2}\Big|_{\psi=0} < 0$ and in this case $A_2|_{(M=M_1=M_c)} = 0$ gives the critical value of $M(M_c)$ below which the SPSs exist. Applying the critical value condition, viz., $M = M_1 = M_c, \psi = 0$ and $\frac{d^2V(\psi)}{d\psi^2}\Big|_{\psi=0} = 0$, we get $M_1 = M_c = 1/\sqrt{3\alpha\beta}$.
The other limit of M can be obtained by introducing the density compression condition ($V(\psi_c) \geq 0$). In our considered model, ψ is limited to $\psi_c = \frac{M_2^2}{2}$ (beyond which the heavy nuclear number density remains undefined), or to $\psi_c = \frac{1}{\alpha}$ (beyond which the electron number density remains undefined). These two limits indicate the second value of M which is given by $M_2 = \sqrt{2/\alpha}$. Therefore, the SPSs exists between the propagation speed M_1 and M_2.

B. Arbitrary Amplitude SPSs

Now, we want to study the fundamental characteristics of arbitrary amplitude SPSs by examining Eq. (9) in terms of various parameters. Equation (11) discloses that $V(\psi)$ and $\frac{dV(\psi)}{d\psi}$ are 0 at $\psi = 0$. This means that the solitary wave solution of Eq. (9) exists if and only if $\frac{d^2V(\psi)}{d\psi^2}\Big|_{\psi=0} < 0$. It is observed that the Pseudo-potential $V(\psi)$ is nonzero for $M < M_1$ ($M_1 = M_c$) and $\psi < 0$, and this condition gives the probability of the formation of negative potential structures (as shown in Fig. 1). From Eqs. (11) and $A_3 = \left(\frac{\gamma}{M^4} + 2\alpha^2\beta\gamma\right)$, SPSs exist with $\psi < 0$ because $A_3 > 0$ for any value of the parameters involved in A_3.

It has already mentioned that the SPSs exist only with $\psi < 0$ for $M_2 < M < M_1$ in a degenerate plasma system like white dwarfs and neutron stars. To verify the condition for the existence of SPSs, we have numerically analyzed the Pseudo-potential $V(\psi)$. The results obtained the numerical analysis are displayed in Figs. 1, 2, 3, 4 and 5 showing the formation of arbitrary amplitude SPSs in neutron stars.

Figs. 1, 2, 3, 4 and 5 clearly indicates that (1) arbitrary amplitude SPSs with $\psi < 0$ can be formed in astrophysical compact objects like nuetron stars; (2) the magnitude of amplitude of SPSs increases when M increases up to $M = 8$ and then decreases when M increases from 8, which is shown in Fig. 3; (3) the width of the SPSs first increases and then decreases with increasing M.

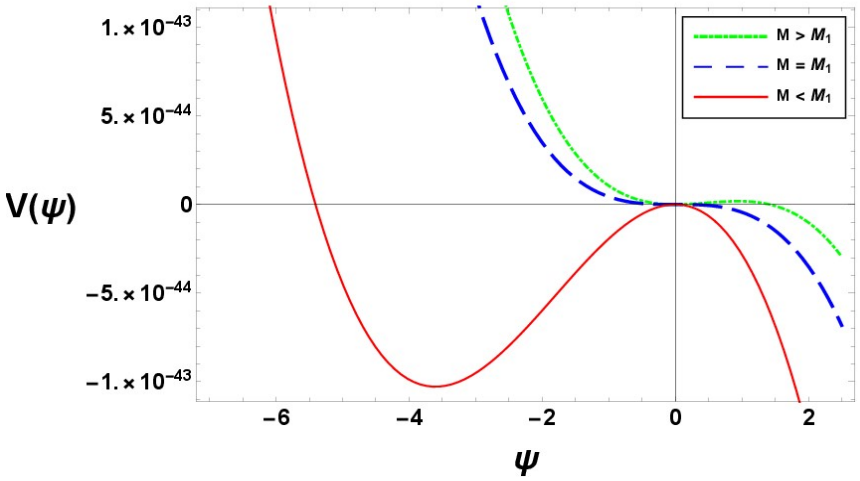

FIG. 1: Behavior of an arbitrary amplitude Pseudo-potential for different values of M. The other parameters are fixed at $n_{e0} = 10^{30}$ cm^{-3}, Z_h =8, and $M_h = 16m_p$ (m_p represents the mass of proton).

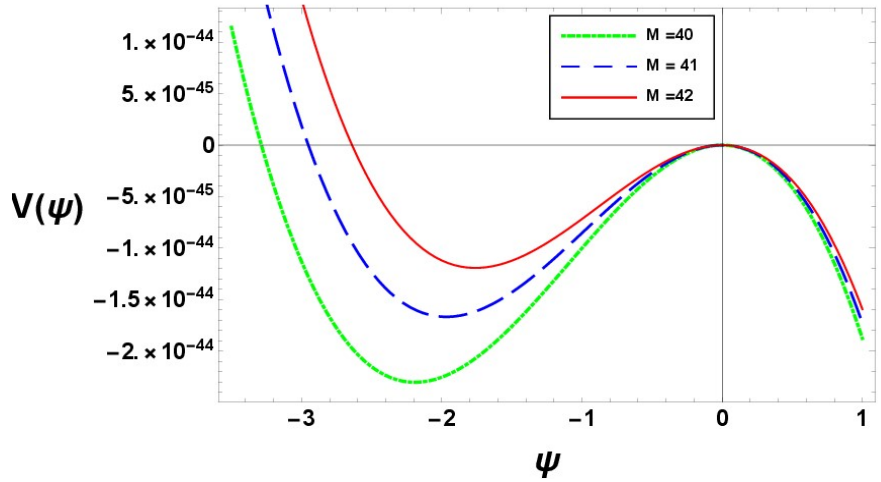

FIG. 2: Formation of arbitrary amplitude SPSs for different values of M with $n_{e0} = 10^{30}$cm^{-3}, Z_h =8, and $M_h = 16m_p$.

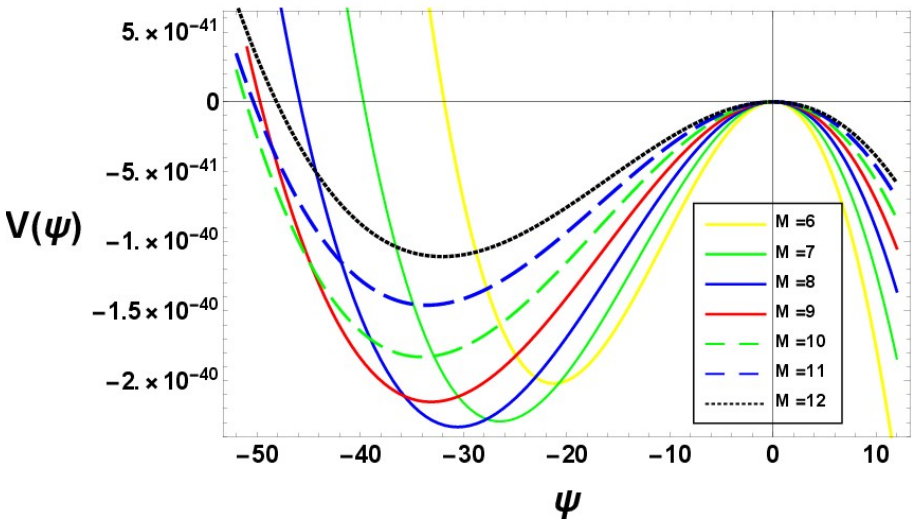

FIG. 3: Variation of arbitrary amplitude SPSs for different values of M. Other parameters are fixed at $n_{e0} = 10^{30}$ cm^{-3}, Z_h =8, and $M_h = 16m_p$.

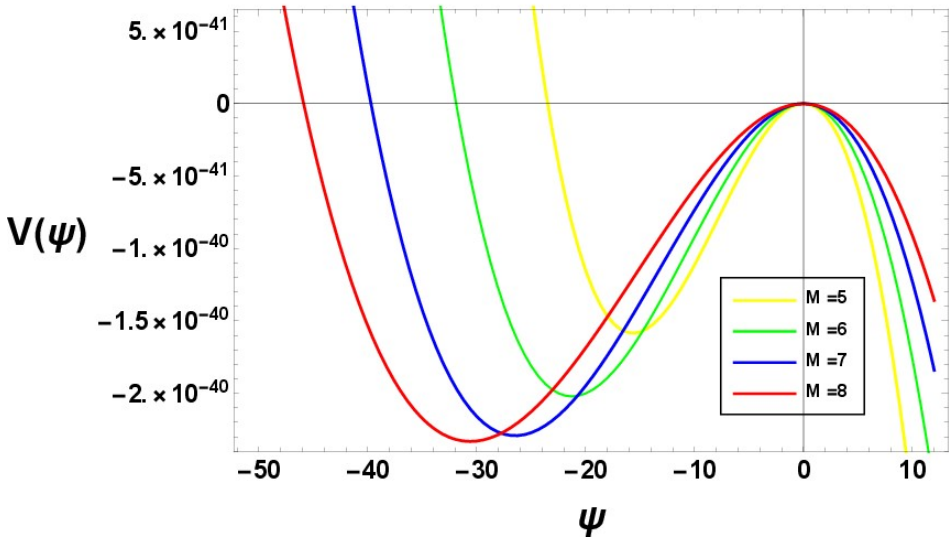

FIG. 4: Variation of arbitrary amplitude SPSs for different values of M when $M \leq 8$. The other parameters are fixed at $n_{e0} = 10^{30}$ cm^{-3}, Z_h =8, and $M_h = 16m_p$.

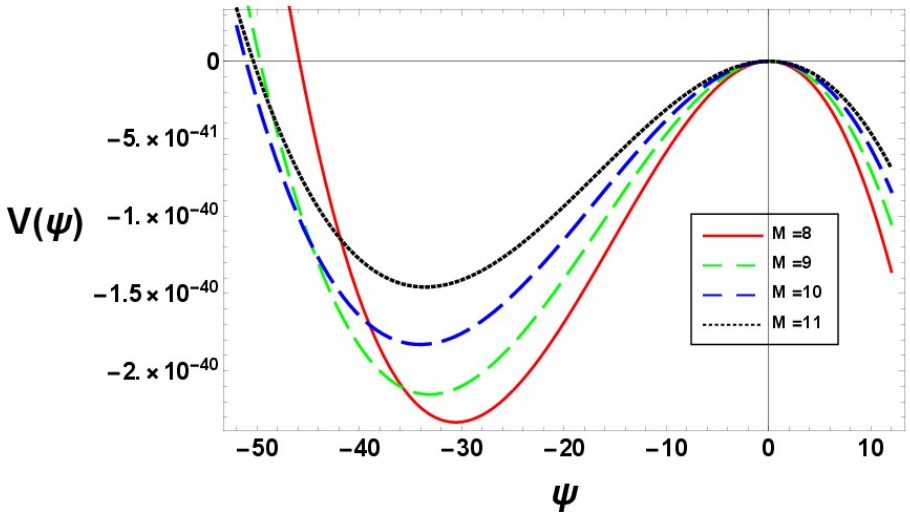

FIG. 5: Variation of arbitrary amplitude SPSs for different values of M when $M \geq 8$. The value of other parameters: $n_{e0} = 10^{30}$ cm^{-3}, Z_h =8, and $M_h = 16m_p$.

III. RESULTS

The results obtained from our current investigation can be pinpointed as follows:

i) The considered plasma model supports negative SPSs only, i.e., only SPSs with $\psi < 0$ can exist.

ii) The arbitrary amplitude SPSs exists in the range $M_2 < M < M_1$.

iii) The amplitude of a SPSs approaches zero for $M \geq M_1$ and for $M \leq M_2$.

iv) The magnitude of amplitude of the SPSs increases when the Mach number M increases up to 8 and then decreases when M increases from 8 (shown in Fig. 3).

v) The width of the SPSs increases when the Mach number M increases from M_2.

vi) As the number density increases, the potential structures become spiky.

IV. CONCLUSION

We have considered a self-gravitating degenerate quantum plasma system consisting of ultra-relativistic inertialess degenerate electrons and inertial nondegenerate heavy nuclei. We have then studied the fundamental characteristics of arbitrary amplitude solitary structures associated with the self-gravitational potential in the considered plasma system. To study arbitrary amplitude SPSs, we have derived the Pseudo-potential and then have numerically analyzed. It may be stressed that the results obtained from our current study concerning the arbitrary amplitude SPSs and their basic features (amplitude, width, etc.) presented here are correct both numerically and analytically and will be useful in understanding the salient features of the solitary self-gravitational potential in degenerate quantum plasmas, which exist in astrophysical compact objects like white dwarfs and neutron stars.

REFERENCES

[1] S. Chandrasekhar, "Dynamical instability of gaseous masses approaching the Schwarzschild limit in general relativity," *Physical Review Letters,* Vol. **12**, no. 15, pp. 437-438, Jan. 1964.

[2] S. Chandrasekhar, "The density of white dwarf stars", *The London, Edinburgh, and Dublin Philosophical Magazine and Journal of Science,* Vol. 11, no. **70**, pp. 592-596, Feb. 1931.

[3] S. Chandrasekhar, "The maximum mass of ideal white dwarfs", *Astrophysical Journal,* Vol. **74**, pp. 81, Jul. 1931.

[4] S. Chandrasekhar, "The highly collapsed configurations of a stellar mass", *Monthly Notices of the Royal Astronomical Society,* Vol. 91, pp. 456-466, Mar. 1931.

[5] S. Chandrasekhar and R. F.Tooper, "The Dynamical instability of the white-dwarf configurations approaching the limiting mass," *Astrophysical Journal, Vol.* **139**, pp. 1396, May. 1964.

[6] A. A. Mamun, "Self-gravito-acoustic shock structures in a self-gravitating, strongly coupled, multi-component, degenerate quantum plasma system," *Physics of Plasmas*, Vol. **24**, no. 10, Oct. 2017.

[7] A. A. Mamun and P. K. Shukla, "Solitary waves in an ultrarelativistic degenerate dense plasma," *Physics of Plasmas*, Vol. 17, no. 10, pp. 104504, Oct. 2010.

[8] A. A. Mamun and P. K. Shukla, "Arbitrary amplitude solitary waves and double layers in an ultra-relativistic degenerate dense dusty plasma," *Physics Letters A*, Vol. 374, no. 41, pp. 4238-4241, Sep. 2010.

[9] S. L. Shapiro and S. A. Teukolsky, Black Holes, White Dwarfs, and Neutron stars, "The Physics of Compact Objects," *Wiley, New York*, 19832, pp. 119-123, 1983.

[10] M. Marklund and G. Brodin, "Dynamics of spin-1 2 quantum plasmas,"*Physical Review Letters,* Vol. **98**, no. 2, pp. 025001, Jan. 2007.

[11] P. K. Shukla and B. Eliasson, "Formation and dynamics of dark solitons and vortices in quantum electron plasmas," *Physical Review Letters,* Vol. **96**, no. 24, pp. 245001, Jun. 2006.

[12] F. Haas, "Variational approach for the quantum Zakharov system," *Physics of Plasmas,* Vol. **14**, no. 4, pp. 042309, Apr. 2007.

[13] M. A. Hossen and A. A. Mamun, "Nonlinear ion-acoustic waves in a degenerate plasma with nuclei of heavy elements," *Physics of Plasmas,* Vol. **22**, no. 10, pp. 102710, Oct. 2015.

[14] M. R. Hossen and A. A. Mamun, "Electrostatic solitary structures in a relativistic degenerate multispecies plasma," *Brazilian Journal of Physics,* Vol. **44**, pp. 673-681, Dec. 2014.

[15] S. Mahmood, A. Mushtaq and H. Saleem, "Ion acoustic solitary wave in homogeneous magnetized electron-positron-ion plasmas," *New Journal of Physics,* Vol. **5**, no. 1, pp. 28, Apr. 2003.

[16] B. Hosen, M. Amina and A. A. Mamun, "Korteweg-de Vries-Burgers equation in a multi-component magnetized plasma with nuclei of heavy elements," *Journal of the Korean Physical Society,* Vol. **69**, pp. 1762-1770, Dec. 2016.

[17] M. Michael, A. Varghese, N. T. Wilington, S. Sebastian, D. E. Savithri, G. Sreekala and C. Venugopal, "Oblique io-acoustic shock waves in a magnetized, multi-species plasma," *In Journal of Physics: Conference Series,* Vol. **836**, no. 1, pp. 012007, Apr. 2017.

[18] A. P. Misra and S. Samanta, "Quantum electron-acoustic double layers in a magnetoplasma," *Physics of Plasmas,* Vol. **15**, no. 12, pp. 123307, Dec. 2008.

[19] G. Manfredi, "How to model quantum plasmas," *Fields Inst. Commun.*, Vol. 46, pp. 263-287, Apr. 2005.

Modeling the light-dependent growth kinetics of the green microalga *Chlorella zofingiensis*

Erdinc ALADAĞ

erdincaladag@gmail.com, ORCID: 0000-0003-1354-0930
Department of Environmental Engineering, Van Yuzuncu Yil University, Van, Turkey

Abstract: Microalgae are photosynthetic microorganisms used as feedstock in many fields, from biofuels to food sources. In this research, *Chlorella zofingiensis*, a green microalgae species that is widely cultivated due to its ability to obtain a variety of products and its applicability in various industrial sectors, was used. Microalgae biomass productivity is affected by many environmental factors such as temperature, light, salinity and nutrient composition. Light intensity plays a key role in microalgae cultivation under autotrophic conditions. The relationship between light intensity and growth rate was investigated using Monod and Haldane kinetic models. The specific growth rates of microalgae cultivated at different light intensities of 25, 50, 100, 250 and 500 μmol photon m^{-2} s^{-1} were calculated as 0.25, 0.31, 0.35, 0.34 and 0.33 d^{-1}, respectively. When the light intensity was increased from 25 to 100 μmol photon m^{-2} s^{-1}, the specific growth rate increased by approximately 40%. The kinetic constants of the Monod equation μ_{max} and K_I were found as 0.36 d^{-1} and 10.70 μmol photon m^{-2} s^{-1}, respectively. The kinetic constants of the Haldane equation μ_{max}, K_I and K_i were found to be 0.42 d^{-1}, 17.11 μmol photon m^{-2} s^{-1} and 1991.26 μmol photon m^{-2} s^{-1}, respectively. *RMSE* and R^2 were calculated to determine the goodness of fit of the Monod and Haldane models with experimental data. *RMSE* values were found to be 0.018 and 0.006 and R^2 values were found to be 0.82 and 0.98, respectively. According to both performance criteria, it can be said that the Haldane model explains the light-dependent microalgal growth better. Mathematical models can be used to predict microalgal growth and optimize operational parameters. These useful tools minimize the necessity for labor-intensive and expensive experiments.

Keywords: *Microalgae, Light, Modelling, Chlorella zofingiensis, Monod, Haldane.*

I. INTRODUCTION

Microalgae are small single-cell plant-like microorganisms that have gained increasing economic and ecological importance in recent years. They produce biomass utilizing carbon dioxide, the primary greenhouse gas, and sunlight, an unlimited natural resource [1]. They also use nutrients such as nitrogen and phosphorus, which are abundant in municipal and industrial wastewater [2]. Furthermore, marine microalgae can grow in salt water instead of drinking water, making it easier to provide water for large-scale cultivation [3]. Besides all these contributions to environmental recycling, microalgae are a source of raw materials for numerous high-value added products that can be utilized in a wide variety of industries such as food, cosmetics, pharmaceuticals, etc [4]. Moreover, microalgal biomass is one of the most hopeful alternatives for biofuel feedstocks owing to its promising sustainable advantages as well as its productivity potential compared to traditional terrestrial crops [5].

Microalgal growth is affected by various environmental conditions. Light intensity is among the most important of these. Light is one of the main requirements for microalgae to grow

autotrophically and is the main source for photosynthetic activity [6]. Light provides the means for cellular multiplication, respiration and photosynthesis [7]. In general, photosynthesis involves light-dependent reactions and dark reactions [8]. During the photosynthesis, photons are absorbed and transformed into energy carriers, and oxygen is released as a by-product of the photolysis [9]. The optimum light intensity required by microalgae for growth and multiplication varies according to species, environmental conditions and nutrient medium composition [10]. Microalgal biomass production generally increases with light intensity. This is due to the utilization and higher absorption of photosynthetic activity in dependence on light intensity [11]. However, the quantity of light, like many other resources, has a saturation point. At higher light intensities beyond this saturation point, photo-inhibition is observed due to photo-oxidation reactions taking place inside the cell, light receptors are damaged and consequently cellular growth is disrupted [12]. This saturation point varies according to the microalgae species and cultivation conditions. Light-dependent growth models are also often used to describe the relationship of microalgae and light irradiance and to determine the saturation point.

Kinetic models are essential tools for the description and characterization of the growth patterns of microalgae [13]. They help to understand how multiple variables affect microalgal growth. They predict biomass concentration under different experimental conditions and thus providing a better understanding of the mechanisms that control microalgal growth [14]. Kinetic models support optimization of bioreactor design, culture conditions, process control, and cultivation strategies [4]. Therefore, they are essential to unlock the full potential of microalgae. They also provide a systematic framework for understanding and controlling their growth dynamics.

This study aims to evaluate the performance of light-dependent microalgal growth kinetic models, focusing on the effect of light intensity on biomass production. *Chlorella zofingiensis*, a widely used microalgae species, was grown at different light intensities and its biomass productivity was periodically monitored. Specific growth rates in the exponential growth phase and kinetic constants of two mathematical models, Monod and Haldane, were determined. Then, the fitting performance of both models with respect to the experimental data was analyzed and the most accurate kinetic growth model was determined.

II. MATERIAL AND METHOD

A. Microalgal Strain and Medium

The green microalga strain *Chlorella zofingiensis* Dönz 1934 (CCALA 944) was obtained from the laboratory of Culture Collection of Autotrophic Organisms (CCALA), Czech Republic was used as the model microalga in this study. First, microalgae were seeded on agar plates. Then, the stock culture was prepared by inoculating pure culture from agar medium into modified Bold's Basal Medium (mBBM) [15] in a Roux bottle. mBBM contains 2.94 mM $NaNO_3$, 0.17 mM $CaCl_2$, 0.30 mM $MgSO_4$, 0.43 mM K_2HPO_4, 1.00 mM KH_2PO_4, 0.43 mM NaCl, 0.17 mM EDTA, 18 µM $FeSO_4$, 0.18 mM H_3BO_3, 61 µM $ZnSO_4$, 15 µM $MnCl_2$, 10 µM MoO_3, 13 µM $CuSO_4$, and 3.3 µM $CoNO_3$. The medium was adjusted to pH 7 and autoclaved before use. The pH of the medium was adjusted to 6.8 and autoclaved prior to use.

B. Microalgal Cultivation

Microalgae were inoculated into 250 mL flasks at 10% by volume with a total volume of 100 mL. The cultures were grown at a temperature of 25±1 °C, agitation speed of 100 rpm and 16:8 light:dark ratio. The batch studies were conducted at 6 different light intensities: 0 (control), 25, 50, 100, 250 and 500 µmol photon m^{-2} s^{-1}. All surfaces of the flasks except the bottom of the flasks were covered with aluminum foil so that the experiments could be carried out simultaneously and under equal conditions. An illumination system consisting of 6 LED

was placed at the bottom of each flask and the light intensity was adjusted using a photometer.

C. Measurement of Microalgal Biomass

The growth of microalgae was monitored every day spectrophotometrically with optical density at 680 nm (OD_{680}). The biomass was also determined gravimetrically by weighing the dry algal samples every two days. The experiments were carried out until the microalgal growth reached the stationary phase.

D. Determination of specific growth rate

The specific growth rate and the doubling time in the exponential phase are calculated using the equation (1) and equation (2), respectively [16].

$$\mu = \frac{\ln X_2 - \ln X_1}{t_2 - t_1} \tag{1}$$

$$t_d = \frac{\ln 2}{\mu} \tag{2}$$

Where, μ (d^{-1}) is the specific growth rate; t_d (d) is the doubling time; X_1 (mg L^{-1}) is the initial biomass concentration; X_2 (mg L^{-1}) is the biomass concentration at the end of the time interval; t_1 (d) is the start time of the experiment and t_2 (d) is the time at the end of the experiment.

E. Mathematical models

In this study, two mathematical models were used for the kinetic modeling of microalgal growth. The Monod model [17] is shown in equation (3) and the Haldane model [18] is shown in equation (4).

$$\mu = \mu_{max} \frac{I}{I + K_I} \tag{3}$$

$$\mu = \mu_{max} \frac{I}{I + K_I + \frac{I^2}{K_i}} \tag{4}$$

Where, μ_{max} is the maximum specific growth rate, I is the light intensity, K_I is the light half-saturation constant and K_i is the photoinhibition constant.

F. Model accuracy

The root mean squared error (*RMSE*) shown in equation (5) and the coefficient of determination (R^2) shown in equation (6) were used to determine the accuracy of the mathematical models [19].

$$RMSE = \sqrt{\frac{\sum_{i=1}^{n} (y_i - \hat{y}_i)^2}{n}} \tag{5}$$

$$R^2 = 1 - \frac{\sum_{i=1}^{n} (y_i - \hat{y}_i)^2}{\sum_{i=1}^{n} (y_i - \bar{y})^2} \tag{6}$$

The experimental values of the specific growth rates are shown as y_i, the predicted values are presented as $\hat{y}_i$, the number of data points is represented as n, and the average of the n samples is shown as $\bar{y}$. A lower *RMSE* value indicates that the predicted values are more

accurate. The R^2 value is the fit of the regression model between the dependent variables and the independent variables. This coefficient ranging between 0 and 1 indicates that the model is more compatible with the actual values as it is closer to 1.

III. RESULTS AND DISCUSSION

The growth curves of microalgae cultivated in batch cultivation at 0 (control), 25, 50, 100, 250 and 500 µmol photon m^{-2} s^{-1} light intensities are shown in Fig. 1. As can be seen in Fig. 1(a), no significant growth was observed in dark culture. At 25, 50 and 100 µmol photon m^{-2} s^{-1} light intensities, microalgae reached the exponential growth phase from day 4. At 250 and 500 µmol photon m^{-2} s^{-1}, exponential growth was observed from day 3. In addition, it is noticed that the biomass increased as the light intensity increased. It can be said that microalgal growth has a strong dependence on light intensity.

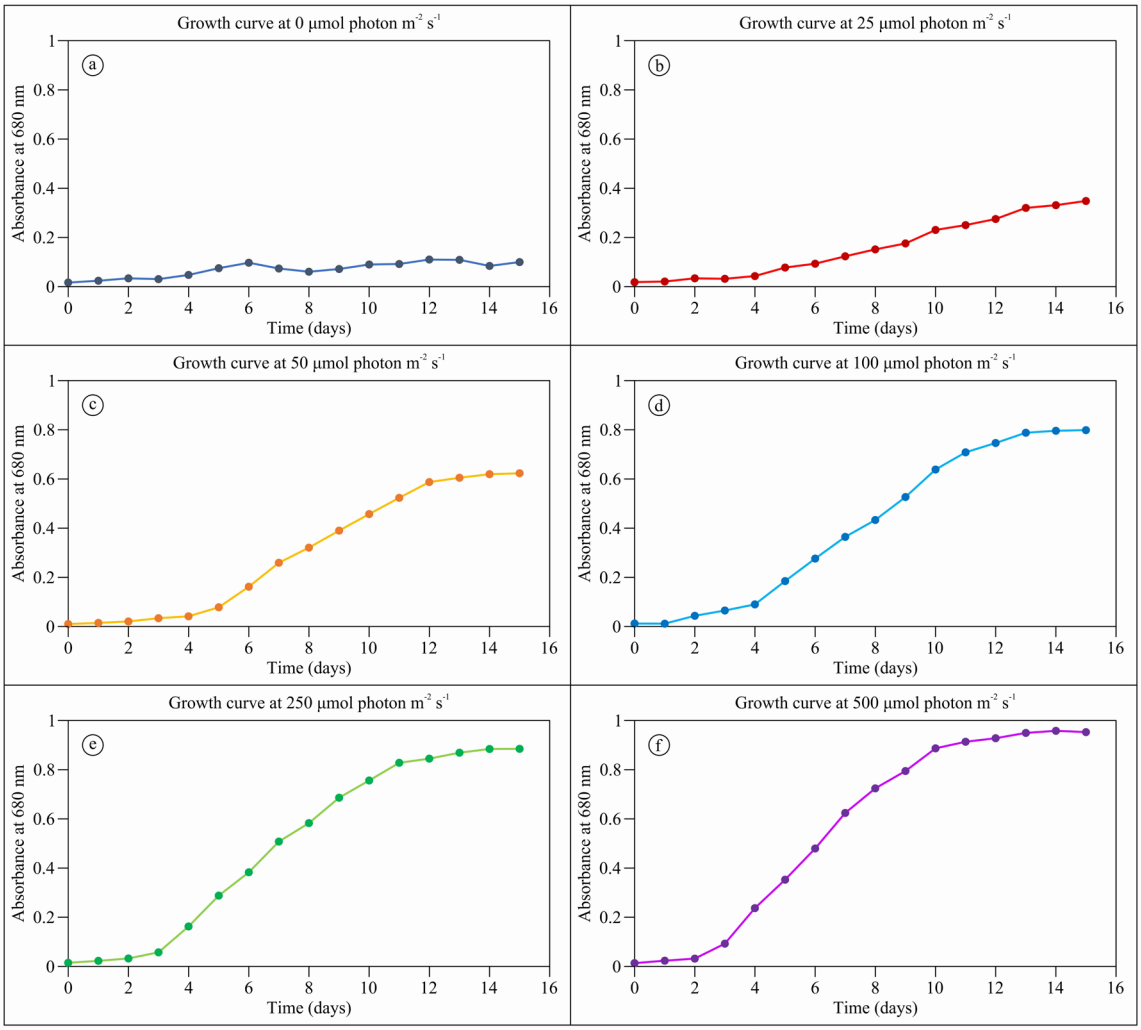

Fig. 1. Growth curves of *Chlorella zofingiensis* at different light intensities.

Table 1 shows the specific growth rates and doubling times at different light intensities in the exponential growth phase. The lowest specific growth rate is 0.25 d^{-1} at 25 µmol photon m^{-2} s^{-1}. The highest specific growth rate was calculated as 0.35 d^{-1} at 100 µmol photon m^{-2} s^{-1}. At 250 and 500 µmol photon m^{-2} s^{-1}, it was 0.34 and 0.33 d^{-1}, respectively. Accordingly, the increase in light intensity after 100 µmol photon m^{-2} s^{-1} did not cause a significant difference in microalgal growth rate. Similarly, doubling times were calculated as 1.99, 2.01, 2.10, 2.21 and 2.77 d at 100, 250, 500 and 25 µmol photon m^{-2} s^{-1}, respectively.

TABLE 1
SPECIFIC GROWTH RATES AND DOUBLING TIMES AT DIFFERENT LIGHT INTENSITIES

Light intensity (µmol photon m^{-2} s^{-1})	μ (d^{-1})	t_d (d)
25	0.25	2.77
50	0.31	2.21
100	0.35	1.99
250	0.34	2.01
500	0.33	2.10

Fig. 2. demonstrates the specific growth rates of C. zofingiensis grown at different light intensities. When the light intensity was increased from 25 to 50 µmol photon m^{-2} s^{-1}, the specific growth rate increased by approximately 24% and when it was increased to 100 µmol photon m^{-2} s^{-1}, it increased by approximately 40%.

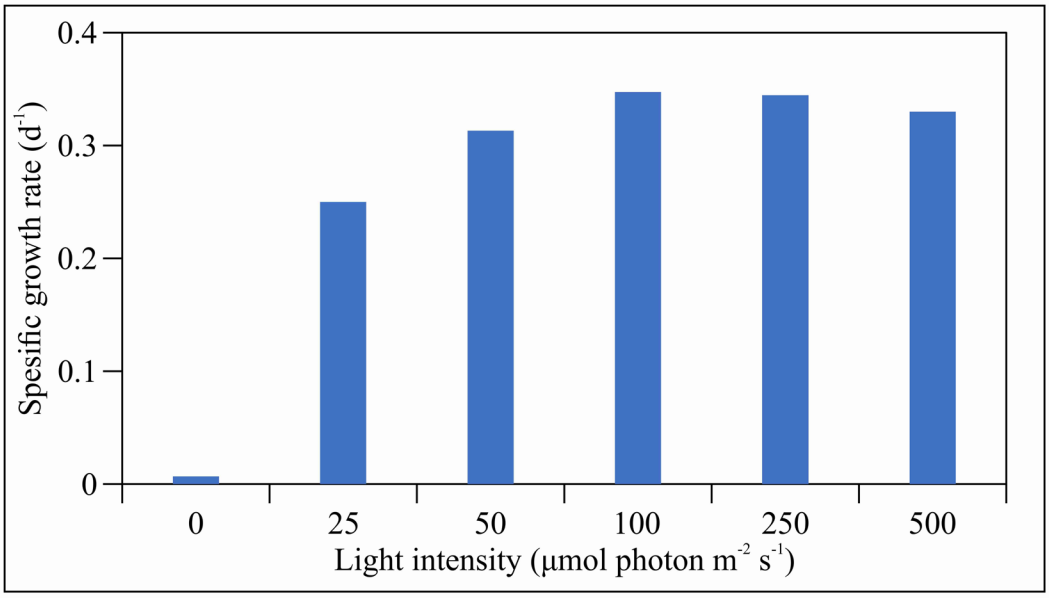

Fig. 2. Specific growth rates at different light intensities.

Table 2 summarizes the kinetic constants for the Monod and Haldane models used in this study. Accordingly, the μ_{max} and K_I coefficients of the Monod model were calculated as 0.36 d^{-1} and 10.70 µmol photon m^{-2} s^{-1}, respectively. The μ_{max}, K_I and K_i coefficients for the Haldane model were found to be 0.42 d^{-1}, 17.11 µmol photon m^{-2} s^{-1} and 1991.26 µmol photon m^{-2} s^{-1}, respectively.

TABLE 2
KINETIC CONSTANTS OF MATHEMATICAL MODELS

Model	μ_{max} (d^{-1})	K_I (µmol photon m^{-2} s^{-1})	K_i (µmol photon m^{-2} s^{-1})
Monod	0.36	10.70	–
Haldane	0.42	17.11	1991.26

Fig. 3 illustrates the specific growth rates at different light intensities by using the kinetic coefficients of the Monod and Haldane models. In the figure, the black dots are the experimental data, the blue dashed line is the Monod model and the red dashed line is the Haldane model. The Monod model provides close results for 25 and 250 µmol photon m^{-2} s^{-1}, while the Haldane model gives results close to almost all actual values. This result indicates that *Chlorella zofingiensis* is photo-inhibited at high light intensities.

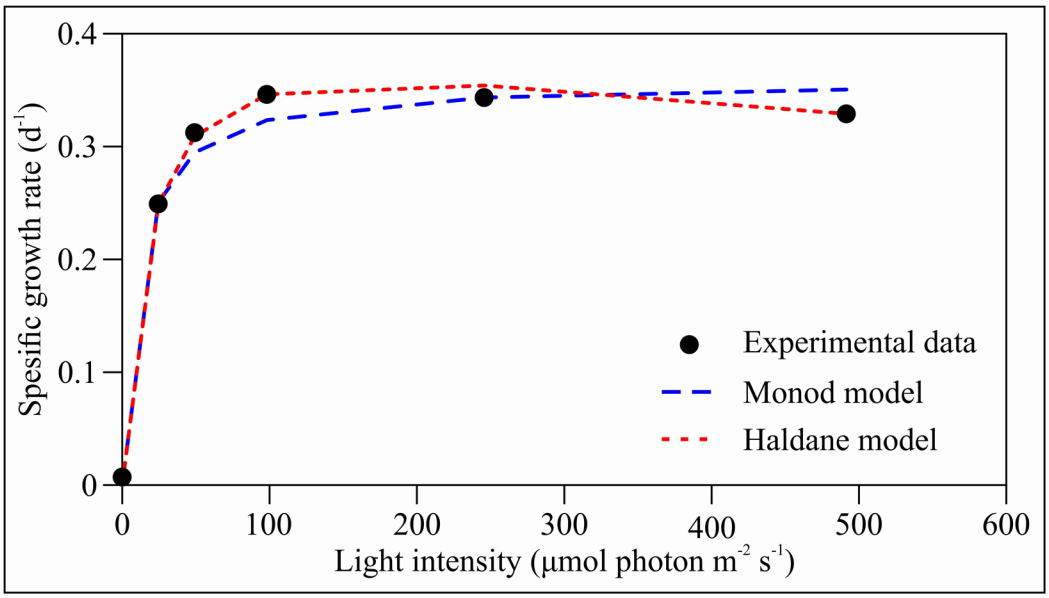

Fig. 3. Mathematical models fit to experimental data.

Table 3 shows the accuracy results of the Monod and Haldane models. *RMSE* values were calculated as 0.018 and 0.006 for Monod and Haldane, respectively. R^2 was determined as 0.82 and 0.98, respectively. Both analysis results show that the Haldane model fits better to the experimental data.

TABLE 3
RESULTS OF GROWTH MODEL PERFORMANCE

Model	*RMSE*	R^2
Monod	0.018	0.82
Haldane	0.006	0.98

IV. CONCLUSION

In this study, *Chlorella zofingiensis* was grown in batch medium and at five different light intensities. Results showed that light intensity strongly affected microalgal biomass production. The highest specific growth rate was obtained at 100 µmol photon m^{-2} s^{-1}. No significant change in specific growth rate was observed at higher light intensities. The relationship between specific growth and light intensity was modeled using the light-dependent Monod and Haldane models. The Haldane model provided the best fit to the experimental data. In future studies, it is necessary to develop models with more parameters such as different microalgae species, illumination rate, wavelength and carbon source. Despite these limitations, the models formulated are valuable tools for understanding the unique behavior of microalgae, optimizing growth conditions and guiding large-scale sustainable microalgae cultivation processes.

REFERENCES

[1] Tang, D., Han, W., Li, P., Miao, X., and Zhong, J. (2011). "CO2 biofixation and fatty acid composition of Scenedesmus obliquus and Chlorella pyrenoidosa in response to different CO2 levels." Bioresource technology, 102(3), pp. 3071-3076.

[2] Kligerman, D. C., and Bouwer, E. J. (2015). "Prospects for biodiesel production from algae-based wastewater treatment in Brazil: A review." Renewable and Sustainable Energy Reviews, 52, pp. 1834-1846.

[3] Borowitzka, M. A., and Moheimani, N. R. (2013). "Sustainable biofuels from algae." Mitigation and Adaptation Strategies for Global Change, 18, pp. 13-25.

[4] Darvehei, P., Bahri, P. A., and Moheimani, N. R. (2018). "Model development for the growth of microalgae: A review." Renewable and Sustainable Energy Reviews, 97, pp. 233-258.

[5] Sajjadi, B., Chen, W. Y., Raman, A. A. A., and Ibrahim, S. (2018). "Microalgae lipid and biomass for biofuel production: A comprehensive review on lipid enhancement strategies and their effects on fatty acid composition." Renewable and Sustainable Energy Reviews, 97, pp. 200-232.

[6] Zonneveld, C. (1998). "Light-limited microalgal growth: a comparison of modelling approaches." Ecological Modelling, 113(1-3), pp. 41-54.

[7] Ramanna, L., Rawat, I., and Bux, F. (2017). "Light enhancement strategies improve microalgal biomass productivity." Renewable and Sustainable Energy Reviews, 80, pp. 765-773.

[8] Sekar, N., and Ramasamy, R. P. (2015). "Recent advances in photosynthetic energy conversion." Journal of Photochemistry and Photobiology C: Photochemistry Reviews, 22, pp. 19-33.

[9] Metsoviti, M. N., Papapolymerou, G., Karapanagiotidis, I. T., and Katsoulas, N. (2019). "Effect of light intensity and quality on growth rate and composition of Chlorella vulgaris." Plants, 9(1), pp. 31.

[10] Li, Y., Zhou, W., Hu, B., Min, M., Chen, P., and Ruan, R. R. (2012). "Effect of light intensity on algal biomass accumulation and biodiesel production for mixotrophic strains Chlorella kessleri and Chlorella protothecoide cultivated in highly concentrated municipal wastewater." Biotechnology and bioengineering, 109(9), pp. 2222-2229.

[11] Choi, Y. K., Kumaran, R. S., Jeon, H. J., Song, H. J., Yang, Y. H., Lee, S. H., ... and Kim, H. J. (2015). "LED light stress induced biomass and fatty acid production in microalgal biosystem, Acutodesmus obliquus." Spectrochimica Acta Part A: Molecular and Biomolecular Spectroscopy, 145, pp. 245-253.

[12] Quaas, T., Berteotti, S., Ballottari, M., Flieger, K., Bassi, R., Wilhelm, C., and Goss, R. (2015). "Non-photochemical quenching and xanthophyll cycle activities in six green algal species suggest mechanistic differences in the process of excess energy dissipation." Journal of plant physiology, 172, pp. 92-103.

[13] Figueroa-Torres, G. M., Pittman, J. K., and Theodoropoulos, C. (2021). "Optimisation of microalgal cultivation via nutrient-enhanced strategies: the biorefinery paradigm." Biotechnology for Biofuels, 14, pp. 1-16.

[14] Esteves, A. F., Gonçalves, A. L., Vilar, V. J., and Pires, J. C. (2024). "Comparative assessment of microalgal growth kinetic models based on light intensity and biomass concentration." Bioresource Technology, 394, 130167.

[15] Kumar, V., Nanda, M., and Verma, M. (2017). "Application of agar liquid-gel transition in cultivation and harvesting of microalgae for biodiesel production." Bioresource technology, 243, pp. 163-168.

[16] Onay, M., and Aladag, E. (2023). "Production and use of Scenedesmus acuminatus biomass in synthetic municipal wastewater for integrated biorefineries." Environmental Science and Pollution Research, 30(6), pp. 15808-15820.

[17] Franz, A., Lehr, F., Posten, C., and Schaub, G. (2012). "Modeling microalgae cultivation productivities in different geographic locations–estimation method for idealized photobioreactors." Biotechnology Journal, 7(4), pp. 546-557.

[18] Fouchard, S., Pruvost, J., Degrenne, B., Titica, M., and Legrand, J. (2009). "Kinetic modeling of light limitation and sulfur deprivation effects in the induction of hydrogen production with Chlamydomonas reinhardtii: Part I. Model development and parameter identification." Biotechnology and bioengineering, 102(1), pp. 232-245.

[19] Aladag, E. (2023). "The influence of meteorological factors on air quality in the province of Van, Turkey." Water, Air, and Soil Pollution, 234(4), 259.

Eksantrik Mesnetli Basit Kirişlerin Serbest Titreşim Analizi

Free Vibration Analysis of Simple Beams With Eccentric Supports

Niyazi ORAL[*,1], Hakan T. Turker[1]

[*]nyzrl16@gmail.com, ORCID: 0009-0008-6359-0139
[1]*Bursa Uludağ Üniversitesi, Mühendislik Fakültesi, İnşaat Mühendisliği Bölümü, Bursa, Türkiye*

Özet: Bu araştırmada, basit mesnetli kirişlerin doğal frekansları incelenmiştir. Standart kiriş teorileri, mesnetlerin kirişin tarafsız ekseni üzerinde olduğunu varsayar; ancak pratik uygulamalarda mesnetler bu konumdan sapabilir. Mesnetlerin bu sapmaları, kirişin dinamik özelliklerinde ve titreşim davranışında belirgin değişikliklere neden olabilir. Mesnet eksantrikliğinin kirişlerin titreşim özelliklerine olan etkisini ortaya koymak için, analitik ve sonlu elemanlar metotları ile bulunan doğal frekanslar karşılaştırılmıştır. Kirişlerin hareket denklemleri, Hamilton prensibi temel alınarak elde edilmiş ve sonrasında sonlu elemanlar modeli kullanılarak kıyaslanmıştır. Araştırmada, iki ucu sabit mesnetli kiriş kullanılmıştır. Araştırma kiriş frekans hesaplamalarında mesnet eksantrikliğinin göz ardı edilmemesi gerektiğini göstermektedir.

Anahtar Kelimeler: *Basit Kiriş, Doğal Frekanslar, Eksantrik Mesnet, Kirişler, Titreşim*

Abstract In this study, the natural frequencies of simply supported beams are examined. Standard beam theories assume that the supports are located on the neutral axis of the beam; however, in practical applications, the supports may deviate from this position. These deviations in the supports can cause significant changes in the dynamic properties and vibration behavior of the beam. To reveal the effect of support eccentricity on the vibration characteristics of beams, the natural frequencies obtained by analytical and finite element methods were compared. The equations of motion of the beams were derived based on Hamilton's principle and then compared using the finite element model. In the research, beams with both ends fixed were used. The study shows that support eccentricity should not be ignored in beam frequency calculations.

Keywords**:** *Simple Beam, Natural Frequencies, Eccentric Support, Beams, Vibration*

I. GİRİŞ

Mühendislikte, mekanik ve yapısal sistemlerde titreşimlerin anlaşılması, makinelerin ve yapıların güvenli bir şekilde tasarlanması, inşa edilmesi ve işletilmesi için büyük bir öneme sahiptir.

Köprüler, binalar ve barajlardaki önemli arızaların birçoğu, rüzgar kaynaklı titreşimler ve depremlerde meydana gelen salınımlı yer hareketleriyle ilişkilidir [1].

Kirişlerin doğal frekansları, özellikle inşaat mühendisliği, havacılık, makine mühendisliği ve otomotiv sektöründe kritik bir öneme sahiptir. Doğal frekanslar, yapıların titreşim analizleriyle doğrudan ilişkilidir ve bu frekansların doğru bir şekilde hesaplanması, yapıların güvenliği ve dayanıklılığı açısından büyük önem taşır [2]. Klasik kiriş teorilerinin varsayımları, eksantrik mesnetlenmiş kirişler için yetersiz kalmakta ve bu teoriler mesnet eksantrikliğini

dikkate almamaktadır. Bu nedenle, eksantrik mesnetlenmiş kirişlerin titreşim analizinde geleneksel yaklaşımlar tam bir çözüm sunamamaktadır.

Son yıllarda yapılan araştırmalar, mesnet eksantrikliğinin kirişlerin doğal frekansları üzerinde belirgin bir etkiye sahip olduğunu göstermiştir [3, 4, 5, 6, 7, 8, 9]. Mesnet eksantrisitesinin artması, kirişin doğal frekanslarında önemli artışlara neden olmaktadır.

Çok sayıda araştırmacı eksantrik olarak mesnetlenmiş kirişlerin titreşim analizini incelemiştir. Dwaikat ve Kodur, mesnetlerde eksantrisitenin çelik kirişlerin yangına altında performansını belirgin bir etkisi olduğunu gözlemlemişlerdir [3]. Eltaher, Alshorbagy ve Mahmoud ise fonksiyonel olarak derecelendirilmiş makro ve nanokirişlerin doğal frekansları üzerindeki tarafsız eksen konumunun etkisini incelemişlerdir. Bu çalışmada, tarafsız eksenin yerinin malzeme özelliklerinin doğrusal olmayan değişimine bağlı olarak doğal frekanslar üzerinde önemli bir rol oynadığı sonucuna varılmıştır [4]. Radice, ise eksantrik sabit mesnetli kirişlerin doğal frekansları üzerindeki etkisini araştırmış ve mesnetlenmenin kiriş kesitinin altında olması durumunda doğal frekansları %55'e kadar artırdığını göstermiştir [5]. Wang ve arkadaşlarının çalışması, FGM kirişler üzerindeki titreşim analizlerinde orta ve tarafsız düzlem formülasyonlarının karşılaştırmasını yaparak her iki formülasyonun da bazı durumlarda benzer sonuçlar verebildiğini, ancak tarafsız düzlemin daha karmaşık olduğunu belirtmiştir [6]. Fernando, Wang ve Roy Chowdhury tarafından yapılan çalışmada ise laminat kirişlerin titreşim analizlerinde, mesnetlerin farklı yüksekliklerde yerleştirilmesinin doğal frekanslar üzerinde önemli etkileri olduğu vurgulanmıştır. Bu çalışma, eksantrik mesnetlerin frekans analizleri üzerinde ne denli kritik bir rol oynadığını ortaya koymaktadır [7]. Türker, eksantrik olarak mesnetlenen kirişlerin eğilme analizine yönelik geliştirdiği modifiye edilmiş kiriş teorisinde, eksantrik mesnetlerin kirişin rijitliği üzerindeki etkilerini incelemiştir [8]. Li, Wen, Shang ve Zhang tarafından yapılan son çalışmada ise eksantrik basit mesnetlerin kirişlerin serbest titreşim özellikleri üzerindeki lokal olmayan etkileri incelenmiş ve eksantrikliğin yalnızca lokal değil, tüm kirişin titreşim davranışını etkileyen önemli bir faktör olduğu belirtilmiştir [9].

Bu çalışmada eksantrik mesnetli kirişlerin serbest titreşim davranışını idare eden diferansiyel denklem Hamilton prensibi ile elde edilmiştir. Diferansiyel denklemin çözümü ile elde edilen frekanslar Sonlu Elemanlar Analizi ile elde edilen sonuçlarla karşılaştırılmıştır.

Çalışmanın sonuçları, mesnet eksantrikliğinin kirişlerin doğal frekansları üzerinde önemli bir etkiye sahip olduğunu ve bu etkinin mühendislik uygulamalarında dikkate alınması gerektiğini göstermektedir.

II. TEORİ

Üzerinde çalışılan kiriş, doğrusal elastik ve homojen bir malzemeden yapılan ve Şekil 1.'de gösterilen kiriş modeldir. Kiriş boyuna eksen koordinatı x ve eğilme ekseni koordinatı z olarak ifade edilmiştir. Elastisite modülü E ve kütle yoğunluğu ρ'dur. Eksantrik mesnet tarafsız eksenden e kadar mesafede konumlandırılmıştır. Burada e1 ve e2 sırasıyla sol ve sağ uçların eksantrisite değeridir. Euler-Bernoulli kiriş teorisinin varsayımları kabul edilerek kesme deformasyonu ve dönme ataleti etkileri ihmal edilmiştir.

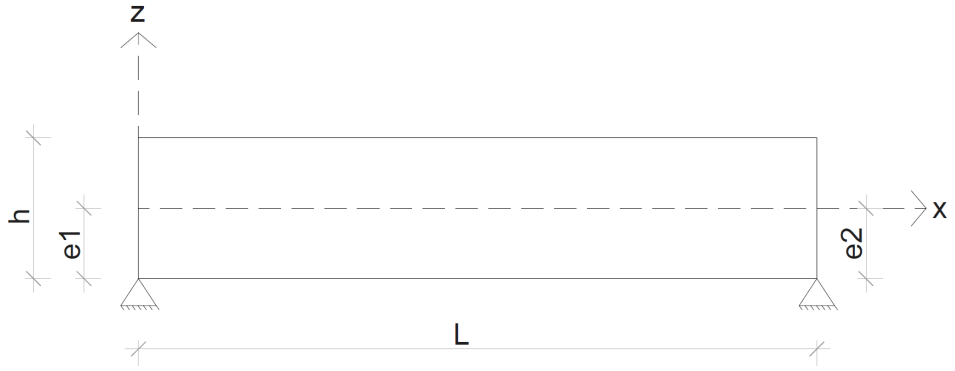

Şekil 1. Eksantrik Olarak Mesnetlenen Basit Kiriş

Boyuna yer değiştirme Denklem (1) ve enine yer değiştirme Denklem (2)'deki gibi tanımlanır.

$$U(x,z,t) = u_0(x,t) - z\frac{\partial w_0(x,t)}{\partial x} \tag{1}$$

Burada $u_0(x, t)$ ve $w_0(x, t)$ tarafsız eksendeki yer değiştirme bileşenleridir.
Hareket denklemleri ve sınır koşulları, Hamilton prensibi yardımıyla enerji minimizasyonunun varyasyonel prensibi ile türetilir. Hamilton prensibi matematiksel olarak Denklem (3)'deki gibi ifade edilir. Burada T kinetik enerjiyi, U iç potansiyel enerjiyi temsil eder.

$$\delta \int_{t1}^{t2} (U - T)\, dt = 0 \tag{2}$$

Denklem (4) kirişte oluşan gerinim bileşenini gösterir. Burada, birinci terim eksenel deformasyonu, ikinci terim ise eğilmeden kaynaklanan deformasyonu tanımlar.

$$\varepsilon_x(x,z) = \frac{\partial u_0(x,t)}{\partial x} - z\frac{\partial^2 w_0(x,t)}{\partial x^2} \tag{3}$$

Gerilme, Hooke yasasına dayalı olarak Denklem (4)'teki gibi gerinim ile ilişkilendirilebilir

$$\sigma_x(x,z) = E\varepsilon_x(x,z) = E\left(\frac{\partial u_0(x,t)}{\partial x} - z\frac{\partial^2 w_0(x,t)}{\partial x^2}\right) \tag{4}$$

İç potansiyel enerjinin matematiksel ifadesi Denklem (6)'daki gibi verilebilir.

$$U = \frac{1}{2}\int_0^l \int_{-h/2}^{h/2} \sigma_x \varepsilon_x b\, dzdx \tag{5}$$

Denklem (4) ve (5), Denklem (6)'da yerine konularak Denklem (7) elde edilir.

$$U = \frac{1}{2}\int_0^l EA\left(\frac{\partial^2 u_0}{\partial x^2}\right)^2 dx + \frac{1}{2}\int_0^l EI\left(\frac{\partial^2 w_0}{\partial x^2}\right)^2 dx \tag{6}$$

Doğrusal elastik malzeme varsayımı altında, iç kuvvet ve eğilme momenti Denklem (8)'de belirtildiği şekilde ifade edilebilir.

$$N_x = EA\frac{\partial u_0}{\partial x}\,, M_x = EI\frac{\partial^2 w_0}{\partial x^2} \tag{7}$$

Denklem (8)'deki iç kuvvet ve eğilme momenti ifadeleri Denklem (7)'de yerlerine konulduklarında Denklem (9) elde edilir.

$$U = \frac{1}{2}\left(\int_0^l N_x\frac{\partial u_0}{\partial x}dx + \int_0^l M_x\frac{\partial^2 w_0}{\partial x^2}dx\right) \tag{8}$$

Denklem (9)'a varyasyonel hesap ve kısmi integrasyon işlemleri uygulandığında Denklem (10) elde edilir.

$$\int_{t1}^{t2}\delta U dt = \int_{t1}^{t2}\left[N_x\delta u_0|_0^l - \int_0^l Ebh\frac{\partial^2 u_0}{\partial x^2}\delta u_0\,dx + M_x\frac{\partial\delta w_0}{\partial x}\Big|_0^l - EI\frac{\partial^3 w_0}{\partial x^3}\delta w_0\Big|_0^l + \int_0^l EI\frac{\partial^4 w_0}{\partial x^4}\delta w_0\,dx\right]dt \tag{10}$$

Kinetik enerjinin matematiksel ifadesi Denklem (11)'deki gibi verilebilir.

$$T = \frac{1}{2}\int_0^l\int_{-h/2}^{h/2}\rho\left[\left(\frac{\partial U}{\partial t}\right)^2 + \left(\frac{\partial W}{\partial t}\right)^2\right]bdzdx \tag{11}$$

Denklem (1) ve (2), Denklem (11)'de yerlerine konularak Denklem (12) elde edilir.

$$T = \frac{1}{2}\int_0^l\int_{-h/2}^{h/2}\rho\left(\frac{\partial u_0}{\partial t} - z\frac{\partial w_0}{\partial x\partial t}\right)^2 bdzdx + \frac{1}{2}\int_0^l\int_{-h/2}^{h/2}\rho\left(\frac{\partial w_0}{\partial t}\right)^2 bdzdx \tag{12}$$

Denklem (12)'ye varyasyonel hesap ve kısmi integrasyon işlemleri uygulandığında Denklem (13) elde edilir.

$$\begin{aligned}\int_{t1}^{t2}\delta T dt &= b\rho\int_{t1}^{t2}\frac{h}{12}^3\frac{\partial^2 w_0}{\partial t\partial x}\frac{\partial\delta w_0}{\partial t}\Big|_0^l \\ &+ b\rho\int_0^l\left(-\frac{h}{12}^3\frac{\partial^3 w_0}{\partial t\partial x^2}\delta w_0\Big|_{t1}^{t2} + \int_{t1}^{t2}\frac{h}{12}^3\frac{\partial^4 w_0}{\partial t^2\partial x^2}\delta w_0 dt\right)dx \\ &+ b\rho\int_0^l\left[h\frac{\partial u_0}{\partial t}\delta u_0\Big|_{t1}^{t2} - \int_{t1}^{t2}h\frac{\partial^2 u_0}{\partial t^2}\delta u_0 dt + \left(h\frac{\partial w_0}{\partial t}\delta w_0\right)\Big|_{t1}^{t2}\right. \\ &\left. - \int_{t1}^{t2}h\frac{\partial^2 w_0}{\partial t^2}\delta w_0 dt\right]dx\end{aligned} \tag{13}$$

Denklem (10) ve (13) Denklem (3)'te yerlerine konularak Denklem (14) elde edilir.

$$\begin{aligned}&\int_{t1}^{t2}(\delta U - \delta T)dt \\ &= \int_{t1}^{t2}\int_0^l\left[\left(b\rho h\frac{\partial^2 u_0}{\partial t^2} - Ebh\frac{\partial^2 u_0}{\partial x^2}\right)\delta u_0\right. \\ &\left. + \left(EI\frac{\partial^4 w_0}{\partial x^4} - b\rho\frac{h}{12}^3\frac{\partial^4 w_0}{\partial t^2\partial x^2} + b\rho h\frac{\partial^2 w_0}{\partial t^2}\right)\delta w_0\right]dxdt \\ &+ \int_{t1}^{t2}\left[\left(N_x\delta u_0 + M_x\frac{\partial\delta w_0}{\partial x}\right)\Big|_0^l - EI\frac{\partial^3 w_0}{\partial x^3}\delta w_0\Big|_0^l\right. \\ &\left. - b\rho\frac{h}{12}^3\frac{\partial^2 w_0}{\partial t\partial x}\frac{\partial\delta w_0}{\partial t}\Big|_0^l\right]dt \\ &+ \int_0^l\left[\left(b\rho\frac{h}{12}^3\frac{\partial^3 w_0}{\partial t\partial x^2}\delta w_0 - b\rho h\frac{\partial w_0}{\partial t}\delta w_0\right)\Big|_{t1}^{t2}\right. \\ &\left. - \left(b\rho h\frac{\partial u_0}{\partial t}\delta u_0\right)\Big|_{t1}^{t2}\right]dx\end{aligned} \tag{14}$$

Denklem (14)'ten hareket denklemleri ve sınır koşulları elde edilir. Denklem (15) kiriş boyuna ekseni doğrultusundaki hareket denklemi Denklem (16) ise eğilme doğrultusundaki hareket denklemidir.

$$\frac{\partial^2 u_0}{\partial t^2} - a^2 \frac{\partial^2 u_0}{\partial x^2} = 0 \tag{15}$$

$$EI \frac{\partial^4 w_0}{\partial x^4} + b\rho h \frac{\partial^2 w_0}{\partial t^2} - b\rho \frac{h^3}{12} \frac{\partial^4 w_0}{\partial t^2 \partial x^2} = 0 \tag{16}$$

Burada $a = \sqrt{\frac{E}{\rho}}$ ve $\rho_l = \rho A$ olarak verilir.

Denklem (16)'daki 3. terim dönme ataletinin etkisini temsil eder. Euler-Bernoulli kiriş teorisinin varsayımları altında bu terim ihmal edildiğinde Denklem (17) elde edilir.

$$EI \frac{\partial^4 w_0}{\partial x^4} + b\rho h \frac{\partial^2 w_0}{\partial t^2} = 0 \tag{17}$$

Değişken ayırma yöntemi uygulandığında, Denklem (15) ve (17)'nin çözümleri Denklem (18) ve Denkem (19)'daki gibi varsayılabilir. Burada U ve W sırasıyla kiriş boyuna eksenindeki ve eğilme ekseninde şekil fonksiyonlarıdır.

$$u_0(x,t) = \sum_{m=1}^{\infty} a_i U(x) \sin(\omega_i t) \tag{18}$$

$$w_0(x,t) = \sum_{m=1}^{\infty} b_i W(x) \sin(\omega_i t) \tag{19}$$

Denklem (18) ve (19), Denklem (15) ve (17)'de yerine konduğunda şekil fonksiyonlarını ifade eden Denklem (20) ve (21) elde edilir. Burada ${\beta_i}^4 = \frac{{\omega_i}^2 \rho_l}{EI}$ olarak verilir.

$$U(x) = A_i \cos\left(\frac{\omega}{a}x\right) + B_i \sin\left(\frac{\omega}{a}x\right) \tag{20}$$

$$W(x) = C_i \cosh(\beta_i x) + D_i \sinh(\beta_i x) + E_i \cos(\beta_i x) + F_i \sin(\beta_i x) \tag{21}$$

Euler-Bernoulli kiriş teorisine göre, kiriş eğildiğinde kesit düzlemi orta yüzeye dik kalır. Bu temel varsayımla kirişin yatay ve düşey deplasman bileşenleri arasında bir ilişki kurulabilir. Orta yüzey yatay yer değiştirme bileşeni u_0 düşey deplasman bileşeni w_0'ın eğimi ile ilişkilidir ve bu ilişki Denklem (22)'de verilmiştir. Bu denklem basit mesnetli kirişin x yönünde hareket edemediğini ifade eder.

$$u_0 + e \frac{\partial w_0}{\partial x} = 0 \tag{22}$$

Deplasmana bağlı küçük değişiklikler (varyasyonlar) incelendiğinde yatay deplasmandaki varyasyonların düşey deplasmanın türevine bağlı oldu görülür ve bu durum Denklem 23'teki gibi ifade edilir.

$$\delta u_0 = -e\delta \frac{\partial w_0}{\partial x} \tag{23}$$

Sabit mesnetin oluşturduğu mesnet kuvvetinin orta düzeleme aktarılmasıyla, sınırdaki iç kuvvetler N ve eğilme momentleri M hesaplanabilir. Denklem (23) Denklem (14)'te yerine konduğunda denklem (24) elde edilir.

$$(M_x - eN_x)|_{x=0}^{x=L} = 0 \tag{24}$$

Bir kirişin kayıcı mesnetli olan ucunda x yönündeki hareket belirsizdir ve Denklem (22)'ye benzer bir durum mevcut değildir. Denklem (22)'deki ilişki sadece eksantrik de olabilen basit mesnet olma durumunda mevcuttur. Eksantrik basit mesnetli olma durumu için sınır koşulları Denklem (25)'deki gibi verilir.

$$u_0 + e\frac{\partial w_0}{\partial x} = 0, \qquad w_0 = 0, \qquad M_x - eN_x = 0 \tag{25}$$

Denklem (8), (15) ve (17)'yi Denklem (25)'e yerleştirdiğimizde, kirişin iki ucunda eksantrik basit mesnetli olma durumu için Denklem (26)'daki sınır koşullarını elde edilir.

$$\begin{aligned} U_i(0) + e_1\frac{\partial W_i(0)}{\partial x} = 0, \qquad W_i(0) = 0, \qquad I\frac{\partial^2 W_i(0)}{\partial x^2} - e_1 bh\frac{\partial U_i(0)}{\partial x} = 0 \\ U_i(L) + e_2\frac{\partial W_i(L)}{\partial x} = 0, \qquad W_i(L) = 0, \qquad I\frac{\partial^2 W_i(L)}{\partial x^2} - e_2 bh\frac{\partial U_i(L)}{\partial x} = 0 \end{aligned} \tag{26}$$

III. NÜMERİK SONUÇLAR

Literatürde Radice [4] verilen iki ucu sabit mesnetli kiriş örneği bu kısımda dikkate alınmıştır. Kirişin geometrik boyutları ve malzeme özellikleri şu şekildedir; L = 762 mm, h = 12.7 mm, E = 69 GPa, ρ = 2730 kg/m³ ve Poisson oranı ν = 0.33. Abaqus'te 2D eleman kullanılarak bir sonlu eleman modeli oluşturulmuş ve doğal frekanslar hesaplanmıştır.

Tablo 1. ve 2.'de farklı eksantrisite durumlarında doğal frekansların nasıl değiştiği incelenmiştir. İlk mod için çıkarılan denklemler ile elde edilen frekansların sonlu elemanlar metodu ve literatür ([4, 7]) ile kıyaslamaları yapılmış ve yüksek oranda doğruluk elde edilmiştir. Eksantrik mesnetin tarafsız eksene mesafesi olan e'nin kiriş yüksekliği olan h'a bölünmesi ile eh=e1/h=e2/h olarak ifade edilmiştir.

Tablo 1. İlk Mod İçin Doğal Frekanslar ve Kıyaslamaları

e_h	Analitik	SEM	Fernando	Radice	Analitik-SEM %Hata	Fernando-Analitik %Hata	Radice-Analitik %Hata
0.000	49.86	49.90	49.86	52.79	0.08	0.00	5.88
0.125	53.39	53.30	53.39	56.35	0.17	0.00	5.54
0.250	61.71	61.40	61.71	64.96	0.50	0.00	5.27
0.375	71.09	70.67	71.10	74.77	0.59	0.01	5.18
0.500	79.48	78.09	79.46	82.22	1.75	0.03	3.45

Tablo 2. 2, 3, 4 ve 5. Mod İçin Doğal Frekanslar ve Kıyaslamaları

Mod-2			Mod-3			Mod-4			Mod-5		
Analitik	**SEM**	**%Hata**	**Analitik**	**SEM**	**%Hata**	**Analitik**	**SEM**	**%Hata**	**Analitik**	**SEM**	**%Hata**
199.45	199.37	0.04	448.75	447.78	0.22	797.79	794.04	0.47	1246.54	1236.7	0.79
199.41	199.42	0.01	452.41	451.36	0.23	797.21	793.59	0.45	1249.83	1239.7	0.81
199.31	199.31	0.00	462.00	460.99	0.22	795.48	791.86	0.46	1259.26	1248.5	0.85
199.14	199.14	0.00	476.76	474.88	0.39	792.57	788.93	0.46	1273.61	1262.2	0.90
198.81	198.89	0.04	492.78	489.00	0.77	788.46	784.55	0.50	1291.22	1278.1	1.02

Şekil 2.'de ilk 5 mod için farklı eksantrisite durumlarına göre normalize edilmiş frekansların değişimini göstermektedir. Burada farklı eksantrisitelerdeki doğal frekanslar eksantrisite olmaması (eh=0) durumundaki frekanslara bölünerek $f_N = \frac{f_{eh,i}}{f_{0h,i}}$ normalize edilmiştir.

En büyük değişiklik mod 1'de olup ileriki modlara gidildikçe eksantrisite etkisinin azaldığı görülmüştür. Bununla birlikte, çift dereceli doğal frekanslar için, her iki uçtaki eksantriklik aynı olduğunda, eksantrikliğin doğal frekans üzerindeki etkisi, tek dereceli frekanslardaki gibi değildir. Eksantrikliğin ikinci dereceli frekanslar üzerinde neredeyse hiçbir etkisi bulunmamaktadır.

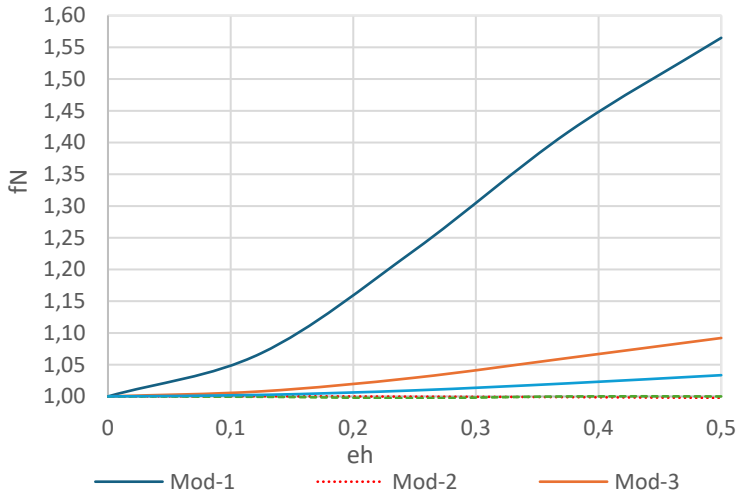

Şekil 2. İlk 5 Mod İçin Farklı Eksantrisite Durumlarına Göre Normalize Edilmiş Frekansların Değişimi

Şekil 3.'de gösterilen birinci ve ikinci mod şekilleri, kirişin farklı titreşim modlarını sergilemektedir. Birinci mod şekli, kirişin tamamının pozitif ve negatif yönlerde hareket ettiği temel bir titreşim modunu temsil ederken, ikinci mod şekli, kirişin pozitif ve negatif yer değiştirmeler arasında bir denge sağladığı daha karmaşık bir titreşim modunu göstermektedir. İlk modda, kirişin tamamı aynı yönde hareket ettiği için eksantrisiteye bağlı asimetrik etkiler kirişin genel dinamik davranışı üzerinde daha belirgin bir rol oynamaktadır. Bunun sonucunda, eksantrisitenin artışıyla birlikte birinci modun frekansında belirgin bir değişiklik gözlemlenmektedir. Ancak ikinci modda, kirişin farklı bölgeleri ters yönlerde hareket ettiğinden bu karşıt hareketler eksantrisitenin etkisini büyük ölçüde dengelemektedir. Özellikle, kısalan ve uzayan bölgelerin simetrik olmasından dolayı, eksantrisitenin frekans üzerindeki etkisi minimal düzeyde kalmaktadır. Bu durum, ikinci modda eksantrisitenin etkisinin gözle görülür şekilde azalmasına yol açmaktadır. Başka bir deyişle, ikinci modda kirişin kısalma ve uzama bölgeleri birbirini dengelediği için eksantrisitenin farklılıklarına rağmen frekansta belirgin bir değişiklik meydana gelmemektedir.

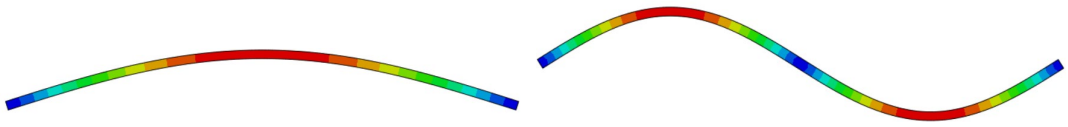

Şekil 3. İlk 2 Mod Şekli

Tablo 3.'de ilk mod için farklı eksantrisite durumları ve farklı L/h'lara göre doğal frekanslar verilmiş ve analitik sonuçlar sonlu elemanlar metodu ile bulunan sonuçlar ile kıyaslanmıştır.

Tablo 3. İlk Mod İçin Farklı Eksantrisite Durumları ve Farklı L/h'lara Göre Doğal Frekanslar

L/h	2		4		6		8		10	
eh	**Analitik**	**SEM**	**Analitik**	**SEM**	**Analitik**	**SEM**	**Analitik**	**SEM**	**Analitik**	**SEM**
0.000	44852.69	31628.00	11218.00	10103.00	4986.16	4753.90	2803.29	2730.40	1795.02	1764.60
0.125	44875.00	34000.00	11978.00	10720.00	5332.33	5054.20	2804.72	2908.40	1921.28	1881.90
0.250	47463.00	36732.00	13747.00	12023.00	6143.87	5746.30	3001.19	3326.60	2218.02	2159.30
0.375	53310.00	39424.00	15730.00	13382.00	7057.55	6490.30	3462.59	3783.10	2552.81	2464.80
0.500	59610.00	41360.00	17506.00	14453.00	7875.28	7101.80	3982.80	4167.00	2852.15	2725.10

Şekil 4. farklı eksantrisite durumları ve farklı L/h'lara göre analitik sonuçlar ve sonlu elemanlar metodu ile bulunan sonuçlar arasındaki %hata'yı göstermektedir. L/h'ın düşük değerlerinde %hata fazla iken L/h arttığında %hata azalmıştır. Bu fark kesme ve dönme ataleti etkisinin çıkarılan hareket denklemlerinde bulunmamasından kaynaklanmaktadır. L/h arttıkça bu etkilere kıyasla eğilme daha baskın hale gelmekte ve %hata azalmaktadır.

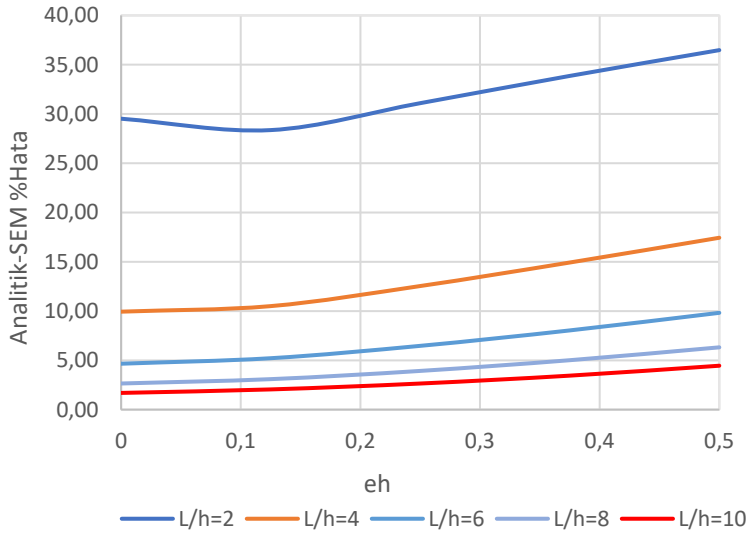

Şekil 4. Farklı Eksantrisite Durumları ve Farklı L/h'lara Göre Analitik ve SEM Sonuçlarının %hata Değişimi

Şekil 5. sonlu elemanlar metodu ile bulunan, farklı eksantrisite durumları ve farklı l/h'lara göre normalize edilmiş frekansların değişimini göstermektedir. L/h arttıkça eksantrisite etkisinin arttığı görülmüştür.

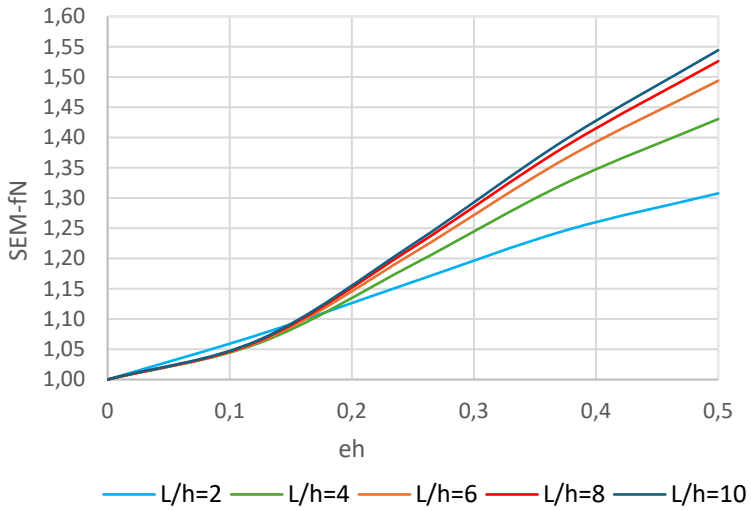

Şekil 5. Farklı Eksantrisite Durumları ve Farklı L/h'lara Göre Normalize Edilmiş Frekansların Değişimi

IV. SONUÇ

Bu çalışma iki ucu sabit eksantrik mesnetli kirişlerin frekansları analitik olarak Hamilton prensibi kullanılarak elde edilmiştir. Elde edilen denklemlerle hesaplanan frekanslar Sonlu Elemanlar ile bulunan frekanslarla kıyaslanarak elde edilen denklemler doğrulanmıştır. Eksantrik mesnet durumunun, mesnetin Tarafsız Eksende olma durumu ile kıyaslanması yapılmıştır. Elde edilen bulgular, mesnetlerin kirişin tarafsız ekseninden sapmasının doğal frekanslarda belirgin artışlara neden olduğunu ve bu sapmanın özellikle birinci modda önemli bir rol oynadığını göstermektedir. Ayrıca, eksantrisitenin etkisinin daha yüksek modlarda azaldığı, çift modlarda frekanslar üzerindeki etkinin minimal seviyede olduğu, kirişin L/h oranı arttıkça eksantrisite etkisinin arttığı, denklemlerin çıkarılmasında kesme etkisi ve dönme ataleti ihmal edildiği için yüksek L/h oranlarında; kesme etkisi ve dönme ataletini dikkate alan sonlu elemanlar modellerine daha fazla yakınsadığı görülmüştür.

KAYNAKLAR

[1] S. S. Rao, Mechanical Vibrations. Pearson Education, 2004.

[2] L. Meirovitch, Fundamentals of Vibrations. McGraw-Hill, 2001.

[3] M. Dwaikat and V. Kodur, "Effect of location of restraint on fire response of steel beams," Fire Technology, 46(1), 109-128, 2010. https://doi.org/10.1007/s10694-009-0085-9

[4] J. J. Radice, "On the effect of local boundary condition details on the natural frequencies of simply-supported beams: Eccentric pin supports," Mechanics Research Communications, 39, 1-8, 2012

[5] M. A. Eltaher, A. E. Alshorbagy and F. F. Mahmoud, "Determination of neutral axis position and its effect on natural frequencies of functionally graded macro/nanobeams," Composite Structures, 99, 193-201, 2013. https://doi.org/10.1016/j.compstruct.2012.11.039https://doi.org/10.1016/j.mechrescom.2011.08.007

[6] C. M. Wang, L. L. Ke, A. N. Roy Chowdhury, J. Yang and S. Kitipornchai, "Critical examination of midplane and neutral plane formulations for vibration analysis of FGM beams," Engineering Structures, 130, 275-281, 2017. https://doi.org/10.1016/j.engstruct.2016.10.051

[7] C. M. Wang, D. Fernando, A. N. Roy Chowdhury and S. Kitipornchai, "Vibration of laminated-beams based on reference-plane formulation: Effect of end supports at

different heights of the beam," Engineering Structures, 159, 245-251, 2018. https://doi.org/10.1016/j.engstruct.2018.01.004

[8] H. T. Türker, "A modified beam theory for bending of eccentrically supported beams," Mechanics Based Design of Structures and Machines, 50(2), 576-587, 2022. https://doi.org/10.1080/15397734.2020.1738246

[9] B. Li, D. Wen, X.-C. Shang and R. Zhang, "Non-local effect of eccentrically simply supported beam on free vibration," Forces in Mechanics, 12, 100218, 2023. https://doi.org/10.1016/j.finmec.2023.100218

Machine Learning-Based IoT Device Classification through Network Traffic Feature Extraction

Mesut GUVEN[1*]

[*]mesuttguve@gmail.com, ORCID: 0000-0002-0957-8541
[1] *TOBB University of Economics and Technology, TR-06560 Ankara,*

Abstract: The rapid proliferation of Internet of Things (IoT) devices in modern networks has raised significant security concerns. Traditional security mechanisms often fall short in identifying and securing IoT devices, particularly when unauthorized or misconfigured devices connect to the network. In this study, we collect network traffic data from a local hub where several IoT devices are connected and analyze the traffic to identify the type of each device. By employing **tshark**, we filter TCP/UDP traffic and extract vital attributes such as IP length, protocol headers, port numbers, and stream lengths to construct a labeled dataset representing various network traffic patterns. To classify and predict the actual type of any connected device, several machine learning algorithms, including K-Nearest Neighbors (KNN), Support Vector Machines (SVM), Logistic Regression, Decision Trees, Random Forests, and XGBoost, are trained on the dataset. The data is preprocessed using Principal Component Analysis (PCA) and standardization. Additionally, a voting classifier is implemented to combine the strengths of these individual models. The models are evaluated in terms of accuracy, precision, recall, and F1-score, with Decision Trees and KNN achieving the highest accuracy of 99.7% and 98.8%, respectively. This approach enhances network security by detecting inconsistencies between a device's behavior and its declared identity in the Data Loss Prevention (DLP) system, flagging unauthorized or suspicious devices. The results demonstrate the effectiveness of using network traffic features to identify IoT device types and provide a robust, scalable solution for securing IoT networks.

Keywords: *Artificial Intelligence, Machine Learning, Cyber Security, Internet of Things, Data Loss Prevention.*

I. INTRODUCTION

The Internet of Things has revolutionized modern living by interconnecting a vast array of devices, from smart home systems to industrial equipment. While IoT enhances convenience, efficiency, and automation, it also presents new vulnerabilities and security risks. With millions of devices continuously being connected, securing IoT ecosystems has become increasingly challenging. Unauthorized devices, misconfigured connections, and malicious intrusions can exploit weak points in a network, leading to data breaches, denial of service attacks, or even hijacking of devices.

Traditional security mechanisms, designed primarily for conventional computing devices, often fail to provide adequate protection for IoT devices due to their distinct characteristics. IoT devices typically communicate through lightweight protocols, have limited computational power, and exhibit unique traffic patterns, making their detection and classification in a network more complex. This necessitates the development of tailored solutions for real-time monitoring, identification, and securing of IoT networks.

In this paper, we propose a machine learning-based approach to classify IoT devices based on their network traffic. By analyzing the distinct patterns of TCP/UDP traffic, we aim to accurately identify device types and detect any inconsistencies between a device's behavior and its declared identity on the network. Such inconsistencies could indicate misconfiguration or unauthorized access, thereby alerting network administrators to potential security breaches.

Our approach focuses on collecting and analyzing network traffic at a local hub, where several IoT devices are connected. Using **tshark**, a packet analyzer, we extract key features from the captured traffic, such as protocol headers, IP lengths, port numbers, and stream lengths. These features are used to create a labeled dataset that reflects the traffic patterns of different IoT devices. We experiment with various machine learning models, including KNN, SVM, Logistic Regression, Decision Trees, Random Forests, and XGBoost, to classify the devices based on their network traffic. The models are further optimized using data preprocessing techniques such as PCA and standardization to enhance classification accuracy. To improve prediction reliability, we implement a voting classifier that combines the strengths of the individual models.

The main contributions of this paper include:

- A method for capturing and extracting key features from IoT device network traffic using **tshark**.
- A comparative analysis of various machine learning algorithms for classifying IoT device types based on traffic patterns.
- A robust solution that can enhance network security by identifying and flagging unauthorized or misconfigured devices.

Our results show that the Decision Tree and KNN models achieve the highest accuracy, providing an efficient, scalable solution for real-time IoT device identification and network security.

The rest of this paper is organized as follows: Section 2 discusses related work in IoT device classification and security. Section 3 describes the dataset and feature extraction process. Section 4 presents the machine learning models and evaluation metrics.

II. RELATED WORK

In recent years, securing IoT devices against malware has become increasingly challenging due to the growing sophistication of attacks and the limited computational resources available for implementing security software on these devices. To address these limitations, advanced anomaly detection methods, such as machine learning, have been proposed for identifying malware-infected IoT devices through gateway analysis. One study presents an architecture that leverages summarized statistical data of network traffic, using algorithms like Isolation Forest and K-means clustering, to achieve high malware detection accuracy while significantly reducing data size and computational demands [1]. In another study, the authors emphasize the vulnerabilities of billions of IoT devices lacking proper security mechanisms and propose a framework utilizing federated learning to enhance malware detection [2]. Their research utilizes the N-BaIoT dataset, which simulates network traffic from various real IoT devices under malware influence, to evaluate the proposed model's efficacy. By comparing the performance of federated learning with traditional centralized methods, the study reveals that federated models can achieve comparable results while preserving data privacy. Moreover, the paper addresses the security challenges associated with federated learning, highlighting the vulnerability of standard aggregation methods to adversarial attacks and proposing alternative aggregation functions as countermeasures. A thorough investigation is conducted by using several ML models, including XGBoost, SVMs, and Deep Convolutional Neural Networks,

using multiple datasets such as IoT-23, NSL-KDD, and TON_IoT datasets [3]. Their findings indicated that XGBoost outperformed both SVM and DCNN, achieving an impressive accuracy of up to 99.98% while demonstrating superior computational efficiency. This highlights the potential of utilizing advanced ML techniques for effective anomaly detection in diverse IoT environments.

The growing cyber security risks posed by IoT devices, particularly concerning large organizations and smart cities is emphasized in another study [3]. They highlight the necessity for smart mechanisms that can automatically detect suspicious activities on IoT devices connected to local networks due to the rapid increase in IoT adoption. The traditional methods for attack detection have become obsolete in the face of increased web traffic and the challenges associated with processing large volumes of data. To address these issues, the study proposes a framework for detecting malicious network traffic, utilizing three widely used classification techniques: SVM, GBDT, and Random Forest. The results indicate that the Random Forest algorithm outperforms the others, achieving an accuracy of 85.34% when evaluated on the NSL KDD dataset [4]. Anomaly detection research within the context of industrial machinery and the IoT is conducted in this study [5]. As IoT enables the collection of vast amounts of data from industrial equipment, traditional manual anomaly detection methods become impractical due to the sheer volume and complexity of the data. This study emphasizes the potential of ML algorithms to automate the detection process, improving safety and reducing downtime. Notably, while existing systematic mapping studies have largely concentrated on network and cybersecurity challenges, this research specifically focuses on the application of ML for anomaly detection in industrial settings. By evaluating 84 studies published between 2016 and 2023, the paper identifies prevalent algorithms, preprocessing techniques, and sensor types utilized in IoT environments. Additionally, it highlights application areas and outlines future challenges and research opportunities in the field.

The rise in successful attacks, particularly from botnets exploiting compromised IoT devices, poses severe security risks and necessitates urgent countermeasures. In this study, the importance of implementing solutions that mitigate threats from their inception is highlighted and the varied nature of these IoT attacks are emphasized [6]. Additionally, it advocates for quarantining infected devices to prevent virus propagation and botnet formation. The authors propose leveraging side-channel attack techniques alongside a machine learning-based algorithm for intrusion detection, demonstrating effective detection of anomalous behavior in smart IoT devices. In this specific study, the discussions of IoT developers on Stack Overflow are investigated to understand the security and ML challenges encountered in IoT device development [7]. An analysis of approximately 53,000 posts reveals that around 12% contain security discussions, while only 0.12% address ML topics, with no overlap between the two. Developers frequently express concerns about securely managing data across IoT devices and show interest in integrating deep neural networks for ML applications, yet they struggle with the resource constraints of IoT devices. These findings highlight the need for innovative solutions to enhance security and support ML adoption in the IoT ecosystem.

In this work, the complexities of security in the IoT are explored, particularly the challenges posed by node heterogeneity [8]. Despite the implementation of traditional security measures like encryption and access control, these approaches have proven insufficient in ensuring security for IoT devices. The paper identifies various types of IoT threats and discusses both shallow and deep machine learning based intrusion detection systems tailored for the IoT environment. The performance of these models is evaluated using five benchmark datasets: NSL-KDD, IoTDevNet, DS2OS, IoTID20, and the IoT Botnet dataset, with performance metrics such as accuracy, precision, recall, and F1-score. The findings reveal that deep machine learning-based IDS significantly outperforms shallow machine learning methods in detecting IoT attacks. In another study, the use of machine learning and blockchain technology to enhance the security and privacy of IoT devices is investigated [9]. The focus is on developing an intrusion detection system that utilizes machine learning algorithms and employs blockchain

to encrypt interactions between IoT devices. The performance of the system and various machine learning algorithms is evaluated on an IoT network using simulated attack data, achieving a remarkable detection accuracy of 99.9% with Random Forest. The findings demonstrate the effectiveness of this approach in identifying attacks on IoT networks. Additionally, the study highlights how blockchain technology can bolster security and privacy by establishing a tamper-proof decentralized communication system.

In this specific study, the vulnerabilities of machine learning models in the IoT ecosystem to adversarial attacks by insider threats are investigated [10]. As machine learning becomes increasingly integral to various applications, the risk posed by capable insider adversaries who can disrupt model behavior during training or testing phases is a significant concern. This paper reviews and organizes the literature on adversarial attacks and defenses from the perspective of insider threats, proposing a taxonomy of adversarial methods applicable to machine learning models in IoT. It discusses the practical implications of these methods in real-life IoT scenarios and explores potential defensive strategies. The aim is to provide a comprehensive overview of existing research and raise awareness about the insider threat landscape, encouraging efforts to protect machine learning models in the IoT environment. In this specific study, the prevalence of malicious attacks on IoT devices is examined, highlighting their increasing occurrence across various environments, including homes, offices, and healthcare [11]. This study proposes offloading machine learning model selection to the cloud while delegating real-time prediction tasks to fog nodes. An ensemble machine learning model is constructed in the cloud based on historical data, facilitating real-time attack detection on fog nodes. Evaluated using the NSL-KDD dataset, the proposed approach demonstrates significant effectiveness, achieving improved execution time, precision, recall, accuracy, and region of convergence curve performance.

Device identification is a crucial aspect of the IoT, where accurate identification of each unique device is essential for critical services like access control and intrusion prevention. Traditional methods, such as using MAC addresses for device identification, face challenges due to vulnerabilities like spoofing. In this specific study, a novel unsupervised approach for IoT device identification which may significantly improve security measures in IoT environments is presented [12]. With this new technique the accurate and reliable device identification is ensured.

III. METHODOLOGY

The dataset used for this study was collected from a local router, with several devices connected to the network. The dataset includes network packets captured in a PCAP file format, with each packet being associated with specific devices identified by their IP addresses. The device types in the dataset are classified into four categories: **PC**, **Mobile**, **Smart TV**, and **Miscellaneous**, which includes other devices like printers or IoT devices. The devices' IP addresses follow the format 192.168.1.#, where # is replaced by a specific identifier corresponding to the device type. For example:

- **PC**: 192.168.1.101
- **Mobile**: 192.168.1.102
- **Smart TV**: 192.168.1.106
- **Miscellaneous (Google Chromecast, Robot Vacuum Cleaner, Amazon Echo)**: 192.168.1.103, 104, 107

In our study, network traffic features were extracted from PCAP files using the tshark tool, part of the Wireshark software suite. We began by filtering the network packets according to device type, as identified by specific IP addresses. Each device category (PC, Mobile, Smart

TV, Miscellaneous) was filtered using predefined IP addresses for TCP and UDP packets. To represent these packets in a feature vector model, some useful features were extracted from each packet. We extracted 15 different features from each packet using tshark's field extraction capabilities. These features include both IP and TCP/UDP header information, providing insight into the behavior and structure of the traffic. The extracted features are represented in Table 1.

TABLE I
FEATURES FROM THE NETWORK ACTIVITY

Feature	Command used to extract the feature
IP Length	tshark -r -e ip.len
IP Header Length	tshark -r -e ip.hdr_
Time-to-Live Protocol	tshark -r -e ip.proto
Time-to-Live	tshark -r -e ip.ttl
Source Port	tshark -r -e tcp.srcport
Destination Port	tshark -r -e tcp.dstport
Window Size	tshark -r -e tcp.window_size_value
TCP Header Length	tshark -r -e tcp.hdr_len
TCP Stream	tshark -r -e tcp.stream
TCP Urgent Pointer	tshark -r -e tcp.urgent_pointer
TCP Length	tshark -r -e tcp.len
UDP Source Port	tshark -r -e udp.srcport
UDP Destination Port	tshark -r -e udp.dstport
UDP Stream	tshark -r -e udp.stream
UDP Length	tshark -r -e udp.length

The labels for each packet are assigned based on the source IP address, allowing for the classification of network activity by device type. In terms of data preprocessing, we handled any missing data by filling them with zeros and scaled the features using standard scaling techniques to normalize the data before training our models. The normalized data was then subjected to Principal Component Analysis (PCA) to reduce the dimensionality while retaining 95% of the explained variance. Even though we executed the PCA, we have used all the features for the classification. But 7 features are the most informative ones among others, and these features are respectively;

- **IP Length** (ip.len): Represents the total length of the IP packet. This feature helps in understanding the size of the transmitted packets and is essential for anomaly detection.
- **IP Header Length** (ip.hdr_len): Indicates the length of the IP header. This can be useful for identifying protocol usage and possible irregularities in packet structures.
- **Time-to-Live (TTL)** (ip.ttl): The TTL value helps determine the packet's lifespan in the network and can indicate the path it has taken. Anomalies in TTL can signify issues like routing loops.
- **Source Port** (tcp.srcport): The port from which the traffic originates. It can be useful for identifying communication patterns and potential attacks.
- **Destination Port** (tcp.dstport): Indicates where the packet is being sent. This feature is critical for analyzing target services and potential vulnerabilities.
- **Window Size** (tcp.window_size_value): The size of the sender's receive window, indicating how much data can be sent before receiving an acknowledgment. This feature is key for performance analysis and detecting congestion.

- **TCP Length** (tcp.len): The length of the TCP segment. This can help assess the nature of the traffic and identify possible anomalous behavior.

These features are presented in Figure 1.

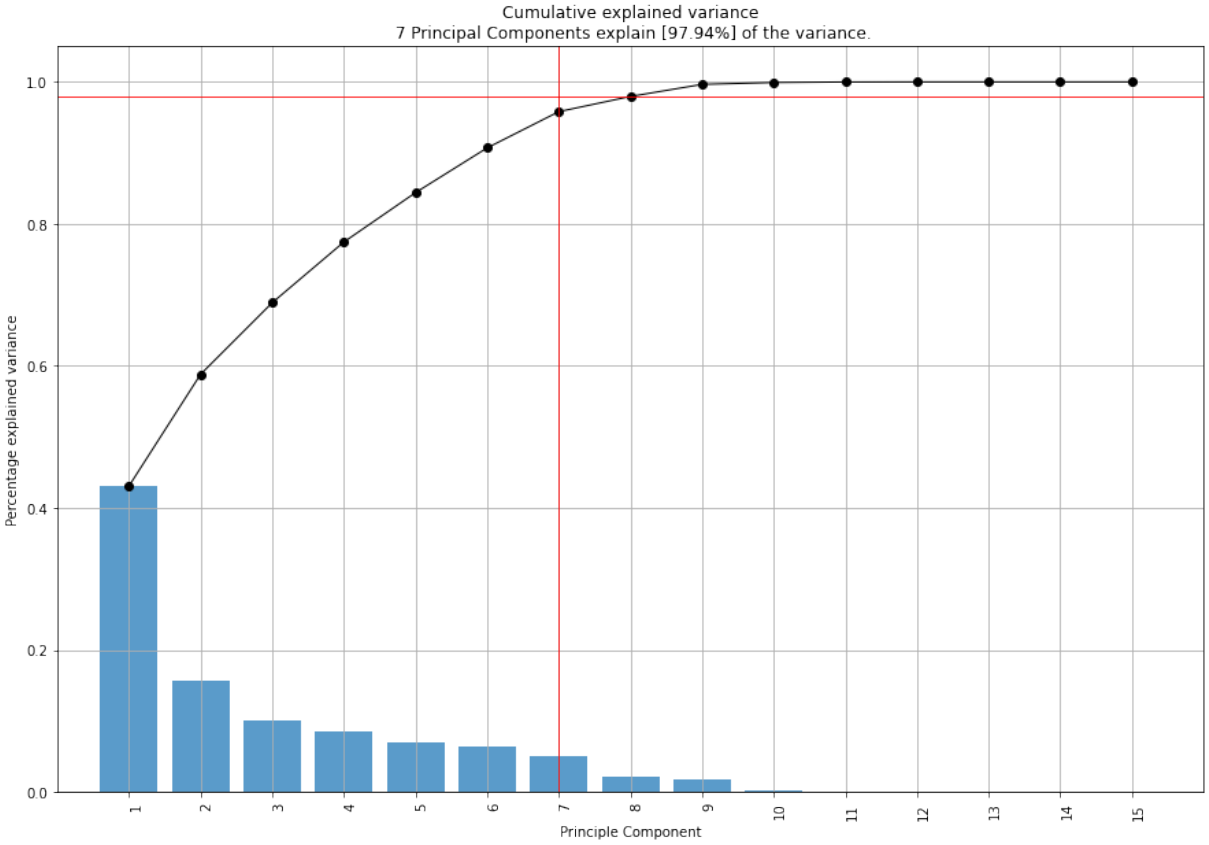

Fig. 1. Result for the PCA analysis.

IV. RESULTS

In our investigation into the efficacy of machine learning algorithms for dynamic malware analysis, we selected a range of classification techniques based on their proven track records in similar domains, their adaptability, and their performance in handling imbalanced datasets. Below, we present the results obtained from various models, including K-Nearest Neighbors, Support Vector Machine, Logistic Regression, Decision Tree, Random Forest, XGBoost, and a Voting Classifier. The results for these algorithms are presented in Table 2.

The results of this study indicate that machine learning algorithms, particularly Decision Trees and ensemble methods like Random Forest and XGBoost, are highly effective for classifying network traffic in the context of dynamic malware analysis. The high accuracy and balanced precision and recall across various models underscore the potential for implementing these techniques in real-world cybersecurity applications.

TABLE II
RESULTS FOR CLASSIFICATION

Model	Metric	Result
K-Nearest Neighbor	Accuracy	0.988
	Precision	0.986
	Recall	0.988
Support Vector Machine	Accuracy	0.964
	Precision	0.972
	Recall	0.966
Logistic Regression	Accuracy	0.984
	Precision	0.980
	Recall	0.979
Decision Tree	Accuracy	0.997
	Precision	0.997
	Recall	0.997
Random Forest	Accuracy	0.995
	Precision	0.995
	Recall	0.995
XGBoost	Accuracy	0.988
	Precision	0.986
	Recall	0.988

V. CONCLUSION

The results of our analysis demonstrate that machine learning algorithms can effectively classify IoT devices based on their network traffic patterns. By employing techniques such as K-Nearest Neighbors, Support Vector Machines, and ensemble methods like Random Forest and XGBoost, we can predict the class (or type) of an IoT device with high accuracy. This capability becomes especially critical in network security, where the dynamic landscape of connected devices presents both opportunities and challenges.

When a new IoT device connects to a network, a deep learning-based detection and prevention (DLP) system can leverage our classification models to assess its assigned type. If there is a discrepancy between the predicted class and the actual type of the device detected, this anomaly may signify a potential cyber threat. Such a situation necessitates immediate and in-depth analysis to determine the cause of the mismatch and to ascertain whether it poses any risk to network integrity.

From this perspective, our findings underline the importance of integrating robust machine learning models into cybersecurity frameworks for IoT environments. By doing so, organizations can enhance their threat detection capabilities, allowing for proactive measures against potential attacks. The ability to recognize and respond to deviations in expected device behavior is crucial for maintaining the security and resilience of IoT networks in an increasingly complex cyber landscape .

REFERENCES

[1] M. Nakahara, N. Okui, Y. Kobayashi, and Y. Miyake, "Machine learning based malware traffic detection on IoT devices using summarized packet data," in *Proceedings of the 5th International Conference on Internet of Things, Big Data and Security (IoTBDS)*, G. Wills and P. Kacsuk, Eds., Prague, Czech Republic, May 7-9, 2020, pp. 78-87. DOI: 10.5220/0009345300780087.

[2] V. Rey, P. M. Sánchez, A. Huertas Celdrán, and G. Bovet, "Federated learning for malware detection in IoT devices," in *Proceedings of the 2022 International Conference on Internet of Things, Big Data and Security (IoTBDS)*, pp. 1-10, 2022.

[3] M. Balega, W. Farag, X.-W. Wu, S. Ezekiel, and Z. Good, "Enhancing IoT Security: Optimizing Anomaly Detection through Machine Learning," *Electronics*, vol. 13, no. 11, Art. no. 2148, June 2024. doi:10.3390/electronics13112148.

[4] M. Anwer, S.M. Khan, M.U. Farooq, and Waseemullah, "Detection of Malicious Network Traffic in IoT Devices," *Engineering Technology & Applied Science Research*, vol. 11, no. 3, pp. 7273-7278, June 2021, doi:10.48084/etasr.4202.

[5] S.F. Chevtchenko, E.D. Rocha, M.C.M. Dos Santos, R.L. Mota, D.M. Vieira, E.C. De Andrade, and D.R.B. De Araujo, "Anomaly Detection in Industrial Machinery Using IoT Devices and Machine Learning: A Systematic Mapping," IEEE Access, vol. 11, pp. 128288-128305, 2023. DOI: 10.1109/ACCESS.2023.3333242.

[6] Myridakis, D., Papafotikas, S., Kalovrektis, K., & Kakarountas, A. (2020). Exploiting Side-Channel Attack Techniques for Smart IoT Devices Protection Using Machine Learning Algorithms. *Electronics*, 9(11), 1799. https://doi.org/10.3390/electronics9111799.

[7] Uddin, G. (2021). *Security and Machine Learning Adoption in IoT: A Preliminary Study of IoT Developer Discussions*. In *2021 IEEE/ACM 3rd International Workshop on Software Engineering Research and Practices for the IoT (SERP4IOT)* (pp. 36-43). IEEE Computer Society. DOI: 10.1109/SERP4IoT52556.2021.00013.

[8] Islam, N., Farhin, F., Sultana, I., Kaiser, M. S., Rahman, M. S., Mahmud, M., Hosen, A. S. M. S., & Cho, G. H. (2021). Towards Machine Learning Based Intrusion Detection in IoT Networks. *CMC-COMPUTERS MATERIALS & CONTINUA*, 69(2), 1801-1821. https://doi.org/10.32604/cmc.2021.018466.

[9] Alsharif, N. A., Mishra, S., & Alshehri, M. (2023). IDS in IoT using Machine Learning and Blockchain. *Engineering Technology & Applied Science Research, 13*(4), 11197-11203. https://doi.org/10.48084/etasr.5992.

[10] Aloraini, F., Javed, A., Rana, O., & Burnap, P. (2022). Adversarial machine learning in IoT from an insider point of view. *Journal of Information Security and Applications*, 70, Article 103341. https://doi.org/10.1016/j.jisa.2022.103341.

[11] Tomer, V., & Sharma, S. (2022). Malicious attacks in IoT environments using fog computing and machine learning. *Future Internet, 14*(4), Article 102. https://doi.org/10.3390/fi14040102.

[12] Koball, C., Rimal, B. P., Wang, Y., Salmen, T., & Ford, C. (2023). Device Identification in IoT: A Machine Learning Approach. *Information*, 14(6), 320. https://doi.org/10.3390/info14060320.

Establishment of *Citrus suhuiensis* Adventitious Root Culture

Noor Illi Mohamad Puad[*,1], Yulis Noor Jannuri[1], Azura Amid[2]

[*]: illi@iium.edu.my, ORCID: 0000-0001-8127-0085
[1]: *Department of Chemical Engineering and Sustainability, Kulliyyah of Engineering, International Islamic University Malaysia (IIUM), Jalan Gombak, 53100 Kuala Lumpur, Malaysia*
[2]: *International Institute for Halal Research and Training (INHART), International Islamic University Malaysia (IIUM), Jalan Gombak, 53100 Kuala Lumpur, Malaysia*

ABSTRACT

Citrus suhuiensis (*C. suhuiensis*) is recognized as a mandarin orange that originated from southern China and developed from the citrus family of *Rutacaeae*. However, the production of citrus, especially mandarin oranges, has declined over the past few years due to low susceptibility to diseases. Plant biotechnology, such as root culture, can potentially increase the propagation rate of citrus plants. This study investigated the effect of different concentrations of auxins on the establishment of *C. suhuiensis* adventitious root culture from its callus, seeds, and leaves explants. The explants were transferred into an MS solid medium supplemented with different concentrations of 1-Naphthaleneacetic acid (NAA) and Indole-3-butyric acid (IBA) (1 - 4 mg/L) to determine which type and concentration of auxin can induce maximum *C. suhuiensis* adventitious root growth. It was found that the callus culture was growing without resulting in root induction. IBA with the concentration of 4 mg/L effectively induced roots from *C. suhuiensis* seed explants as it gave the highest root length of 10.23 cm. This is because IBA is more potent and influences the root induction from seeds more than NAA. Contrarily, 4 mg/L NAA was significant for leaf explants in *C. suhuiensis* root induction as it gave the longest root length of 0.8 cm. The findings in this study serve as a basis for the scaling-up of root culture and *in vitro* cultivation of *C. suhuiensis.*

Keywords— *Adventitious roots; Citrus plants; Citrus suhuiensis; Plant growth regulator, Auxin.*

Preparation of Ti_3SiC_2 Max Phase Via Sol-Gel Process

Gizem Ozge Kayan[1], Ipek Akin [*1]

[*]: akinipe@itu.edu.tr, ORCID: 0000-0002-3159-7650
[1]: *Metallurgical and Materials Engineering Department, Istanbul Technical University, Istanbul, Turkiye*
[2]: *Metallurgical and Materials Engineering Department, Istanbul Technical University, Istanbul, Turkiye*

ABSTRACT

MAX phases are characterized by the general formula $M_{n+1}AX_n$ (n = 1, 2, 3). M stands for a transition metal, A for an element of group 3A or 4A and X for C or N. MAX phases are polycrystalline, nano-sized and layered structures of ternary carbides and nitrides. Ti_3SiC_2 MAX phases are generally produced by hot isostatic press, hot press, and spark plasma sintering methods by their pure elements or carbide (TiC or SiC) compounds. Synthesis at high temperatures, high pressure, and long holding times can cause decomposition of Ti_3SiC_2 and it is also not economical to start from pure elements. In this study, possible problems were considered and sol-gel method for Ti_3SiC_2 synthesis was investigated. The synthesis of Ti_3SiC_2 consists of two stages which are sol-gel method and heat treatment. The raw materials of Ti_3SiC_2 were synthesized by using metal alkoxides such as Ti-, Si- and C sources via sol-gel method. After this, raw materials were conducted to heat treatment at 1150-1400 °C with 60 mins holding time under argon (Ar) atmosphere. The maximum yield of Ti_3SiC_2 with 90% purity was achieved by heat treatment of inorganic-organic hybrid MAX phase raw materials obtained by partial hydrolysis of 2:1 Ti:Si-alkoxide ratio prepared by sol-gel method under argon at 1350 ºC for 60 minutes. Acid purification processes were applied to increase the purity of the MAX phase produced, for example to remove impurities such as SiO_2 and TiO_2. As the authors knowledge there is no study in the literature on the synthesis of Ti_3SiC_2 MAX phases by sol-gel method.

Acknowledgment
This work was supported by the Scientific and Technological Research Council of Turkey (TUBITAK) for their financial support of this research, under project number 122M818.

Keywords— *Ti_3SiC_2, MAX phase, Sol-Gel, Heat Treatment*

Investigation of the Oxidation Behavior and Mechanical Properties of TiB_2-$MoSi_2$ Composites

Taha Can Yasgul, Beste Ecem Kayar, Gizem Ozge Kayan, Gultekin Goller, Ipek Akin*

*akinipe@itu.edu.tr, ORCID: 0000-0002-3159-7650
Metallurgical and Materials Engineering Department, Istanbul Technical University, Istanbul, Turkiye

ABSTRACT

Binary compounds composed of transition metals such as Zr, Hf, Ti, Nb and Ta, combined with boron, carbon or nitrogen, are known as ultra-high temperature ceramics (UHTCs). UHTCs are characterized as high temperature ceramics that have melting temperatures above 3000°C and are suitable for use in operating conditions above 2000°C due to their high temperature stability.

Titanium diboride (TiB_2), a member of the transition metal diboride family, possesses a high melting point, high hardness, and good thermal shock resistance. However, its application is limited by challenges in sintering and low fracture toughness. To address these limitations, this study aims to enhance the sinterability and fracture toughness of TiB_2 by incorporating molybdenum disilicide ($MoSi_2$) into the matrix, forming high-density composites.

In this study, composites with three different compositions were synthesized using the spark plasma sintering (SPS) technique (7.40 MK VII, SPS Syntex Inc.). The TiB_2 matrix was reinforced with 2.5 vol%, 5 vol%, and 10 vol% $MoSi_2$. The powder mixtures were placed into graphite molds and sintered using SPS at 1720°C under a pressure of 40 MPa, with a dwell time of 5 min. The bulk densities of the samples were measured using the Archimedes' method. Phase analysis was conducted through X-ray diffraction (XRD), and microstructural characterization was performed using scanning electron microscopy (SEM). Mechanical properties, including Vickers microhardness and fracture toughness, were evaluated, and the oxidation behavior of the composites was tested by furnace oxidation at 1100°C for 90 min.

Density measurements revealed that the sample containing 2.5 vol% $MoSi_2$ achieved a relative density of over 97%. XRD phase analysis indicated that the crystal structure of $MoSi_2$ transformed from a tetragonal to a hexagonal close-packed structure due to the elevated temperature during SPS. Additionally, $TiSi_2$ was detected in the sample with 10 vol% $MoSi_2$. The addition of $MoSi_2$ resulted in an approximately 6% increase in fracture toughness compared to monolithic TiB_2. Moreover, the oxidation resistance of the composite with 10 vol% $MoSi_2$ improved ~4 times compared to monolithic TiB_2.

Keywords— *TiB_2, $MoSi_2$, SPS, Composite*

Investigation Of the Densification, Mechanical Properties and Oxidation Behavior of CrB_2-SiC Composites

Beste Ecem Kayar, Gizem Ozge Kayan, Taha Can Yasgul, Gultekin Goller, Ipek Akin*

*akinipe@itu.edu.tr, ORCID: 0000-0002-3159-7650
Metallurgical and Materials Engineering, Istanbul Technical University, Istanbul, Turkey

ABSTRACT

Chromium diboride (CrB_2) is one of the advanced ceramics with high melting temperature (2200 °C), high hardness (~20 GPa), good corrosion and oxidation resistance. The potential applications are hard coatings on cutting parts and thin films produced by magnetron sputtering. The strong covalent bonding character and low self-diffusion coefficient of CrB_2 restrict the full densification during sintering in monolithic form. In order to overcome this problem, ceramic matrix composites are produced by incorporating various reinforcements such as, silicon carbide (SiC) and molybdenum disilicide ($MoSi_2$). SiC, in particular, acts as a sintering aid and enhances oxidation resistance by forming a protective borosilicate glass layer on the surface when exposed to air.

In this study, CrB_2-SiC binary composites containing 0, 10, 15, and 20 vol.% SiC were produced by spark plasma sintering (SPS) at 1600°C, under a pressure of 40 MPa, and with a holding time of 5 min. The consolidated samples were characterized through density measurements using the Archimedes' principle and mercury porosimetry, phase analysis via X-ray diffraction (XRD), microstructural analysis using scanning electron microscopy (SEM), and mechanical property assessment through Vickers microhardness testing. Additionally, oxidation behavior was investigated using thermogravimetric analysis (TGA) over a temperature range of 25-1100°C and furnace oxidation tests at 900, 1000, and 1100°C for 180 min. Elemental analysis was conducted to identify the elements formed during oxidation.

According to the characterization results, the relative density of monolithic CrB_2 was approximately 97%, and the addition of SiC increased the density to over 98%. XRD patterns confirmed the absence of any secondary phase formation, showing only the characteristic peaks of CrB_2 and SiC. The fracture mode for all compositions was predominantly transgranular. Vickers hardness increased by approximately 13% with the addition of 15 vol.% SiC, while the addition of 20 vol.% SiC enhanced the indentation fracture toughness of monolithic CrB_2 by ~36%. Oxidation resistance improved significantly, with CrB_2-SiC composites (containing 15-20 vol.% SiC) exhibiting approximately 40 times better performance compared to monolithic CrB_2 after furnace oxidation at 1100°C. The composite with 15 vol.% SiC showed the best overall combination of densification, microstructure, mechanical properties, and oxidation resistance among all the compositions studied. No prior research has been reported in the literature regarding the addition of SiC particles into the CrB_2 matrix. Oxidation resistance improved significantly, with CrB_2-SiC composites (containing 15-20 vol.% SiC) exhibiting approximately 30 times better performance compared to monolithic CrB_2 after furnace oxidation at 1100°C. The composite with 15 vol.% SiC showed the best overall combination of densification, microstructure, mechanical properties, and oxidation resistance among all the compositions studied.

This research was supported by ITU Scientific Research Projects Coordination Unit with a project code FHD-2023-44882.

Keywords—*CrB_2, CrB_2-SiC composites, spark plasma sintering, oxidation resistance*

Local well-posedness and blow-up solutions of a fourth-order pseudo-parabolic equation

Dilara Karslıoğlu[*,1]

[*]: dilara.karslioglu@yeditepe.edu.tr, ORCID: 0000-0001-7141-73

[1]: *Department of Mathematics, Yeditepe University, İstanbul, Turkey*

ABSTRACT

In this note, the initial and periodic boundary value problem was solved for the fourth-order pseudo-parabolic equation with gradient non-linearity and pseudo term.
Local existence-uniqueness result for mild solutions was found for any initial data by using Banach fixed point theorem. In addition, the existence of blow-up solutions was proved and a lower bound for the blow-up time was obtained.
Pseudo-parabolic equations play a crucial role in modeling complex physical phenomena where traditional parabolic or hyperbolic equations are insufficient. Their ability to capture memory effects and non-local behavior and to ensure the smoothness of solutions makes them valuable in various scientific and engineering applications
Moreover, In this research, it was observed that two different types of equations have different solution spaces and these spaces converge to each other. It was also observed that the solutions of pseudo-parabolic equations are smoother than the solutions of parabolic equations.

Keywords— *Fourth order pseudo parabolic equation; Gradient non-linearity; Existence-uniqueness; Blow-up; Lower blow-up time*

Evaluation of the Degree of Biological Decay of Wood Based on Climate Index Values in Türkiye

Seren Seda ARI[*,1], Çağatay TAŞDEMİR[1,2], Eylem DİZMAN TOMAK[1,2]

[*]: serensedaari@gmail.com, ORCID: 0009-0004-4615-1055
[1]: *Department of Forest Products (Grad. School), Bursa Technical University, 16310 Bursa, Türkiye*
[2]: *Department of Forest Industry Engineering, Bursa Technical University, 16310 Bursa, Türkiye*

ABSTRACT

Wood is an organic material, so it is susceptible to degradation by various biological agents. When temperatures range between 20-27°C and humidity levels are between 65-70%, the conditions become ideal for fungal growth. In our country, wood materials typically used in outdoor environments fall within these ranges, making them vulnerable to fungal damage. Therefore, understanding climate index values is crucial for assessing the degree of fungal damage risk to outdoor wood materials in our country and providing insights into the technical and practical measures needed to minimize the adverse effects of potential decay hazards. This study aims to classify the climate of provinces in our country and calculate climate index values using meteorological data from 2012-2023. In doing so, the study aims to link these values to the biological decay of wood. For this purpose, the Erinç climate classification and Scheffer Climate Index values were calculated based on temperature and precipitation parameters over the last 11 years. These values were then categorized according to decay risk levels. The results indicate a slight increase in Scheffer Climate Index values in recent years and a decrease in the precipitation effectiveness index. This trend could be related to rising temperatures and decreasing precipitation over the past 11 years. The highest precipitation effectiveness index was observed in the Eastern Black Sea region, while the lowest was recorded in Southeastern and Central Anatolia. The precipitation effectiveness index, directly proportional to precipitation levels, produced results consistent with regional expectations. Among all provinces, Rize in the Eastern Black Sea region had the highest precipitation effectiveness index, while Aksaray in the Central Anatolia region had the lowest. According to the Scheffer Climate Index values, the region with the highest risk of decay is the Eastern Black Sea. In contrast, regions such as the Central Black Sea, Western Black Sea, and Marmara exhibited moderate decay conditions. Decay conditions were identified as low in the other areas, with Southeastern Anatolia having the lowest index value. The highest Scheffer Climate Index values (> 80) were found in the Eastern Black Sea provinces of Rize, Giresun, Ordu, and Trabzon. In contrast, the lowest values (< 10) were recorded in the Eastern Anatolian provinces of Bitlis and Van, the Central Anatolian province of Karaman, and the Southeastern Anatolian province of Batman. In regions with a high risk of decay, it is essential to use impregnated wood for outdoor applications. As is the case globally, increasing global warming in our country is causing significant changes in the climate. As a result, wood used in outdoor environments is greatly affected by seasonal factors, which may alter its service life over time. Particularly in recent years, the decrease in precipitation and the corresponding increase in temperature and global solar radiation are likely to result in changes to the factors that cause damage to wood. Given the expected rise in fungal attacks and insect and termite attacks in the coming years, it is necessary to promote the use of impregnated or modified wood products for outdoor applications and raise public awareness about these issues.

Keywords— *Erinç Climate Classification; Scheffer Climate Index; Wood Decay; Impregnation*

The Role of CuIr Alloys and Magnetic Damping in NiFe Thin Films

Mustafa Tokaç[*,1]

[*]: *mustafa.tokac@alanya.edu.tr*, ORCID: 0000-0001-5614-2292
[1]: *Department of Fundamental Sciences, Faculty of Engineering, Alanya Alaaddin Keykubat University, Antalya, Türkiye*

ABSTRACT

In the rapidly evolving field of spintronics, the manipulation of spin currents is a crucial factor for developing efficient and powerful devices. One of the most significant discoveries in this domain has been the spin-Hall effect, which allows the generation of spin currents in non-magnetic materials without the need for an external magnetic field or a ferromagnetic (FM) layer. The spin-Hall effect is directly related to the spin-orbit interaction, an effect that occurs prominently in materials with heavy atoms, like those in the 5d transition metal group. This relationship opens the door to using alloys formed by 5d metals and lighter elements such as Cu in FM/NM structures to enhance the performance of spintronic devices.

In this study, the potential of these materials was explored by examining how non-magnetic layers affect the magnetic properties of NiFe thin films. NiFe films with thicknesses of 5, 7, and 10 nm were fabricated using magnetron sputtering. These films were then capped with 3 nm layers of CuIr and Pt to study the influence of the non-magnetic layers on the magnetic damping properties of NiFe. The vector network analyzer ferromagnetic resonance (VNA-FMR) was employed in this study, providing detailed information on the magnetization processes within the multilayers. From the VNA-FMR data, the Gilbert damping constant was extracted, a parameter that describes how fast the magnetization precession decays back to equilibrium. This constant is vital for understanding energy dissipation in magnetic systems, as materials with strong spin-orbit coupling tend to exhibit higher damping due to enhanced spin-flip scattering, which broadens the FMR linewidth. Among the non-magnetic layers tested, CuIr stood out as a promising alternative to traditional heavy metals like platinum, which are widely used in spintronic devices. The CuIr alloy, due to its high spin-orbit interaction, showed potential to influence the magnetic damping in NiFe films, a property crucial for efficient spin current generation and manipulation. By reducing damping or controlling it precisely, new generations of spintronic devices could be developed, offering faster, more energy-efficient operations.

Keywords—*Magnetization dynamics, Thin films, Gilbert damping, Ferromagnetic resonance.*

Processing and Characterization of $CoCrFeNiAl_x$ (x=0.2 x=0.6 x=1 x=1.5 mol) High Entropy Alloy by Mechanical Alloying and Spark Plasma Sintering

Yusuf Baran Cicek[*1], Gultekin Goller[1]

[*]: yusufbarancicek@gmail.com, ORCID: 0009-0006-0860-8004
[1]: *Metallurgical and materials engineering, Istanbul Technical Universit1, Istanbul, Türkiye*

ABSTRACT

High entropy alloys (HEAs) are materials consisting of at least 5 elements, where the composition of each element is between 5% and 35%. For a 5-element equiatomic alloy, the proportion of each element is 20%. HEAs have various superior properties compared to conventional alloys, especially high strength, high hardness value. High entropy alloys have 4 main effects called four core effects. These are high entropy effect, lattice distortion effect, slow diffusion effect and cocktail effect, which are extremely important for the evaluation and development of material properties. The main objective of this study is to produce and optimize $CoCrFeNiAl_x$ (x=0.2 x=0.6, x=1, x=1.5 mol) high entropy alloy powders by mechanical alloying and to study the change of material properties by sintering process with boron carbide addition. The powders were prepared with a 10:1 ball-to-powder ratio to ensure the optimum grinding condition. The mechanical alloying process was then carried out with 2-4-6-8 and 20 hours of grinding at 800 rpm for both systems. The spark plasma sintering process of the unreinforced material was carried out at 840°C, 40 MPa pressure and 3 minutes sintering time, while the sintering of the material containing 2% boron carbide was carried out at 900°C, the same pressure and sintering time. Density measurements were made according to the archimedes principle. The density of the unreinforced material was 6.39 g/cm^3 ± 0.04, while the density of the reinforced material was 6.91 g/cm^3 ± 0.02. The average hardness value of the unreinforced material was 415.07 HV ± 12.35. As a result of the study, phase analysis was carried out by x-ray diffraction technique.

Keywords— *High Entropy Alloys, Mechanical Alloying, Spark Plasma Sintering, Material Characterization, X-Ray Diffraction Technique, Microstructure Characterization*

Influence of Halogen Heater and Fluidized Bed Drying on Color, Total Phenolic Content and Drying Kinetics of Green Pepper (*Capsicum* L.)

Elif Sena YÜCEL[*1], Fatma Kevser ERAFŞAR[2], Elif ÇELİK[3]

[*]: esenayucel@gmail.com, ORCID: 0000-0001-5868-5434
[1,3]: *Department of Food Engineering, Kahramanmaraş Sütçü İmam University, K.Maraş,Turkey*
[2]: *Department of Food Technology, Kahramanmaraş İstiklal University, K.Maraş, Turkey*
[3]: *Department of Food Engineering, Kahramanmaraş Sütçü İmam University, K.Maraş,Turkey*

ABSTRACT

Drying is a process that involves the simultaneous transfer of heat and mass, resulting in the reduction of moisture content in food products. The study aimed to evaluate color values, total phenolic content and drying kinetics on different drying temprature (50, 60 and 70°C) of halogen heater drying (HHD) and fluidized bed drying (FBD) on green pepper (*Capsicum* L.). Drying kinetics were evaluated for drying rate, moisture ratio, effective diffusion coefficient (D_{eff}), activation energy (Ea). Drying curves were obtained by recording sample weights in 15-min periods for the drying the time for the samples to reach 8-10% humidity level on a wet basis. The effective diffusion coefficients were found to be between $-8.11x10^{-9}$ and $-2.84x10^{-8}$ m^2/s in the HHD and $-1.62\ x10^{-8}$ and $-3.65x10^{-8}$ m^2/s in the FBD. The activation energy ranged from 60.42 to 70.83 kJ/mol and 58.33 to 65.07 kJ/mol in HHD and FBD, respectively. The total phenolic content of the samples ranged from 354.00 to 651.49 mg gallic acid/kg in the HHD and 538.17 to 665.47 mg gallic acid/kg in the FBD. Additionally, it was found that the samples dried in the HHD had a better rehydration capacity and rate compared to those dried in the FBD. However, when comparing color values, the samples dried in the FBD were found to be closer to the fresh sample compared to those dried in the HHD.

Also, the drying curves were fitted to six mathematical models. The model with the highest regression coefficient (R^2) and the lowest chi-square (χ^2), and root mean square error (RMSE) was selected as the best model. For the samples dried in the HHD the Jena&Das model provided the best fit for describing the thin-layer drying of greenpepper, whereas the Aghbashlo model was more suitable for the FBD. The study concluded that increased the drying temperature of the samples reduced the drying time by 50-57.7%, increased the effective diffusion coefficient, and allowed drying with lower activation energy in the production of dried green pepper for both drying methods.

Keywords: *Mathematical Modelling, Drying Kinetics, Total Phenolic Content, Halogen Heater Drying, Fluidized Bed Drying*

Tuz Hidrat Faz Değişim Malzemeleri ve Performanslarını İyileştirmek için Kullanılan Nanoparçacıklar

Salt Hydrate Phase Change Materials and Nanoparticles Used to Improve Their Performance

Sinem KILIÇKAP IŞIK[*,1]

[*]: sinemisik@bingol.edu.tr, ORCID: 0000-0002-1044-5092

[1]: *Department of Mechanical Engineering, Faculty of Engineering and Architecture, Bingöl University, Bingöl, Türkiye*

ÖZET

Nüfus ve enerji talebinin artması ile sürdürülebilir enerji üretimi ve özellikle enerjinin depolanması konuları çok önemli hale gelmiştir. Özellikle mevcut enerjiyi depolamak, enerji talebinin karşılanması, güneş ve rüzgar gibi yenilenebilir enerji kaynaklarından elde edilen enerjinin kesintisiz ve istikrarlı olması, enerjideki fiyat artışlarının önlenmesi açısından çok önemlidir. Bu amaçla, termal enerji depolama yöntemlerinden en önemlisi olan gizli ısı depolama yönteminde kullanılan tuz hidratlar, son zamanların araştırma konularından biri olmuştur. Tuz hidratlar, ısı depolama ve serbest bırakma özelliğine sahip, sabit sıcaklıkta faz değiştiren, faz değişimi sırasında hacim değişikliği az olan, büyük miktarda enerji depolayan, düşük maliyetli, toksik olmayan malzemelerdir. Tuz hidratların, diğer faz değişim malzemelerine göre ulaşılabilirliği daha yüksektir. Yapılarında su molekülleri (nH_2O) bulunmaktadır. Gıda taşımacılığı, güneş enerjisi gibi yenilenebilir enerji sistemleri, bina uygulamaları, ısıtma ve soğutma uygulamaları gibi çok çeşitli uygulama alanları sunmaktadır. Günümüzde yaygın olarak kullanılan tuz hidrat faz değişim malzemelerinden bazıları şunlardır; $Na_2SO_4 \cdot 10H_2O$ (sodyum sülfat dekahidrat, glauber tuzu), $CaCl_2.6H_2O$ (kalsiyum klorür hekzahidrat, $CH_3COONa.3H_2O$ (sodyum asetat trihidrat), $Mg(NO_3)_2.6H_2O$ (magnezyum nitrat hekzahidrat, $KF.4H_2O$ (potasyum florür tetrahidrat), $LiClO_3.3H_2O$ (lityum klorat trihidrat), $LiNO_3.3H_2O$ (lityum nitrat trihidrat), $Na_2CO_4 \cdot 10H_2O$ (sodyum karbonat dekahidrat), $CaBr_2.6H_2O$ (kalsiyum bromür hekzahidrat), $MgCl_2.6H_2O$ (magnezyum klorür hekzahidrat), $Na_2HPO_4 \cdot 12H_2O$ (disodyum hidrojen fosfat dodekahidrat), $MgCl_2.6H_2O$ (magnezyum klorür hekzahidrat), $NH_4Al(SO_4)_2 \cdot 12H_2O$ (amonyum alüminyum sülfat dodekahidrat, amonyum şap, şap), $Na_2S_2O_3.5H_2O$ (sodyum tiosülfat pentahidrat), $Na_3PO_4 \cdot 10H_2O$ (sodyum fosfat dekahidrat).

Tuz hidrat faz değişim malzemelerinin avantajlarının yanında bazı dezavantajları da bulunmaktadır. Düşük termal iletkenliklerini ve enerji depolama kapasitelerini iyileştirmek, faz ayrışmasını önlemek ve aşırı soğuma davranışlarını azaltmak için nanomalzemeler kullanılmaktadır. Bu amaçla kullanılan nanomalzemeler arasında, grafen ve grafenden elde edilen diğer nanoparçacıklar (GO, rGO, GNP, N-doped grafen, GQDs gibi), metal ve metal oksit nanoparçacıkları, tek ve çok duvarlı karbon nanotüpler, silika nanoparçacıkları, grafit, genişletilmiş grafit, boron nitride nanotüpleri, polimerler ve farklı malzemelerin birleşmesiyle oluşan nanokompozitler yer almaktadır.

Keywords—*Enerji Depolama; FDM; Tuz Hidratlar; Nanoparçacıklar*

ABSTRACT

With the increasing population and energy demand, sustainable energy production, particularly energy storage, has become very important. In particular, storing the existing energy, meeting the energy demand, ensuring that the energy obtained from renewable energy sources such as solar and wind is uninterrupted and stable, and preventing price increases in energy are very important. For this purpose, salt hydrates used in the latent heat storage method, which is the most important of the thermal energy storage methods, have become one of the recent research topics. Salt hydrates are low-cost, non-toxic materials that have the property of storing and releasing heat, phase change at a constant temperature, having little volume change during phase change, and storing large amounts of energy. Salt hydrates are more accessible than other phase change materials. They contain water molecules (nH_2O) in their structures. They offer a wide range of application areas such as food transportation, renewable energy systems such as solar energy, building applications, and heating and cooling applications. Some of the salt hydrate phase change materials widely used today are as follows; $Na_2SO_4 \cdot 10H_2O$ (sodium sulfate decahydrate, glauber's salt), $CaCl_2.6H_2O$ (calcium chloride hexahydrate, $CH_3COONa.3H_2O$ (sodium acetate trihydrate), $Mg(NO_3)_2.6H_2O$ (magnesium nitrate hexahydrate, $KF.4H_2O$ (potassium fluoride tetrahydrate), $LiClO_3.3H_2O$ (lithium chlorate trihydrate), $LiNO_3.3H_2O$ (lithium nitrate trihydrate), $Na_2CO_4 \cdot 10H_2O$ (sodium carbonate decahydrate), $CaBr_2.6H_2O$ (calcium bromide hexahydrate), $MgCl_2.6H_2O$ (magnesium chloride hexahydrate), $Na_2HPO_4 \cdot 12H_2O$ (disodium hydrogen phosphate dodecahydrate), $MgCl_2.6H_2O$ (magnesium chloride hexahydrate), $NH_4Al(SO_4)_2 \cdot 12H_2O$ (ammonium aluminium sulfate dodecahydrate, ammonium alum, alum), $Na_2S_2O_3.5H_2O$ (sodium thiosulfate pentahydrate), $Na_3PO_4 \cdot 10H_2O$ (sodium phosphate decahydrate).

Despite the advantages of salt hydrate phase change materials, there are also some disadvantages. Nanomaterials are used to improve their low thermal conductivity and energy storage capacity, prevent phase separation and reduce their supercooling behaviour. Nanomaterials used for this purpose include graphene and other nanoparticles obtained from graphene (GO, rGO, GNP, N-doped graphene, GQDs, etc.), metal and metal oxide nanoparticles, single and multi-walled carbon nanotubes, silica nanoparticles, graphite, expanded graphite, boron nitride nanotubes, polymers and nanocomposites formed by combining different materials.

Keywords— *Energy Storage; PCM; Salt Hydrates; Nanoparticles*

Kısa Elyaf Takviyeli Kompozit Timoshenko Kirişlerinin Titreşiminde Dönel Yay Mesnetlerinin Etkisi

Effect of Rotational Spring Supports on Vibration of Short-Fiber-Reinforced Composite Timoshenko Beams

Büşra UZUN[*,1]

[*]: buzun@uludag.edu.tr, ORCID: 0000-0002-7636-7170
[1]: *Bursa Uludağ Üniversitesi, Mühendislik Fakültesi, İnşaat Mühendisliği Bölümü, Görükle Kampüsü, 16059, Bursa / TÜRKİYE*

ÖZET

Bu çalışmada, her iki ucundan dönel yaylar ile dönmeye karşı kontrol altına alınmış ve Timoshenko kiriş teorisi ile ele alınan kısa elyaf takviyeli kompozit kirişlerin serbest titreşim analizi incelenmiştir. Ayrıca, kısa elyaf takviyeli kompozit kirişler dönel yayların yanısıra her iki ucundan basit mesnetler ile sabitlenmiştir. Takviye elemanı olarak kullanılan kısa elyaflar, kompozitin matris malzemesinde rastgele yönlendirilmiş olarak ele alınmıştır. İlk olarak, literatürde iyi bilinen Timoshenko kiriş teorisinin serbest titreşimini ifade eden denklemler verilmiştir. Dönel yay mesnetlerinin etkisini incelemeye imkan veren analitik çözümün elde edilebilmesi için yer değiştirme fonksiyonu Fourier sinüs serisi seçilirken dönme fonksiyonu Fourier kosinüs serisi seçilmiştir. Ardından, benimsenen sınır koşullarında serbestlik sağlaması için Stoke dönüşümü uygulanmış ve bir özdeğer problemi elde edilmiştir. Elde edilen bu özdeğer problemi hem kısa elyaf takviyeli kompozit kirişlerin malzeme özelliklerini hem de dönel yay parametrelerini içermektedir. Kısa elyaf takviyeli kompozit Timoshenko kirişlerin uçlarındaki dönel yay parametrelerinin rijitlikleri çok düşük ayarlandığında sonuçlar her iki ucu basit mesnetli kirişlerin sonuçlarını vermektedir. Bu dönel yay parametrelerinin rijitliklerinin çok yüksek ayarlanması ise sonuçları her iki ucu ankastre mesnetli kirişlerin sonuçlarına getirir. Bu çözümün avantajı dönel yay parametrelerini keyfi bir şekilde ayarlama imkanı vermesi ve böylece hem deforme olabilir hem de rijit sınır koşullarına sahip kısa elyaf takviyeli kompozit Timoshenko kirişlerinin serbest titreşim frekanslarını hesaplayabilmesidir. Sunulan çözüm ile değişik kısa elyaf ve matris malzeme özelliği kombinasyonlarının kompozit Timoshenko kirişlerinin serbest titreşim frekanslarına etkisi farklı dönel yay rijitlikleri düşünülerek incelenmiştir. Kısa elyaf elastisite modülünün matrisin elastisite modülüne oranı arttıkça frekanslar artarken kısa elyaf kütle yoğunluğunun matrisin kütle yoğunluğuna oranı arttıkça frekanslar düşmektedir. Kompozit kirişin her iki ucundaki dönel yayların rijitliklerinin artması titreşim frekanslarının artmasına neden olmaktadır. Hem eşit hem de farklı rijitliklerde ayarlanabilen bu dönel yaylar kompozit kirişlerin diğer özelliklerini değiştirmeden frekansların kontrol edilebilmesine imkan sağlamaktadır.

Anahtar Kelimler— *kısa elyaf takviyeli kompozit kiriş; titreşim; Timoshenko kiriş teorisi; Stoke dönüşümü; dönel yay*

ABSTRACT

In this study, the free vibration analysis of short-fiber-reinforced composite beams controlled against rotation by rotational springs at both ends and treated by Timoshenko beam theory is investigated. In addition to rotational springs, short-fiber-reinforced composite beams are also rested on simply supports at both ends. The short fibers used as reinforcing elements are considered randomly oriented in the matrix material of the composite. First, the equations expressing the free vibration of the Timoshenko beam theory, well known in the literature, are given. The displacement function is chosen as Fourier sine series while the rotation function is Fourier cosine series to obtain an analytical solution that allows to study the effect of rotational springs. Then, the Stokes' transform is applied to provide freedom in the adopted boundary conditions and an eigenvalue problem is obtained. This eigenvalue problem involves both the material properties of the short-fiber-reinforced composite beams and the rotational spring parameters. When the stiffnesses of the rotational spring parameters at the ends of the short-fiber-reinforced composite Timoshenko beams are set too low, the results give the results of simply-supported beams at both ends. Setting the stiffnesses of these rotational spring parameters too high brings the results to the results of beams with clamped supports at both ends. The advantage of this solution is that it allows arbitrary setting of the rotational spring parameters and thus can calculate the free vibration frequencies of short-fiber-reinforced composite Timoshenko beams with both deformable and rigid boundary conditions. With the presented solution, the effect of different combinations of short fiber and matrix material properties on the free vibration frequencies of composite Timoshenko beams is investigated by considering different rotational spring stiffnesses. The frequencies increase as the ratio of short fiber modulus of elasticity to matrix modulus of elasticity increases, while the frequencies decrease as the ratio of short fiber mass density to matrix mass density increases. Increasing the stiffness of the rotational springs at both ends of the composite beam causes the vibration frequencies to increase. These rotational springs, which can be set at both equal and different stiffnesses, allow the frequencies to be controlled without changing the other properties of the composite beams.

Keywords— *short-fiber-reinforced beam; vibration; Timoshenko beam theory; Stokes transform; rotational spring*

Morphological Features in Radiological Images: Python-Based Image Processing Solutions

Muhammet Üsame ÖZİÇ[*,1]

[*]: muozic@pau.edu.tr, ORCID: 0000-0002-3037-2687
[1]: *Department of Biomedical Engineering, Pamukkale University, Denizli, TÜRKİYE*

ABSTRACT

Radiological imaging systems are widely used in hospitals to examine undesired anomalies that occur in the human body. Many types of anomalies such as tumors, cysts, masses, bleeding, abscesses, inflammation, pneumonia and plaques can be analyzed and monitored in detail using computed tomography, X-ray, ultrasound and magnetic resonance imaging techniques. Periodic monitoring is crucial for longitudinal follow-up of detected or suspected anomalies. For this purpose, images of individuals are obtained from the same regions at certain time intervals (months or weeks) with radiologic imaging systems. By comparing the morphological characteristics of the anomalies in the relevant regions in the previous and subsequent images, important information that directly affects the diagnosis and treatment processes such as the direction of disease progression, tumor growth rate, extent of spread, and increase in volume is provided. The acquisition of morphological features in radiological images is usually performed manually in hospitals. Automated or semi-automated measurement systems can reduce the time and errors caused by manual measurement. In this study, we investigated the functions and application solutions offered by OpenCV and Scikit-image libraries with Python programming language to determine the morphological features of a liver tumor in computed tomography images. Morphological features were obtained using a mask from a liver Computed Tomography image in the "Medical Segmentation Decathlon" database. These masks were drawn by experts and have been made available for exploring artificial intelligence methods in segmentation and other features. In this study, masks were used only for the determination of morphological features, and segmentation operations related to artificial intelligence were excluded from the scope of the study. We determined the real-world size of a pixel in millimeters from the 'info' files of NIfTI format images. Using Python, OpenCV and Scikit-image libraries, morphological features of the tumor region were obtained and how to measure the real-world size of these features was investigated. The study showed that Python image processing solutions provide practical functions and tools for determining morphological features. At the end of the study, we discussed the advantages and limitations of these libraries in the context of medical imaging.

Keywords—*Computed Tomography; Morphological Features; OpenCV; Python; Scikit-image; Tumor*

Optimizing Load-Bearing Capacity of Sand: The Role of Stiffness Modulus Ratio

Aykut EROL[*,1], Hakan YALÇIN[2], Gül AKPINAR EROL[1]

[*]: aykuterol@erciyes.edu.tr, ORCID: 0000-0003-3206-8133
[1]: Department of Civil Engineering, *Erciyes University, Kayseri, TÜRKİYE*
[2]: *Department of Civil Engineering, Abdullah Gül University, Kayseri, TÜRKİYE*

ABSTRACT

Soil deformation characteristics are influenced by factors such as effective stress, relative density, strain level, and stress-strain history. The mechanical behavior of cohesionless soil, including stress-strain and dilatancy responses, is notably affected by changes in confining pressure. Soil behavior is inherently non-linear, meaning soil stiffness varies with the stress levels within the soil mass. In the Hardening Soil (HS) model, soil behavior is represented more accurately by incorporating three distinct soil stiffness moduli. This model also considers the stress dependence of soil stiffness and the dilatancy behavior specific to sand. Additionally, the yield surface in the HS model can expand as plastic strains accumulate. Advanced models like the HS model can also account for loading history through parameters such as the overconsolidation ratio (OCR) or pre-overburden pressure (POP).

The stiffness parameters E_{50}^{ref}, E_{ur}^{ref}, and E_{oed}^{ref} correspond to reference pressures and are crucial for modeling soil behavior. Specifically, E_{50}^{ref} (secant modulus) is used to represent the soil's response to plastic deformations during primary deviatoric loading. In contrast, E_{ur}^{ref} (unloading-reloading modulus) characterizes the soil's elastic behavior during unloading and reloading phases; this parameter can often be calculated using a specific equation. The reference value E_{oed}^{ref} (odeometric modulus) is commonly used in soil mechanics to represent the modulus of elasticity from oedometer tests. In instances where direct measurement of E_{50} or E_{ur} from experimental data is not feasible, it is often beneficial to employ the approximation E_{ur}^{ref} / E_{50}^{ref} = 2.00 to 6.00, with a commonly accepted mean value of 3.00. This stiffness modulus ratio serves as a comparative metric, effectively characterizing the stiffness behavior of soil under varying loading conditions.

This research employs finite element software to perform comprehensive numerical simulations. The study is structured into two principal phases: validation and soil analysis. During the validation phase, the full-scale loading tests executed by Briaud and Gibbens (1997) on square footings resting on sandy substrates have been meticulously replicated and assessed using finite element modeling (FEM). This methodology facilitates the development of a rigorously calibrated and validated finite element model, subsequently utilized for generating an extensive dataset.

In this study, the effect of varying stiffness modulus ratios (E_{ur}^{ref} / E_{50}^{ref} = 2.00, 3.00, 4.00, 5.00, 6.00, 7.00) on the load-bearing capacity of sand is examined through finite element analysis utilizing the HS method. The findings of this study indicate that the stiffness modulus ratio notably influences the load-bearing capacity of sand, with a pronounced effect observed between ratios of 2.00 and 3.00. Beyond this threshold, the tendency for diminishing returns in load-bearing capacity suggests the need to establish an optimal stiffness ratio for engineering applications that balances performance with material efficiency.

Keywords—*Hardening Soil; Stiffness Modulus; Bearing Capacity; Finite Element*

Analysis of Piled Concrete Foundation for an Offshore Structure

Hakan YALÇIN*[1], Aykut EROL[2], Gül AKPINAR EROL[2]

*hakan.yalcin@agu.edu.tr, ORCID: 0000-0003-3346-1893
[1] *Department of Civil Engineering, Abdullah Gül University, Kayseri, TÜRKİYE*
[2] *Department of Civil Engineering, Erciyes University, Kayseri, TÜRKİYE*

ABSTRACT

Numerous essential offshore structures are supported by wide-diameter rigid piles for support, including bridges, wind turbine systems, and marine construction platforms. Offshore foundations are responsible for transmitting the complete loads of offshore structures to the seabed and ensuring their stability. Any structural failure within these foundations can lead to a collapse of the entire offshore structure. Environmental loads including wind and waves may cause lateral strains on offshore piles. These loads can cause long-lasting soil deformations and create excessive pore water pressures in saturated soils. This is a critical factor to consider in designing structures and managing construction projects. In this study, to enhance the precision and efficacy of the design process for offshore foundation systems subjected to axial and lateral wave loads, a finite element analysis has been executed to ascertain the stresses and displacements in a concrete pile under comparable loading conditions.

The results indicated that the maximum bending moments existed at a distance of 3 to 6 times of the pile diameter from the seabed level. As the soil's relative density increases, the point where the largest bending moment occurs approaches the pile head. Also, the effect of pile length on ultimate lateral resistance decreases as the pile length increases. Lastly, the soil type has a significant role in predicting the deformation behavior of the laterally loaded piles. While ultimate resistance is crucial for sands throughout the pile design, deformation values are vital for clays.

Keywords—*Offshore pile, Finite element analysis, soil deformation, foundation*